NAGOYA UNIVERSITY

EFFECT OF SURFACE TRANSFORMATION AND TRANSFER FILM ON FRICTION OF CARBONACEOUS HARD COATINGS

by

Nor Azmmi Bin Masripan

A thesis submitted in partial fulfillment for the degree of Doctor of Engineering

in the

DEPARTMENT OF MECHANICAL SCIENCE AND ENGINEERING

GRADUATE SCHOOL OF ENGINEERING

2013

NAGOYA UNIVERSITY

Abstract

DEPARTMENT OF MECHANICAL SCIENCE AND ENGINEERING
GRADUATE SCHOOL OF ENGINEERING

Doctor of Engineering

by Nor Azmmi Bin Masripan

In this thesis, we present the effect of surface transformation and transfer layer on the friction of carbonaceous hard coatings. Carbonaceous hard coatings have been used in recent years as coatings for tribological components; especially for vehicles, in order to reduce friction and wear, which consequently increases the life-span and working efficiently of components. Carbonaceous hard coatings are used in many industrial applications, due to their excellent tribological properties of low friction, high wear resistance, and chemical inertness. Another essential advantage of carbonaceous hard coatings is that it provides a low friction coefficient; either under dry conditions or boundary lubrication in oil. This particular advantage has attracted more research to understand the tribological behaviour of carbonaceous hard coatings, as a guideline for future usage. Consequently, we performed two experiments; one in dry and the other in oil conditions. In the first experiment, we investigated the effect of the transfer layer on the ultra-low friction of CNx coating under blowing dry Ar. Meanwhile, the second experiment investigated the effect of the transformed layer, in terms of their thickness and hardness on friction under boundary lubrication, in additive-free mineral-based oil.

In a dry condition, CNx coating can provide a low friction coefficient of 0.003 under blowing Ar, in an ambient environment, with help from the formation of a transfer layer at the sliding interface. Following the friction test, an ex-situ observation showed that the transfer layer could be found easily on the counter part's surface. Therefore, we think that an in-situ observation is needed to observe the formation of the transfer layer that influences the friction behaviour under a dry condition. However, no reports exist about an in-situ observation of the formation of a transfer layer during friction testing in a dry condition. We have developed a new experimental apparatus, based on a ball-on-disc tribometer. We used a transparent sapphire hemisphere ball (α-Al_2O_3) as a counterpart against a CNx coated disc for friction testing. With help of an optical microscope and a CCD camera, images of the formation of a transfer layer can be recorded through the transparent sapphire hemisphere ball during the friction test.

The friction test's results show that the friction coefficient under blowing Ar, decreases from 0.18 to a steady state value of 0.003. An in-situ observation showed that the friction coefficient decreased rapidly, as the transfer layer started to generate at the contact interface. As the thickness of the transfer layer increased to 500 nm, the friction coefficient had a constant value at 0.003. Meanwhile, an ex-situ observation was performed using Raman analysis of the transfer layer, and found the transfer layer structure to be similar to graphite. The results showed that the formation of a graphite-like transfer layer from the CNx coating played an essential role in the low friction mechanism of CNx.

In the other experiment, we performed a friction test of a DLC coated sliding bearing (SUJ2) against an S55C disc under boundary lubrication conditions, in an additive-free mineral-based oil. Since the low friction mechanism under this condition was still unclear, we tried to investigate the low friction mechanism from a different point of view i.e., through the thickness and hardness of the transformed layer through an ex-situ observation. The thickness of the transformed layer was measured on wear track of DLC's coating using reflectance spectroscopy, and the hardness of the transformed layer was calculated using the depth of a scratch test, using Atomic Force Spectroscopy (AFM).

We prepared three types of DLC, which we named DLC1, DLC2, and DLC3, with different hardness's of 47.1, 11.8, and 6 GPa, respectively. The tribological properties of DLCs were investigated using a pin-on-disc tribometer, and friction tests were performed under boundary lubrication conditions, in an additive-free

mineral-based oil, at different oil temperatures of 24, 80, 120 and 160 °C. The experiment's results showed that DLC1 provided the lowest friction coefficient and wear rate of 0.03 and in the order of $10^{-11} mm^3/Nm$,respectively. The transformed layer was found at the topmost surface of DLC coating after the friction test. The pressure-induced graphitization was responsible for the DLCs structure changing from sp^3 into sp^2. The pressure-induced graphitization, which was confirmed by Raman analysis, showed that the value of I_D/I_G increased with increasing oil temperatures.

Reflectance spectroscopy was used to measured the thickness of transformed layer after friction test. In this work, we did find that the friction decreased by increasing the ratio of the thickness of the transformed layer, t and the deviation of roughness, σ^*. It was found that, the friction coefficient decreased significantly when the t/σ^* value higher than 1.

We performed an AFM scratch test to determine the nano characteristics of the transformed layer in terms of its hardness. We found that the hardness of the transformed layer decreased significantly at oil temperatures above 80 °C, compared to the hardness of the as-deposited DLC.

The empirical-based friction model map, which presents the thickness and hardness of the transformed layer, correlated to friction coefficient data in a graphical manner, was able to provide us with information of how the thickness and hardness of the transformed layer influenced the friction's behaviour. The combination of a thick transformed layer (more than 100 nm) and a moderate hardness of the transformed layer (2.8-4.3 GPa) can provide low friction. This combination avoids direct contact between the mating surfaces and the hard bulk DLC. Therefore, the mating surface can slide smoothly on the low shear strength of the transformed layer, without touching the hard bulk DLC.

Acknowledgements

First and foremost I would like to express my heartfelt gratitude to my advisor Professor Noritsugu Umehara. It has been an honor to be his Ph.D. student. He has taught me, both consciously and unconsciously, how good experimental tribology is done. I could not have asked for better role models, each inspirational, supportive, and patient.

I would also like to thank my examiners, Professor Kenji Fukuzawa, Professor Nagahiro Saito, and Associate Professor Hiroyuki Kousaka, who provided encouraging and constructive feedback. I am very grateful for their thoughtful and detailed comments.

This work was collaborate with DAIDO Metal Co. Ltd, and I would like to thank to Mr. Shigeru Inami, Mr. Koji Zushi and Mr. Mashahito Fujita for their generous support.

I owe a debt of gratitude to Associate Professor Dr. Hiroyuki Kousaka, Assistant Professor Dr. Takayuki Tokoroyama, Dr. Yosuke Tsukiyama and Mr. Shinko Senda for their involvement and support in different aspects of my research project, as well as the various group meetings that expanded my understanding.

I owe a special thanks to my research partner, Mr. Kenji Ohara, Mr. Yuki Miyahira, Mr. Hidenori Nishimura and all members from the Advanced Materials and Manufacturings for their invaluable help during laboratory works. I am very happy to be a part of the Umehara Laboratory.

Special thanks to Malaysian government and Universiti Teknikal Malaysia Melaka (UTeM) for financial support under Skim Latihan Akademik Bumiputera (SLAB), without it, my study at Nagoya University, Japan would have not been possible.

I owe a lot to my parents, Masripan Bin Abu and Rokeyah Binti Yasman, who loved me at every stage of my life. There is no enough words to thank for your sacrifice to make my life meaningful.

I am very much indebted to my family, my wife Norazah Binti Amir, daughters Alifah Ilyana and Alifah Raschika, and son Alif Hakim, who supported me in every possible way to see the completion of this work. I love you all so much.

I also thank my friends especially Dr. Mohd. Fadzli Bin Abdollah for providing support and friendship that I needed.

Above all, I owe it all to Almighty ALLAH S.W.T for granting me the wisdom, health and strength to complete my works.

Contents

List of Figures

List of Tables

Chapter 1

Introduction

1.1 Introduction to tribology

The word tribology is combination between *tribo*, "rub" in classic Greek, and $-logy$, "knowledge of ". Widely used as an engineering term since 1966, it is a new discipline in the field of mechanical engineering and materials science correlating to the study of friction, lubrication, and wear [1]. The problem posed by friction when moving heavy objects using the sliding method has challenged mankind for a thousand years. During early tribology history, the Egyptians first used water, and later natural oils as lubricants to reduce friction at the sliding interface in order to move massive stones over great distances for the construction of pyramids. A breakthrough in tribology technology occurred with the introduction of a rolling part such as a wheel and bearing to further reduce friction.

Friction and wear are basic problems in the tribology system due to abrasion on the contact surface of two moving parts leading to a reduction in the lifespan of the tribology component. Friction is defined as a tangential force against the sliding motion of a body in an opposite direction. Wear is the result from the friction process where the greater the friction, the higher the wear. Therefore, in the tribology system, it is essential to separate two relative moving contact surfaces in order to minimize friction and wear. The focus of this study is the application of a liquid as a lubricant at the contact interface.

The demand for tribological technology increased in tandem with industrial growth and this led to the need for a better understanding of its aspects in various areas.

The role of tribology became more significant of late when researches acknowledged the looming problem of an energy crisis in the not too distant future. As such, the onus is on tribologists to increase knowledge in this area and come up with an efficient system that does not lose too much energy to the forces of friction.

1.2 Industrial needs of hard coating

It has been reported that friction, lubrication, and wear have a significant influence on the efficiency and lifespan of mechanical components employed in industries. In the long run, this influence plays a deciding role in the economic development of a nation. The report emphasized that viewing tribology from a scientific and technological perspective is crucial in order to avoid major economic losses [2]. The concern here is not only related to the economy, but also to the environment, as machinery and vehicles with high efficiency will significantly reduce CO_2 emission. It has been acknowledged that the major source of rising CO_2 emission can be traced to cars and trucks [3]. This environmental problem continues to escalate with the increasing demand for transportation which leads to a heightening of the greenhouse effect. Studies revealed that when it comes to transportation, passenger cars are responsible for 45% of total energy use and emissions [4]. The most fundamental part of a car system is the internal combustion engine which converts chemical energy into mechanical energy. The potential energy is generated by the internal combustion engine during the process of fuel burning. This energy is then converted into mechanical power which moves the car. However, part of the energy is diverted towards overcoming the adherent friction in the car system. Friction in the engine and transmission system contributes to about 17% of total energy losses in areas such as the piston assembly, the valve train, and the bearings and seals as reported in [5].

Friction behavior is dependent on whether the lubrication involved is boundary lubrication, mixed lubrication or hydrodynamic lubrication as illustrated by the recognized “Stribeck-curve” shown in Figure 1.1 [6]. However, tribological engine components will experience all three kinds of lubrication conditions because the speed of the engine is constantly changing during driving. Of the three, the one that matters most in the “Stribeck-curve” is boundary lubrication because of its potential for high friction and wear. Boundary lubrication occurs during starts, stops, shock-loads, direction changes, and when the vehicle is moving at a slow

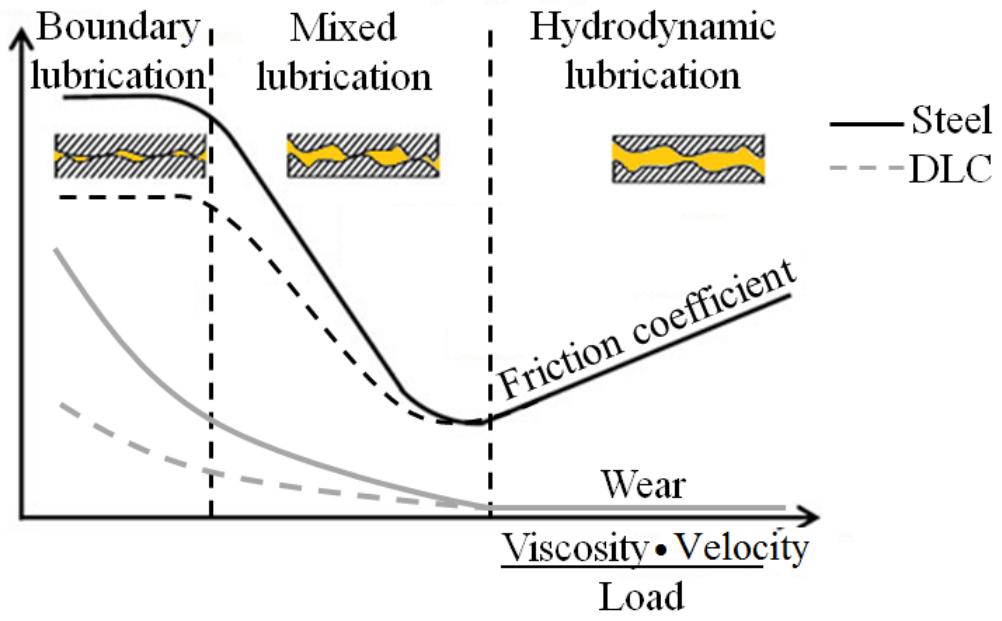

FIGURE 1.1: Possible improvements based on Stribeck diagram by DLC coating application.[6]

to intermediate speed. This can be attributed to the almost complete absence of an oil film between two contact surfaces. The topmost surfaces fully contact each other and the sliding or rolling motion results in high friction. High friction leads to high fuel consumption because the system needs more power to overcome the resistance. At the same time, high friction also causes the component to undergo more wear which culminates in a reduction of its lifespan.

Figure 1.2 shows the number of cycles to failure for material combinations employed for a friction test under boundary lubrication conditions [7]. The combination of DLC-steel displays a significantly longer lifespan of the component compared to a steel-steel and DLC-DLC combination. This result indicates that hard coating can improve the tribological properties of a component in terms of friction coefficient and wear as depicted in Figure 1.1. Tribologists are challenged to come up with a suitable coating material that can improve tribological behavior in terms of low friction and high wear resistance under specific conditions.

Industrial applications that involve tribological components include internal combustion engines for automobiles, material processing, gas turbine engines, rail transportation etc. The coating material selected for a particular application depends on the device and its operating conditions as well as the required performance and lifespan of the component [8]. Some examples on the use of coating

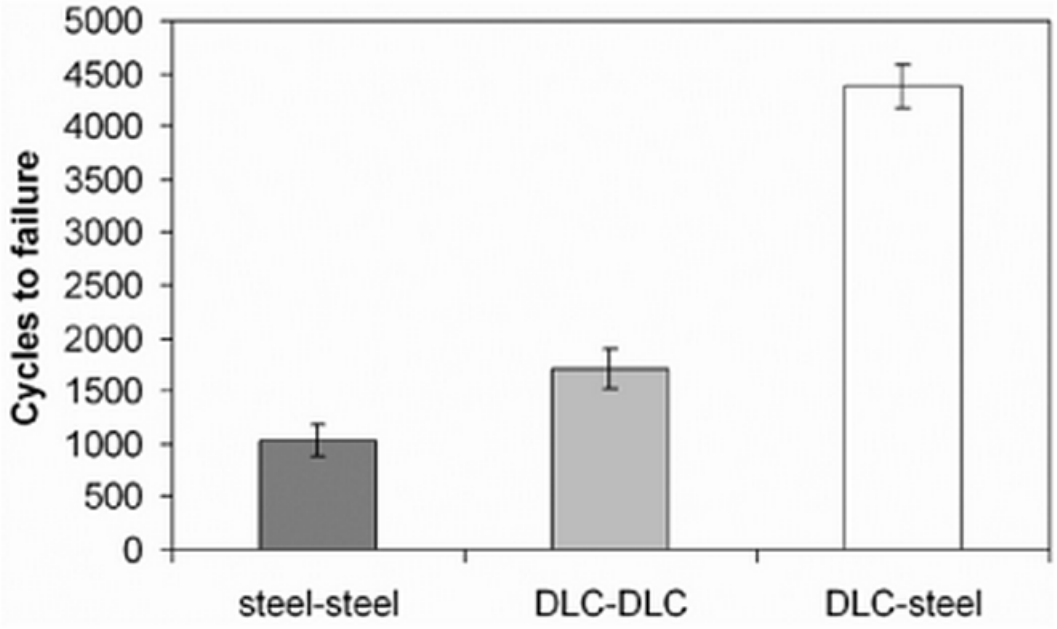

FIGURE 1.2: Cycles to failure for combination of steel-steel, DLC-DLC and DLC-steel under boundary lubrication condition.[7]

technology for increasing the tribological performance of internal combustion engines for automotive applications are shown in Figure 1.3 [9]. Tribological components will experience different contact conditions depending on their application. These conditions include contact stress at normal load, sliding abrasion, impact, surface fatigue, fretting and chemical dissolution. Table 1.1 shows the guideline for coating selection which depends on dominating contact conditions [10].

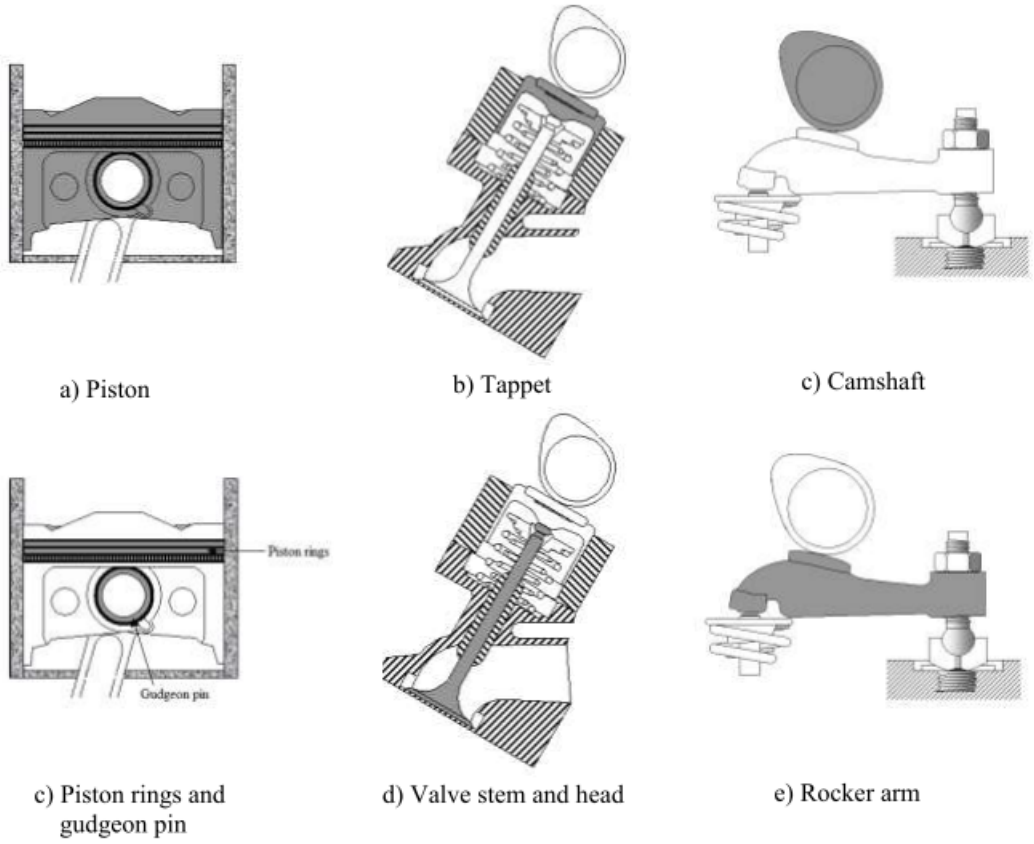

FIGURE 1.3: Components that can be coated with DLC for use in an automotive engine.[9]

TABLE 1.1: Guideline for coating selection.[10]

Contact type	Dominating contact condition	Required surface properties	Recomended coatings
Sliding	Low friction sliding Mild wear	Low shear strength at surface to layer Good load support	DLC, MoS_2, diamond
Abrasion	(a) Third-particle indentations	(a)Good-microtoughness and load support	TiN, TiAlN, TiC, Al_2O_3, CrN
	(b) Two-body ploughing	(b) High hardness to resist plastic deformation	
Impact	Concentrated impacting stress wave Abrasive wear	Good macrotoughness Good elasticity	Multilayer
Fatique	Continuous large stress waves	Good macrotoughness, Good load support	TiN, DLC Multilayer
Fretting	High-frequency large stress wave, Wear debris in contact continuously	Good elasticity, Low shear strength surface layer, Not producing hard wear debris	MoS_2, Cu-Ni-In, Multilayer
Chemical dissolution	High temperature	Non-soluble, Thermally conductive	TiN, TiAlN, TiC, WC, CrAlN, DLC, diamond
Lubricated sliding	Coating giving load support for lubricant film and acting as emergency layer	Interaction with lubricant additives, Texturing to support lubricant prevalence	DLC, TiN, TiC,CrN

1.3 Carbon coatings

Carbon is a unique material which can provide high hardness and good thermal conductivity in the form of a diamond, as well as softness and high lubricity in the form of graphite. Carbon exists in many forms in carbon-based allotropes. These forms include white carbon (ceraphite), nanotubes, buckyballs, other fullerenes, carbon-carbon composites, glassy carbons, and carbon nanofibres. Diamond-like carbon (DLC), carbon nitride, and boron nitride are a few examples of thin coating technology in which carbon, widely used in engineering technology, is the key element. Carbon is the preferred choice due to its outstanding tribological properties which contribute towards the reduction of friction and wear.

Carbon coatings can have different mechanical properties because they consist of sp^3, sp^2 and sp^1 as shown in Figure 1.4 [11]. These combinations can provide a great variety of crystalline and disordered structures. A diamond consists of a sp^3 configuration where four carbon atoms bond with each other to build a tetrahedral structure which in turn makes a strong σ bond to an adjacent atom. These structures provide high mechanical hardness, chemical and electrochemical inertness, and a wide band gap. In the sp^2 configuration, as in graphite, the three of four valence electrons enter trigonally directed sp^2 orbitals. These form σ bond in a plane. The fourth electron of the sp^2 atom enters a $p\pi$ orbital which lies normal to the σ bonding plane [11]. Graphite has a strong intra-layer σ bonding and a weak Van der Waals bonding between its layers [12]. As these layers can be separated and slide easily, the resulting friction is low [13, 14]. In the sp^1 configuration, two of the four valence electrons enter σ, each forming an σ bond directed along the $\pm x$-axis, and the other two electrons enter $p\pi$ orbitals in the y and z directions [11].

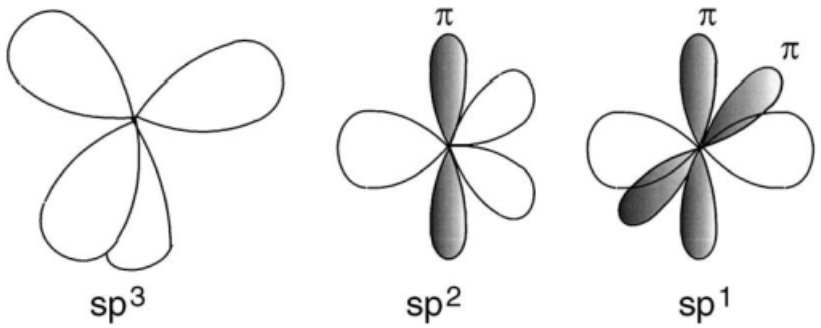

FIGURE 1.4: sp^3, sp^2 and sp^1 hybridised bonding.[11]

1.3.1 Diamond-like carbon (DLC)

DLCs are commonly used as a hard coating in many industrial applications due to their excellent tribological properties of low friction, high wear resistance, and chemical inertness.

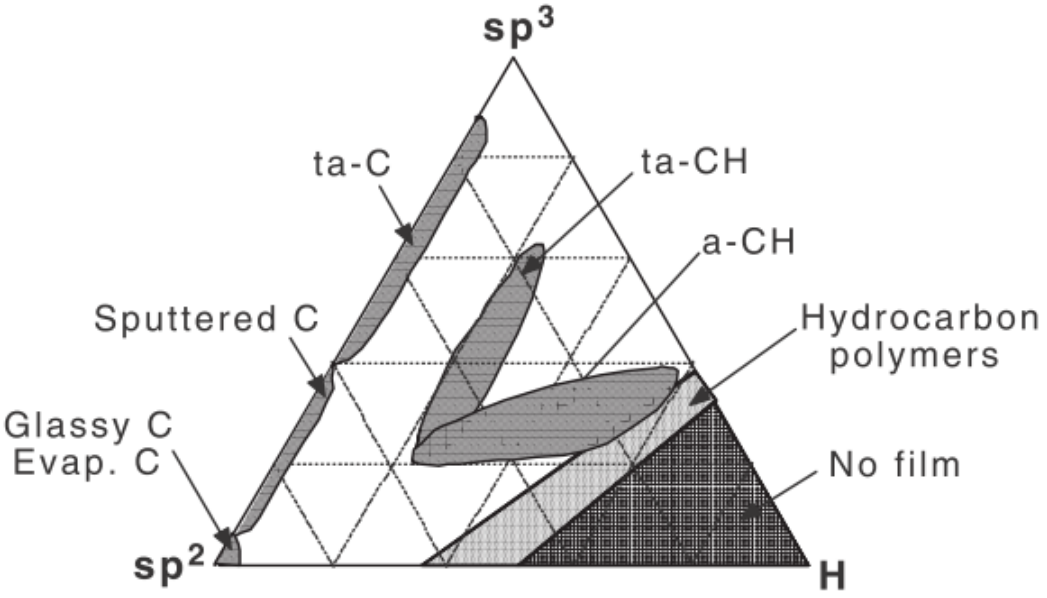

FIGURE 1.5: Ternary phase diagram for various DLC films with respect to their sp^2, sp^3 and hydrogen contents.[15]

Ferrari and Robertson studied the different types of DLCs using spectroscopic techniques to define their structure and chemical content. Figure 1.5 shows the ternary phase diagram by dividing various DLCs into different regions based on the fraction of sp^3 or sp^2 and hydrogen content [15].

Generally, the mechanical and tribological properties of DLCs depend on the sp^3/sp^2 ratio. However, the additional dopant material such as silicon, hydrogen, and metal/carbide, can also contribute different tribological properties to the DLC coating. Examples of diamond-like carbon are hydrogen-free amorphous carbon (a-C), hydrogenated GLC (a-C: H), tetrahedral amorphous carbon (ta-C) and hydrogenated tetrahedral amorphous carbon (ta-C: H). The other types of DLC which contain the dopant elements silicon and metal/carbide will be termed Si-DLC and Me-DLC respectively. Hydrogenated DLC coatings are generally soft with low internal stress. Thus, with good adhesion, it is possible to apply thicker film on the substrate [16]. However, hydrogen-free DLC coatings have a high degree of hardness and consequently high internal stress. As such, it is difficult to

deposit thicker hydrogen-free DLC. Generally, the thickness of hydrogen-free DLC is limited to 1 μm [11].

There are two types of deposition techniques commonly used for deposition of DLC coatings and these are Plasma Vapour Deposition (PVD) and Chemical Vapour Deposition (CVD). The PVD procedure involves atomistic deposition processes, in which material is vaporized from a solid or liquid state in the form of atoms or molecules, and then transported in the form of a vapour through a vacuum or a low pressure gaseous (or plasma) environment to the substrate where it condenses. Typically, PVD processes are used to deposit films with thickness in the range of a few nanometres to thousands of nanometres. Typical PVD deposition rates are 10-100$\mathring{A}$ (1-10 nanometers) per second [17]. There are several types of PVD coating techniques such as vacuum evaporation, sputter deposition (in a plasma environment or in a vacuum), ion plating and Ion Beam Assisted Deposition (IBAD).

Thermal Chemical Vapour Deposition (CVD) is the deposition of atoms or molecules by substantial temperature reduction or decomposition of a chemical vapour precursor which contains the material to be deposited. Deposition at a low temperature is facilitated by the introduction of plasmas into CVD reactors. The plasmas are typically generated by radio-frequency (rf) techniques and the process is called plasma-enhanced CVD (PE-CVD) [17].

The tribological behavior of DLC films differ according to their individual properties. Other factors that can significantly influence the tribological performance of DLC films are test conditions and the environment. The result from a previous study showed that the friction coefficient for various DLCs and test conditions vary widely in a range of 0.001-0.7 [18]. With regard to hardness, the hydrogenated DLCs are generally softer than hydrogen-free DLCs. Table 1.2 displays a few examples of the mechanical properties of various carbon films employing different deposition methods. Soft DLCs scratch easily while DLCs with high hardness possess high wear resistance properties with generally low wear rates of 10^{-11}mm^{3}N^{-1}m^{-1}.

TABLE 1.2: Mechanical properties of various carbon films employing different deposition methods.

Film	Deposition method	H (GPa)	Thickness (nm)
a-c:H [19]	PECVD	14	1140
		18	550
ta-C [20]	FCVA	80	76
ta-C [15]	PLD	27	120
a-C [21]	Sputtering	39	29
		42	46
		85	38

1.3.2 Carbon nitride (CNx)

CNx is also carbon coating material that has very good tribological properties like DLC. It is expected if the CNx can be harder than diamond if the CNx possess the ideal structure of β-C_3N_4 [22, 23]. Table 1.3 displays a few examples of the mechanical properties of amorphous CNx (a-CNX) films employing different deposition methods.

TABLE 1.3: Mechanical properties of CNx films by different deposited method.

Film	Deposition method	H (GPa)	Thickness (nm)
a-CNx [24]	MS	5.6	280
a-CNx [25]	FCVA	65 (high N %)	100
		40 (low N %)	100
a-CNx [26]	IBAD	25	1000

1.3.3 Friction mechanism of carbon coatings

The frictional behavior of carbon coatings can be influenced by intrinsic factors and extrinsic factors. Intrinsic factors come into play when the influence of friction behavior comes from the properties of the coating material itself. These include sp^3 and sp^2 content, the amount of hydrogen present, the doping material involved, and their bonding structure. The influence of frictional behavior from external sources such as chemical reaction and the physical and mechanical interaction during moving contact between two surfaces are defined as extrinsic factors. Both factors play significant roles in the friction and wear mechanisms of carbon coatings.

The effects of physical roughness on DLCs containing dopants like tungsten (a-C:W) and chromium (a-C:Cr) were examined using the ball-on-disk test. The friction coefficient rose from 0.1 to 0.7 with increasing surface roughness R_q of 7 to 390 nm respectively. The friction coefficient was closely related to the surface roughness of the coating as higher roughness contributed to a higher friction coefficient. The higher friction for rougher surfaces could be due to the oxidized particles of coating material filled the scratches. Shearing the oxidized particles

causes a higher friction. It was found that the wear rate for the a-C:W is not dependent on surface roughness. However, the a-C:Cr coating displayed a different behavior with the surface roughness influencing the wear rate [27].

The environmental effect on friction and wear behavior of DLCs was evaluated under four conditions. These conditions were dry air, O_2, N_2 and vacuum. The results revealed that the environment has a significant influence on friction and wear behavior. The N_2 environment exhibited the lowest friction coefficient of 0.06 and a low wear rate $2.2\times10^{-9}mm^3N^{-1}m^{-1}$. The highest friction coefficient of 0.17 was attributed to the vacuum environment, and the lowest wear resistance of $5.2\times10^{-9}mm^3N^{-1}m^{-1}$ to the O_2 environment [28]. The importance of hydrogen content in DLC films was investigated in an open air and a dry N_2 environment. t was suggested that the low friction mechanism of hydrogenated DLC films is due to the passivation of the dangling surface bonds of carbon atoms by hydrogen [29]. Another study reported that the formation of friction layers at the topmost contact surface of DLCs influences the friction behavior. The generation of friction layers was affected by the testing environment [30].

DLC is hybridized structure that containing sp^3 and sp^2. The graphitization occurred during friction when the sp^3 structure converted into the sp^2 structure due to a friction-induced graphitization mechanism [31–33]. The transfer layer formed on a counterface through the graphitization process provides low shear strength between hexagonal planes in the graphite structure allowing for the possibility of reducing friction to 0.02 [34, 35].

An investigation on the friction properties of DLC/DLC contacts in base oil using 12 different types of DLCs such as a-C:H:W, Si-DLC, ta-C and a-C:H with different mechanical properties was carried out by Vengudusamy et al. They found that the friction properties in this situation depended on the DLC type. The lowest friction of 0.05 was exhibited by ta-C in a boundary lubrication condition. The low friction mechanism in the boundary lubrication was attributed to surface graphitization [36]. The effect of temperature on the DLC performance in base oil was studied by Kalin et al. The lowest friction coefficient was achieved at a high temperature of 150 °C. The Raman analysis clearly showed that graphitization provides a slippery surface and this condition contributes to low friction levels [37].

Nitrogenated DLC or Carbon Nitride (CNx) is widely used as a coating material

in magnetic hard disk applications due to its excellent tribological properties [38–40]. Intensive studies were conducted on these properties in the environments of a vacuum, Ar, N_2, CO_2, O_2 and air against the counter material of Si_3N_4. It emerged that the N_2 environment had a significant effect on friction coefficient with a reading of below 0.01. Blowing dry N_2 gas directly onto the contact interface in an air environment effectively reduced the friction coefficient to about 0.017 [41]. The low friction mechanism was analyzed using an Auger Electron Spectroscopy (AES) and an X-ray Photoelectron Spectroscopy (XPS) where the desorption of N_2 atoms from the top layers of coating led to the CNx structure transforming into a graphite-like structure. This provides a slippery surface that reduces the friction coefficient [26].

1.4 Purpose of this study

Carbonaceous hard coatings can provide low friction either in a dry condition or boundary lubrication in oil. After the friction test, an ex-situ observation in dry conditions showed that the transfer layer could easily found on the counter part's surface. This transfer layer was believed to be responsible for the low friction, with the transfer layer acting as a third body. The transfer layer separated the direct contact between the two surfaces and controlled the friction's behavior. Therefore, in-situ observation was needed to observe the formation of a transfer layer that influenced the friction behavior under dry conditions. However, no reports exist about in-situ observations of the formation of a transfer layer during friction testing under dry conditions.

Consequently, we developed a new experimental apparatus that was based on a ball-on-disc tribometer. We used a transparent sapphire hemisphere ball (α-Al_2O_3) as a counter part for friction testing against a CNx coated disc. With the help of an optical microscope and a CCD camera, images of the formation of a transfer layer were recorded during the friction test. Information from these images was used to determine the thickness of the contact area and the transfer layer. It was possible that the area of the transfer layer could have changed the contact pressure leading to the material properties of the transfer layer. Meanwhile, an ex-situ observation was performed to analyze the transfer layer, wear track, and wear debris, using Raman spectroscopy, SEM, AFM and AES.

However, the transfer layer could not be found on the counter part's surface using ex-situ observation after friction, in the case of oil lubrication. The oil would not allow the adhesive bonding of the transfer layer to the counterpart. However, after ex-situ surface analysis of the carbonaceous coating worn area, using Raman analysis after the friction test, the results showed that the carbonaceous hard coating structure had changed and was then known as the transformed layer. This change was due to graphitization; where the structure of sp^3 converted to sp^2 . Sp^2 rich topmost surface could provide a low shear strength that resulted from the low friction. We believe that due to a lack of oil in boundary lubrication friction test, the properties of the carbonaceous hard coating topmost surface (transformed layer) could control the friction's behavior. It is therefore very important to investigate the mechanical properties of the topmost contact interface. Further analysis of

the transformed layer, in terms of its thickness and hardness, could provide more information about the mechanism of low friction in oil under boundary lubrication.

We used three different hardness's of DLC that were coated on sliding bearings made of steel (SUJ2) as a substrate and a S55C steel disc as a counterpart. Boundary lubrication friction tests were conducted using a pin-on-disc tribometer. An additive-free mineral based oil was used as a lubricant to avoid the influence of any additives on both the friction and wear behaviors of DLC. After the friction tests, the worn area on the DLC coating was examined using Raman analysis, reflectance spectroscopy, and AFM scratch testing. Raman analysis was used during the friction tests to verify the graphitization process that generated the transformed layer at the topmost sliding interface. The thickness of the transformed layer was measured using reflectance spectroscopy. An AFM scratch test was used to determine the hardness of the transformed layer.

From the experimental results of the friction test in dry conditions, we attempted to relate the significant role of the transfer layer formation at the contact sliding interface to the friction behavior of the CNx coating under blowing dry Ar.

For the friction test in boundary oil lubrication conditions, the generation of a thin transformed layer at the topmost sliding interface of the DLC coating could be the main factor for low friction. We investigated the nano characteristics of transformed layer in term of its thickness and hardness. Then, we attempted to propose a friction model of low friction under boundary lubrication conditions in an additive-free mineral based oil.

In summary, the objectives of this study were as follows:

1. To clarify the effect of the CNx transfer layer area on the mating sapphire hemisphere on the friction properties under blowing dry Ar.
2. To clarify the effect of as-deposited hardness of DLC on friction and wear after friction test under boundary lubrication conditions in an additive-free mineral based oil.
3. To clarify the effect of the transformed layer's thickness on the tribological properties of the sliding bearing under boundary lubrication conditions in an additive-free mineral based oil.
4. To clarify the effect of the transformed layer's hardness on friction under boundary lubrication conditions in an additive-free mineral based oil.
5. To propose friction map and friction model for low friction of carbonaceous hard coatings.

1.5 Outline of dissertation

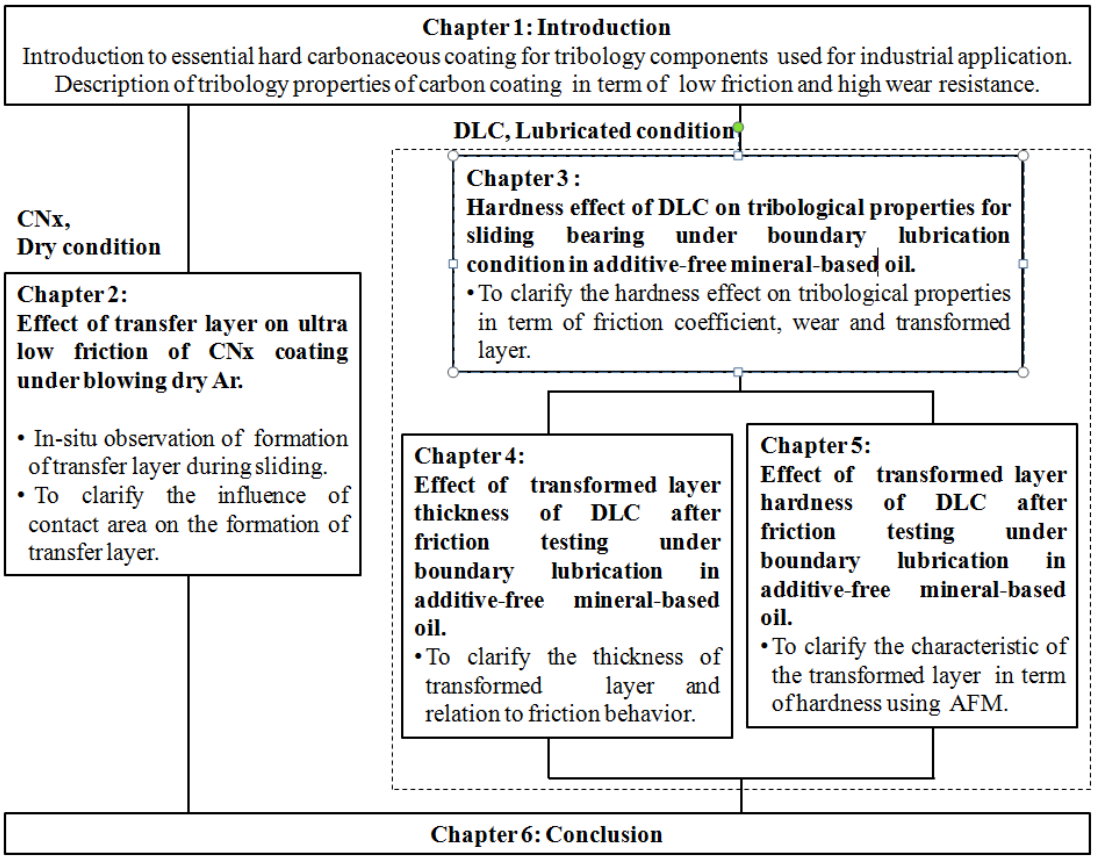

FIGURE 1.6: Outline of dissertation.

Chapter 2

Effect of transfer layer on ultra low friction of CNx coating under blowing dry Ar

2.1 Introduction

Carbonaceous hard coatings are used because those have good tribological properties, such as low friction, high hardness, and high wear resistance. Carbon Nitride (CNx) is expected as excellent materials with excellent tribological properties. CNx is a hybridized material that is composed of sp^3 and sp^2 Carbon-Nitrogen (C-N) bonding. CNx showed ultra low friction that is less than 0.01 of friction coefficient in dry Nitrogen gas [41]. The authors has tried to know the ultra low friction mechanism of CNx on the basis of surface analysis with Raman spectroscopy, XPS and AES because ultra low friction was observed after a number of repeated sliding in dry Nitrogen. As a result, we proposed the ultra low friction mechanism as the formation of thin graphite like layer that thickness is about 20 nm on the surface of CNx, the formation of transfer layer of graphite like wear particles and smoothing of friction surface [42]. However we have done the ex-observation after sliding test. Therefore we do not know the specific effect of the formation of transfer layer on the mating surface. In order to overcome this issue, we developed a friction tester with in-situ observation of transfer layer under sliding against a sapphire hemisphere in different species of gas such as Argon (Ar), Nitrogen (N_2) and ambient air.

In the case of ultra low friction under dry nitrogen and dry Argon, friction coefficient decreased with the increasing of the thickness of transfer layer. On the other hand, friction coefficient did not decrease with the increasing of the thickness of transfer layer in the case under ambient gas [43]. These results show the transfer layer from CNx to mating surface has the essential role in the ultra low friction mechanism of CNx.

In this chapter, we investigated the effect of the area of transfer layer on mating sapphire hemisphere on friction properties under blowing Ar gas. There is a possibility that the area of transfer layer can change contact pressure lead to the material properties of transfer layer. In-situ observation of transfer layer formation, and attachment at the sliding contact point, was observed using an optical microscope. Images were captured using a CCD camera. Meanwhile, an ex-situ observation was performed to analyze the transfer layer, wear track and wear debris, using Raman spectroscopy, SEM, AFM, and AES.

2.2 Experimental procedure

2.2.1 Test specimen

The Si(100) wafer disk was coated with a 100 μm thickness of CNx using Ion Beam Assisted Deposition (IBAD) method in this study. Further details of coating procedure can be seen in [26]. The nitrogen content in the CNx is about 10 %. A CNx surface roughness of 0.72 nmRa was measured using AFM. The hardness of the CNx coating was measured at approximately 25.2 GPa using nano indenter, with a maximum indentation load of 20 μN. A transparent sapphire hemisphere, with a radius of 4 mm, a hardness of about 35 GPa, and surface roughness of 30 nmRa, was chosen as a counter face.

2.2.2 Friction test

Figure 2.1 shows a ball-on-disk equipment with in-situ observation of contact point during sliding under blowing Ar gas. An electric motor was used to rotate the CNx coating, which was fixed on a rotatable disk holder, and the sapphire hemisphere was used as a stationary counter face at the upper side. The friction test was performed using the ball-on-disk tribometer, with a sliding speed of 83.8 mm/s, and a sliding track of 6 mm. The experiment was performed under ambient conditions, with room a temperature of 24 °C and a relative humidity of about 26 %. Dry Ar, with a 99.9999 % purity, was used in this experiment. Dry Ar came directly from the gas cylinder to the contact point between the CNx coating and the sapphire hemisphere, with a volume rate of 5 l/min throughout the sliding test. The O_2 content and humidity were measured at sliding interface using TORAY Oxygen Analyzer (LC-750) and Thermo Recorder (TR-72U) in order to clarify the impurities of blowing Ar. A normal load of 0.1 N was applied constantly to the sapphire hemisphere with a leaf spring. The initial mean Herztian's contact pressure was calculated at about 177 MPa, with a contact diameter of approximately 10 μm. The test's specimens were cleaned in an ultrasonic bath in acetone for 15 minutes before and after the friction test, in order to avoid any contamination on the specimen surface during testing and other analysis.

Transfer layer formation phenomena during contact sliding, which was generated by friction between the transparent sapphire hemisphere and the CNx coating,

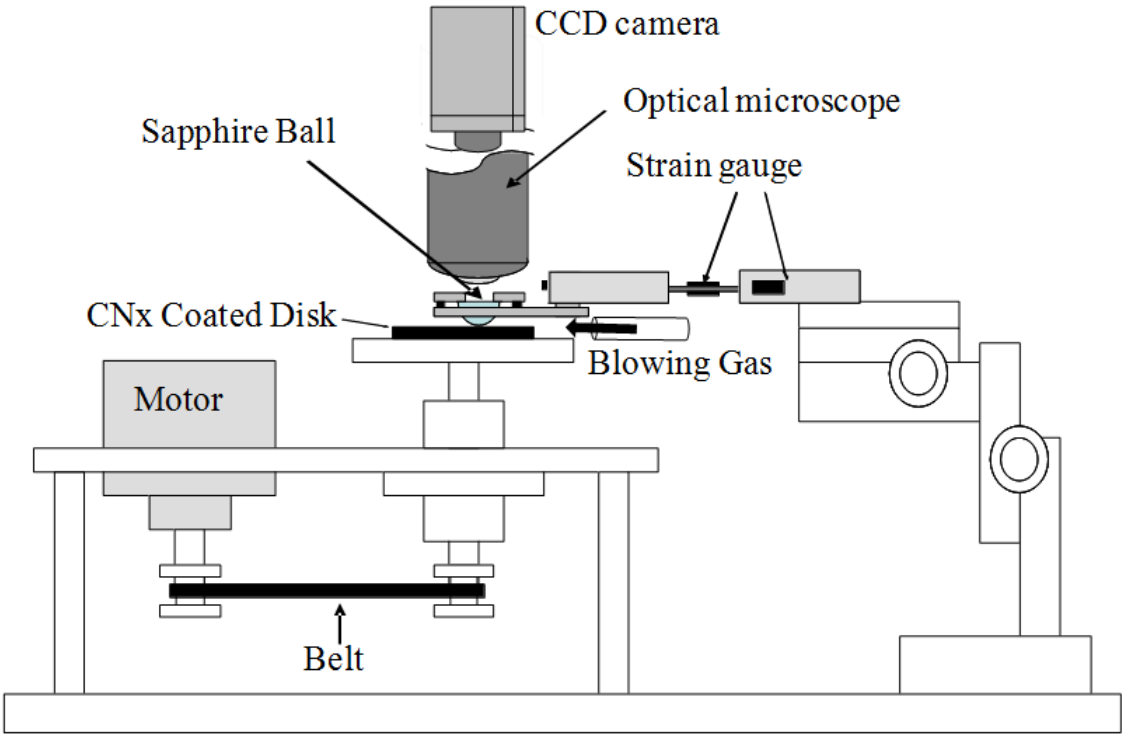

FIGURE 2.1: Test rig based on pin-on-disk method. Combination of optical microscope and CCD camera were used to observe the in-situ frictional behavior CNx coated disk against Sapphire hemisphere.

can be observed with optical microscope using CCD camera, through the sapphire hemisphere. Newton's ring can also be seen in the images and was used to estimate transfer layer thickness during the friction test. Pictures were taken every five cycles for 10,000 cycles.

2.2.3 Estimation of the thickness of transfer layer

The transfer layer thickness can be estimated by comparing the Newton's ring diameter images that were captured during the sliding test with an initial state image. The movement of Newton's ring can be observed during the sliding test. Inward movements of Newton's ring were caused by the elevation of the sapphire hemisphere, which corresponded to the increasing transfer layer thickness. The change of Newton's ring diameter during sliding test can be observed and measured from the images. The use of Newton's ring to quantify transfer layer thickness is given in [44, 45]. Pythagoras' theorem was used to estimate transfer layer thickness, as in Eqs. 2.1 and 2.2 and referring to the schematic illustration of transfer layer formation, as shown in Figure 2.2.

$$h = (X_2 + Z) - (X_1 + Z) \tag{2.1}$$

$$h = \sqrt{R^2 - {r_2}^2} - \sqrt{R^2 - {r_1}^2} \tag{2.2}$$

where h is transfer layer thickness; R is the radius of the sapphire hemisphere; Z is the height between the measured Newton's ring from the contact surface, $y_{1,2}$ are the height between the top of the sapphire hemisphere and the Newton's ring (*1*: before sliding, *2*: during sliding), $r_{1,2}$ are the estimated radius of Newton's ring (*1*: before sliding, *2*: during sliding).

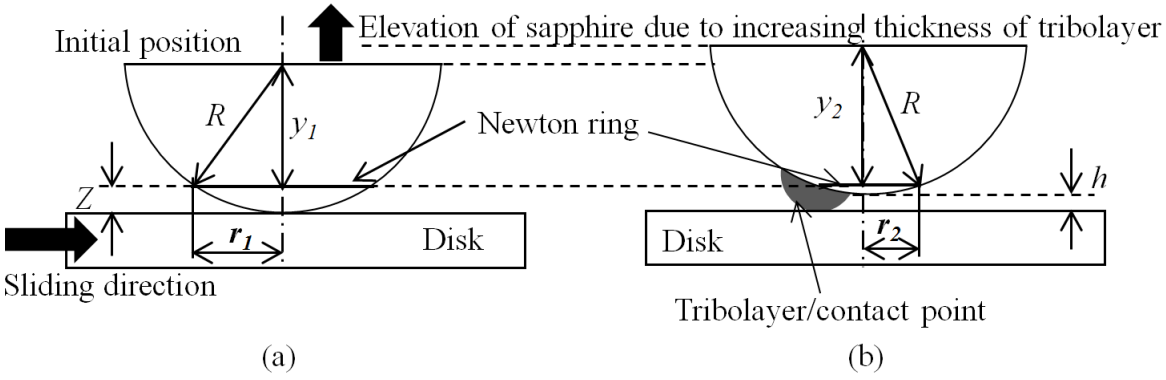

FIGURE 2.2: Schematic illustration ofrelationship between transfer layer and Newton's ring during sliding test for estimation of transfer layer thickness. (a) Initial state and (b) during sliding with the formation of transfer layer.

2.2.4 Raman and AES analyses

The Raman spectra was obtained using a Jasco Laser Raman spectrophotometer NRS-1000 equipped with a second harmonic Nd:YAG laser with a maximum laser power and wavelength of 10 mW and 532 nm, respectively. However, only 1% of the maximum power was applicable for the measurement without burning the surface and also to avoid the influence of the substrate underneath. The AES (ULVAC PHI-650) was used to obtain the depth profiles of chemical composition of test specimen with beam energy of 5 kV and a probe current of 100 nA. Before the measurement, the test specimen surface was cleaned by ion sputtering with a sputtering energy and a probe current of 3 kV and 25 mA, respectively.

2.3 Results and discussion

2.3.1 Effect of the thickness of transfer layer on friction coefficient

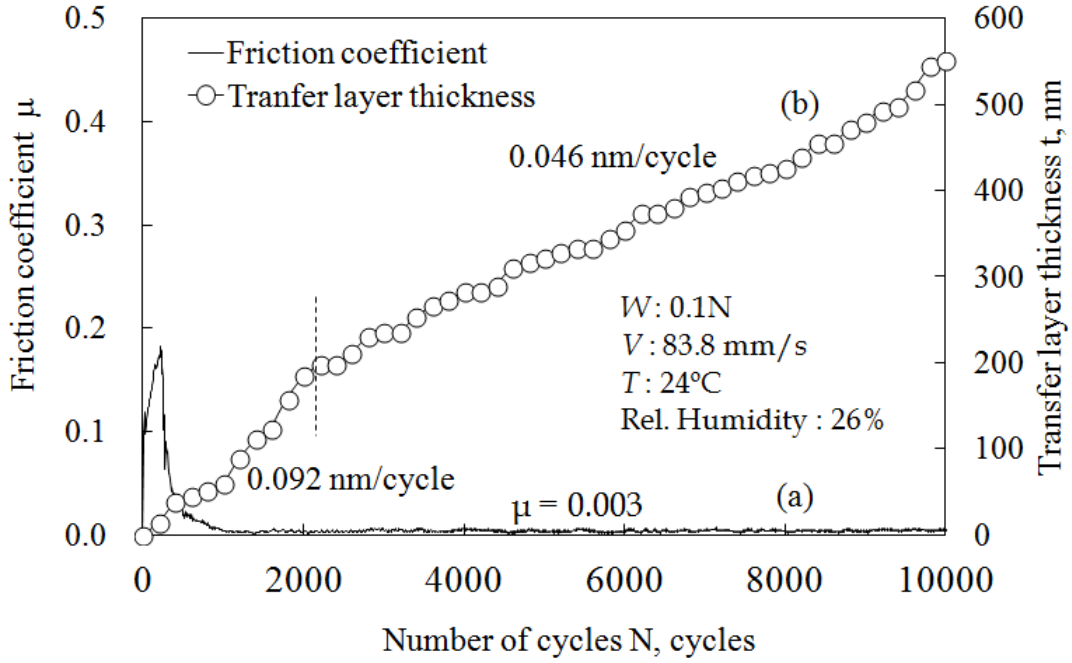

FIGURE 2.3: (a) The frictional behavior of CNx coating against Sapphire hemisphere as a function of sliding cycles and (b) Transfer layer thickness as a function of sliding cycles.

Figure 2.3 shows the coefficient of CNx coating against the sapphire hemisphere during the repeated sliding test under blowing dry Ar, as a function of the number of cycles. At approximately 300 cycles, the friction coefficient increased from 0.1 to 0.18. Then at 1000 cycles, the friction coefficient decreased drastically from 0.18 to 0.003. After a short running-in period, the friction coefficient was consistently ultra low until 10,000 cycles. Figure 2.4 shows images of transfer layer through a transparent sapphire hemisphere in each sliding cycles from 0 to 10,000 cycles.

The other experimental results show that the friction coefficient increased suddenly, due to a detachment of the transfer layer from the contact surface, as shown in Figure 2.5. Later, the transfer layer built-up again at the contact point, and the friction coefficient decreased slowly until it achieved a super low friction again. The images in Figure 2.4 show that the initial real contact point was at the centre (zero cycle), but later it deviated to the front of the sliding direction (400

cycles), where it remained for the rest of the sliding test, as illustrated in Figure 2.2.

Figure 2.4 shows the microscope images of Newton's rings that formed around the contact point of the two surfaces (i.e., the sapphire hemisphere and the CNx coating) with different diameters and light intensities. The Newton's rings were formed due to interference between the light waves reflected from the top and bottom surfaces.

The Newton's ring's diameters were measured and used to estimate transfer layer thickness using Eq. 2.2 from Pythagoras' theorem. The Newton's ring becomes smaller due to the elevation of the sapphire hemisphere corresponding to the formation of a transfer layer at the contact point, as illustrated in Figure 2.2. The results show that the friction coefficient decreased whilst the transfer layer thickness increased. See Figure 2.3(a). In addition, the higher rate of transfer layer generation (about 0.092 nm/cycle) was seen from the beginning of sliding test during the running-in period until approximately 2000 cycles. Then, the transfer layer generation rate became lower (at about 0.046 nm/cycle) from 2000 cycles onwards, and the friction coefficient reached a super low friction of 0.003, where it remained until 10,000 cycles. An ultra low friction of 0.003 was achieved when the transfer layer thickness was around 60 nm after 1000 sliding cycles. The transfer layer thickness increased consistently to 550 nm at 10,000 cycles, whilst the friction coefficient kept constant at super low. The higher rate of transfer layer generation during the running-in period showed that more graphitization occurred then, than the steady state period. This result indicates that more wear debris was produced from sliding at the beginning, due to the direct surface contact between the sapphire hemisphere and the coating disk. The wear debris accumulated at the sliding contact and became a thin transfer layer through compaction. As the transfer layer became thicker, the wear rate of the CNx coating decreased because the transfer layer could act as a protective layer to reduce wear.

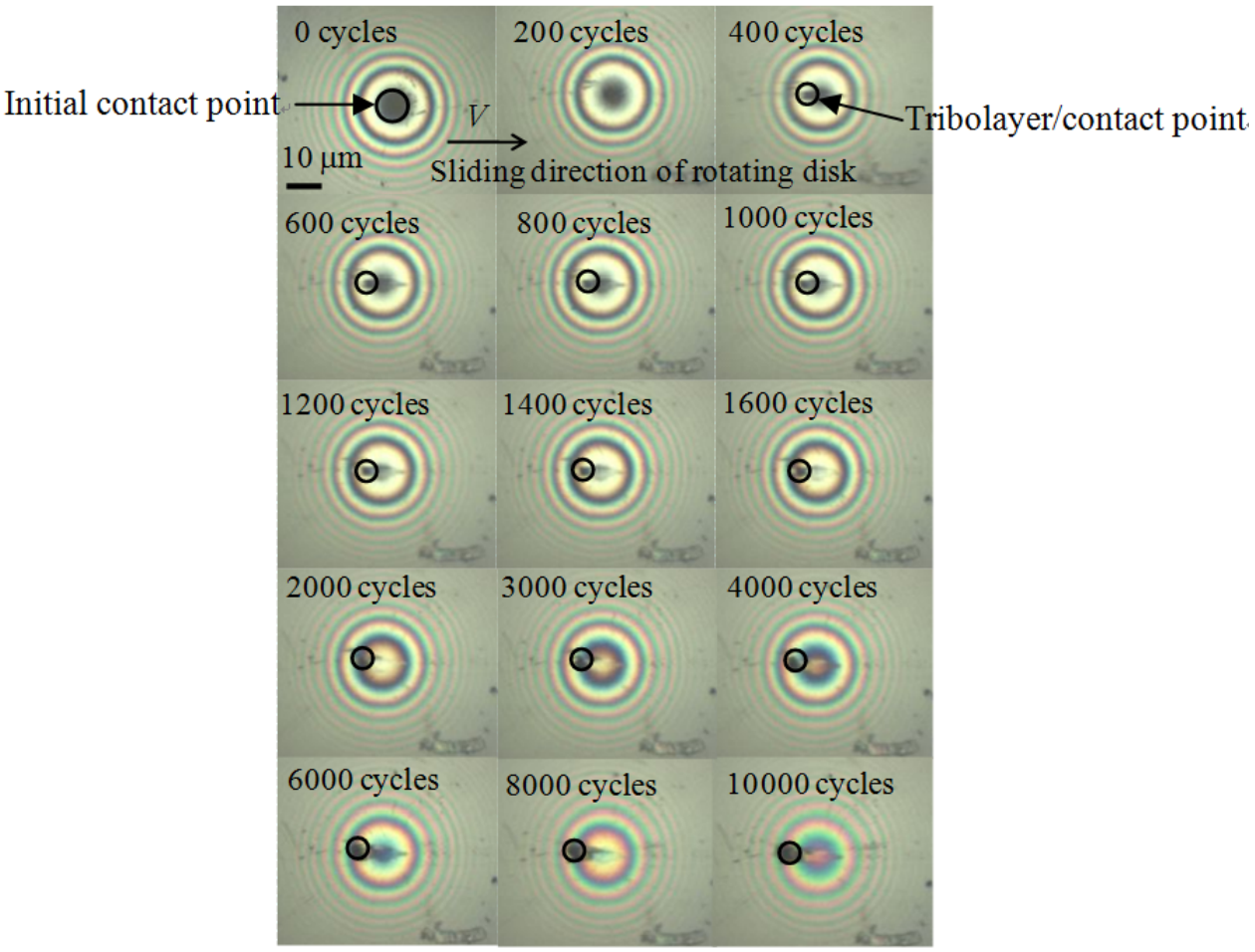

FIGURE 2.4: Microscopic images of Newton's ring and real contact area for estimation of transfer layer thickness and mean Hertzian's contact pressure respectively.

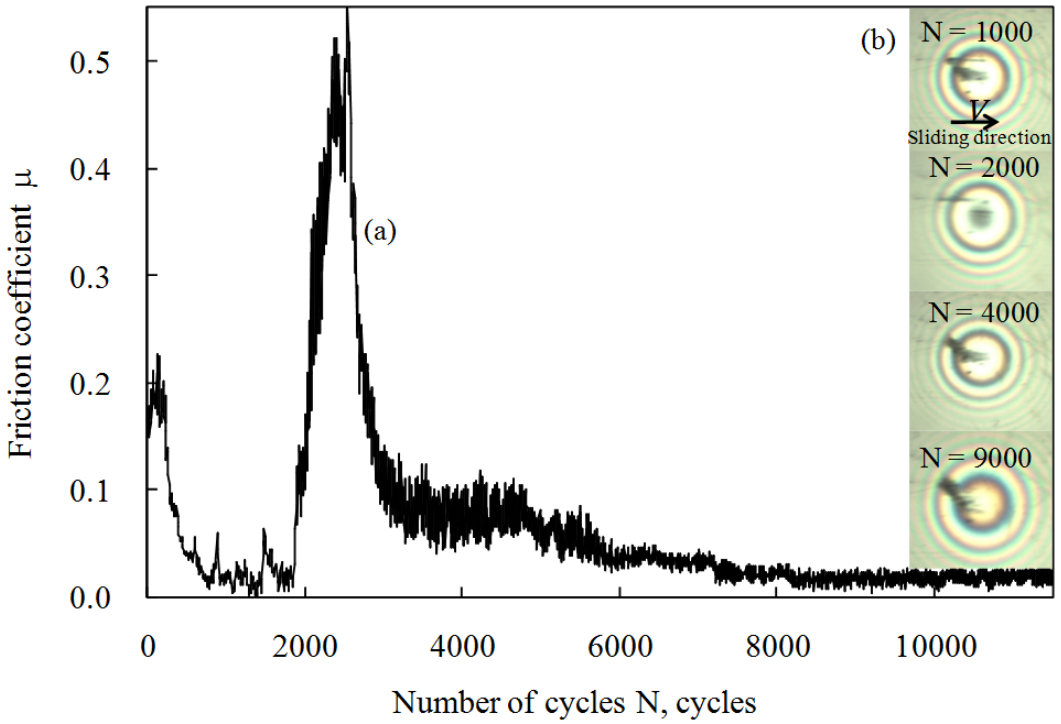

FIGURE 2.5: (a) Sudden increase of friction coefficient during sliding between CNx coatings against Sapphire hemisphere as a function of sliding cycles (b) Images of transfer layer and Newton's ring.

2.3.2 Effect of area of transfer layer and contact pressure on friction coefficient

As shown in Figure 2.4, the initial image of the dark circle at zero cycles shows the direct contact point between the sapphire hemisphere and the CNx coating. At the beginning of friction test, the contact between the sapphire hemisphere and the CNx coating forming the Hertzian's contact as shown in Figure 2.4 at 0 and 200 cycles. However, from 400 cycles of sliding rotation, transfer layer was generated, and the contact point moved from centre to the front side of the sliding direction. At this point, there was no more Hertzian's contact. The accumulation of wear debris at contact interface segregated the direct contact between sapphire hemisphere and CNx coating. The measured contact radius, decreased from 0 to 10000 cycles around 13 μm initially to 4 μm (10000 cycles). The changing contact radii were measured carefully from the captured images using CCD to be used later for the estimation of contact area, A. The measured radius of the Hertzian's contact point was 13 μm at initially state (i.e., zero cycles), which was confirmed by calculating the contact radius of 10 μm using Hertzian's contact mechanics; as per Eqs. 2.3 and 2.4 [46]. The different values, between measured and calculated Hertzian's contact point radii, are due to inaccurate measurements of the contact point using optical images. It is very difficult to obtain accurate value of Hertzian's contact radius by measurement because of the blurring of the contact edge as shown in Figure 2.4 (0 cycles). The difference between the measured contact point radius, r_c and the calculated Hertzian's contact radius, a was within a few micrometers, and are also reported elsewhere [45].

$$a = \left(\frac{3WR}{4E^*}\right)^{1/3} \tag{2.3}$$

where

$$\frac{1}{E^*} = \frac{1-{\upsilon_1}^2}{E_1} - \frac{1-{\upsilon_2}^2}{E_2} \tag{2.4}$$

Here, W is the applied load, R is the sapphire hemisphere's radius, E^* is the effective elastic modulus, υ_1 and υ_2 are the Poisson's ratio of the sapphire hemisphere and the CNx, respectively, and E_1 and E_2 are the Young's modulus of the sapphire hemisphere and the CNx, respectively. A measured contact point radius, r_c was used to calculate the mean pressure P_m using Eqs. 2.5 and 2.6.

$$P_m = \frac{W}{A} \tag{2.5}$$

where,F is the applied load, and A is the estimated contact area.

$$A = \pi {r_c}^2 \tag{2.6}$$

where, r_c is the measured contact radius.

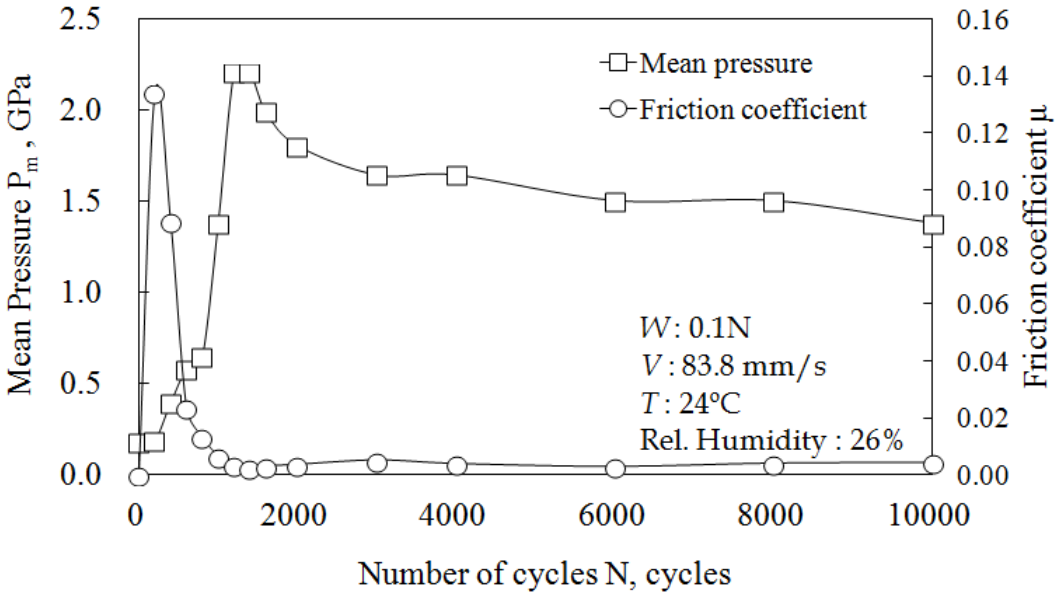

FIGURE 2.6: Relation between mean Hertzian's contact pressure and friction coefficient as a function of sliding cycles.

Figure 2.6 shows the relation between the estimated mean contact pressure and the friction coefficient, as a function of sliding cycles. The contact pressure increased drastically from 0.174 to 2.25 GPa, where the friction coefficient was shown to decrease to a super-low level of 0.003 until 10,000 cycles of rotation. Then, the

contact pressure decreased slowly from 2.25 to 1.5 GPa. The friction coefficient achieved a steady state condition at around 0.003, when the pressure was at a high value of around 1.5 GPa.

Another essential relation shown in this study is how the estimated mean Herztian's contact pressure affects the generation of the transfer layer as shown in Figure 2.7. It was observed that the thickness of transfer layer increase gradually, although the contact pressure slightly decrease after 2000 sliding cycle.

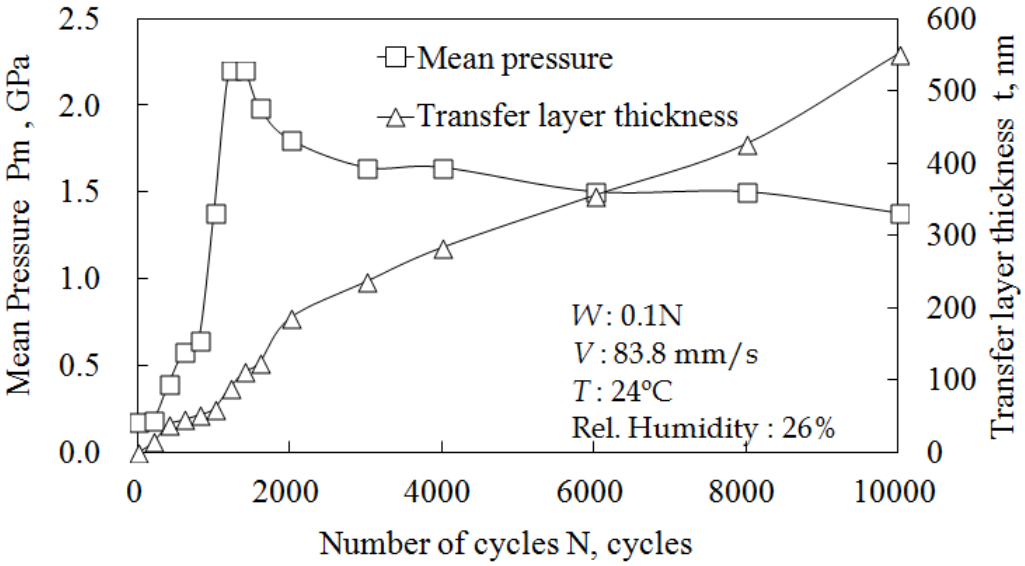

FIGURE 2.7: Relation between estimated mean Hertzian's constant pressure and transfer layer thickness as a function of sliding cycles.

2.3.3 Phase transition of CNx coating at sliding contact interfaces

CNx is a material with a combination of sp^3 and sp^2 carbon bonds, which the nitrogen substitutes into the sp^2-bonded ring to a saturation level of about one nitrogen to every three carbon atoms. This CNx structure provides good tribological properties, such as low friction, high hardness, and high wear resistance. CNx graphitization occurred when desorption of nitrogen atoms from the CNx matrix was caused by raising the annealing temperature. Generally, the transition temperature of CNx is about 200 °C, which corresponds to a sp^3-sp^2 transition temperature [47]. However, during sliding, the transition temperature can be decreased to a lower value, due to the high contact stress [48, 49]. The CNx transition

temperature can be calculated according to the Clapeyron law [50], with the functions of contact pressure and specific volume of low and high nitrogen contents of carbon nitride, as per Eq. 2.7.

$$T = T_c exp\left(\frac{-|\Delta v|}{L}\Delta p\right) \tag{2.7}$$

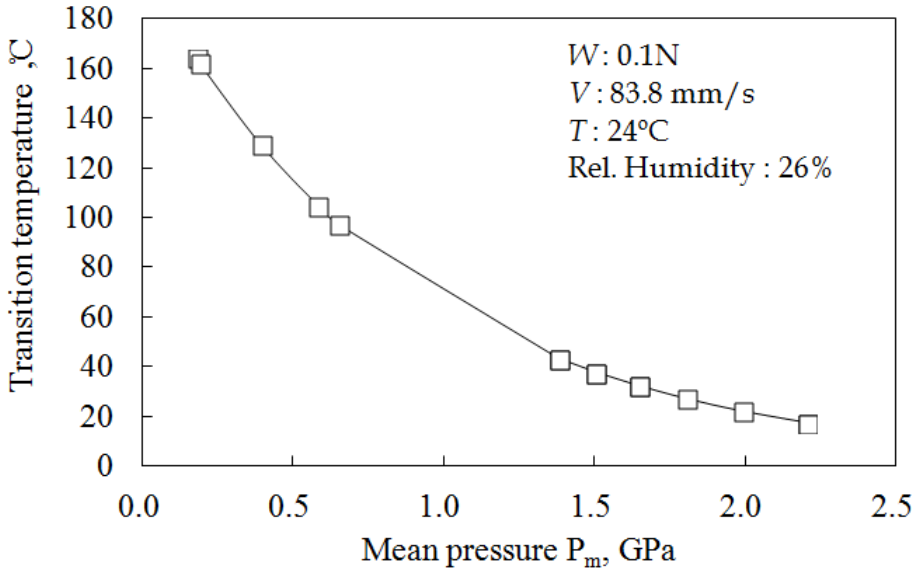

FIGURE 2.8: Calculated transition temperature of CNx coating as a function of Hertzian's contact pressure referring to Clapeyron law.

where T_c is the critical phase transition temperature of CNx (200 °C) [47], Δv is the difference between specific volume of low nitrogen content ($0.303{*}10^{-3}m^3kg^{-3}$) and high nitrogen content ($0.746 * 10^{-3}m^3kg^{-3}$) [21], Δp is the difference between Hertzian's contact pressure and atmospheric pressure. As explained previously, the contact area decreased throughout the sliding test, corresponding to increased contact pressure. Figure 2.8 shows that the phase transition temperature of CNx coatings decreased with an increase of Herztian's contact pressure at the sliding interface. Hence, a high contact pressure results in a lower transition temperature sp^3- sp^3 to as low as 20 °C. This explains that the graphitization process possibly occurred under high contact stress at room temperature, since the experiment was performed under room temperature (about 24 °C).

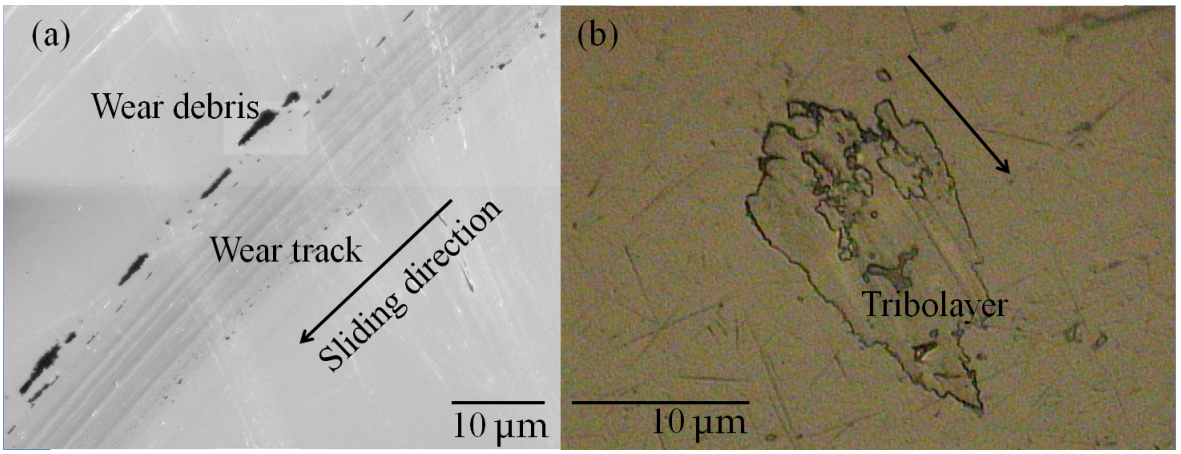

FIGURE 2.9: a) SEM observation of wear track and debris on CNx coating disk after sliding test.(b) Microscopic image of transfer layer on the sapphire hemisphere after sliding test.

2.3.4 Ex-observation of wear track with Optical microscope (OM), Raman spectroscopy and Auger Electron Spectroscopy (AES)

After the sliding test, the CNx coating and sapphire hemisphere was observed using SEM and an optical microscope. Figure 2.9(a) shows a picture of the compacted wear debris along the wear track on the CNx coating after the sliding test. No wear debris was found within the wear track because the wear debris was ejected outside of the wear track during the sliding. The generated transfer layer was transferred from the coating surface to the sapphire hemisphere's surface. The microscope image shows that the transfer layer is strongly adhered to the sapphire hemisphere, as shown in Figure 2.9(b).

Figure 2.10(a)-(d) show the Raman spectra of the as-deposited wear track, the transfer layer, and the wear debris, respectively. The Raman spectra shape, of the as-deposited of CNx, is comparable to other researcher's results [51]. The shape of Raman spectra on the wear track, after the sliding test, was the same as the as-deposited CNx; with the same Raman shift, G peak of 1576.5 1/cm. However, the Raman shifts of the G peak for both the wear debris and transfer layer show a different value of 1588.8 1/cm. This shifting G peak value, from a low to a higher frequency, means that transition of sp^3-sp^2 (also known graphitization) occurred during the sliding test [52].

The Raman shape of the wear debris and the transfer layer is comparable with pure graphite, as reported by other researchers [53]. This means that the graphitic material was removed from the CNx coating's wear track and accumulated as a transfer layer; which then adhered to the sapphire hemisphere and partially became wear debris.

Figure 2.11(a)-(c) show the results for Ar KLL, C KLL, N KLL, and O KLL peaks through AES analysis, between 150 and 550 eV on as-deposited CNx, wear track and wear debris, respectively. The kinetic energy of Ar KLL, C KLL, N KLL, and O KLL were approximately 220, 258, 374, and 510 eV, respectively. The intensity of the N KLL peaks on the wear debris is approximately zero. This means that there was almost no N content in the wear debris compared to the as-deposited CNx, and the wear track. This proves that desorption of N from the CNx coating during sliding was responsible for the graphitization process. Under high pressure stress, the C-N bonds tend to release their N content to become a more stable graphite-like structure [48, 50].

AES analysis does not detect the Ar content on the wear track or the debris after the sliding test. This means that the Ar gas, as an inert gas, was not involved in the tribochemical reaction with the dangling bonds [54]; which probably influenced the tribological performance. Oxygen molecules were not found on the coating surface, both before and after the sliding test. No oxidation process occurred on the coating surface before, during, or after the friction test, that influenced the results of the sliding test and the analysis.

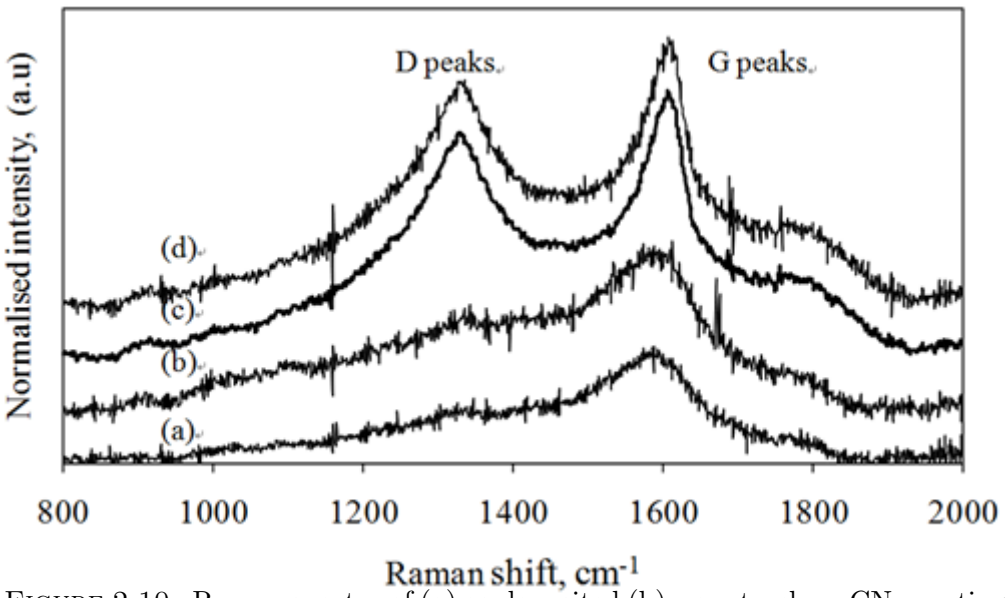

FIGURE 2.10: Raman spectra of (a) as-deposited (b) wear track on CNx coating (c) transfer layer on sapphire hemisphere and (d) wear debris on CNx coating.

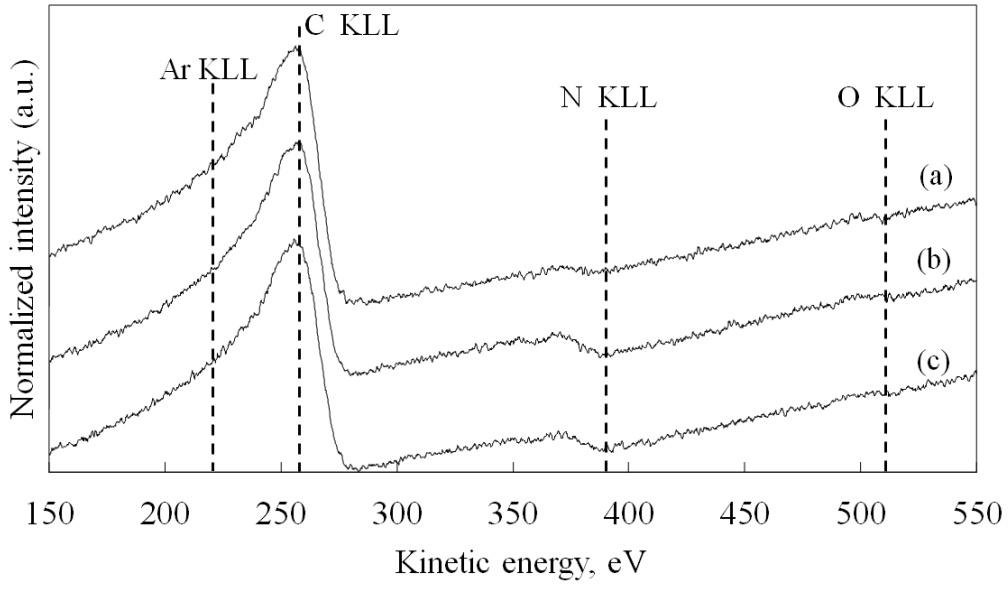

FIGURE 2.11: AES analysis for Ar, C, N and O content on CNx coating (a) as-deposited, (b) wear track and (c) wear debris.

2.3.5 Effect of transfer layer on ultra low friction of CNx coating

An ultra low friction level of 0.003 was observed during the sliding test, between the CNx coatings against the sapphire hemisphere, under blowing dry Ar gas directly onto the contact interface. In-situ observation confirmed that the generation of transfer layer at the contact point was responsible for reducing the friction coefficient to a super low level. It was also observed that the friction coefficient increased at the beginning of the friction test (up to 300 cycles), then the friction coefficient dropped to an ultra-low level of 0.18 to 0.003 at 1000 cycles. Sharp asperities that broke-off at the CNx coating's surface interface, which contributed to the nano particles, caused the increasing friction coefficient at the beginning of the sliding test.

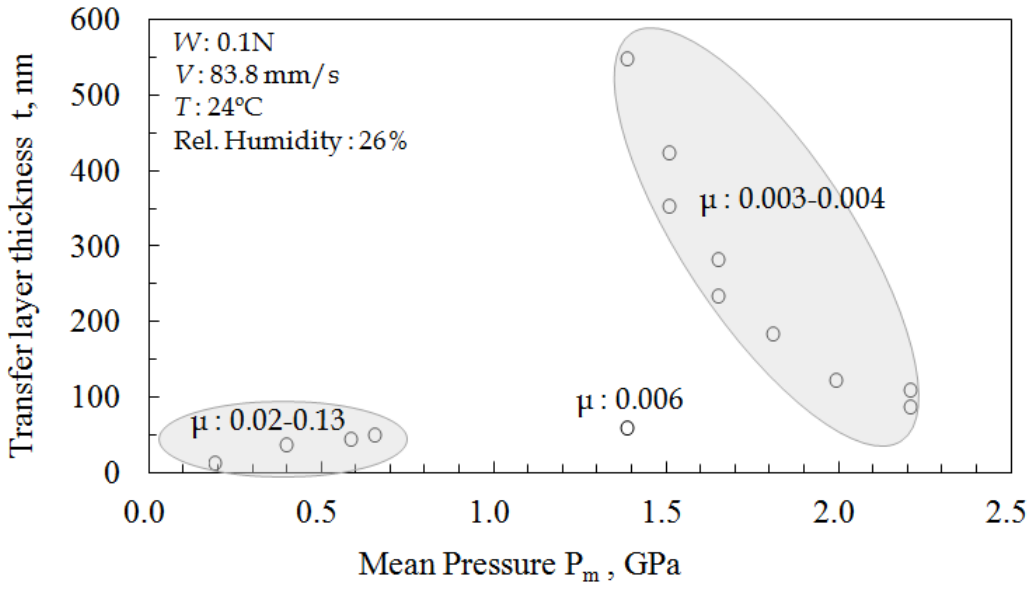

FIGURE 2.12: Relation between the thickness of transfer layer and contact pressure to friciton coefficient.

It is believed that the formation of the transfer layer began after 200 cycles (see Figure 2.4), by the compaction of nano wear particles between the CNx coating and the sapphire hemisphere. Accumulation of the transfer layer at the contact surface completely separated the contact between the CNx coating and the sapphire hemisphere. This provided a steady state value of super low friction between 1000 to 10,000 cycles. The transfer layer thickness was calculated and a significant relation between the friction coefficient and the transfer layer was found, which with a constantly increasing transfer layer, drops the friction coefficient to a lower

level. Super low friction can be achieved at a steady state through a sufficiently thick transfer layer at the contact interface, where it will remain throughout the sliding test. Figure 2.3 shows that a steady state of super low friction of 0.003 was achieved at 1000 cycles, with a sufficient transfer layer thickness of 60 nm. Further consistent increments of the transfer layer do not affect the friction coefficient anymore.

Figure 2.12 shows the relation between the thickness of transfer layer and contact pressure to friction coefficient. It was observed that the thickness of transfer layer below 50 nm, the value of friction coefficient is high in the range of 0.02-0.13. The super low friction achieved in the range 0.003-0.004 when the thickness of transformed layer above than 100 nm. A high contact pressure enhanced the generation of transfer layer at sliding contact interface. The accumulation of transfer layer at sliding interface increased the thickness of transfer layer.

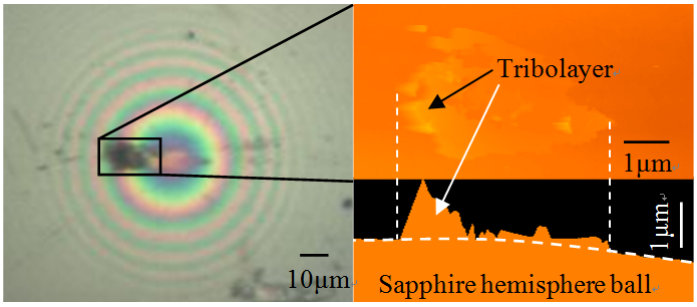

FIGURE 2.13: Microscopic and AFM images of transfer layer on sapphire hemisphere.

Figure 2.13 shows the ex-situ observation of the transfer layer on the sapphire hemisphere using AFM, after the sliding test. The thickness of the transfer layer was measured at approximately 550 nm. This value is comparable with that calculated at the end of the sliding test of 10,000 cycles, as discussed in Section 2.3.1. The transfer layer thickness is much higher than the RMS value of of 30 nm for the CNx coating and the sapphire hemisphere. It is believed that a steady state of super low friction was not influenced further by surface properties, such as the surface roughness of the CNx coatings and the sapphire hemisphere after 1000 cycles, but was fully controlled by the transfer layer; as long as the transfer layer was attached to the contact interface [55]. The Raman spectra of the transfer layer and the wear debris, as shown in Figure 2.10, proved that the transfer layer had graphite-like structures, which contributed to the super low friction during the friction test [56, 57]. AES analysis showed that no Ar molecule was found on the test specimen after the sliding test. As an inert gas, the function of Ar is to

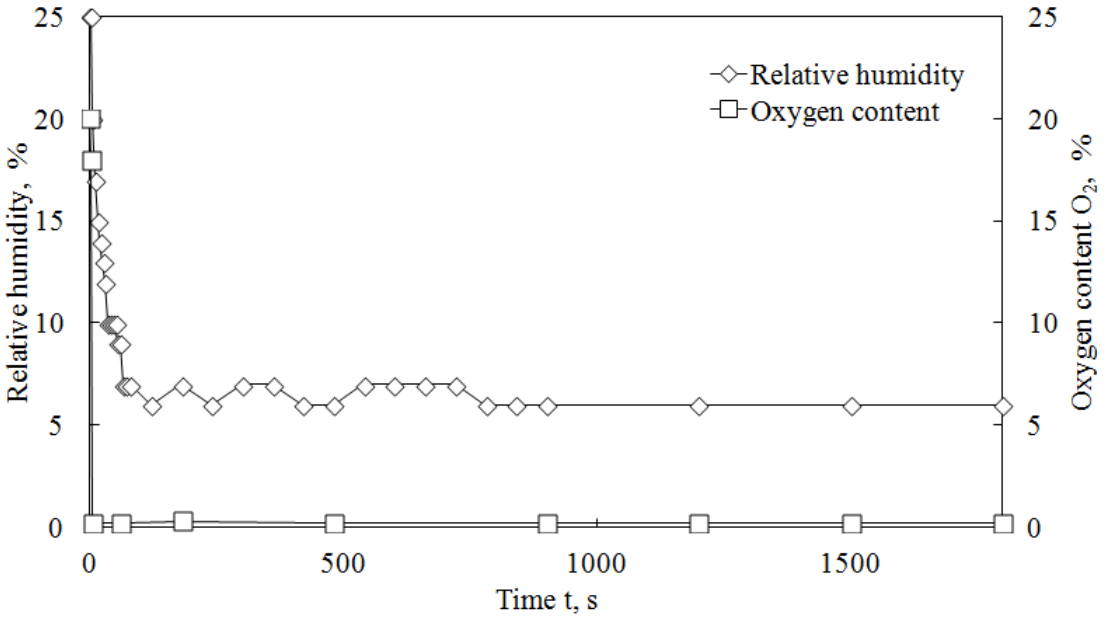

FIGURE 2.14: In-situ observation of relative humidity and oxygen content at sliding contact interface under blowing Ar.

protect accessibility of water and oxygen molecules from the environment to the sliding interface, which subsequently prevents chemical reaction that can cause an increment of friction coefficient [54]. Figure 2.14 shows the in-situ observation of relative humidity and O_2 content at the sliding interface during the sliding test. The relative humidity reduces significantly from 25 to 6 % after 1 minute. In addition, the O_2 content reduced drastically from 20 to 0.2 % after the Ar gas blew directly to the sliding contact interface. The very low value of relative humidity and O_2 was consistent throughout the sliding test. The influence of relative humidity and O_2 on friction coefficient is considered to be small in this experiment. High humidity and oxygen can cause high friction during friction test, as reported elsewhere [43, 54, 57]. As an inert gas, dry Ar gas flowed into the disorderly graphite structure without involving chemical interaction which attributed to the passivation of dangling covalent bonds [54]. This caused the atomic displacements from disorder into inter-lamellar layer of the lattice, which provided a highly slippery layer for super low friction, as reported elsewhere [57]. Since, no transfer layer was attached to the wear track of the CNx coating and the strongly adherent surface of the transfer layer on the sapphire hemisphere, it is suggested that a super low friction mechanism on the CNx coating against the sapphire hemisphere was provided by a low shear strength between the graphite-like transfer layer and the CNx coating.

2.4 Conclusions

In-situ observation successfully identified the transfer layer generation, which contributed to the friction behaviour of the CNx coating against the sapphire hemisphere. From this study, the following conclusions are as follows:

1. The transformation of CNx to graphite-like transfer layer is a consequence of high contact pressure 1.5 GPa at the contact interface.
2. The desorption of N content from the CNx coating during sliding was responsible for graphitization.
3. The shape of Raman spectra of the transfer layer is comparable with pure graphite.
4. Existing of a graphite-like transfer layer with the thickness of 60 nm between the CNx coating and the sapphire hemisphere, will significantly reduce the friction coefficient to an ultra low of 0.003.

The permanent attachment of a transfer layer at the contact interface is very important to maintain an ultra low friction during the friction test.

Chapter 3

Hardness effect of DLC on tribological properties for sliding bearing under boundary lubrication condition in additive-free mineral-based oil

3.1 Introduction

Many methods have been introduced in order to reduce friction and wear or as to increase the life span of mechanical components, and the efficiency of fuel consumption for engines. Surface topography, surface texturing, and the introduction of a lubricant at the contact of moving components have a significant influence on friction and the wear behaviour of engine components [58]. It has been reported that about 17% of energy is used to overcome friction in the engine and transmission system of passenger cars [5]. Thus, a new technology for engine systems is needed to increase fuel economy by introducing low friction materials, coatings, and lubricants [59–61].

Surface coating technology for engine components has been used in recent years under lubrication conditions in order to achieve ultra-low friction and low wear rates. One of the promising coating materials is diamond-like carbon (DLC) which

mainly provides high hardness, chemically inert, low friction and high wear resistance [62]. The tribological behaviour of DLCs depends on their structure, test environment and temperature [63]. High friction and wear occur mainly in a boundary lubrication regime. Although a DLC coating provides low friction and wear in these conditions, however what causes this good performance has not been fully clarified. It is important to understand the behaviour of DLC in terms of the structure changes that take the place in of DLC under these conditions in oil lubricants that have no additives.

In this chapter, we focus on the tribological behaviour of DLC with different hardness as a surface coating against steel as a mating surface under a boundary lubrication regime in an additive-free mineral-based oil lubrication.

3.2 Experimental details

DLC coatings with different hardness were deposited using plasma vapor deposition (PVD) and chemical vapor deposition (CVD) equipment on the same sliding roller of high carbon chrome steel (SUJ2) as the substrate. All the specimens were obtained from outside sources. Hydrogen-free DLC coating (DLC1) with a thickness of 1 μm was produced by an arc-PVD process. The detailed information of the arc-PVD process can be found elsewhere [64]. The Hydrogenated DLC coatings (DLC2 and DLC3) with the thickness of 4 and 10 μm respectively, were produced by a plasma enhanced CVD process . Different hardness was obtained by introducing different RF biases. S55C disks were used as counterpart for the friction test. Table 3.1 shows the mechanical properties of the as-deposited DLC coated sliding bearing and S55C disk.

Table 3.1: Properties of as-deposited DLC coated sliding bearing and disk.

Name	Roughness (R_a, nm)	Deposition method	Thickness (μm)
DLC1	50	PVD (FCVA)	1
DLC2	50	CVD (Plasma assisted CVD)	4
DLC3	50	CVD (Plasma assisted CVD)	10
S55C Disk	20	-	-

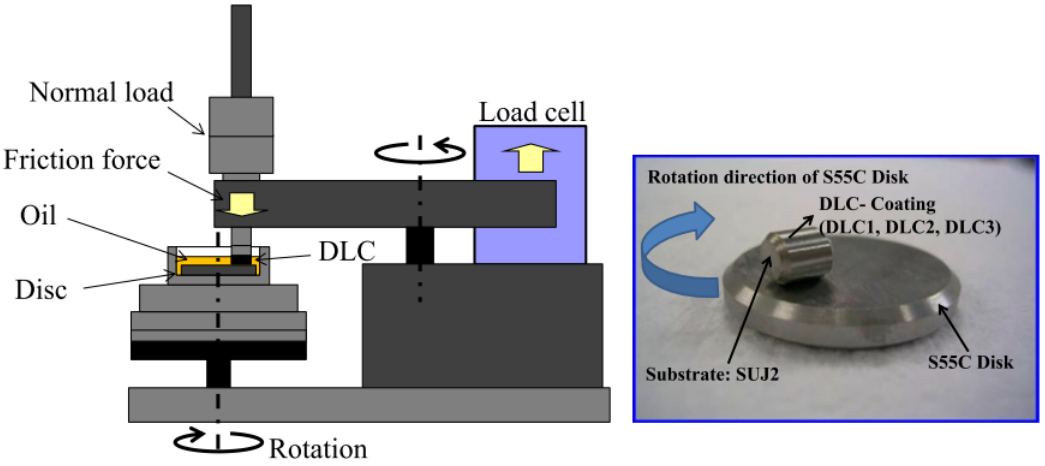

FIGURE 3.1: Schematic illustration of the pin-on-disk type tribometer.

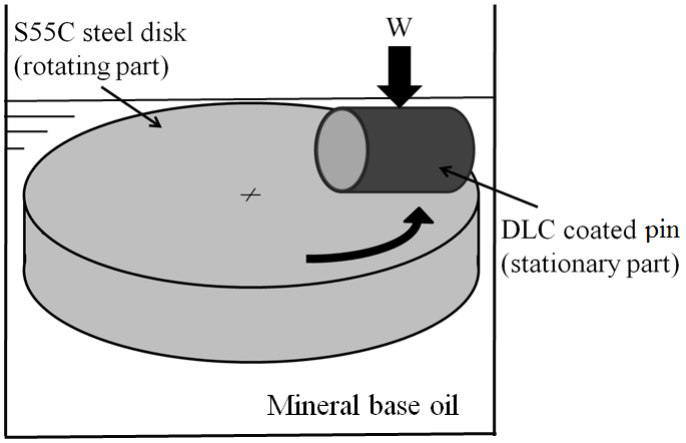

FIGURE 3.2: Schematic diagram of roller on disk friction test.

Pin on disk friction tests were carried out in order to investigate the effect of the hardness of DLC on the friction and wear behaviors under a constant load, W of 10 N (Hertzian's contact pressure of 208 MPa) at different oil temperatures of 25, 80, 120 and 160 °C. Figure 3.1 shows the schematic illustration of the pin-on-disk type tribometer of the friction test. The DLC-coated roller as the stationary part, is loaded in boundary lubrication conditions against a rotating disk of S55C immersed in an additive-free mineral-based oil as shown in Figure 3.2. The additive-free mineral-based oil had a kinetic viscosity of 95.2 mm^2/s (at 40 °C) and 10.8 mm^2/s (at 100 °C). The use of an additive-free mineral-based oil in this experiment enables the observation of the performance on the friction and wear of the DLC coating itself without any influence from the additive in lubricant. A contact load of 10 N was applied to the sliding bearing with a diameter of 4 mm and length of 5 mm during the sliding test with a sliding speed of 65 mm/s. The wear loss of the DLC films was investigated after 100 m sliding distance. The

worn surfaces of the films were observed by using an optical microscope and atomic force microscopy. Before sliding tests, the specimens were cleaned carefully in an ultrasonic bath with acetone solvent for 15 minutes. After the sliding tests, the tested specimens were cleaned in an ultrasonic bath with benzene for 15 minutes in order to remove all oil from the surface.

All the experiments were performed under a boundary lubrication regime where the calculated Λ value was less than unity. The Λ value, which was calculated using the EHL (elastohydrodynamic lubrication) theory, was controlled in the range of 0.07-0.1. The minimum film thickness of the oil and the dimensionless Λ value were calculated using Eqs. 3.1-3.6 [65].

$$h_{min} = 3.63RU^{0.68}G^{0.49}W^{-0.073}(1 - e^{-0.68k}) \tag{3.1}$$

where R is the radius of the roller,

U is the dimensionless speed parameter,

$$U = \frac{V\eta}{E^* R_x} \tag{3.2}$$

where

$$V = \left(\tilde{u}^2 + \tilde{v}^2\right)^{1/2} \tag{3.3}$$

G is the dimensionless materials parameter,

$$G = \xi E^* \tag{3.4}$$

W is the dimensionless load parameter,

$$W = \frac{w_z}{E^* R_x^2} \tag{3.5}$$

$$\Lambda = \frac{h_{min}}{\sqrt{R_{q,a}^2 + R_{q,b}^2}} \tag{3.6}$$

where η is the absolute viscosity at p=0 and constant temperature, E^* is the effective modulus of elasticity, R_x is the effective radius in x direction, $\tilde{u}$ is the mean surface velocity in x direction, $\tilde{v}$ is the mean surface velocity in y direction, ξ is the pressure-viscosity coefficient of the lubricant dependent on temperature and w_z is the normal load component.

The nanoidentation measurement system from Elionix (ENT-1100a) was used to measure the hardness of the as-deposited DLC. All measurements were carried out at a maximum indentation load of 1000 μN. The indentation depth was less than 10% of the thickness of the DLC coating in order to avoid the influence of the substrate material [66]. The structures of DLC coating surfaces were obtained before and after the friction test by using Raman spectroscopy in order to identify the structural changes in the topmost layer of DLC. The Raman spectra were obtained using a Jasco Laser Raman spectrophotometer NRS-1000 equipped with a second harmonic Nd:YAG laser with a maximum laser power and wavelength of 10 mW and 532 nm, respectively. However, only 1% of the maximum power was suitable for the measurement without burning the surface and also to avoid the influence of the steel substrate underneath. Three measurements were taken in order to reduce the uncertainty of the results from fitting the Raman peaks. Spectroscopy ellipsometry from Photal Otsuka Eletronics (FE-3000) was used to measure the thickness of transformed layer after the sliding test. Experimetal details about the measurement of the thickness of transformed layer is explained in the Chapter 4.

3.3 Results and discussion

3.3.1 Correlation between results with Raman spectroscopy and spectroscopic ellipsometry

The low friction coefficient obtained during the friction test is caused by structure changes in the surface of the DLC coating, which corresponds to graphitization. Graphitization during the rubbing was reported in many papers either under oil lubrication conditions [37, 67, 68] or dry conditions [52, 69]. Graphitization can be confirmed from the Raman spectra when the D and G peaks shifted to higher frequencies than the as-deposited DLC, and the intensity of the D peaks increased [37, 67]. The other indicator for graphitization from the Raman spectra is the ratio of I_D/I_G, in which the higher values of the I_D/I_G ratio of the DLC after rubbing compared to the as-deposited DLC mean the transformation of sp^3 to sp^2 [70].

Figure 3.3 shows the Raman shift of the D and G peaks, as well as the I_D/I_G ratios of all the DLCs at the various test temperatures before and afterthe sliding. Figure 3.4 and 3.5 show clearly, the shifting of the D and G peaks to higher frequencies as well as the increasing I_D/I_G values for all kinds of DLCs with increasing test temperatures, which correlate to graphitization. This means that the DLC structure at the topmost of the contact surface transforms from sp^3 to sp^2 and it is dependent on the oil temperature. Consequently, the topmost DLC coating becomes softer due to graphitization compared to the original surface, which results in more mechanical damage and wear [71, 72]. The wear results, indicate that the wear loss increases with increasing oil temperature. This means that the contact surface during rubbing becomes softer at higher temperatures under boundary lubrication conditions than at lower oil temperatures.

Spectroscopic ellipsometry was used to measure the transformed layer on the topmost DLC surfaces after the friction test. Figure 3.6 shows the thickness of transformed layer of all the DLCs at all the test temperatures. All the DLCs showed a significant increment in term of transformed layer thickness, where the thickness increases with increasing oil temperature. DLC1 shows the highest thickness 195 nm in the transformed layer at oil temperature of 120 °C. The thickness of transformed layer of DLC2 and DLC3 at oil temperature of 160 °C are 146 and 104 nm, respectively. The correlation between the D peaks from the Raman spectra and

transformed layer thickness from spectroscopic ellipsometry are shown in Figure 3.7. All the DLCs show the same trend, where the thickness of transformed layer increases with an increase in the intensity of the D peak.

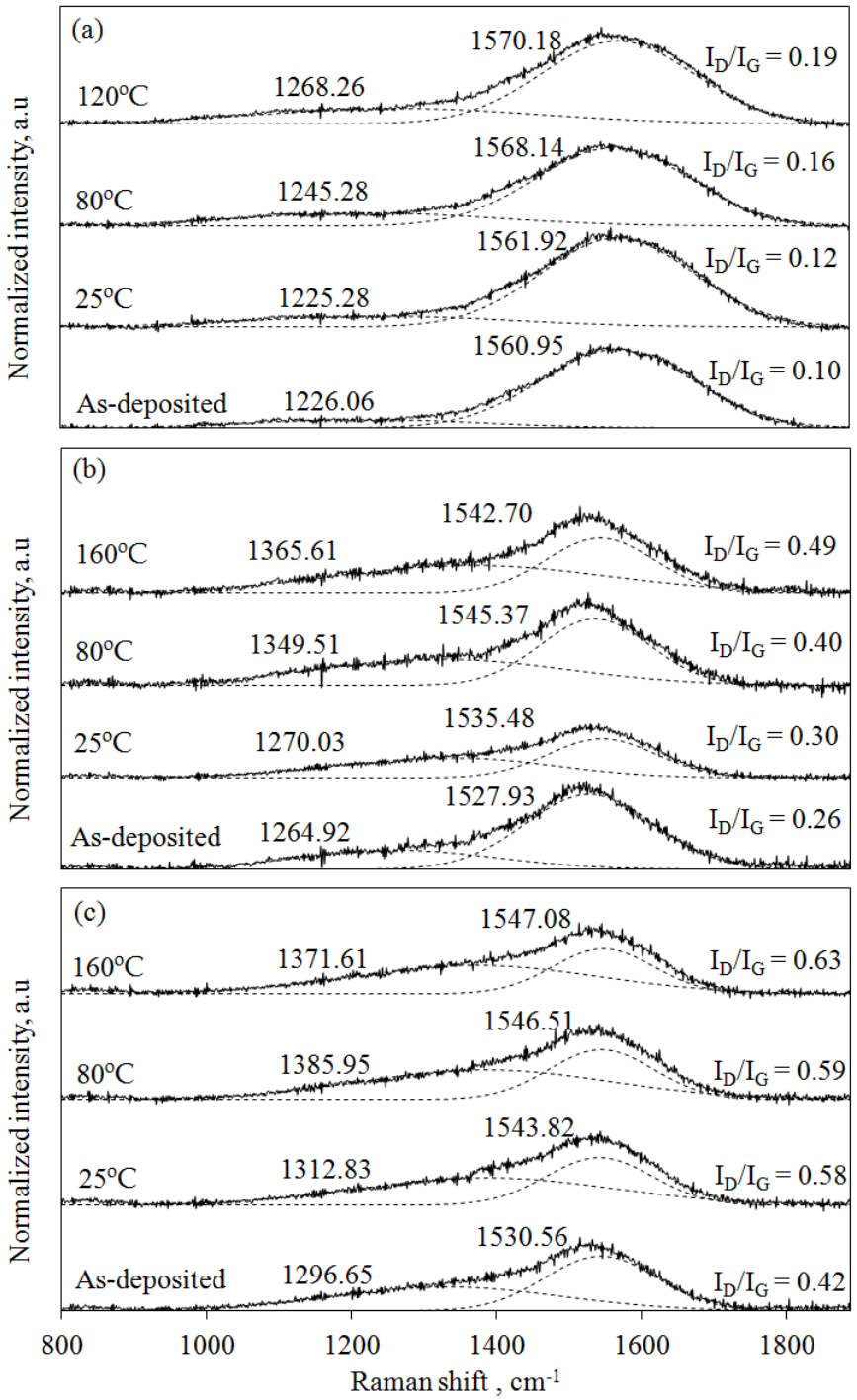

FIGURE 3.3: Raman spectroscopy of as-deposited DLC coatings before and after friction tests under different temperatures for (a) DLC1, (b) DLC2 and (c) DLC3.

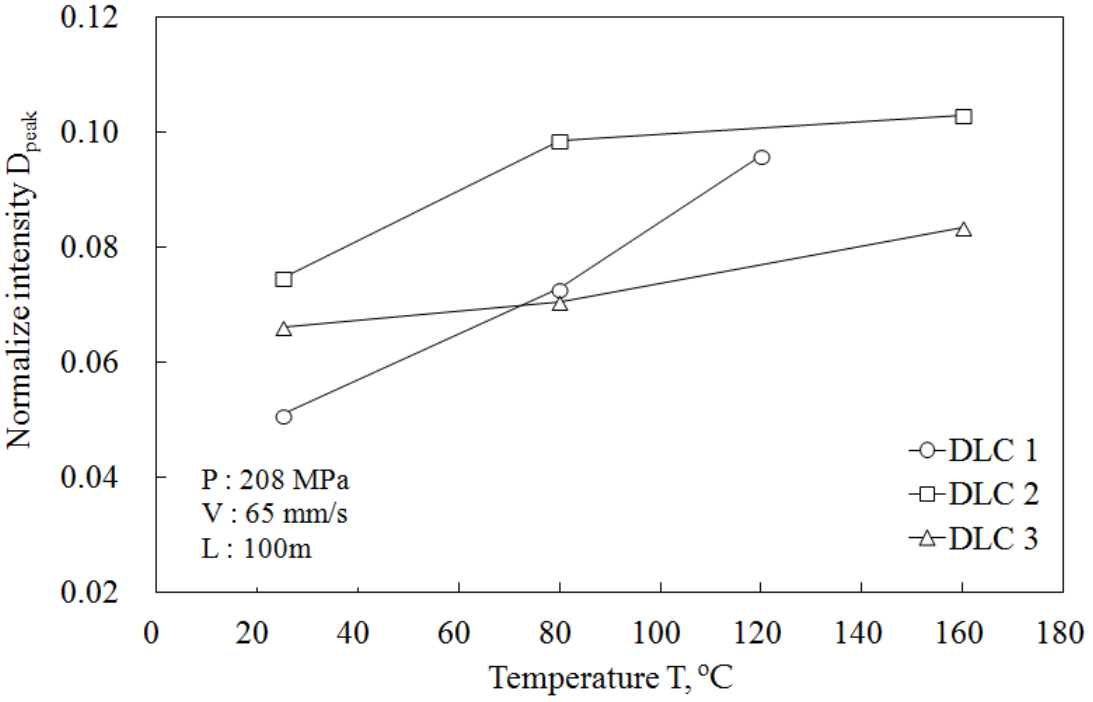

FIGURE 3.4: Intensity of D peak of DLC obtained by Raman spectroscopy as a function of oil temperature.

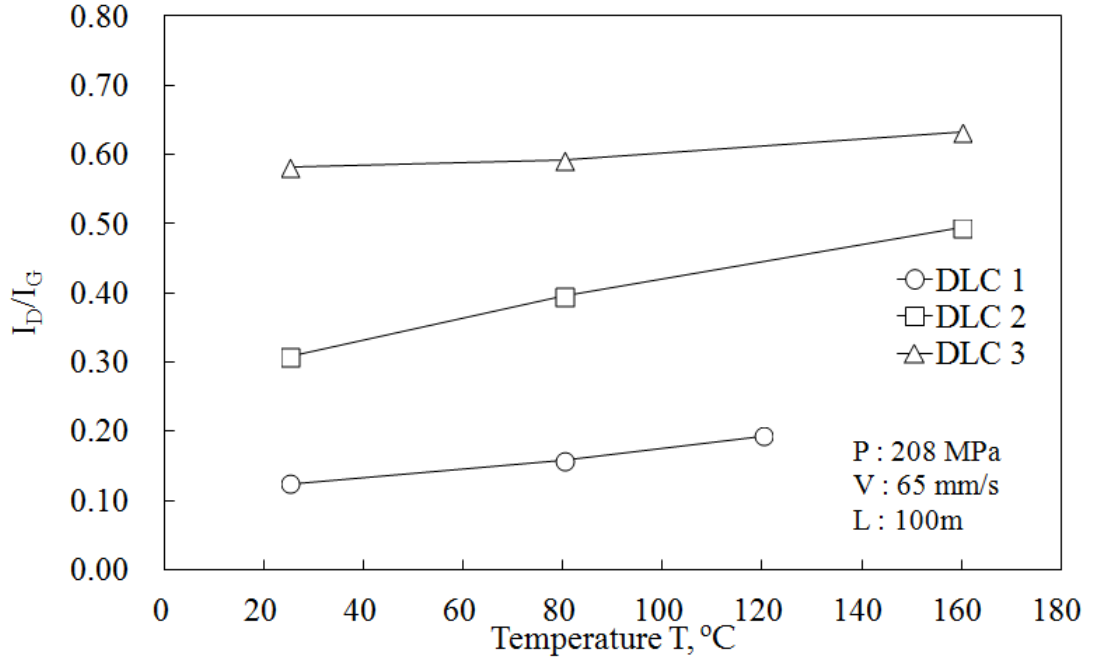

FIGURE 3.5: I_D/I_G ratio of DLC obtained by Raman spectroscopy as a function of oil temperature.

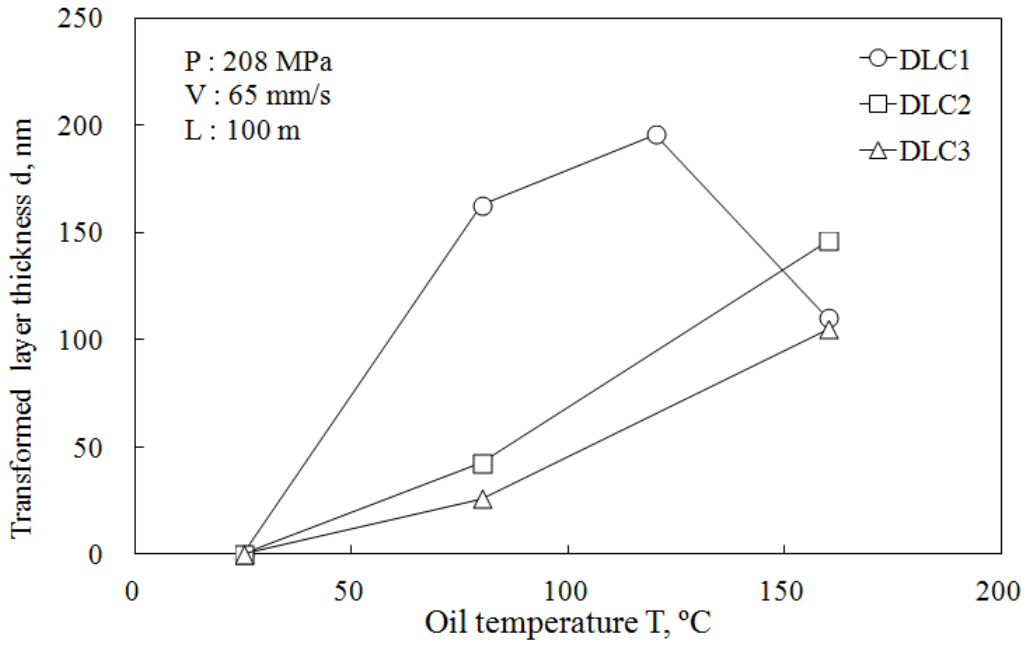

FIGURE 3.6: Thickness of the transformed layer after sliding in oil detected on wear track using spectroscopic ellipsometry as a function of oil temperature.

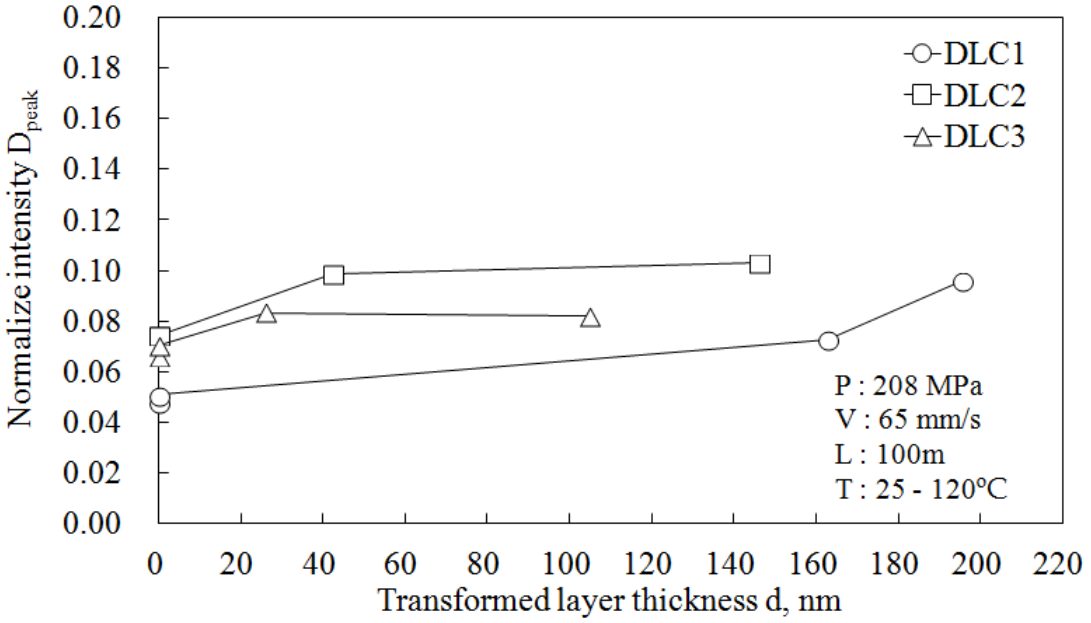

FIGURE 3.7: Correlation between intensity of D peaks and the thickness of transformed layer .

3.3.2 Hardness

The hardness was measured using a nanoindenter. An average of ten measurements was used to determine the hardness of the DLC coating in order to obtain a good statistical representation. The hardness of the DLC coatings DLC1, DLC2 and DLC3 were 47.1, 11.8 and 6.05 GPa, respectively as shown in Figure 3.8. Figure 3.9 shows the results of the indentation depths, where the depths of DLC1, DLC2 and DLC3 were 26.5, 70.04 and 90.2 nm at maximum indentation load of 1000 μN, respectively. This order is in agreement with the hardness of DLC coatings.

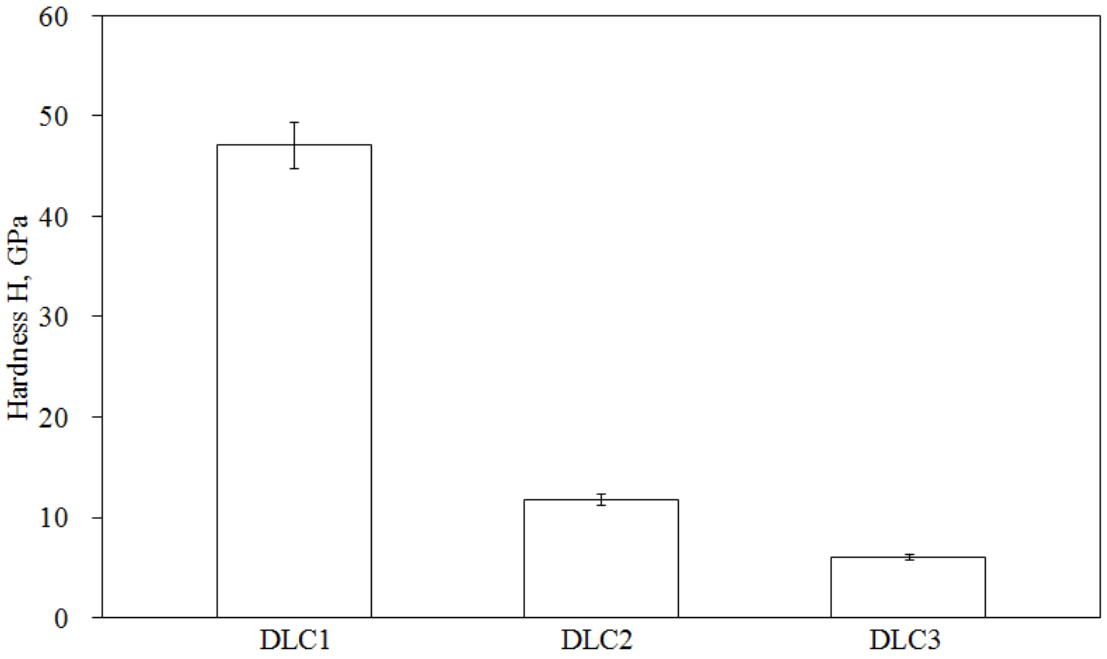

FIGURE 3.8: The hardness of DLC1, DLC2 and DLC3.

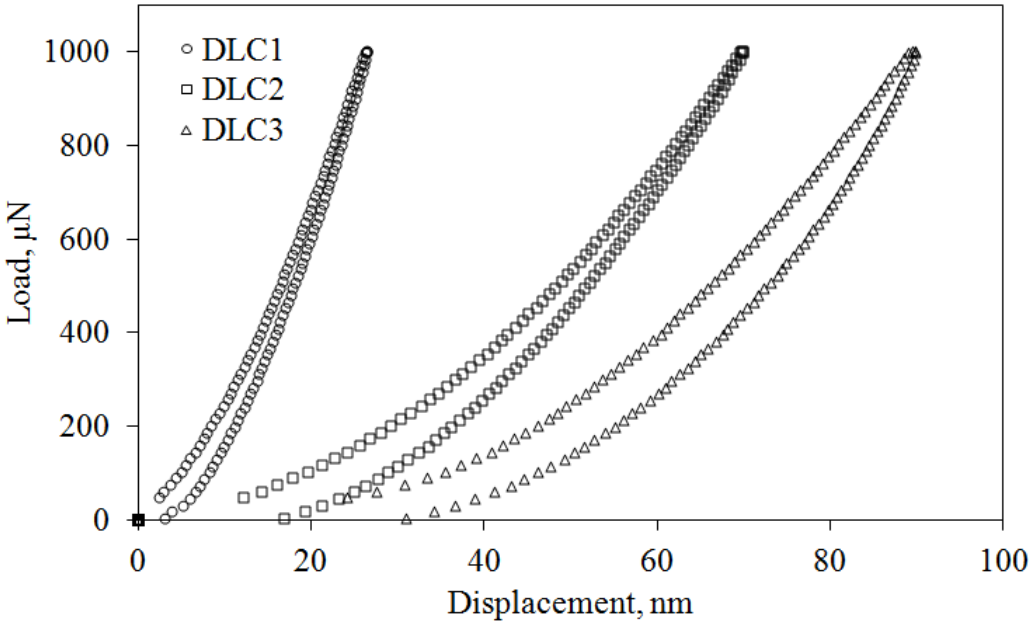

FIGURE 3.9: Load-displacement curves of different DLC by nanoindenter.

3.4 Friction and wear behaviors

Figure 3.10 shows the results of the friction coefficient of DLC1, DLC2 and DLC3 at different oil temperatures. All the DLCs showed the same friction behaviour where after the running-in, the friction coefficient reached a relatively steady and low value. It can be observed that DLC1 with the highest hardness showed a reduction of friction coefficient from 0.05 to 0.03 with increasing oil temperatures of 25, 80 and 120 °C. But DLC2 and DLC3 showed an increase in the friction coefficient at all oil temperatures. Figure 3.11 shows the relation between hardness and the average friction coefficient, where DLC1 with the highest hardness shows the lowest friction coefficient. Since, all the DLCs have the same initial surface roughness and have been coated on the same substrate, the friction behaviors depend strongly on the hardness of the DLC.

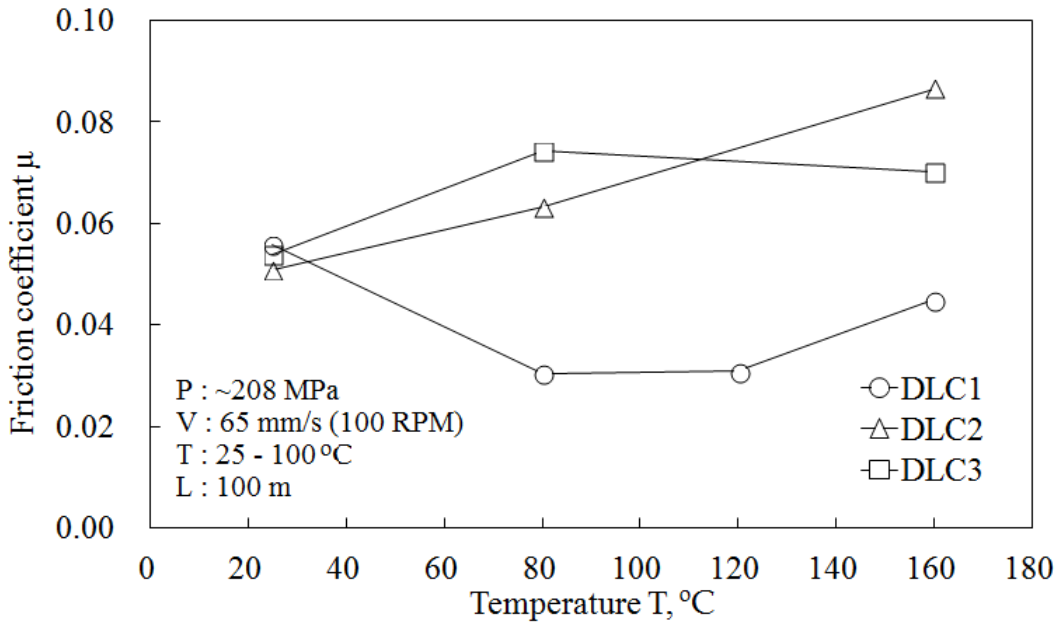

FIGURE 3.10: Friction coefficient of DLC as a function of oil temperature.

The wear loss of the DLC coatings can be obtained by observing the wear scar on the surface of the DLC coated roller. The wear volume, V (mm^3) of the DLC coating was measured by using the worn width and length of the DLC coated roller in an optical microscope and was calculated by using Eq. 3.7.

$$V = \left[R^2\left(\frac{\pi}{2} - Cos^{-1}\frac{b}{2R}\right) - \frac{b}{2}\sqrt{R^2 - \left(\frac{b}{2}\right)^2} \right] L \tag{3.7}$$

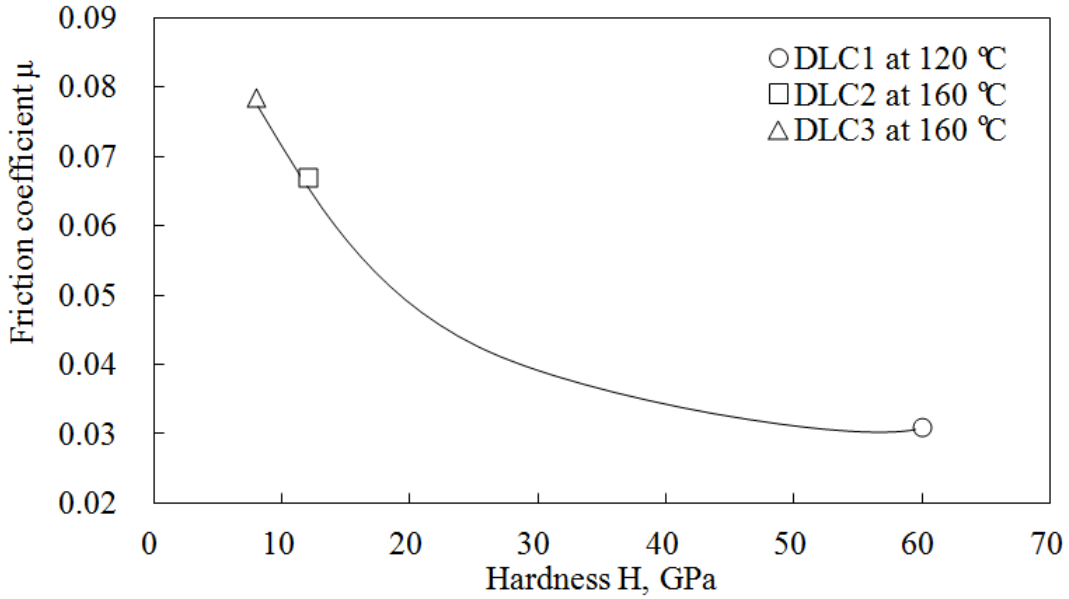

FIGURE 3.11: Correlation between friction coefficient and hardness of DLC.

where R is the radius of the roller (mm); b is the wear width (mm) and L is the wear length (mm).

The specific wear rate, W_s (mm^3/Nm) has been calculated using Archard wear equation as represented by Eq. 3.8.

$$W_s = \frac{V}{WL} \tag{3.8}$$

The effect of temperature on the wear behaviour of DLCs is shown in Figure 3.12. All the DLC showed the same trend with an increase in the specific wear rate as the oil temperature increased. The wear of the surface coatings increased with increasing oil temperature for all the DLCs mainly because of changes in the mechanical properties of the DLC coatings. The transformed layers at the contact interface were softer than the original DLC, and thus caused more wear [37]. The hardest DLC1 showed the lowest wear rate, followed by DLC2, and DLC3, which suffered the most wear. The specific wear rate of DLC1 was in the order of 10^{-11} mm^3/Nm, and DLC2 and DLC3 were at the order of 10^{-9} mm^3/Nm.

The relationship between the inverse hardness of DLC and the specific wear rate is shown in Figure 3.13. The specific wear rate decreases significantly with increases in the hardness of DLC.

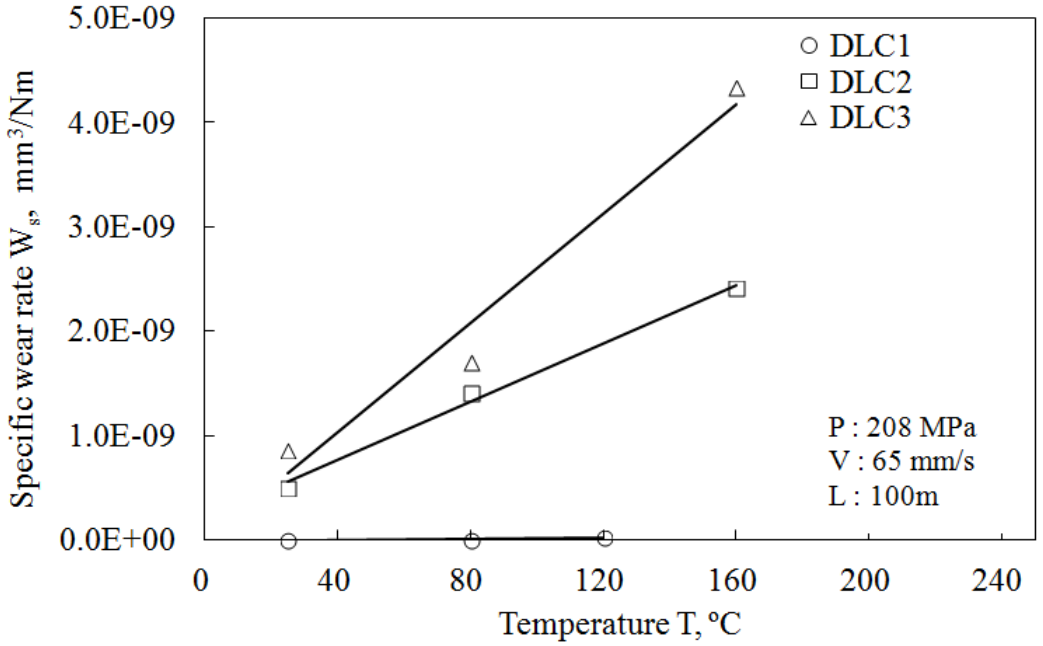

FIGURE 3.12: Specific wear rate of DLC as a function of oil temperature.

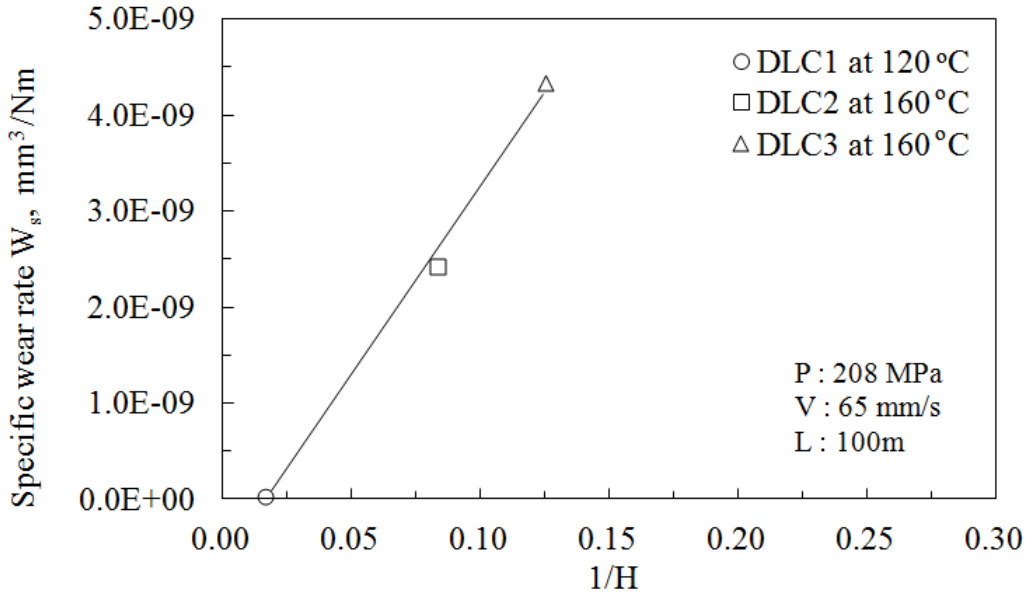

FIGURE 3.13: Relation between specific wear rate and inverse hardness of DLC.

It is suggested that the graphite-like transformed layer with low shear strength at contact interface could be responsible for the low friction coefficient. This is the most reasonable explanation for the low friction coefficient in this experiment for two reasons. Firstly, the influence of the lubricant is considered to be small because the oil film is very thin under the boundary lubrication conditions. The second reason is the absence of a low friction additive agent in the oil. On the other hand, we believed that the graphite-like transformed layer has some character such

as thickness and hardness that probably influence the friction behaviour. These nano characteristics is reported in the Chapter 4 and 5.

3.5 Conclusions

The tribological properties of different hardness of DLCs sliding against steel under boundary lubrication condition in additive-free mineral-based oil were investigated in order to determine the influence of the as-deposited DLC hardness on friction behaviour. The following conclusions were reached as follows:

1. The friction coefficient decreased with an increasing of the hardness of as-deposited DLC.
2. The specific wear rate decreases significantly with an increasing in the hardness of as-deposited DLC.
3. The formation of graphite-like transformed layer is due to graphitization process during friction test.

Further analysis on graphite-like transformed layer is needed in order to get the information about the nano character in term of its thickness and hardness.

Chapter 4

Effect of thickness of transformed layer on friction behaviour

4.1 Introduction

Diamond-like carbon (DLC) coatings are well known for their excellent low-friction and wear-resistance properties [11, 73]. Currently, these coatings are widely used in various mechanical systems. However, there are no clear systematic guidelines concerning for the use of DLC coatings in lubricated mechanical systems. This lack of guidelines in the use of DLC coatings is believed to be because the mechanism for the low friction of the DLC coating is unclear and because there are few models of DLC friction. Of course, there has been a report on the superlubricity mechanism for the ultra-low friction of glycerol-lubricated ta-coatings [74]. Furthermore, this report demonstrates that the adsorbed molecules from the oil additives play a critical role in obtaining ultra low friction. However, it is unclear what mechanism is valid for oil that does not contain any additives or mineral oil. Additionally, it has been reported that the transformed layer, which is a structure of a DLC surface enriched with sp^2 carbon, can reduce the friction of DLC under dry conditions [75].

However, it is only a qualitative factor, and this transformed layer cannot be easily observed under oil lubrication. Therefore, there is a need for quantitative methods to measure the thickness of the transformed layer of DLC under oil lubrication. A model for the friction of DLC under oil boundary lubrication is required to describe how the transformed layer of DLC functions. Several methods have been

developed for measuring the structure of DLC. For example, typical methods for this purpose include Raman spectroscopy, EELS, NEXAFS, NMR, PBS-ERDA and ESR. However, these methods are complex measurement techniques, and excessive amounts of time and costs are required to measure the DLC. Therefore, reflectance spectroscopy is considered to be a simple, rapid and low-cost method because once the optical models are defined, the thickness of the target film can be easily calculated. Spectroscopic reflectometry is a measurement technique that is based on an interferometric measurement. This method is a new method for the control of the thickness and the quality of the DLC. Reflectance spectrometry can measure the optical constant and film thickness of thin films from 1 to 5 nm in thickness based on the spectroscopic analysis of reflected light [76]. Furthermore, this system can measure the thickness with high resolution and accuracy. Therefore, spectroscopic reflectometry is expected to be an effective method for measuring the DLC film.

DLC films are thought to be predominantly amorphous, in which small clusters of microcrystalline structures with sp^3 and sp^2 bonding and an amorphous matrix coexist [77]. Therefore,the DLC can change its own structure from sp^3 to sp^2 with mechanochemical reaction under friction. Sanchez-Lopez et al. reported that friction-induced structural transformations of diamond-like carbon affect its friction coefficient under various atmospheres, such as in ambient air (RH 30-40 %),dry air (RH 1 %) and dry nitrogen (0-1 %) [74] . Mabuchi et al. observed that the DLC transformed its rich sp^2 carbon layer after sliding, which was obtained from friction under oil lubrication. They used transmission electron microscopy (TEM) and determined that the thickness of the transformed layer was a few nanometers [78] . This transformed layer had a π^* plasmon peak, which indicating that the transformed layer included a high content of sp^2 carbon. Therefore, it is believed that this transformed layer also had optical properties which were different than those of the original DLC. Consequently, the transformed layer could affect the friction coefficient of the DLC layer under oil boundary conditions. Therefore, the transformed layer of the DLC coating could be observed using reflective spectroscopy, and its thickness could also be quantitatively measured.

The transformed layer of the DLC on the original DLC surface can be considered to be a bi-layer [79] . However, there are no experimental examinations concerning this model because of the lack of quantitative measurement systems for the

transformed layer of DLC. Therefore, the purpose of this study is to develop are reflective spectroscopy method to quantitatively measure the transformed layer.

This chapter is composed of three parts. The first part details the optical model to explain the reflectance intensity spectrum of the DLC wear scar after sliding in oil. The second part reports on the influence of the oil temperature, contact pressure and sliding distance on the thickness of the transformed layer. In the third part, the relationship between the thickness of the transformed layer and the friction coefficient is clarified from the viewpoint of the friction model of DLC under oil boundary lubrication.

4.2 Experimental method and procedure

4.2.1 Test specimens and friction test

All materials and friction tests are same as in the Section 3.2.

Additional, the transformed layer thickness was measured using spectroscopic reflectometry measurement system (FE3000 made by Otsuka Electronics) as shown in Figure 4.1.

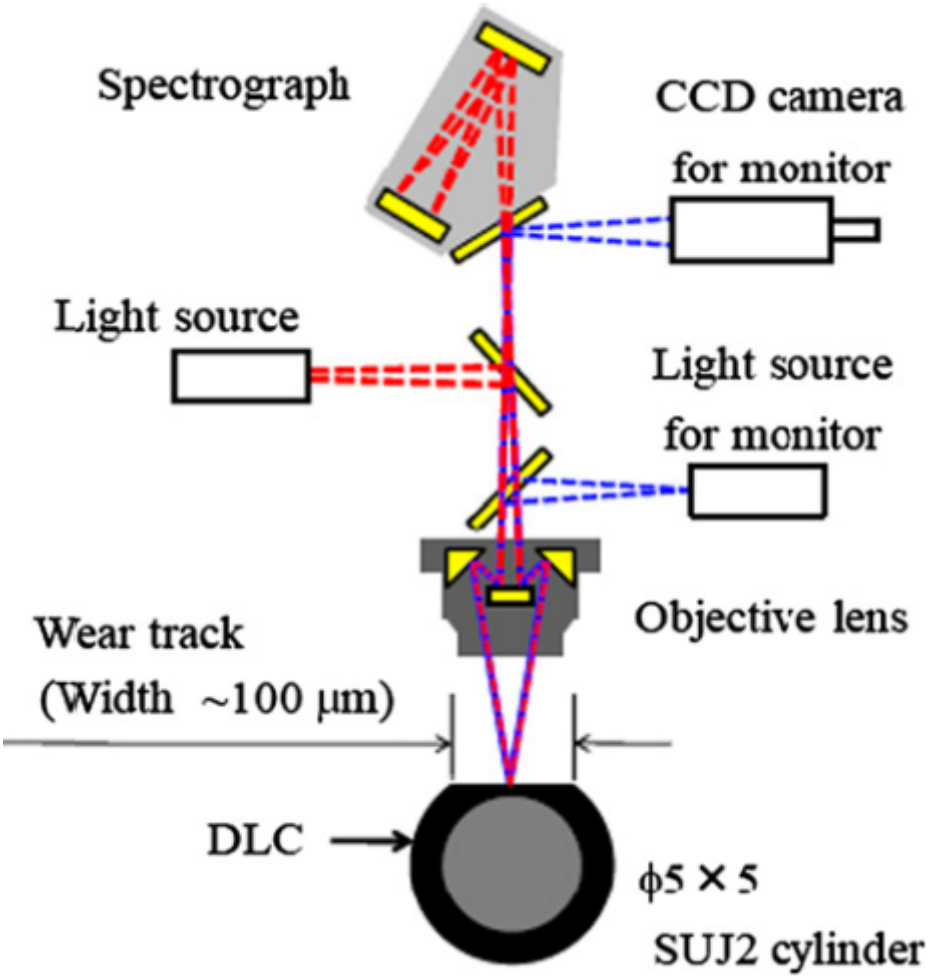

FIGURE 4.1: Schematic illustration of the reflectance spectrometry measurement for analysing the wear track on pin.

4.3 Spectroscopic reflectometry

A proper optical model for the material is needed in order to analyse the thickness and optical constant of the material using spectroscopic reflectometry. In this study, the materials, including DLC1, DLC2 and DLC3, were considered to have transformed layers on their topmost surfaces after the sliding test in additive-free mineral-based oil. Therefore, it was hypothesized that the specimens had two different layers on the SUJ2 substrate in the model. Figure 4.2 presents the cross-sectional image of the DLC1 coating cut using the FIB (Focused Ion Beam) and its elemental analysis by EDS (Energy Dispersive Spectroscopy). Figure 4.2 shows the DLC1 coating after sliding under an oil temperature of 80 °C within the region of the wear scar. The image was obtained by EDS/SEM with a tilting stage angle of 60 °. The SEM image showed different colour intensities with regard to different kinds of materials. The topmost surface showed that the transformed layer formatted during the friction test. The EDS analysis confirmed that the transformed layer consisted of the element carbon.

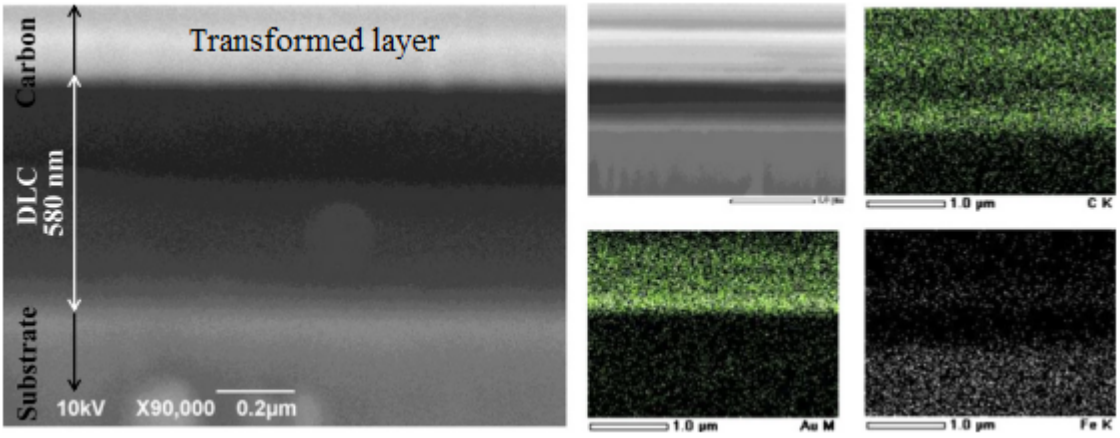

FIGURE 4.2: The cross-sectional image of the DLC1 coating cut by FIB and elemental analysis using EDS/SEM.

In this image, the bulk DLC, which is located between the transformed layer and the SUJ2 substrate., has a thickness of 580 nm. After recording an image, the real coating thickness (bulk DLC and transformed layer) was calculated to be 667 nm for DLC1. From this thickness, the optical properties of the original DLC1 film and the thickness and optical properties of the transformed layer could be estimated.

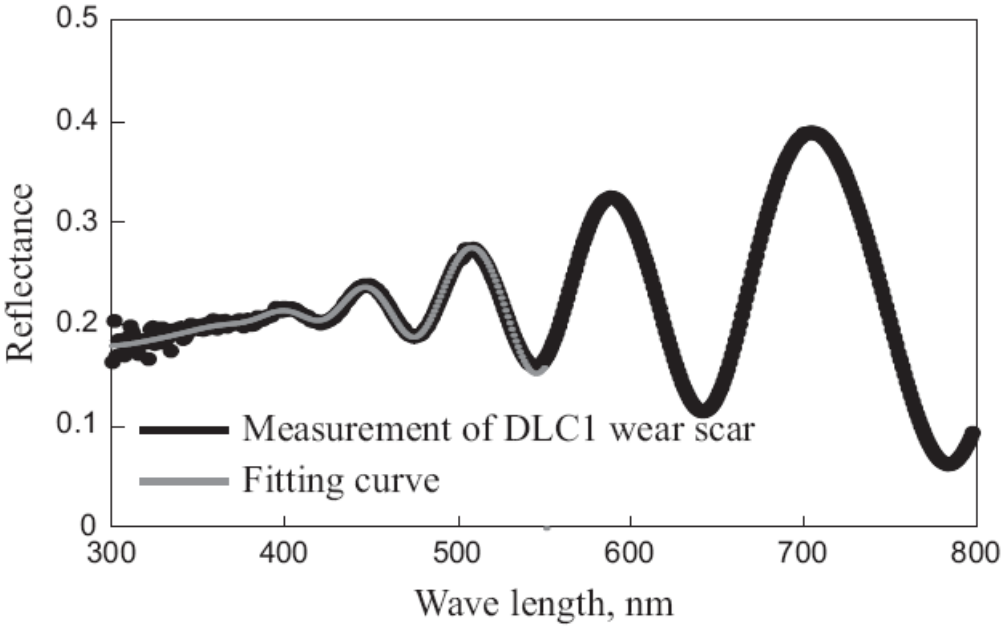

FIGURE 4.3: Reflectance intensity spectrum of the friction scar on the DLC1 coating after sliding.

Figure 4.3 presents the result of the reflectance intensity in the spectrum of a friction scar of DLC1 after sliding in oil. Figure 4.3 exhibits a fringe pattern along with the wavelength, which clearly indicates that the specimen contained a bi-layer. By fitting the spectrum with a theoretical curve, it was possible to estimate the thickness of the transformed layer on DLC1 after sliding in oil. The spectrum was fitted with the theoretical curve within the wavelength range of 300-550 nm. This wavelength range was selected because the penetration depth of 550-800 nm light was too deep to measure the optical properties of the transformed layer. Therefore, the penetration depth was calculated from the extinction index of the original DLC1 layer. Subsequently, the wavelength range was selected, for which the penetration depth of light was less than tens of nanometres, as shown in Figure 4.4.

Therefore, the optical model for DLC1 could be obtained as a bi-layer with a 10 nm transformed layer on the DLC1 films over the SUJ2 substrates. The optical models for DLC2 and DLC3. were also considered. It was determined that these two coatings had quite different models from that of the DLC1 coating, as a single-layer model. The reason for this difference was that the extinction index was too high to transmit the those films to the substrates.

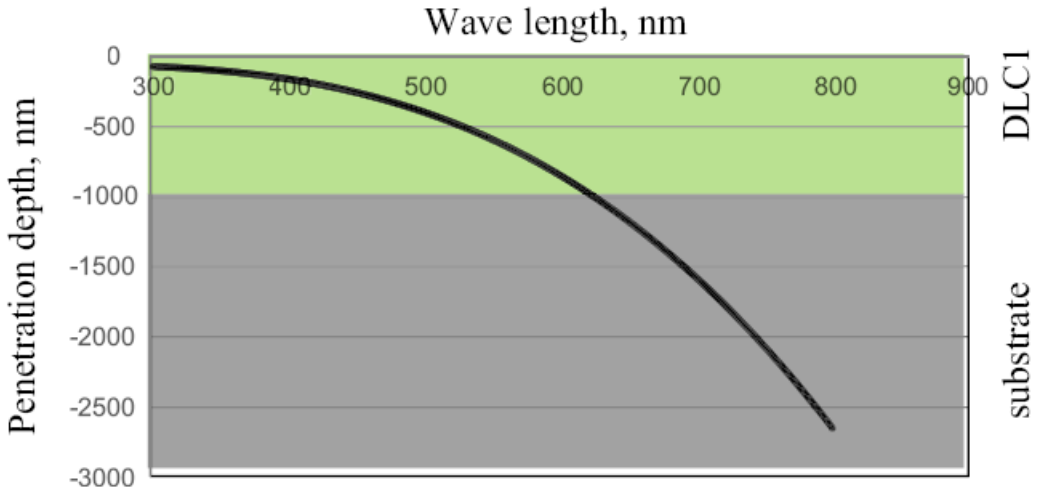

FIGURE 4.4: Penetration depth for each wavelength of light and the corresponding thickness of the DLC coating.

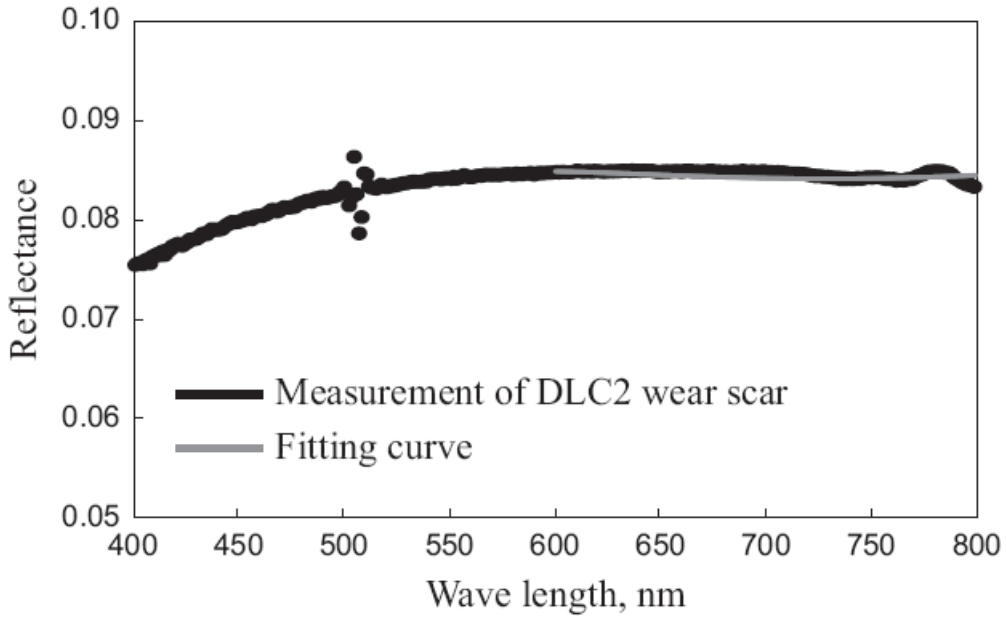

FIGURE 4.5: Reflectance intensity spectrum of the friction scar on the DLC2 coating after sliding.

Figure 4.5 shows the typical result of the reflectance intensity of a friction scar in the DLC coating (DLC2 and DLC3) after sliding in oil under different wavelengths. Figure 4.4 shows that no long wavelengths could penetrate those films, which is why there are no obvious fringe images in Figure 4.5. Figure 4.6 shows the penetration depth of each wavelength of light through the coating.

However, the penetration depths of light at 600-800 nm were sufficient to transmit the transformed layers of those DLCs. There, the optical model for the DLC2 and DLC3 coatings were obtained after sliding as a single model of transformed layers on the DLC2 and DLC3 substrates.

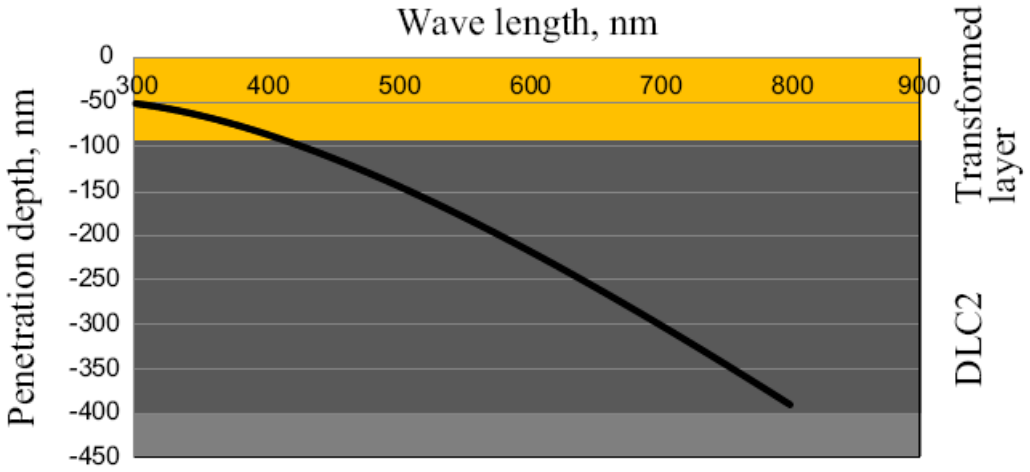

FIGURE 4.6: Penetration depth of each wavelength of light through the coating.

4.4 Results

4.4.1 The effect of oil temperature on the reflectance intensity

Figures 4.7-4.9 show the influence of the oil temperature on the intensity of the reflectance spectra of the wear scar in the DLC1, DLC2 and DLC3 films after sliding.

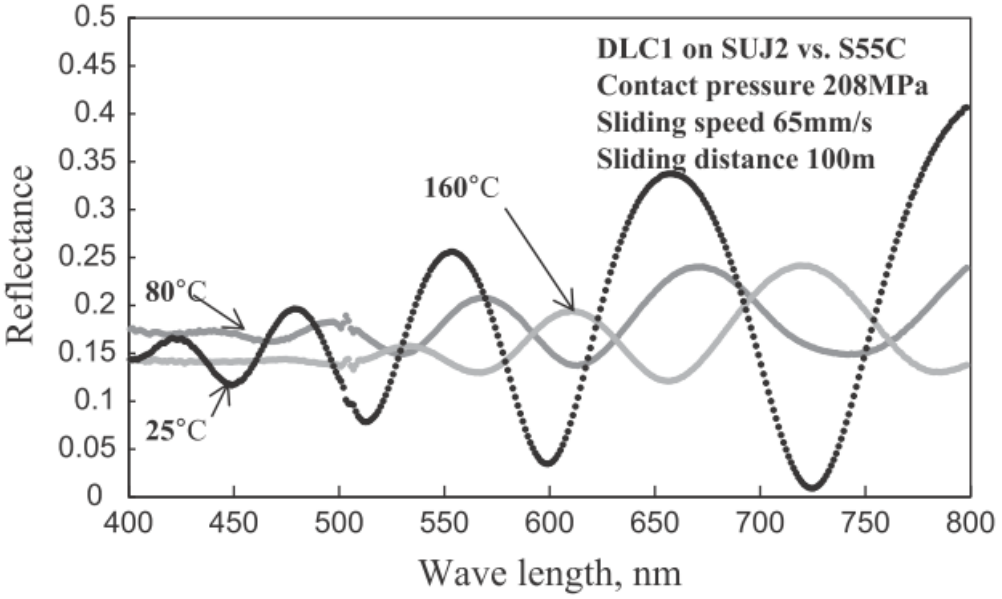

FIGURE 4.7: Reflectance intensity spectrum of the friction scar in the DLC1 coating after sliding under various contact pressures.

Figure 4.7 reveals that the reflectance intensity of DLC1 decreased with increasing oil temperature and phase (fringe pattern starting point) shifts to larger wavelengths with increasing oil temperature. In contrast, Figures 4.8 and 4.9 show a fringe image at wavelengths greater than 750-800 nm for DLC2 and DLC3. The fringe image in the wavelength range of 750-800 nm disappeared with increasing oil temperature.

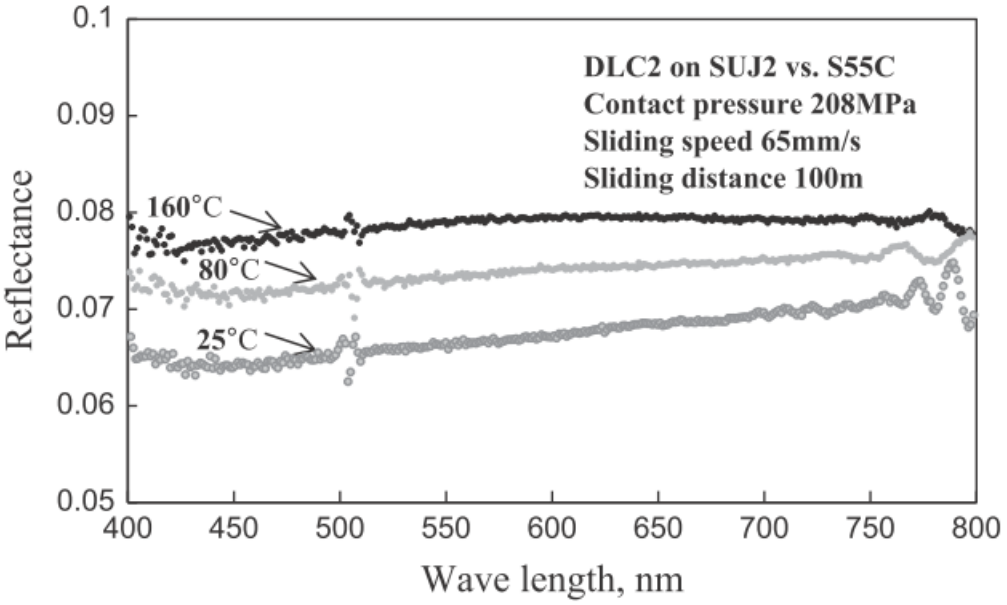

FIGURE 4.8: Reflectance intensity spectrum of the friction scar in the DLC2 coating after sliding under various contact pressures.

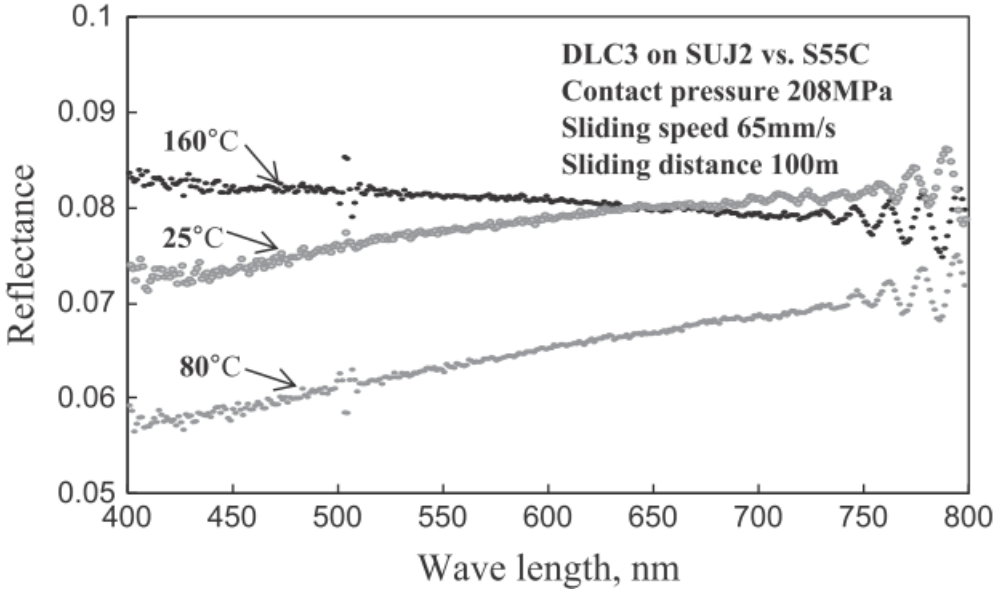

FIGURE 4.9: Reflectance intensity spectrum of the friction scar in the DLC3 coating after sliding under various contact pressures.

4.4.2 The effects of contact pressure and sliding distance on the reflectance intensity

After several friction tests with different contact pressures, Figure 4.10 shows the influence of contact pressure on the reflectance intensity of the friction scar in the DLC1 coating. The reflectance intensity decreased with increasing contact pressure and phase shifting was observed.

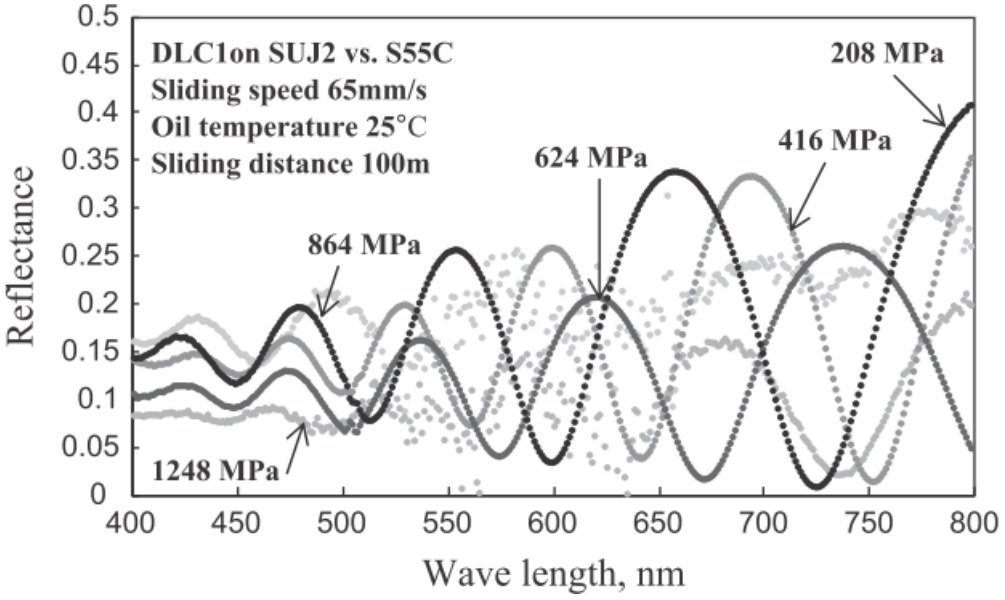

FIGURE 4.10: Reflectance intensity spectrum of the friction scar in the DLC1 coating after sliding under various contact pressures.

Figure 4.11 shows the influence of the sliding distance on the reflectance intensity of the friction scar in the DLC1 coating. The reflectance intensity decreased with increasing sliding distance, and phase shifting was observed.

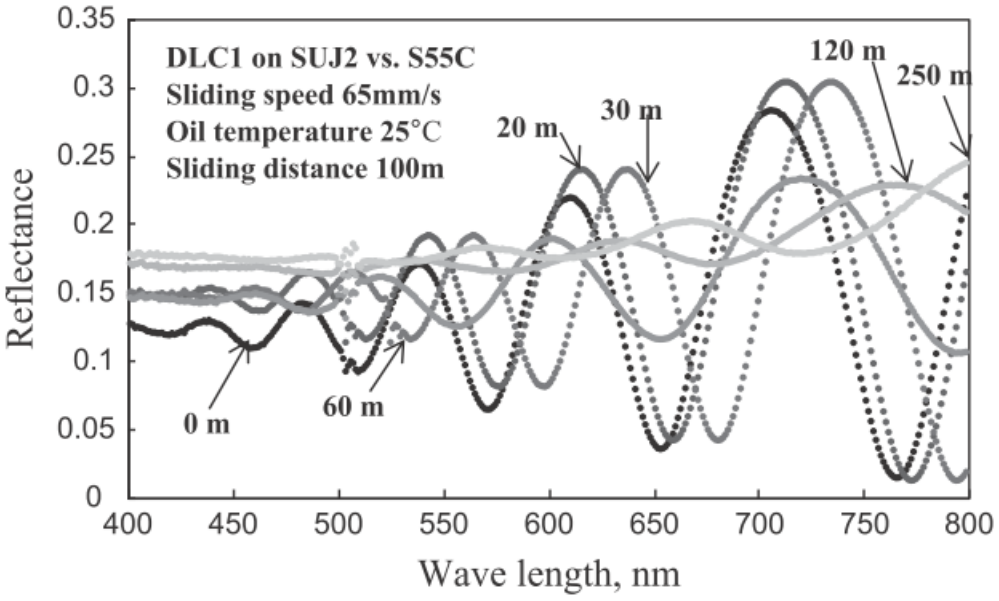

FIGURE 4.11: Reflectance intensity spectrum of the friction scar in the DLC1 coating after sliding under various sliding distances.

4.4.3 The effects of friction conditions on the thickness of the transformed DLC layer using spectroscopic reflectometry

After several friction tests, the relationships between the thickness of the transformed layer and the friction coefficient under various oil temperatures, contact pressures and sliding distances, were summarized. Figures 4.12-4.14 show the effects of the friction conditions on the thickness of the transformed layers, which were obtained from the results of Figures 4.7-4.11 with the theoretical curve fittings.

4.4.3.1 The effect of oil temperature on the thickness of the transformed DLC layer using spectroscopic reflectometry

Figure 4.12 shows the relationship between the thickness of the transformed layer and oil temperature. It can be seen that the thickness of the transformed layer increased with increasing oil temperature for all the DLC coatings. The hydrogen-free DLC coating (DLC1) exhibited a thick transformed layer at each oil temperature. When the friction coefficient of DLC1 decreased, the thickness of the transformed layer of DLC1 simultaneously increased. However, the friction coefficients of the DLC2 and DLC3 coatings increased with increasing thickness of the transformed layers on these films.

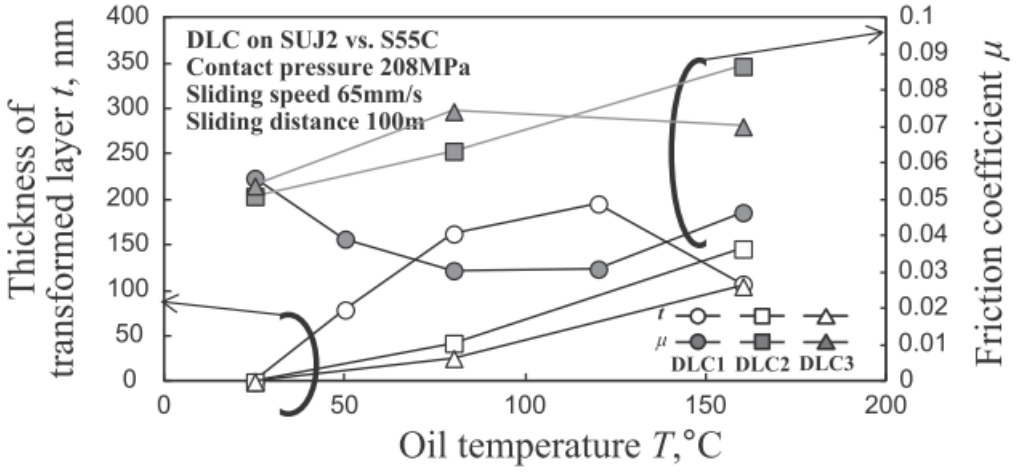

FIGURE 4.12: Effect of oil temperature on the thickness of the transformed layer and friction coefficient of various DLC coatings after sliding in the based oil.

4.4.3.2 The effects of contact pressure on the thickness of the transformed DLC layer using spectroscopic reflectometry

Figure 4.13 shows the effect of contact pressure on the thickness of the transformed layer and the friction coefficient of DLC1 after sliding in based oil at room temperature. The effects of the contact pressures on the thicknesses of the transformed layers were substantially less than the influence of the oil temperature. Subsequently, there was no obvious correlation between the friction coefficient and the thickness of the transformed layer.

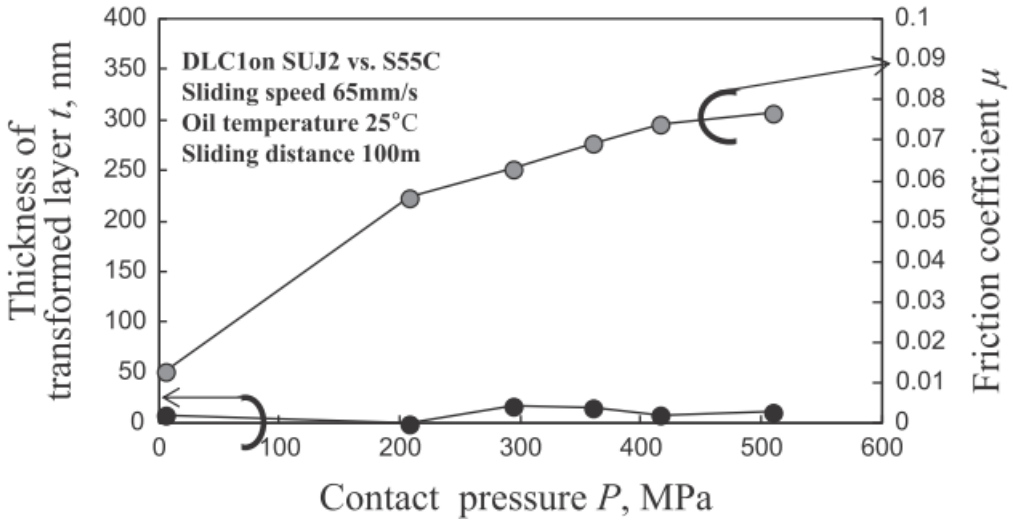

FIGURE 4.13: Effect of contact pressure on the thickness of the transformed layer, t, and friction coefficient, μ, of the DLC1 coating after sliding in the based oil at a temperature of 25 $°C$.

4.4.3.3 The effects of sliding distance on the transformed layer thickness of DLC with spectroscopic reflectometry

Figure 4.14 shows the effects of the sliding distance on the thickness of the transformed layer and the friction coefficient of DLC1 after sliding in the based oil with a temperature of 80 °C and approximately under 104 MPa of contact pressure. The thickness of the transformed layer increased with increasing sliding distance. In contrast, the friction coefficient decreased with increasing sliding distance. At the beginning of the friction test, there was no generation of the transformed layer. After several meters of sliding distance, the transformed layer was generated and increased with an increase in the sliding distance. The thickness of the transformed layer on the DLC coating outside the scar surface was measured at oil temperatures of 80 and 160 °C. The result showed that no transformed layer was generated under annealing temperatures at 80 and 160 °C. Since, the experimental oil temperature is below the transition temperature of 300 °C for DLC, the sliding distance is also one of the factors for the graphitization process which leads to pressure-induced graphitization [48, 49].

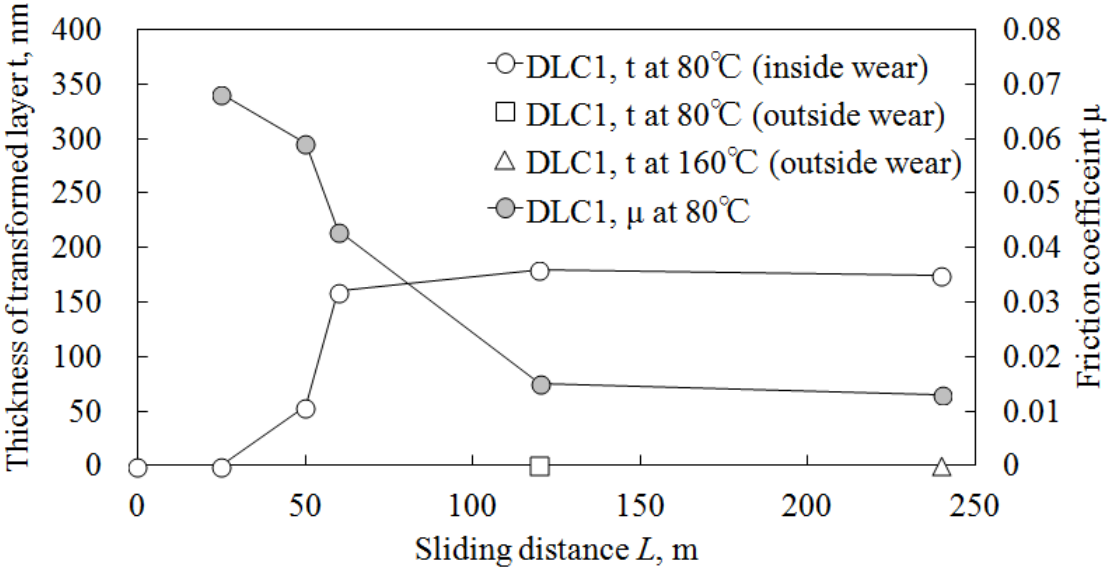

FIGURE 4.14: Effect of sliding distance on the thickness of the transformed layer, t, and the friction coefficient, μ, of the DLC1 coating after sliding in the mineral-based oil at a temperature of 80 °C.

4.4.4 The effects of the friction condition on the surface roughness of the DLC coatings using spectroscopic reflectometry

From the viewpoint of the friction coefficient, the surface roughness was assumed to have a significant effect. Dayson reported on the possibility of breaking of the solid lubricant film from this compound surface model [80]. Therefore, the deviation of roughness height, σ^* was measured on the wear track of DLC1, DLC2 and DLC3 using AFM, and these results are shown in Figures 4.15-4.17.

4.4.4.1 The effects of oil temperature on the surface roughness of the DLC coatings using spectroscopic reflectometry

Figure 4.15 shows the relationship between σ^* and the oil temperature. The DLC1 exhibited a remarkable change in σ^* with increasing oil temperature. However, it was difficult to correlate the σ^* of all the DLCs with oil temperature.

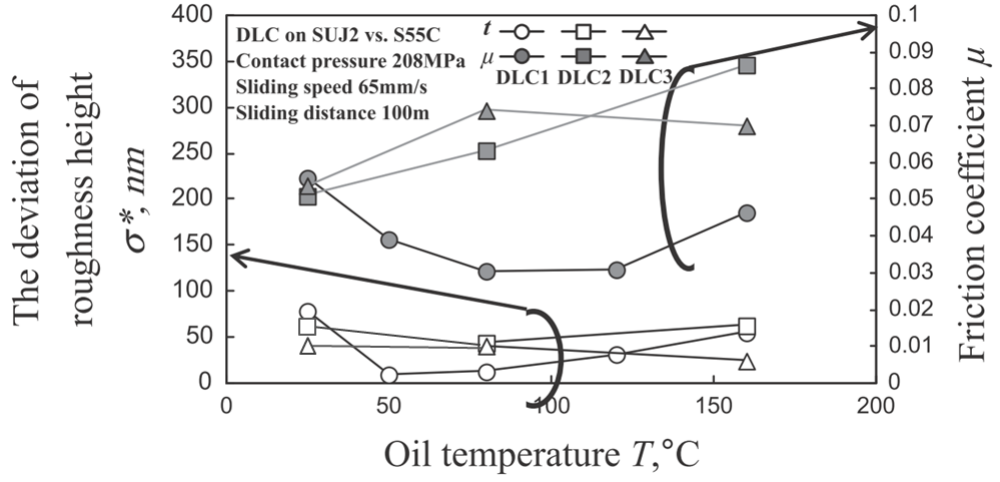

FIGURE 4.15: Effect of oil temperature on the deviation of the roughness height, σ^* and friction coefficient, μ, of various DLC coatings after sliding in the mineral-based oil.

4.4.4.2 The effects of the contact pressure on the surface roughness of the DLC coatings using spectroscopic reflectometry

Figure 4.16 shows the effects of the contact pressures on the $\sigma^*$and the friction coefficient of DLC1 after sliding in additive-free mineral-based oil. at room temperature. The σ^* decreased as the contact pressure increased from 200 to 300 MPa, and remained constant with further increases of contact pressure. It was clear that the contact pressure did not have a significant effect on either σ^*.

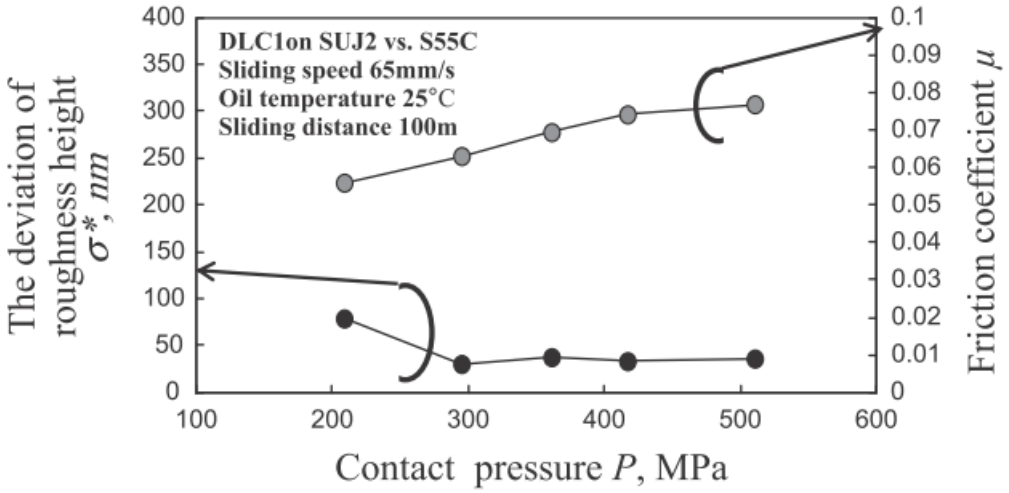

FIGURE 4.16: Effect of contact pressure on the deviation of the roughness height,σ^* and the friction coefficient, μ, of the DLC1 coating after sliding in the mineral-based oil with a temperature of 25 $°C$.

4.4.4.3 The effects of sliding distance on the surface roughness of the DLC coatings using spectroscopic reflectometry

Figure 4.17 shows the effect of the sliding distance on the σ^* and the friction coefficient of DLC1 after sliding in mineral-based oil with a temperature of 80 $°C$ and approximately under 104 MPa of contact pressure. The σ^* first increased to 50 nm with increasing sliding distance and then σ^* decreased to 10 nm after 50 m of sliding distance. In contrast, the friction coefficient decreased with increasing sliding distance. Therefore, there was no clear correlation between the sliding distance and σ^*.

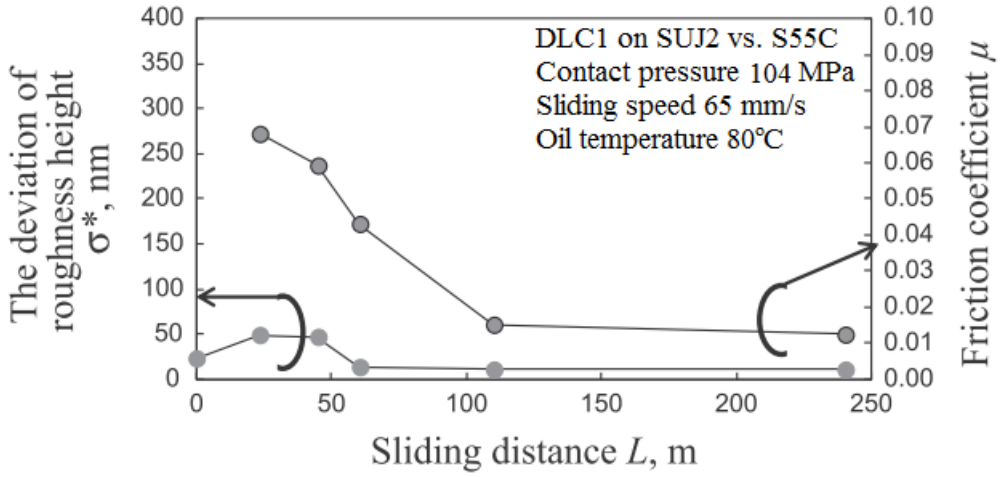

FIGURE 4.17: Effect of sliding distance on the deviation of the roughness height, σ^* and friction coefficient, μ,of the DLC1 coatings after sliding in the mineral-based oil with a temperature of 80 $°C$.

4.5 Discussion

Figure 4.18 shows the friction coefficient, μ as a function of the transformed layer thickness, t. In case of increasing of oil temperature, the friction coefficient of DLC1 decreases with an increasing of the thickness of transformed layer. The effect of sliding distance of DLC1 shows that the friction coefficient decreases with an increasing of the thickness of transformed layer. However, the effect of pressure, the thickness of transformed layer was not increased with an increasing of contact pressure. DLC2 and DLC3 shows the friction coefficient increase with an increasing of the thickness of transformed layer. From this result, it is difficult to find concrete relation between the friction coefficient and the thickness of transformed layer.

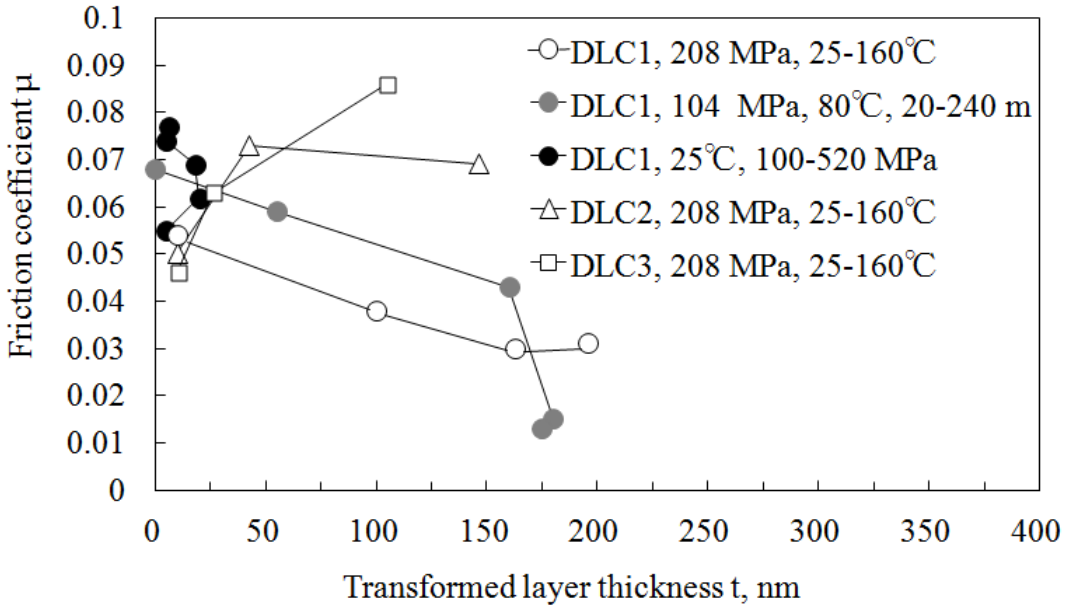

FIGURE 4.18: Relation between transformed layer thickness, t and friction coefficient, μ.

Figure 4.19 shows the friction coefficient, μ as a function of the deviation of the roughness height, σ^*. The friction coefficient increases drastically with an increasing of the deviation of roughness height in the range of 10-20 nm. Then, the σ^* don't have significant influence on friction coefficient when the σ^* value higher than 20 nm.

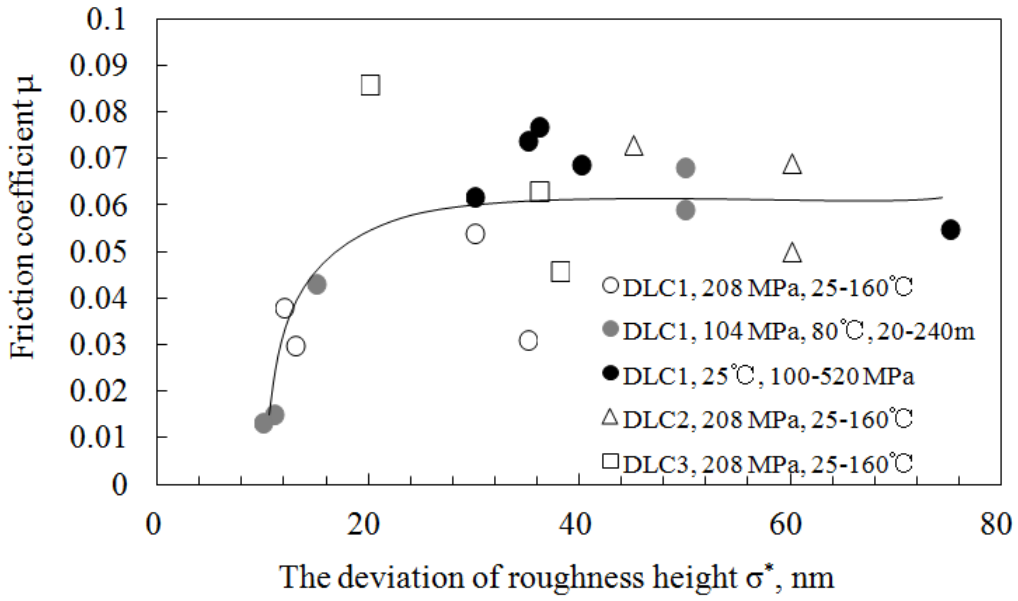

FIGURE 4.19: Relation between the deviation of the roughness height, σ^* and friction coefficient, μ.

Figure 4.20 shows the effect of t/σ^* on the friction coefficient of various DLC coatings after sliding in the mineral-based oil. The friction coefficient did not change when the value of t/σ^* below than 1. The friction coefficient decreases significantly with an increasing of t/σ^* value above 1. This figure showed that the low friction coefficient can achieve if the thickness of transformed layer much higher than the the σ^* value.

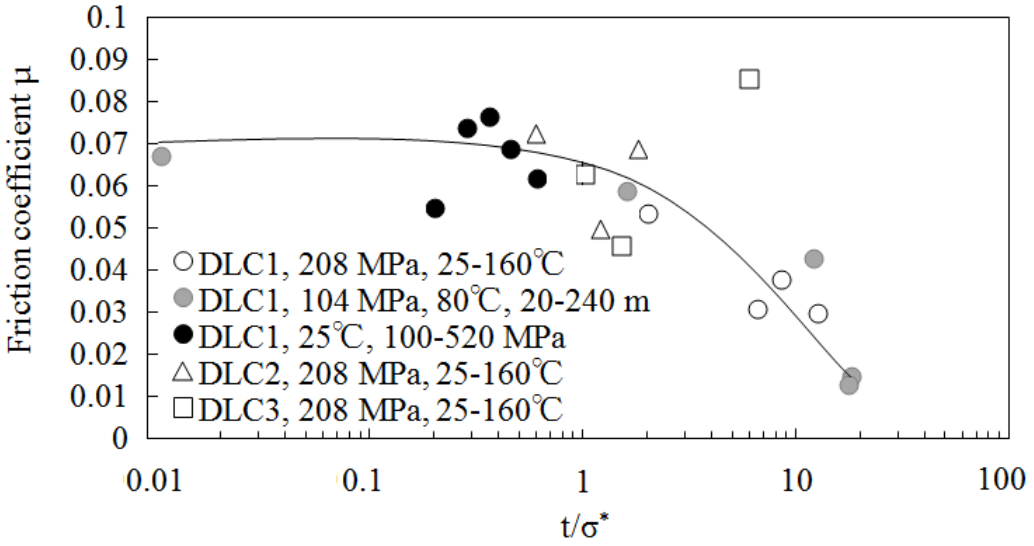

FIGURE 4.20: The effect of t/σ^* on the friction coefficient of various DLC coatings after sliding in the mineral-based oil.

4.6 Conclusions

The thickness of transformed layer of DLC sliding against steel under boundary lubrication condition in additive-free mineral-based oil were successfully measured by using reflectance spectroscopy. From the experimental results, following conclusions are as follows:

1. The thickness of the transformed layer has an effect to reduce friction coefficient in the case of DLC1.
2. It was observed that the temperature and the sliding distance has a significant effect on DLC1 for generating transformed layer during sliding test.
3. The significant decrement of friction coefficient when the t/σ^* value is higher than 1, where t is the thickness of transformed layer of DLC and σ^* is the effective root mean square roughness.

Chapter 5

Characteristics of transformed layer of DLC after friction test under boundary lubrication in additive-free mineral-based oil

5.1 Introduction

Diamond-like carbon (DLC) provide very excellence performance in term of friction coefficient and wear resistance under boundary lubrication in mineral based oil with or without additives [81–84]. DLC became more interesting as a coating material in tribological applications especially in the automotive industry in order to reduce the fuel consumption [5], because of their significant tribological properties such as low friction, high hardness, and high wear resistance. Improvements in coating technology have made the DLC coating suitable for various machine components that operate under severe conditions i.e under boundary lubrication. The low friction mechanism in the DLC coating under friction tests in either dry or boundary-lubricated conditions is due to the formation of a graphite-like layer in the non- lubricated [37, 52, 69, 85] or transformed layer [37, 86] which provides low shear strength at the contact interface. The transition phase of the as-deposited DLC to graphite-like structure at the topmost sliding interface is due to graphitization by conversion of sp^3 to sp^2. This transition phase has been reported in

other studies as a friction-induced transformation of the topmost sliding interface of the DLC coating [87, 88].

However, the nano characteristic of the transformed layer has not been studied in-terms of its hardness which is believed to have a significant effect in the tribological performance, such as a low friction coefficient under boundary lubrication conditions. The most important finding in this study is the scratch hardness of the transformed layer at the topmost of the sliding interface of the DLC from the AFM scratch test under different oil temperatures.

5.2 Experimental details

5.2.1 Friction test and Raman analysis

The detailed explanation about materials, friction test and Raman analysis are same as in the Section 3.2.

5.2.2 Scratch test

A scratch hardness test was performed to find the hardness of the transformed layer that is believed to have been formed at the topmost worn surface during the friction test. The scratch test was carried out using a commercial AFM (SII, SPA-400) in ambient temperature and humidity of 25 °C and 40 %, respectively. The poly-crystal diamond (PCD) tip cantilever from the Nano World AG, which has a tip radius of 150 nm and a spring constant of 42 Nm^{-1}, was used to perform the scratch test. Figure 5.1 shows the scanning and the scratch area when the scanning process was done before and after the scratch hardness test in order to obtain different surface profiles of the worn area. The load was applied to the cantilever for the scanning and hardness scratch of 50 and 1000 nN, respectively. The AFM stage speed of 1 μms^{-1} was set for both the scanning and scratch hardness test. The scratch movement of the PDC tip was programmed to be the same in all the tests. As shown in Figure 5.1, the initial position of the scratch hardness was at the bottom-left corner of the scratch area and then moved in a straight line by 500 nm along the y axis with a constant normal load and scratch speed. Then the PCD tip detached from the surface, and moved to the bottom position and was translated by 4 nm of x axis. These movements were repeated for 125 times for 1 cycle in order to create a scratch area of 500×500 nm^2.

The advantage of the scratch method compared to the nano-indentation in terms of the determination of the thin layer hardness is that the influence of the substrate hardness can be minimized [89]. The hardness of the transformed layer can be directly calculated using the depth of the scratch area (h') that is measured after 1 cycle of the scratch test as shown in Figure 5.2. The scratch hardness is commonly defined as a normal load per one half of the projected contact area by a single line scratch [90, 91]. In this experiment, the scratch test was done in area, a. So, the effective contact was defined as only one quarter of the vertically projected area.

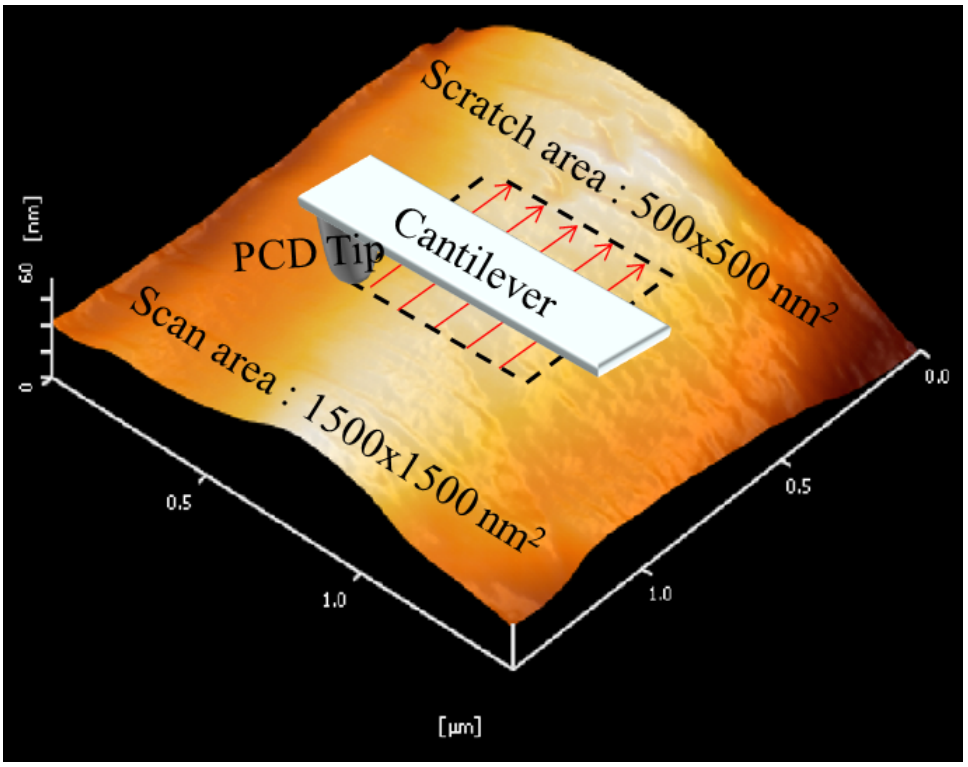

FIGURE 5.1: Schematic diagram of scan and nanoscratch test area at worn surface of DLC coating after friction test.

Figure 5.2 shows the schematic diagram of the nano-scratch test. The appropriate scratch hardness H formula that was used to calculate the hardness of the transformed layer is as follows [92].

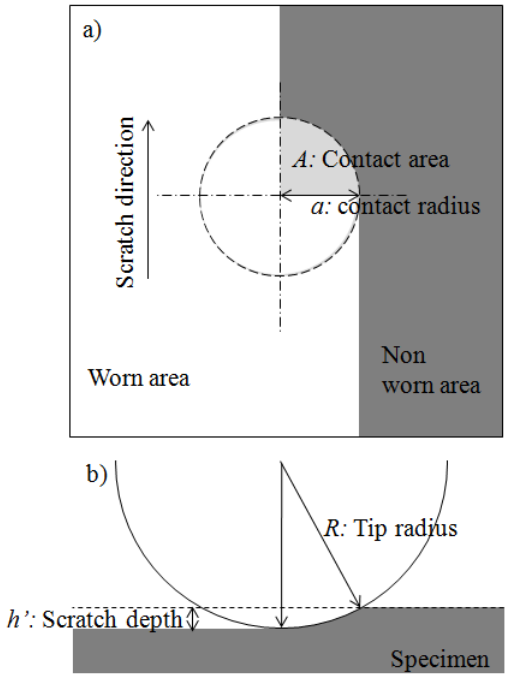

FIGURE 5.2: Schematic diagram of nano-scratch area a) top-view b) side-view.

$$H = \frac{4W}{\pi a^2} = \frac{4W}{\pi(2kRh' - k^2h'^2)} \tag{5.1}$$

$$k = \frac{R - \sqrt{R^2 - \frac{(4W)}{\pi H}}}{h'} \tag{5.2}$$

where W is the scratch test applied load, a is the radius of the projected area of contact, R is the tip radius, k is the correction factor, h' is the scratch depth and H is the hardness of the known material.

The AFM scratch hardness is depend on the stiffness of the PCD tip cantilever that used for scratch test. The correction factor, k can be determine by scratching the known material. This k value is used for calculating the hardness of transformed layer.

5.3 Results and discussion

5.3.1 Raman spectroscopy results

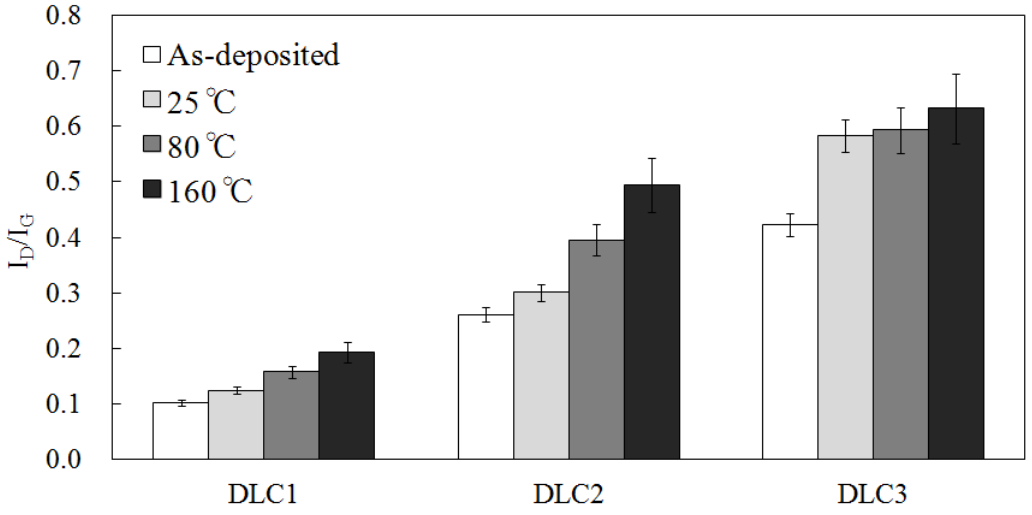

FIGURE 5.3: I_D/I_G ratios by Raman spectroscopy on wear track for each DLC as a function of oil temperature.

Raman analysis is used commonly used to investigate the changes in the DLC structure. The DLC structure can be indicated using Raman spectra by the height of disordered (D) peak near a wavelength of 1380 cm^{-1} and the graphite (G) peak near a wavelength of 1580 cm^{-1} [15]. Figure 5.3 shows the I_D/I_G values of each coating as a function of the oil temperature. Soft DLCs showed higher intensities of I_D/I_G ratios compared to harder DLCs. These results are similar to the data reported by other researchers [15]. In addition, all DLCs showed the same trend where the I_D/I_G value tended to increase after the friction test by elevated temperatures. These shows that the phase transition of sp^3 - sp^2 occurred at the topmost sliding interface during the friction test. The higher value of I_D/I_G indicated that more sp^3 transformed into sp^2 through graphitization. Generally, the transition temperatures for DLC coatings are in the range of 300-500 °C. However, according to the Clayperon law, the phase transition temperature of DLC coatings decreases with an increase in the Hertzian's contact stress. The phase transition of DLC could be reduced to a lower value of 100 °C during the sliding test [50]. This shows that the DLC coating surface can be transformed from sp^3 into sp^2 at lower than phase transition temperatures due to increased contact stress during sliding. It suggests that the friction-induced graphitization was responsible for the structural

changes. These surface modifications created a graphite-like transformed layer at the sliding interface.

5.3.2 Dependence of scratch depth on oil test temperature

A scratch test was carried out to investigate the hardness properties of transformed layer of all DLCs after the friction test in different oil test temperatures from 25 to 160 °C. Figure 5.4(a) shows the surface topography after the scratch hardness test on DLC1, DLC2 and DLC3 with different oil temperatures of the friction test. These AFM images showed that an apparent worn area was created after the scratch test. Figure 5.4(b) shows the cross-sectional profile of the worn area. All types of DLCs showed the same behaviour in that the scratch depth increased with increases in oil temperature. The deepest scratch depth for all the DLCs showed at a high oil test temperature with the value of 5.5, 12.7 and 29.2 nm for DLC1, DLC2 and DLC3, respectively. This scratch depth was used later for the determination of the hardness of the transformed layer.

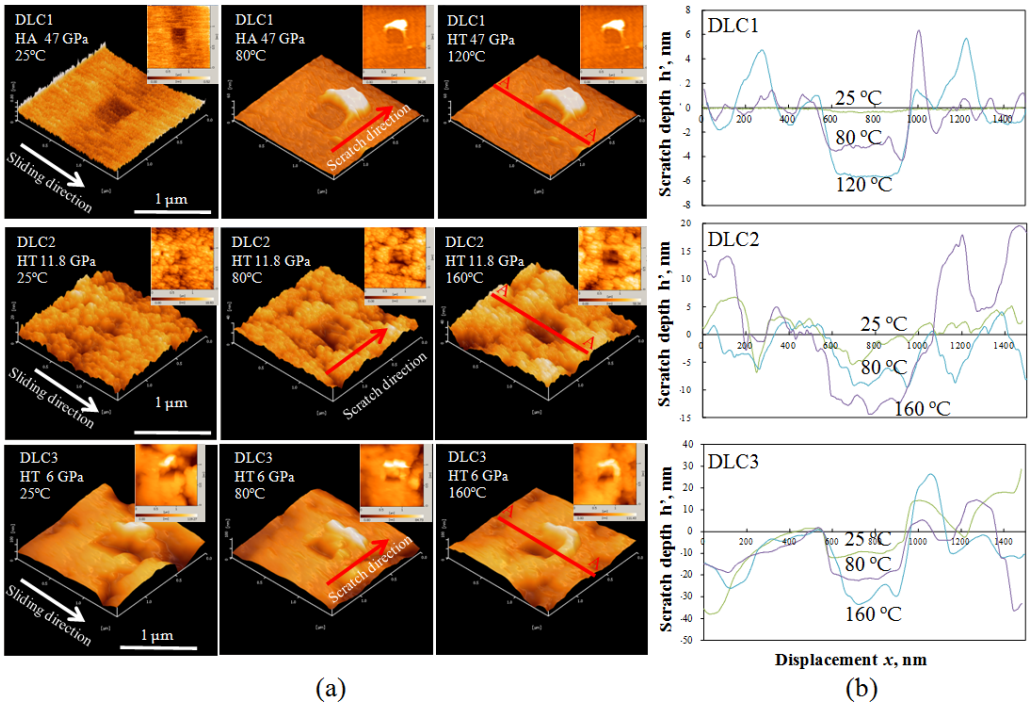

FIGURE 5.4: a) Surface topography after scratch hardness test b) cross-section profile of A-A and wear depth at different oil test temperatures.

In Figure 5.5, the scratch depth values of all the DLCs have been plotted as a function of the oil temperature. The increase in the scratch depth by increasing the oil temperature showed that the DLC coating became softer during the

friction test and was influenced by the oil temperature [37]. As explained in the previous subsection, the structure of the coating at the sliding contact interfaces has transformed the DLC into a graphite-like layer due to the friction-induced graphitization process [50]. The graphite-like transformed layer has a more sp^2 structure compared to the as- deposited DLC. The friction-induced graphitization process softened the contact interface during sliding.

5.3.3 Scratch hardness of transformed layer

The scratch hardness was calculated by Eqs. 5.1 and 5.2 using the applied normal load and the scratch depth. The scratch depth was measured from the cross-sectional profile of the scratch area from AFM as shown in Figure 5.4(b). The scratch hardness results were plotted as a function of oil temperature as shown in Figure 5.6.

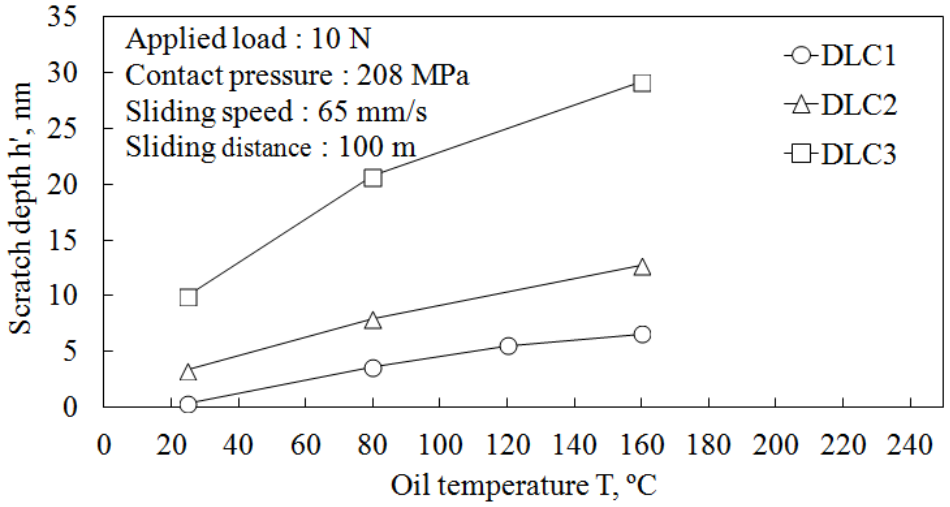

FIGURE 5.5: Scratch depth as a function of oil temperature for DLC1, DLC2 and DLC3.

The result showed a significant decrease in the scratch hardness of the transformed layer compared to the as-deposited DLC by the elevated oil temperature for all types of DLCs. The hardness of the transformed layers was lower than the hardness of the S55C mating material. In addition, the scratch hardness of the transformed layer decreased by increasing the oil temperature. The hardness of the transformed layer of DLC1 showed drastic reduction from the as-deposited coating hardness of 47 GPa to 4.3 GPa at 80 °C. The low hardness of the transformed layer with the sp^2-rich structure provided a low shear strength at the contact interface that influenced the friction behaviour. The lowest scratch hardness of 0.5 GPa was shown by the softest coating (DLC3) at an oil temperature of 160 °C, and the hardest coating (DLC1) showed the lowest scratch hardness of 2.5 GPa at an oil temperature of 160 °C.

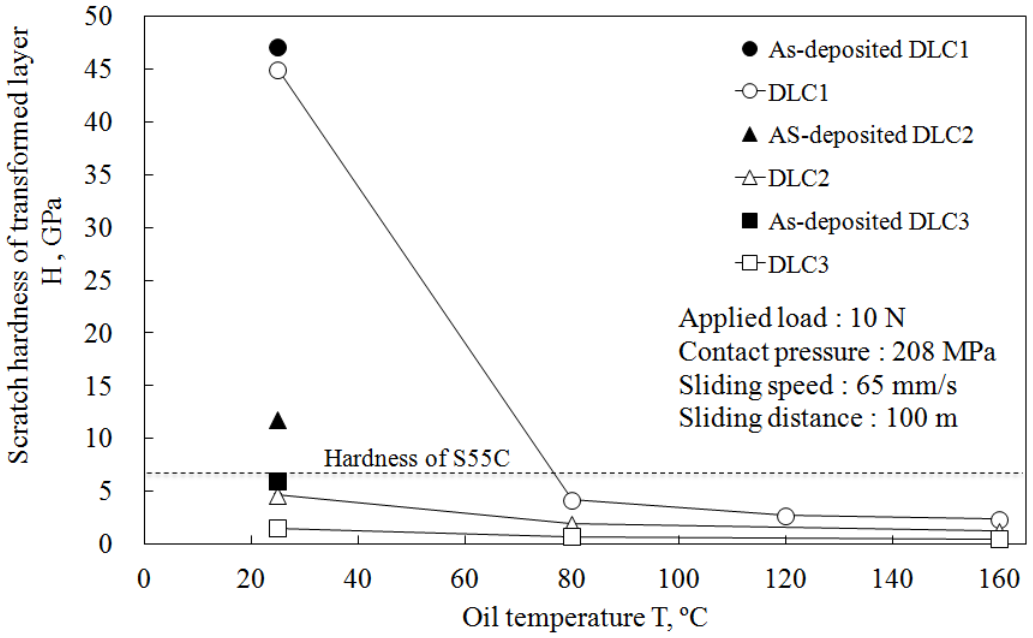

FIGURE 5.6: Scratch hardness as a function of oil temperature for DCL1, DLC2 and DLC3.

5.3.4 Dependence of friction coefficient on the scratch hardness of the transformed layer

The relation between friction coefficient and oil temperatures is discussed in section 3.4. The friction coefficient of DLC1 decreased from 0.05 to 0.03 with an increase in oil temperature. However, the friction coefficient of DLC1 increased from 0.03 to 0.04 when the oil temperature increased from 120 to 160 °C. DLC2 and DLC3 showed the opposite behaviour, where the friction coefficient increased with elevated oil temperatures, and the value was higher than DLC1. From these results, it is difficult to explain why the different hardness of as-deposited DLC showed different friction behaviour.

In order to understand the situation, the friction coefficient was plotted as a function of the hardness of the transformed layer. Figure 5.7 shows the relation between the friction coefficient and the hardness of the transformed layer. This figure can be divided into 3 regions. The first region is the soft transformed layer, where the friction coefficient is high and the value is around 0.08. Then the friction coefficient decreased as the hardness of the transformed layer increased. The lowest friction coefficient of 0.03 was achieved at a moderate hardness of the transformed layer

within the range of 2.8-4.3 GPa. However, any further increment of the hardness of the transformed layer results an increasing in the friction coefficient.

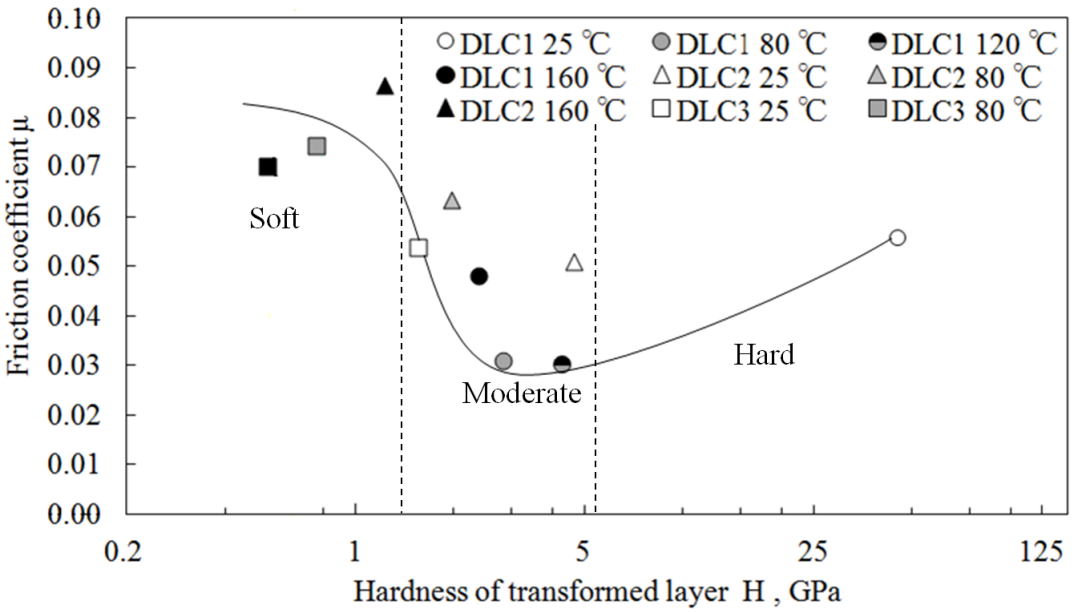

FIGURE 5.7: Friction coefficient as a function of hardness of transformed layer for DLC1, DLC2 and DLC3.

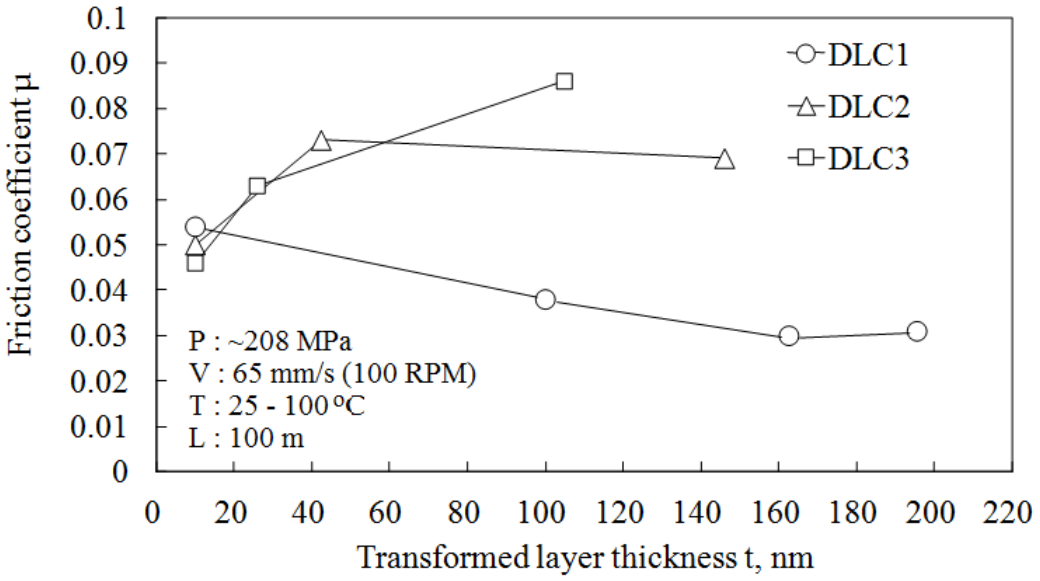

FIGURE 5.8: Friction coefficient as a function of transformed layer thickness.

Figure 5.8 shows the friciton coefficient as a function of transformed layer thickness as reported in Chapter 4. The friction coefficient of DLC1 decreased with an increasing oil temperature. In contrast, DLC2 and DLC3 showed an increasing in the friction coefficient as the oil temperature increased.

Further investigation is needed in order to understand the influence of the thickness and hardness of the transformed layer on the friction behaviour. Therefore, the friction coefficient map as a function of the thickness and hardness of the transformed layer is developed as shown in Figure 5.9. A high friction coefficient in the range of 0.07 - 0.08 is given by the combination LH-TnTL and LH-TkTL. The thickness of the transformed layer did not play a significant role in these combinations because the transformed layer was too soft. It was thought that the high friction coefficient in the soft region was because the asperities of the mating surface could penetrate easily into the transformed layer, and subsequently the mating surface had full contact with hard bulk DLC as shown in 5.10(a). The graphite-like transformed layer did not function as a slippery surface because the direct contact between the mating surface and the bulk DLC controlled the behaviour.

The combination of LH, MH, HH, and Tn gives the friction coefficient in the range of 0.05 - 0.07. In this case, the hardness of the transformed layer did not influence the friction coefficient. Because of the thickness of the transformed layer, the asperities of the mating surface could touch the hard bulk DLC as shown in Figure 5.10(c). The friction between the hard bulk DLC surfaces with the mating surface still provided a high friction coefficient.

The lowest friction coefficient of 0.03 was given by the MH-TkTL combination. Because of its moderate hardness, the transformed layer, could avoid direct contact between the asperities of the mating surface and the hard bulk DLC. Subsequently, the mating surface could smoothly slide on the transformed layer because the graphite-like transformed layer provided a slippery surface.

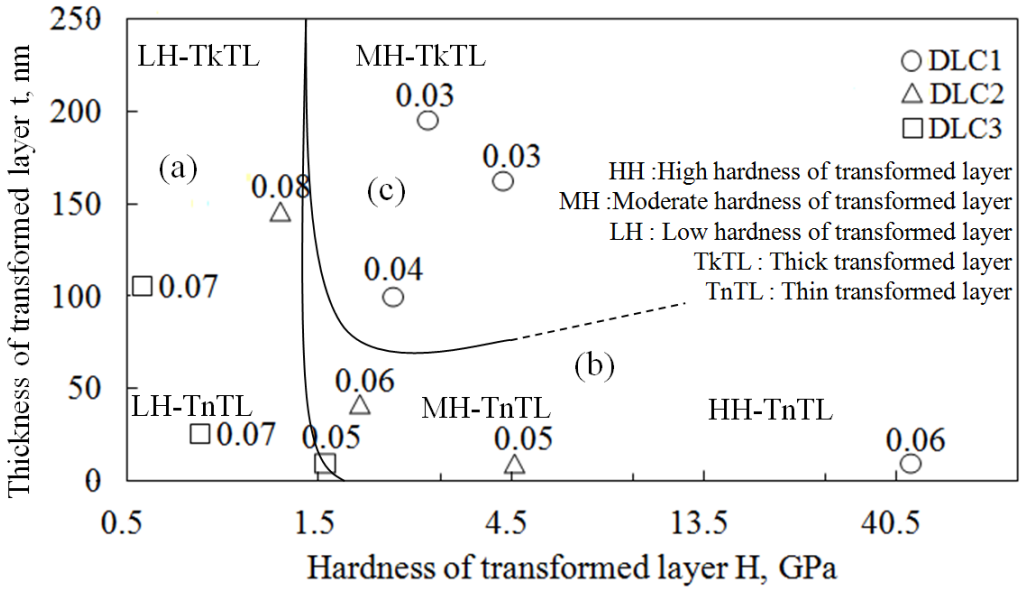

FIGURE 5.9: Friction coefficient map as a function of the thickness and hardness of the transformed layer.

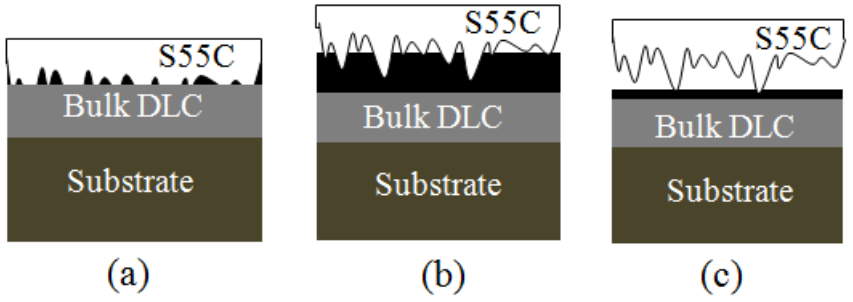

FIGURE 5.10: Friction model regarding the combination of thickness and hardness of the transformed layer. (a) LH-TkTL and LH-TnTL. (b) MH-TnTL and MH-TnTL. (c) MH-TkTL.

5.4 Conclusion

DLC is well known as a coating material that has essential properties for tribological applications due to its low friction coefficient, high hardness and wear resistance. The low friction coefficient that achieved during the friction test was due to the phase transformation of the hard DLC coating into a soft graphite-like transformed layer. This study presented the scratch hardness of the transformed layer was obtained from the AFM scratch test that governs the friction behaviour of DLC. A friction map was also developed as a function of the thickness and hardness of the transformed layer. The following conclusions were reached as follows:

1. The hardness of the transformed layer depends on the oil temperature, where the sliding interface of DLC softened during the friction test due to graphitization.

2. It is suggested that the combination of moderate hardness and thick transformed layer leads to a low friction.

Chapter 6

Conclusion

Carbonaceous hard coatings attract more attention for coating technology especially for tribological components, because of their high hardness, low friction and high wear resistance. Carbonaceous hard coatings can also provide low friction either under dry conditions or boundary lubrication in oil. After the friction test, an ex-situ observation in dry conditions showed that the transfer layer could easily be found on the surface. of the counterpart. This transfer layer is believed to be responsible for the low friction, with the transfer layer acting as a third body and providing a slippery interlayer between the carbonaceous and mating surface. The transfer layer separated the direct contact between the two surfaces and controlled the friction behaviour. Therefore, an in-situ observation was needed to observe the formation of a transfer layer that influenced the friction behaviour under dry conditions. However, no reports exist about in-situ observations of the formation of a transfer layer during friction testing under dry conditions.

However, the transfer layer could not be found on the surface of the counterpart using ex-situ observation after friction, in the case of oil lubrication. The oil would not allow the adhesive bonding of the transfer layer to the counterpart. However, after the ex-situ surface analysis of the carbonaceous coating worn area, the results of a Raman analysis after the friction test, showed that the carbonaceous hard coating structure had changed and was then known as the transformed layer.

This change was due to graphitization, where the structure of sp^3 was converted to sp^2 . The sp^2 rich topmost surface could provide a low shear strength that resulted the low friction. It is believed that due to a lack of oil in the boundary lubrication friction test, the properties of the carbonaceous hard coating topmost

surface (transformed layer) could control the friction behaviour. It is therefore very important to investigate the mechanical properties of the topmost contact interface.

The findings in this work can be summarized as follows:

1. In-situ observation successfully identified the transfer layer generation, which contributed to the friction behaviour of the CNx coating against the sapphire hemisphere. From this study, the following conclusions are as follows:

   (a) The transformation of CNx to graphite-like transfer layer is a consequence of high contact pressure 1.5 GPa at the contact interface.

   (b) The desorption of N content from the CNx coating during sliding was responsible for graphitization.

   (c) The shape of Raman spectra of the transfer layer is comparable with pure graphite.

   (d) Existing of a graphite-like transfer layer with the thickness of 60 nm between the CNx coating and the sapphire hemisphere, will significantly reduce the friction coefficient to an ultra low of 0.003.

   The permanent attachment of a transfer layer at the contact interface is very important to maintain an ultra low friction during the friction test.

2. The tribological properties of different hardness of DLCs sliding against steel under boundary lubrication condition in additive-free mineral-based oil were investigated in order to determine the influence of the as-deposited DLC hardness on friction behaviour. The following conclusions were reached as follows:

   (a) The friction coefficient decreased with an increasing of the hardness of as-deposited DLC.

   (b) The specific wear rate decreases significantly with an increasing in the hardness of as-deposited DLC.

   (c) The formation of graphite-like transformed layer is due to graphitization process during friction test.

3. The thickness of transformed layer of DLC sliding against steel under boundary lubrication condition in additive-free mineral-based oil were successfully measured by using reflectance spectroscopy. From the experimental results, following conclusions are as follows:

   (a) The thickness of the transformed layer has an effect to reduce friction coefficient in the case of DLC1.

   (b) It was observed that the temperature and the sliding distance has a significant effect on DLC1 for generating transformed layer during sliding test.

   (c) The significant decrement of friction coefficient when the t/σ^* value is higher than 1, where t is the thickness of transformed layer of DLC and σ^* is the effective root mean square roughness.

4. DLC is well known as a coating material that has essential properties for tribological applications due to its low friction coefficient, high hardness and wear resistance. The low friction coefficient that achieved during the friction test was due to the phase transformation of the hard DLC coating into a soft graphite-like transformed layer. This study presented the scratch hardness of the transformed layer was obtained from the AFM scratch test that governs the friction behaviour of DLC. A friction map was also developed as a function of the thickness and hardness of the transformed layer. The following conclusions were reached as follows:

   (a) The hardness of the transformed layer depends on the oil temperature, where the sliding interface of DLC softened during the friction test due to graphitization.

   (b) It is suggested that the combination of moderate hardness and thick transformed layer leads to a low friction.

References

[1] Dowson, D., 2nd edition, Professional engineering published limited, London, UK, Tribology Transactions, (1998).

[2] Jost, P., Lubricant tribology, Education and Research Report, London, Department Education and Science, Her Majestry's Stationary Office, (1998).

[3] Taylor, R.I., Improved fuel efficiency by lubricant design: A review, Proceedings of the Institution of Mechanical Engineers, 214J (2000) 1-15.

[4] Fessler, R.R., Fenske, G.R.I., Multiyear program plan: Reducing friction and wear in heavy vehicles, U.S. Department of Energy, Office of Heavy Vehicle Technologies, Workshop Report, Argonne National Laboratory, Argonne, (1999).

[5] Holmberg, K., Andersson, P., Erdemir, A., Global energy consumption due to friction in passenger cars, Tribology International, 47 (2012) 221-234.

[6] Hogmark, S., Progress report on WG3: Tribochemistry, Triboscience and Tribotechnology, Workgroup meeting, Prague, (2005).

[7] Podgornik, B., Vizintin, J., Jacobson, S., Hogmark, S., Tribological behaviour of WC/C coatings operating under different lubricant regimes, Surface and Coatings Technology, 177-178 (2004) 558-565.

[8] Bhusan, B., Introduction to Tribology, John Wiley & Sons, Inc., New York, (2002).

[9] Hainsworth, S.V., Uhure, N., Diamond-like carbon coatings for tribology applications, Int. Mater. Rev., 52 (2007) 153-158.

[10] Stachowiak, G.W., Wear: Materials, Mechanisms and Practice, John Wiley & Sons, Inc., New York, (2006).

[11] Robertson, J., Diamond-like amorphous carbon, Materials Science and Engineering, R: Reports, 37 (2002) 129-281.

[12] Kelly, B.T., Physics of graphite, Applied Science Publishers, London, (1981).

[13] Kelly, B.T., Essentials of materials science, McGraw-Hill, Inc., New York, US, (1976).

[14] Bushan, B., Principles and applications of tribology, John Wiley & Sons, Inc., New York, USA, (1999).

[15] Ferrari, A.C., Robertson J., Interpretation of Raman spectra of disordered and amorphous carbon, Physic Rev. B., 61 (2000) 14095-14106.

[16] Moon, M.W., Jensen, H.M., Hutchinson, J.W., Oh, O.H., Evans, J., Mech. Phys. Solids, 50 (2002) 2355-2365.

[17] Mattox, D.M., Handbook of physical vapor deposition (PVD) processing film formation, adhesion, surface preparation and contamination control, Noyes Publication, (1998).

[18] Erdemir, A., Donnet, C., Modern tribology handbook, Boca Raton, FL., CRC Press, (2000) 871-908.

[19] Bruno, P., Cicala, G., Losacco, A.M., Decuzzi, P., Mechanical properties of PECVD hydrogenated amorphous carbon coatings via nanoindentation and nanoscratching techniques, Surface and Coatings Technology, 180 (2004) 259-264.

[20] Ferrari, A.C., Robertson, J., Pastorelli, R., Beghi, M.G., Bottanii, C.E., Elastic constants of tetrahedral amorphous carbon films by surface Brillouin scattering, Applied Physics Letters, 75 (1999) 1893-1895.

[21] Hu, J., Lieber, C., Yang P., Nitrogen-driven sp^3 to sp^2 transformation in carbon nitride materials, Physical Review B, 57 (1998) 3185-3188.

[22] Liu, A.I., Cohen, M.L., Prediction of new low compressibility solid, Science, 245 (1989) 841-842.

[23] Cohen, M.L., Predicting useful materials, Science, 261 (1993) 307-308.

[24] Wang, D.F., Kato, K., Friction studies of ion beam, assisted carbon nitride coating sliding against diamond tip in water vapour, Wear, 217 (1998) 307-311.

[25] McCann, R., Roy, S.S., Papakonstantinou, P., Abbas, G., McLaughlin, G.A., The effect of thickness and arc current on the structural properties of FCVA synthesised ta-C and ta-C:N films, Diamond Related Materials, 14 (2004) 983-988.

[26] Tokoroyama, T., Goto, M., Umehara, N., Nakamura, T., Honda, F., Effect of nitrogen atoms desorption on the friction of the CNx against Si_3N_4 ball in nitrogen gas, Tribology letters, 22 (2006) 215-220.

[27] Svahn, F., Kassman-Rudolphi, A., Wallen, E., The influence of surface roughness on friction and wear of machine element coatings, Wear, 254 (2003) 1092-1098.

[28] Zhang, W., Tanaka, A., Wazumi, K., Koga Y., Effect of environment on friction and wear properties of diamond-like carbon film, Thin Solid Films, 413 (2002) 104-109.

[29] Erdemir, A., Fenske, G.R., Terry, J., Wilbur, P., Effect of source gas and deposition method on friction and wear performance of diamond-like carbon films, Surface and Coatings Technology, 94-95 (1997) 525-530.

[30] Yoon, E.S., Kong, H., Lee, K.R. Tribological behavior of sliding diamond-like carbon films under various environments, Wear, 217 (1998) 262-271.

[31] Fontaine, J., Donnet, C., Grill, A., LeMogne, T., Tribochemistry between hydrogen and diamond-like carbon films, Surface and Coatings Technology, 146-147 (2001) 286-291.

[32] Fontaine, J., Belin, M., Le Mogne, T., Grill A., How to restore superlow friction of DLC: The healing effect of hydrogen gas, Tribology International, 37 (2004) 869-877.

[33] Donnet, C., Le Mogne, T., Ponsonnet, L., Belin, M., Grill A., Patel V., Jahnes, C., The respective role of oxygen and water vapor on the tribology of hydrogenated diamond-like carbon coatings, Tribology Letters, 4 (1998) 259-265.

[34] Liu, Y., Erdemir, A., Meletis, E.I., Influence of environmental parameters on the frictional behavior of DLC coatings, Surface and Coatings Technology, 93-95 (1997) 363-168.

[35] Liu, Y., Meletis, E. I., Evidence of graphitization of diamond-like carbon films during sliding wear, Journal of Materials Science, 32 (1997) 3491-3495.

[36] Vengudusamy, B., Mufti, R.A., Lamb, G.D., Green J.H., Spikes, H.A., Friction properties of DLC/DLC contacts in base oil, Tribology International, 44 (2011) 922-932.

[37] Kalin, M., Roman, E., Vizintin, J., The effect of temperature on the tribological mechanisms and reactivity of hydrogenated, amorphous diamond-like carbon coatings under oil-lubricated conditions, Thin Solid Films, 515 (2007) 3644-3652.

[38] Khurshudov, A.G., Kato, K., Tribological properties of carbon nitride overcoat for thin-film magnetic rigid disks, Surface and Coatings Technology, 86-87 (1996) 664-671.

[39] Fernandez, A., Fernandez-Ramos, C., Sanchez-Lopez, J.C., Preparation, microstructural characterisation and tribological behaviour of CNx coatings, Surface and Coatings Technology, 163-164 (2003) 527-534.

[40] Qi, J., Chan, C.Y., Bello, I., Lee, C.S., Lee, S.T., Luo, J. B., Wen, S.Z., Film thickness effects on mechanical and tribological properties of nitrogenated diamond-like carbon films, Surface and Coatings Technology, 145 (2001) 38-43.

[41] Kato, K., Umehara, N., Adachi, K., Friction, wear and N_2-lubrication of carbon nitride coatings: A review, Wear, 254 (2003) 1062-1069.

[42] Umehara, N., Tatsuno, M., Kato, K., Nitrogen lubricated sliding between CNx coatings and ceramic balls, Proceedings of the International Tribology Conference, Nagasaki, (2000) 1007-1012.

[43] Miyahira, Y., Tokoroyama, T., Umehara N., Effect of atmosphere gas on ultra low friction properties of CNx coating, The Japan Society of Mechanical Engineers, (2010) 1116-1120 (In Japanese).

[44] Chromik, R.R., Baker, C.C., Voevodin, A.A., Wahl, K.J., In situ tribometry of solid lubricant nanocomposite coatings, Wear, (2007) 1239-1252.

[45] Wahl, K.J., Chromik, R.R., Lee, G.Y., Quantitative in situ measurement of transfer film thickness by a Newton's rings method, Wear, 264 (2008) 731-736.

[46] Johnson, K.L., Contact mechanics, Cambridge University Press, (1985).

[47] McCulloch, D.G., Merchant, A.R., The effect of annealing on the structure of cathodic arc deposited amorphous carbon nitride films, Thin Solid Film, (1996) 99-102.

[48] Zhou, Z.F., Li, K.Y., Bello, I., Lee, C.S., Lee, S.T., Study of tribological performance of ECR-CVD diamond-like carbon coatings on steel substrates: Part 2. The analysis of wear mechanism, Wear, 258 (2005) 1589-1599.

[49] Haque, T., Morina, A., Neville, A., Kapadia, R., Arrowsmith, A., Effect of oil additives on the durability of hydrogenated DLC coating under boundary lubrication conditions, Wear, 266 (2009) 147-157.

[50] Huu, T.L., Zaidi, H., Paulmier, D., Voumard, P., Transformation of sp^3 to sp^2 sites of diamond like carbon coatings during friction in vacuum and under water vapour environment, Thin Solid Films, (1996) 126-130.

[51] Tokoroyama, T., Umehara, N., Effect of nitrogen atom included in CNx coatings on friction sliding against Si_3N_4 ball in nitrogen gas, International Symposium on Micro-Nano Mechatronics and Human Science, (2007) 568-591.

[52] Liu, Y., Erdemir, A., Meletis, E.I., An investigation of the relationship between graphitization and frictional behavior of DLC coatings, Surface and Coatings Technology, 86-87 (1996) 564-568.

[53] Reich, S., Thomsen, C., Raman spectroscopy of graphite, Philosophical Transactions of the Royal Society of London A., 362 (2004) 2271-228.

[54] Sanchez-Lopez, J.C., Belin, M., Quiro, C., Elizalde, E., Friction mechanisms of amorphous carbon nitride films under variable environments: A triboscopic study, Surface and Coatings Technology, 160 (2002) 138-144.

[55] Scharf, T.W., Singer, I.L., Tribology of diamond-like carbon films: Fundamental and applications, Springer, (2008) 210-237.

[56] Zaidi, H., Robert, F., Paulmier, D., Influence of absorbed gases on the surface energy of graphite: consequences on the friction behavior, Thin solid films, 264 (1995) 46-51.

[57] Kumar, N., Dash, S., Tyagi, A.K., Raj, B., Super low to high friction of turbo static graphite under various atmospheric test conditions, Tribology International, 44 (2011) 1969-1978.

[58] Kovalchenko, A., Ajayi, O., Erdemir, A., Fensk, G., Etsion, I., The effect of laser texturing of steel surfaces and speed-load parameters on the transition of lubrication regime from boundary to hydrodynamic, Tribology Transactions, 47 (2010) 299-307.

[59] Beardsley, M.B., Happoldt, P.G., Kelley, K.C., Rejda, E.F., Socie, D.F., Thermal barrier coatings for low emission, high efficiency diesel engine applications, SAE, 01 (1999) 2255-2265.

[60] Johnson, D.R., Diamond, S., Heavy vehicle propulsion materials: Recent progress and future plans, SAE, 01 (2001) 2061-2070.

[61] Singh, G., Graves, R.L., Storey, J.M., Partridge, W.P., Thomas, J.F., Penetrante, B.M., Brusasco, R.M., Merritt, B.T., Vogtlin, G.E, Aardahl, C.L., Habeger, C.F., Balmer, M. L., Emission control research to enable fuel efficiency, SAE, 01 (2000) 2198-2215.

[62] Kalin, M., Velkavrhand, I., Vizintinand, J., Ozbolt L., Review of boundary lubrication mechanisms of DLC coatings used in mechanical applications, Meccanica, 43 (2008) 623-637.

[63] Semenov, A.P., Khrushchov, M.M., Influence of environment and temperature on tribological behavior of diamond and diamond-like coatings, Journal of Friction and Wear, 31 (2010) 142-158.

[64] Hosfall, R.H., Commercial applications using non-hydrogenated carbon films for industrial uses such as cutting tools and wear components, Proceedings of the 41st Annual Technical Conference, Society of Vacuum Coaters, (1998) 60-65.

[65] Hamrock, B.J., Schmid, S.R., Jacobson, B. O., Fundamentals of fluid film lubrication, CRC Press, (2004).

[66] Fischer-Cripps, A.C., Critical review of analysis and interpretation of nanoindentation test data, Surface and Coatings Technology, 200 (2006) 4153-4165.

[67] Tamor, M. A., Vassell, W.C., Raman "fingerprint" of amorphous carbons films, Journal Applied Physics, 76 (1999) 3823-3830.

[68] Prawer, S., Nugent, K.W., Lifshiz, Y., Lempert, G.D., Grossman, E., Kulik, J., Avigal, I., Kalish, R., Systematic variation of the Raman spectra of DLC films as a function of sp^2:sp^3 composition, Diamond and Related Materials, 5 (1996) 433-438.

[69] Sanchez-Lopez, J.C., Erdemir, A., Donnet, C., Rojasa, T.C., Friction-induced structural transformations of diamond-like carbon coatings under various atmospheres, Surface and Coatings Technology, 163 (2003) 444-450.

[70] Scheibe, H.J., Drescher, D., Alers, P., Raman characterization of amorphous carbon films, Fresenius' Journal of Analytical Chemistry, 353 (1995) 695-697.

[71] Waara, P., Hannu, J., Norrby, T., Byheden, A., Additive influence on wear and friction performance of environmentally adapted lubricants, Tribology International, 34 (2001) 547-556.

[72] Spikes, H., The history and mechanisms of ZDDP, Tribology Letters, (2004) 17-3.

[73] Kalin, M., Dohda, K., Jahanmir, S., Erdemir, A., Vizintin. J., Diamond-like carbon films, Tribology of mechanical systems, NewYork: ASME Press, (2004) 139-156.

[74] De Barros Bouches, M.I., Matta, C., Kano, M., Superlubricity mechanism of diamond-like carbon with glycerol, Coupling of experimental and simulation studies, Journal of Physics: Conference Series, (2007) 89-90.

[75] Sanchez-Lopez, J.C., Erdemir, A., Donnet, C., Rojas, T.C., Friction-induced structural transformations of diamond like carbon coatings under various atmospheres, Surface and Coatings Technology, (2003) 163-164.

[76] Johnston, G.J., Wayte, R., Spikes, H.A., The measurement and study of very thin lubricant films in concentrated contacts, Tribology Transactions, 34 (1991) 187-194.

[77] Spencer, E.G., Schmidt, P.H., Joy, D.C., Sansalone, F.J., Ion beam deposited polycrystalline diamond-like films, Applied Physics Letters, 29 (1976) 118-120.

[78] Higuchi, T., Mabuchi, Y., Structure transformation of hydrogen free DLC surface with friction, Proceedings of the JAST tribology conference, Tokyo, (2011) 135-140.

[79] Momozono, S., Nakahara, T., Effects of mechanical properties of solid-like film and substrate, film thickness and roughness parameters on static boundary friction, Proceedings of the 3rd Asia international conference of tribology, Kanazawa, (2006) 85-86.

[80] Dayson, C., The friction of very thin solid film lubricants on surface of finite roughness, STLE Transactions, 14 (1971) 105-115.

[81] De Barros Bouchet, M.I., Martin, J.M., Le-Mogne, T., Vacher, B., Boundary lubrication mechanisms of carbon coatings by MoDTC and ZDDP additives, Tribology International, 38 (2005) 257-264.

[82] Stallard, J., Mercs, D., Jarratt, M., Teer, D.G., Shipway, P.H., A study of the tribological behaviour of three carbon-based coatings, tested in air, water and oil environments at high loads, Surface and Coatings Technology, 177 (2004) 545-551.

[83] Ouyung, J.H., Sasaki, S., Friction and wear characteristics of a Ti-containing diamond-like carbon coating with an SRV tester at high contact load and elevated temperature, Surface and Coatings Technology, 195 (2005) 234-244.

[84] Miyake, S., Tadashi, F., Yasuda, Y., Okamoto, Y., Kano, M., Improvement of boundary lubrication properties of diamond-like carbon (DLC) films due to metal addition, Tribology International, 37 (2004) 751-761.

[85] Liu, Y., Erdemir, A., Meletis, E.I., An investigation of the relationship between graphitization and frictional behavior of DLC coatings, Surface and Coatings Technology, 86 (1996) 564-568.

[86] Ohara, K., Masripan, N.A., Umehara, N., Kousaka, H., Tokoroyama, T., Inami, S., Zushi, K., Fujita, M., Evaluation of transformed layer of DLC after sliding in oil with spectroscopic reflectometry, Tribology International, (2013) in press.

[87] Erdemir, A., Bindal, C., Pagan, J., Wilbur, P., Characterization of transfer layers on steel surfaces sliding against diamond-like hydrocarbon films in dry nitrogen, Surface and Coatings Technology, 76 (1995) 559-563.

[88] Voevodin, A.A., Phelps, A.W., Zabinski, J.S., Donley, M.S., Friction induced phase transformation of pulsed laser deposited diamond-like carbon, Diamond and Related Materials, 5 (1996) 1264-1269.

[89] Beegan, D., Chowdhury, C., Laugier, M.T., Comparison between nanoindentation and scratch test hardness (scratch hardness) values of cooper thin films on oxidised silicon, Surface and Coatings Technology, 201 (2007) 5804-5808.

[90] Ahn, J., Mittal, K.L., MacQueen, R.H., Adhesion measurement of thin films, thick films and bulk coatings, ASTM, 640 (1978) 74.

[91] Thomas, A., Walters, R.P., Wear and scratch hardness of 304 stainless steel investigated with a single scratch test, Wear, 74 (1993) 713-720.

[92] Kimura, H., Tsukiyama, Y., Tokoroyama, T., Umehara, N., Evaluation of mechanical properties of the superficial layer of CNx with ultra low friction in N_2 gas, Transactions of the Japan Society of Mechanical Engineer Series C, 772 (2010) 3794-3799.

Publication lists

[1] **Nor Azmmi Bin Masripan**, Yuki Miyahira, Hidenori Nishimura, Takayuki Tokoroyama, Noritsugu Umehara, Yoshio Fuwa. Effect of transfer layer on ultra low friction of CNx coating under blowing dry Ar. Triboligy Online,
8,3 (2013) 219-226.

[2] **Nor Azmmi Bin Masripan**, Kenji Ohara, Noritsugu Umehara, Hiroyuki Kousaka, Takayuki Tokoroyama,Shigeru Inami, Koji Zushi, Masahito Fujita Hardness effect of DLC on tribological properties for sliding bearing under boundary lubrication condition in additive-free mineral base oil.
Tribology International, (2013) in press.

[3] Kenji Ohara, **Nor Azmmi Bin Masripan**, Noritsugu Umehara, Hiroyuki Kousaka, Takayuki Tokoroyama, Shigeru Inami, Koji Zushi, Masahito Fujita. Evaluation of the transformed layer of DLC coatings after sliding in oil using spectroscopic reflectometry. Tribology International, (2013) in press.

International Conference

[1] **Nor Azmmi Bin Masripan**, Yuki Miyahira, Hidenori Nishimura, Takayuki Tokoroyama, Noritsugu Umehara, Yoshio Fuwa. Effect of transfer layer on ultra low friction of CNx coating under blowing dry Ar. International Tribology conference Hiroshima 2011, 30 Oct. – 3 Nov. 2011.

[2] **Nor Azmmi Bin Masripan**, Kenji Ohara, Noritsugu Umehara, Hiroyuki Kousaka, Takayuki Tokoroyama,Shigeru Inami, Koji Zushi, Masahito Fujita Hardness effect of DLC on tribological properties for sliding bearing under boundary lubrication condition in additive-free mineral base oil.
39th Leeds-Lyon Symposium on Tribology, 4-7 Sept. 2012, Leeds Trinity University College, Leeds.

[3] Kenji Ohara, **Nor Azmmi Bin Masripan**, Noritsugu Umehara, Hiroyuki Kousaka, Takayuki Tokoroyama, Shigeru Inami, Koji Zushi, Masahito Fujita Evaluation of the transformed layer of DLC coatings after sliding in oil using spectroscopic reflectometry. 39th Leeds-Lyon Symposium on Tribology, 4-7 Sept. 2012, Leeds Trinity University College, Leeds.

NAGOYA UNIVERSITY

Abstract

DEPARTMENT OF MECHANICAL SCIENCE AND ENGINEERING
GRADUATE SCHOOL OF ENGINEERING

Doctor of Engineering

by Nor Azmmi Bin Masripan

In this thesis, we present the effect of surface transformation and transfer layer on the friction of carbonaceous hard coatings. Carbonaceous hard coatings have been used in recent years as coatings for tribological components; especially for vehicles, in order to reduce friction and wear, which consequently increases the life-span and working efficiently of components. Carbonaceous hard coatings are used in many industrial applications, due to their excellent tribological properties of low friction, high wear resistance, and chemical inertness. Another essential advantage of carbonaceous hard coatings is that it provides a low friction coefficient; either under dry conditions or boundary lubrication in oil. This particular advantage has attracted more research to understand the tribological behaviour of carbonaceous hard coatings, as a guideline for future usage. Consequently, we performed two experiments; one in dry and the other in oil conditions. In the first experiment, we investigated the effect of the transfer layer on the ultra-low friction of CNx coating under blowing dry Ar. Meanwhile, the second experiment investigated the effect of the transformed layer, in terms of their thickness and hardness on friction under boundary lubrication, in additive-free mineral-based oil.

In a dry condition, CNx coating can provide a low friction coefficient of 0.003 under blowing Ar, in an ambient environment, with help from the formation of a transfer layer at the sliding interface. Following the friction test, an ex-situ observation showed that the transfer layer could be found easily on the counter part's surface. Therefore, we think that an in-situ observation is needed to observe the formation of the transfer layer that influences the friction behaviour under a dry condition. However, no reports exist about an in-situ observation of the formation of a transfer layer during friction testing in a dry condition. We have developed a new experimental apparatus, based on a ball-on-disc tribometer. We used a transparent sapphire hemisphere ball (α-Al_2O_3) as a counterpart against a CNx coated disc for friction testing. With help of an optical microscope and a CCD camera, images of the formation of a transfer layer can be recorded through the transparent sapphire hemisphere ball during the friction test.

The friction test's results show that the friction coefficient under blowing Ar, decreases from 0.18 to a steady state value of 0.003. An in-situ observation showed that the friction coefficient decreased rapidly, as the transfer layer started to generate at the contact interface. As the thickness of the transfer layer increased to 500 nm, the friction coefficient had a constant value at 0.003. Meanwhile, an ex-situ observation was performed using Raman analysis of the transfer layer, and found the transfer layer structure to be similar to graphite. The results showed that the formation of a graphite-like transfer layer from the CNx coating played an essential role in the low friction mechanism of CNx.

In the other experiment, we performed a friction test of a DLC coated sliding bearing (SUJ2) against an S55C disc under boundary lubrication conditions, in an additive-free mineral-based oil. Since the low friction mechanism under this condition was still unclear, we tried to investigate the low friction mechanism from a different point of view i.e., through the thickness and hardness of the transformed layer through an ex-situ observation. The thickness of the transformed layer was measured on wear track of DLC's coating using reflectance spectroscopy, and the hardness of the transformed layer was calculated using the depth of a scratch test, using Atomic Force Spectroscopy (AFM).

We prepared three types of DLC, which we named DLC1, DLC2, and DLC3, with different hardness's of 47.1, 11.8, and 6 GPa, respectively. The tribological properties of DLCs were investigated using a pin-on-disc tribometer, and friction tests were performed under boundary lubrication conditions, in an additive-free

mineral-based oil, at different oil temperatures of 24, 80, 120 and 160 °C. The experiment's results showed that DLC1 provided the lowest friction coefficient and wear rate of 0.03 and in the order of $10^{-11} mm^3/Nm$,respectively. The transformed layer was found at the topmost surface of DLC coating after the friction test. The pressure-induced graphitization was responsible for the DLCs structure changing from sp^3 into sp^2. The pressure-induced graphitization, which was confirmed by Raman analysis, showed that the value of I_D/I_G increased with increasing oil temperatures.

Reflectance spectroscopy was used to measured the thickness of transformed layer after friction test. In this work, we did find that the friction decreased by increasing the ratio of the thickness of the transformed layer, t and the deviation of roughness, σ^*. It was found that, the friction coefficient decreased significantly when the t/σ^* value higher than 1.

We performed an AFM scratch test to determine the nano characteristics of the transformed layer in terms of its hardness. We found that the hardness of the transformed layer decreased significantly at oil temperatures above 80 °C, compared to the hardness of the as-deposited DLC.

The empirical-based friction model map, which presents the thickness and hardness of the transformed layer, correlated to friction coefficient data in a graphical manner, was able to provide us with information of how the thickness and hardness of the transformed layer influenced the friction's behaviour. The combination of a thick transformed layer (more than 100 nm) and a moderate hardness of the transformed layer (2.8-4.3 GPa) can provide low friction. This combination avoids direct contact between the mating surfaces and the hard bulk DLC. Therefore, the mating surface can slide smoothly on the low shear strength of the transformed layer, without touching the hard bulk DLC.

Acknowledgements

First and foremost I would like to express my heartfelt gratitude to my advisor Professor Noritsugu Umehara. It has been an honor to be his Ph.D. student. He has taught me, both consciously and unconsciously, how good experimental tribology is done. I could not have asked for better role models, each inspirational, supportive, and patient.

I would also like to thank my examiners, Professor Kenji Fukuzawa, Professor Nagahiro Saito, and Associate Professor Hiroyuki Kousaka, who provided encouraging and constructive feedback. I am very grateful for their thoughtful and detailed comments.

This work was collaborate with DAIDO Metal Co. Ltd, and I would like to thank to Mr. Shigeru Inami, Mr. Koji Zushi and Mr. Mashahito Fujita for their generous support.

I owe a debt of gratitude to Associate Professor Dr. Hiroyuki Kousaka, Assistant Professor Dr. Takayuki Tokoroyama, Dr. Yosuke Tsukiyama and Mr. Shinko Senda for their involvement and support in different aspects of my research project, as well as the various group meetings that expanded my understanding.

I owe a special thanks to my research partner, Mr. Kenji Ohara, Mr. Yuki Miyahira, Mr. Hidenori Nishimura and all members from the Advanced Materials and Manufacturings for their invaluable help during laboratory works. I am very happy to be a part of the Umehara Laboratory.

Special thanks to Malaysian government and Universiti Teknikal Malaysia Melaka (UTeM) for financial support under Skim Latihan Akademik Bumiputera (SLAB), without it, my study at Nagoya University, Japan would have not been possible.

I owe a lot to my parents, Masripan Bin Abu and Rokeyah Binti Yasman, who loved me at every stage of my life. There is no enough words to thank for your sacrifice to make my life meaningful.

I am very much indebted to my family, my wife Norazah Binti Amir, daughters Alifah Ilyana and Alifah Raschika, and son Alif Hakim, who supported me in every possible way to see the completion of this work. I love you all so much.

I also thank my friends especially Dr. Mohd. Fadzli Bin Abdollah for providing support and friendship that I needed.

Above all, I owe it all to Almighty ALLAH S.W.T for granting me the wisdom, health and strength to complete my works.

Contents

List of Figures

List of Tables

Chapter 1

Introduction

1.1 Introduction to tribology

The word tribology is combination between *tribo*, "rub" in classic Greek, and $-logy$, "knowledge of ". Widely used as an engineering term since 1966, it is a new discipline in the field of mechanical engineering and materials science correlating to the study of friction, lubrication, and wear [1]. The problem posed by friction when moving heavy objects using the sliding method has challenged mankind for a thousand years. During early tribology history, the Egyptians first used water, and later natural oils as lubricants to reduce friction at the sliding interface in order to move massive stones over great distances for the construction of pyramids. A breakthrough in tribology technology occurred with the introduction of a rolling part such as a wheel and bearing to further reduce friction.

Friction and wear are basic problems in the tribology system due to abrasion on the contact surface of two moving parts leading to a reduction in the lifespan of the tribology component. Friction is defined as a tangential force against the sliding motion of a body in an opposite direction. Wear is the result from the friction process where the greater the friction, the higher the wear. Therefore, in the tribology system, it is essential to separate two relative moving contact surfaces in order to minimize friction and wear. The focus of this study is the application of a liquid as a lubricant at the contact interface.

The demand for tribological technology increased in tandem with industrial growth and this led to the need for a better understanding of its aspects in various areas.

The role of tribology became more significant of late when researches acknowledged the looming problem of an energy crisis in the not too distant future. As such, the onus is on tribologists to increase knowledge in this area and come up with an efficient system that does not lose too much energy to the forces of friction.

1.2 Industrial needs of hard coating

It has been reported that friction, lubrication, and wear have a significant influence on the efficiency and lifespan of mechanical components employed in industries. In the long run, this influence plays a deciding role in the economic development of a nation. The report emphasized that viewing tribology from a scientific and technological perspective is crucial in order to avoid major economic losses [2]. The concern here is not only related to the economy, but also to the environment, as machinery and vehicles with high efficiency will significantly reduce CO_2 emission. It has been acknowledged that the major source of rising CO_2 emission can be traced to cars and trucks [3]. This environmental problem continues to escalate with the increasing demand for transportation which leads to a heightening of the greenhouse effect. Studies revealed that when it comes to transportation, passenger cars are responsible for 45% of total energy use and emissions [4]. The most fundamental part of a car system is the internal combustion engine which converts chemical energy into mechanical energy. The potential energy is generated by the internal combustion engine during the process of fuel burning. This energy is then converted into mechanical power which moves the car. However, part of the energy is diverted towards overcoming the adherent friction in the car system. Friction in the engine and transmission system contributes to about 17% of total energy losses in areas such as the piston assembly, the valve train, and the bearings and seals as reported in [5].

Friction behavior is dependent on whether the lubrication involved is boundary lubrication, mixed lubrication or hydrodynamic lubrication as illustrated by the recognized “Stribeck-curve” shown in Figure 1.1 [6]. However, tribological engine components will experience all three kinds of lubrication conditions because the speed of the engine is constantly changing during driving. Of the three, the one that matters most in the “Stribeck-curve” is boundary lubrication because of its potential for high friction and wear. Boundary lubrication occurs during starts, stops, shock-loads, direction changes, and when the vehicle is moving at a slow

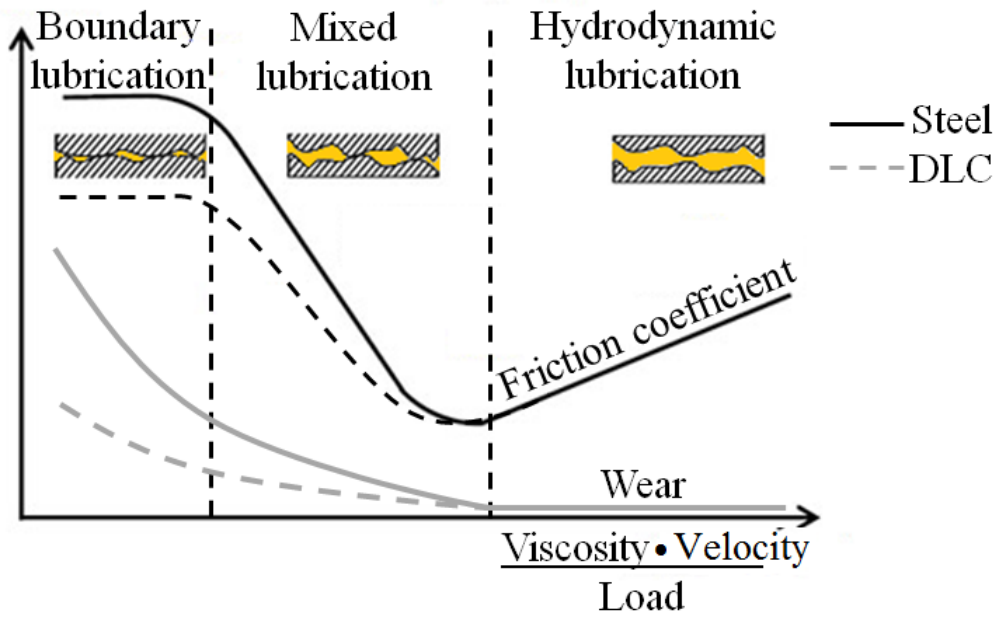

FIGURE 1.1: Possible improvements based on Stribeck diagram by DLC coating application.[6]

to intermediate speed. This can be attributed to the almost complete absence of an oil film between two contact surfaces. The topmost surfaces fully contact each other and the sliding or rolling motion results in high friction. High friction leads to high fuel consumption because the system needs more power to overcome the resistance. At the same time, high friction also causes the component to undergo more wear which culminates in a reduction of its lifespan.

Figure 1.2 shows the number of cycles to failure for material combinations employed for a friction test under boundary lubrication conditions [7]. The combination of DLC-steel displays a significantly longer lifespan of the component compared to a steel-steel and DLC-DLC combination. This result indicates that hard coating can improve the tribological properties of a component in terms of friction coefficient and wear as depicted in Figure 1.1. Tribologists are challenged to come up with a suitable coating material that can improve tribological behavior in terms of low friction and high wear resistance under specific conditions.

Industrial applications that involve tribological components include internal combustion engines for automobiles, material processing, gas turbine engines, rail transportation etc. The coating material selected for a particular application depends on the device and its operating conditions as well as the required performance and lifespan of the component [8]. Some examples on the use of coating

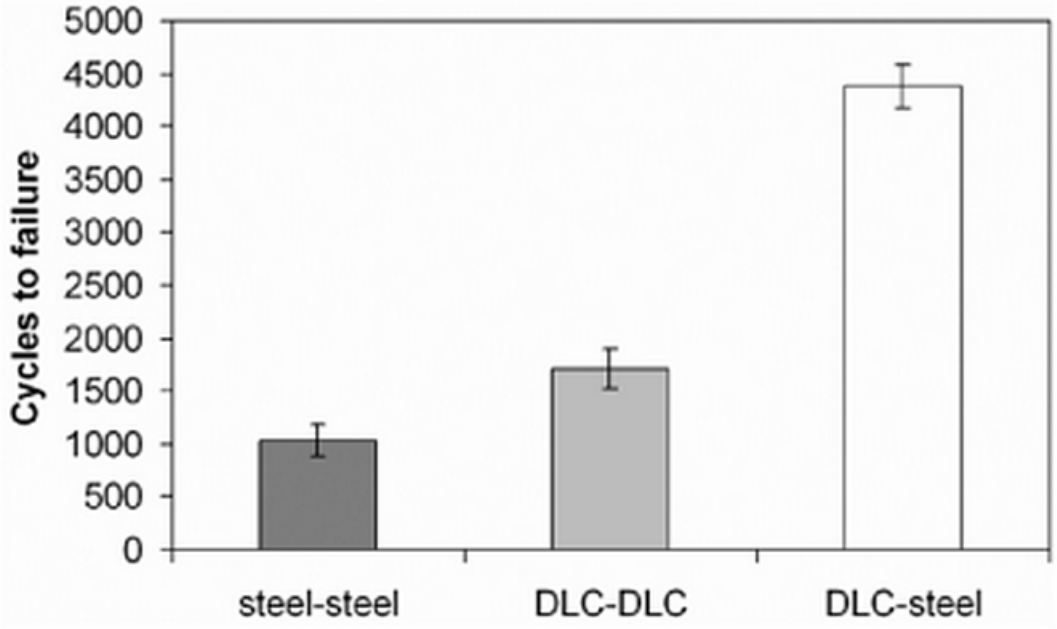

FIGURE 1.2: Cycles to failure for combination of steel-steel, DLC-DLC and DLC-steel under boundary lubrication condition.[7]

technology for increasing the tribological performance of internal combustion engines for automotive applications are shown in Figure 1.3 [9]. Tribological components will experience different contact conditions depending on their application. These conditions include contact stress at normal load, sliding abrasion, impact, surface fatigue, fretting and chemical dissolution. Table 1.1 shows the guideline for coating selection which depends on dominating contact conditions [10].

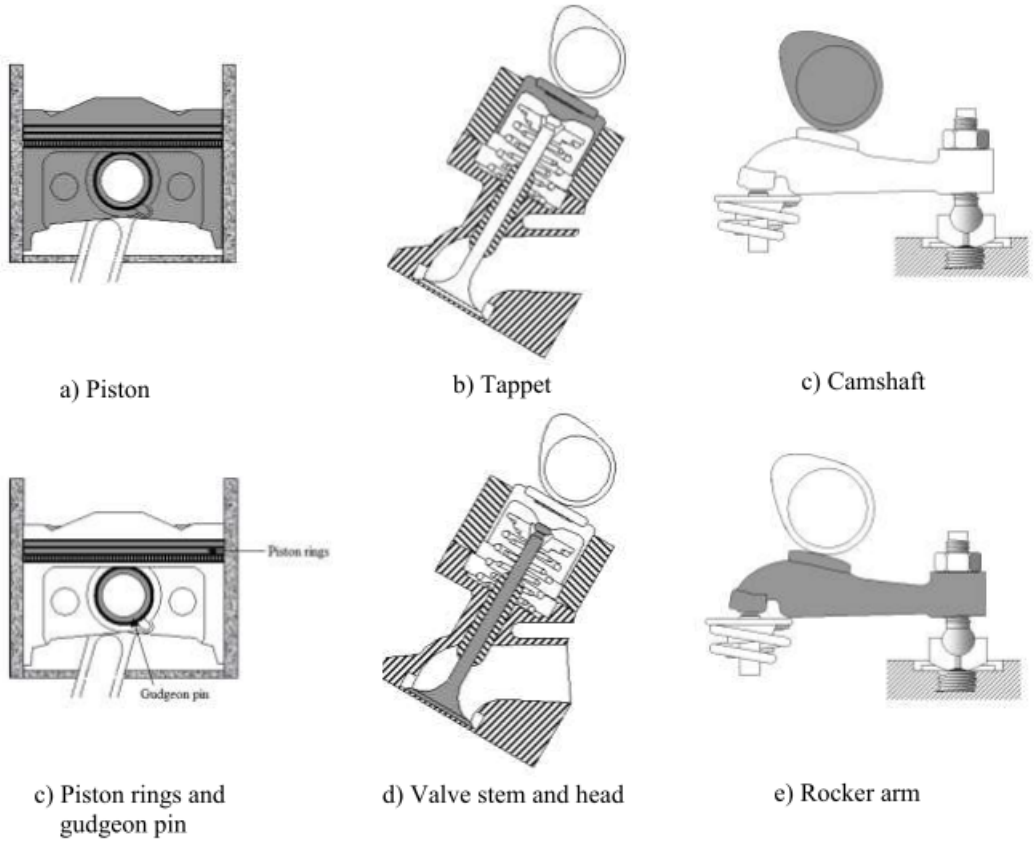

FIGURE 1.3: Components that can be coated with DLC for use in an automotive engine.[9]

TABLE 1.1: Guideline for coating selection.[10]

Contact type	Dominating contact condition	Required surface properties	Recomended coatings
Sliding	Low friction sliding Mild wear	Low shear strength at surface to layer Good load support	DLC, MoS_2, diamond
Abrasion	(a) Third-particle indentations	(a)Good-microtoughness and load support	TiN, TiAlN, TiC, Al_2O_3, CrN
	(b) Two-body ploughing	(b) High hardness to resist plastic deformation	
Impact	Concentrated impacting stress wave Abrasive wear	Good macrotoughness Good elasticity	Multilayer
Fatique	Continuous large stress waves	Good macrotoughness, Good load support	TiN, DLC Multilayer
Fretting	High-frequency large stress wave, Wear debris in contact continuously	Good elasticity, Low shear strength surface layer, Not producing hard wear debris	MoS_2, Cu-Ni-In, Multilayer
Chemical dissolution	High temperature	Non-soluble, Thermally conductive	TiN, TiAlN, TiC, WC, CrAlN, DLC, diamond
Lubricated sliding	Coating giving load support for lubricant film and acting as emergency layer	Interaction with lubricant additives, Texturing to support lubricant prevalence	DLC, TiN, TiC,CrN

1.3 Carbon coatings

Carbon is a unique material which can provide high hardness and good thermal conductivity in the form of a diamond, as well as softness and high lubricity in the form of graphite. Carbon exists in many forms in carbon-based allotropes. These forms include white carbon (ceraphite), nanotubes, buckyballs, other fullerenes, carbon-carbon composites, glassy carbons, and carbon nanofibres. Diamond-like carbon (DLC), carbon nitride, and boron nitride are a few examples of thin coating technology in which carbon, widely used in engineering technology, is the key element. Carbon is the preferred choice due to its outstanding tribological properties which contribute towards the reduction of friction and wear.

Carbon coatings can have different mechanical properties because they consist of sp^3, sp^2 and sp^1 as shown in Figure 1.4 [11]. These combinations can provide a great variety of crystalline and disordered structures. A diamond consists of a sp^3 configuration where four carbon atoms bond with each other to build a tetrahedral structure which in turn makes a strong σ bond to an adjacent atom. These structures provide high mechanical hardness, chemical and electrochemical inertness, and a wide band gap. In the sp^2 configuration, as in graphite, the three of four valence electrons enter trigonally directed sp^2 orbitals. These form σ bond in a plane. The fourth electron of the sp^2 atom enters a $p\pi$ orbital which lies normal to the σ bonding plane [11]. Graphite has a strong intra-layer σ bonding and a weak Van der Waals bonding between its layers [12]. As these layers can be separated and slide easily, the resulting friction is low [13, 14]. In the sp^1 configuration, two of the four valence electrons enter σ, each forming an σ bond directed along the $\pm x$-axis, and the other two electrons enter $p\pi$ orbitals in the y and z directions [11].

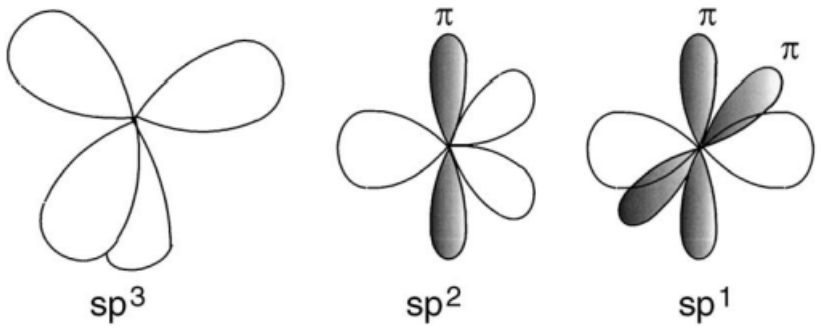

FIGURE 1.4: sp^3, sp^2 and sp^1 hybridised bonding.[11]

1.3.1 Diamond-like carbon (DLC)

DLCs are commonly used as a hard coating in many industrial applications due to their excellent tribological properties of low friction, high wear resistance, and chemical inertness.

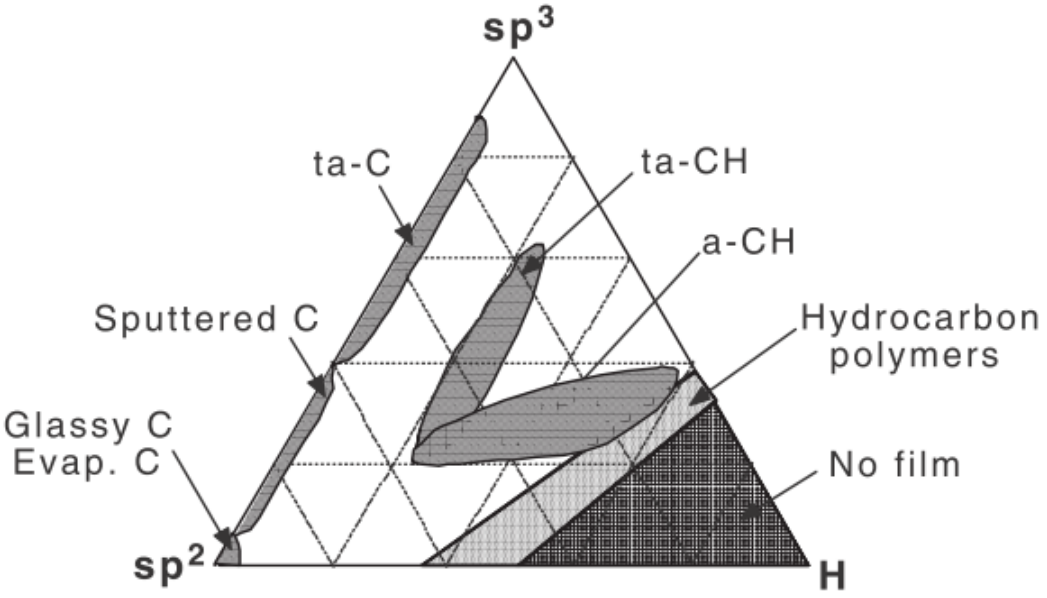

FIGURE 1.5: Ternary phase diagram for various DLC films with respect to their sp^2, sp^3 and hydrogen contents.[15]

Ferrari and Robertson studied the different types of DLCs using spectroscopic techniques to define their structure and chemical content. Figure 1.5 shows the ternary phase diagram by dividing various DLCs into different regions based on the fraction of sp^3 or sp^2 and hydrogen content [15].

Generally, the mechanical and tribological properties of DLCs depend on the sp^3/sp^2 ratio. However, the additional dopant material such as silicon, hydrogen, and metal/carbide, can also contribute different tribological properties to the DLC coating. Examples of diamond-like carbon are hydrogen-free amorphous carbon (a-C), hydrogenated GLC (a-C: H), tetrahedral amorphous carbon (ta-C) and hydrogenated tetrahedral amorphous carbon (ta-C: H). The other types of DLC which contain the dopant elements silicon and metal/carbide will be termed Si-DLC and Me-DLC respectively. Hydrogenated DLC coatings are generally soft with low internal stress. Thus, with good adhesion, it is possible to apply thicker film on the substrate [16]. However, hydrogen-free DLC coatings have a high degree of hardness and consequently high internal stress. As such, it is difficult to

deposit thicker hydrogen-free DLC. Generally, the thickness of hydrogen-free DLC is limited to 1 μm [11].

There are two types of deposition techniques commonly used for deposition of DLC coatings and these are Plasma Vapour Deposition (PVD) and Chemical Vapour Deposition (CVD). The PVD procedure involves atomistic deposition processes, in which material is vaporized from a solid or liquid state in the form of atoms or molecules, and then transported in the form of a vapour through a vacuum or a low pressure gaseous (or plasma) environment to the substrate where it condenses. Typically, PVD processes are used to deposit films with thickness in the range of a few nanometres to thousands of nanometres. Typical PVD deposition rates are 10-100$\mathring{A}$ (1-10 nanometers) per second [17]. There are several types of PVD coating techniques such as vacuum evaporation, sputter deposition (in a plasma environment or in a vacuum), ion plating and Ion Beam Assisted Deposition (IBAD).

Thermal Chemical Vapour Deposition (CVD) is the deposition of atoms or molecules by substantial temperature reduction or decomposition of a chemical vapour precursor which contains the material to be deposited. Deposition at a low temperature is facilitated by the introduction of plasmas into CVD reactors. The plasmas are typically generated by radio-frequency (rf) techniques and the process is called plasma-enhanced CVD (PE-CVD) [17].

The tribological behavior of DLC films differ according to their individual properties. Other factors that can significantly influence the tribological performance of DLC films are test conditions and the environment. The result from a previous study showed that the friction coefficient for various DLCs and test conditions vary widely in a range of 0.001-0.7 [18]. With regard to hardness, the hydrogenated DLCs are generally softer than hydrogen-free DLCs. Table 1.2 displays a few examples of the mechanical properties of various carbon films employing different deposition methods. Soft DLCs scratch easily while DLCs with high hardness possess high wear resistance properties with generally low wear rates of 10^{-11}mm^{3}N^{-1}m^{-1}.

TABLE 1.2: Mechanical properties of various carbon films employing different deposition methods.

Film	Deposition method	H (GPa)	Thickness (nm)
a-c:H [19]	PECVD	14	1140
		18	550
ta-C [20]	FCVA	80	76
ta-C [15]	PLD	27	120
a-C [21]	Sputtering	39	29
		42	46
		85	38

1.3.2 Carbon nitride (CNx)

CNx is also carbon coating material that has very good tribological properties like DLC. It is expected if the CNx can be harder than diamond if the CNx possess the ideal structure of β-C_3N_4 [22, 23]. Table 1.3 displays a few examples of the mechanical properties of amorphous CNx (a-CNX) films employing different deposition methods.

TABLE 1.3: Mechanical properties of CNx films by different deposited method.

Film	Deposition method	H (GPa)	Thickness (nm)
a-CNx [24]	MS	5.6	280
a-CNx [25]	FCVA	65 (high N %)	100
		40 (low N %)	100
a-CNx [26]	IBAD	25	1000

1.3.3 Friction mechanism of carbon coatings

The frictional behavior of carbon coatings can be influenced by intrinsic factors and extrinsic factors. Intrinsic factors come into play when the influence of friction behavior comes from the properties of the coating material itself. These include sp^3 and sp^2 content, the amount of hydrogen present, the doping material involved, and their bonding structure. The influence of frictional behavior from external sources such as chemical reaction and the physical and mechanical interaction during moving contact between two surfaces are defined as extrinsic factors. Both factors play significant roles in the friction and wear mechanisms of carbon coatings.

The effects of physical roughness on DLCs containing dopants like tungsten (a-C:W) and chromium (a-C:Cr) were examined using the ball-on-disk test. The friction coefficient rose from 0.1 to 0.7 with increasing surface roughness R_q of 7 to 390 nm respectively. The friction coefficient was closely related to the surface roughness of the coating as higher roughness contributed to a higher friction coefficient. The higher friction for rougher surfaces could be due to the oxidized particles of coating material filled the scratches. Shearing the oxidized particles

causes a higher friction. It was found that the wear rate for the a-C:W is not dependent on surface roughness. However, the a-C:Cr coating displayed a different behavior with the surface roughness influencing the wear rate [27].

The environmental effect on friction and wear behavior of DLCs was evaluated under four conditions. These conditions were dry air, O_2, N_2 and vacuum. The results revealed that the environment has a significant influence on friction and wear behavior. The N_2 environment exhibited the lowest friction coefficient of 0.06 and a low wear rate $2.2\times10^{-9}mm^3N^{-1}m^{-1}$. The highest friction coefficient of 0.17 was attributed to the vacuum environment, and the lowest wear resistance of $5.2\times10^{-9}mm^3N^{-1}m^{-1}$ to the O_2 environment [28]. The importance of hydrogen content in DLC films was investigated in an open air and a dry N_2 environment. t was suggested that the low friction mechanism of hydrogenated DLC films is due to the passivation of the dangling surface bonds of carbon atoms by hydrogen [29]. Another study reported that the formation of friction layers at the topmost contact surface of DLCs influences the friction behavior. The generation of friction layers was affected by the testing environment [30].

DLC is hybridized structure that containing sp^3 and sp^2. The graphitization occurred during friction when the sp^3 structure converted into the sp^2 structure due to a friction-induced graphitization mechanism [31–33]. The transfer layer formed on a counterface through the graphitization process provides low shear strength between hexagonal planes in the graphite structure allowing for the possibility of reducing friction to 0.02 [34, 35].

An investigation on the friction properties of DLC/DLC contacts in base oil using 12 different types of DLCs such as a-C:H:W, Si-DLC, ta-C and a-C:H with different mechanical properties was carried out by Vengudusamy et al. They found that the friction properties in this situation depended on the DLC type. The lowest friction of 0.05 was exhibited by ta-C in a boundary lubrication condition. The low friction mechanism in the boundary lubrication was attributed to surface graphitization [36]. The effect of temperature on the DLC performance in base oil was studied by Kalin et al. The lowest friction coefficient was achieved at a high temperature of 150 °C. The Raman analysis clearly showed that graphitization provides a slippery surface and this condition contributes to low friction levels [37].

Nitrogenated DLC or Carbon Nitride (CNx) is widely used as a coating material

in magnetic hard disk applications due to its excellent tribological properties [38–40]. Intensive studies were conducted on these properties in the environments of a vacuum, Ar, N_2, CO_2, O_2 and air against the counter material of Si_3N_4. It emerged that the N_2 environment had a significant effect on friction coefficient with a reading of below 0.01. Blowing dry N_2 gas directly onto the contact interface in an air environment effectively reduced the friction coefficient to about 0.017 [41]. The low friction mechanism was analyzed using an Auger Electron Spectroscopy (AES) and an X-ray Photoelectron Spectroscopy (XPS) where the desorption of N_2 atoms from the top layers of coating led to the CNx structure transforming into a graphite-like structure. This provides a slippery surface that reduces the friction coefficient [26].

1.4 Purpose of this study

Carbonaceous hard coatings can provide low friction either in a dry condition or boundary lubrication in oil. After the friction test, an ex-situ observation in dry conditions showed that the transfer layer could easily found on the counter part's surface. This transfer layer was believed to be responsible for the low friction, with the transfer layer acting as a third body. The transfer layer separated the direct contact between the two surfaces and controlled the friction's behavior. Therefore, in-situ observation was needed to observe the formation of a transfer layer that influenced the friction behavior under dry conditions. However, no reports exist about in-situ observations of the formation of a transfer layer during friction testing under dry conditions.

Consequently, we developed a new experimental apparatus that was based on a ball-on-disc tribometer. We used a transparent sapphire hemisphere ball (α-Al_2O_3) as a counter part for friction testing against a CNx coated disc. With the help of an optical microscope and a CCD camera, images of the formation of a transfer layer were recorded during the friction test. Information from these images was used to determine the thickness of the contact area and the transfer layer. It was possible that the area of the transfer layer could have changed the contact pressure leading to the material properties of the transfer layer. Meanwhile, an ex-situ observation was performed to analyze the transfer layer, wear track, and wear debris, using Raman spectroscopy, SEM, AFM and AES.

However, the transfer layer could not be found on the counter part's surface using ex-situ observation after friction, in the case of oil lubrication. The oil would not allow the adhesive bonding of the transfer layer to the counterpart. However, after ex-situ surface analysis of the carbonaceous coating worn area, using Raman analysis after the friction test, the results showed that the carbonaceous hard coating structure had changed and was then known as the transformed layer. This change was due to graphitization; where the structure of sp^3 converted to sp^2 . Sp^2 rich topmost surface could provide a low shear strength that resulted from the low friction. We believe that due to a lack of oil in boundary lubrication friction test, the properties of the carbonaceous hard coating topmost surface (transformed layer) could control the friction's behavior. It is therefore very important to investigate the mechanical properties of the topmost contact interface. Further analysis of

the transformed layer, in terms of its thickness and hardness, could provide more information about the mechanism of low friction in oil under boundary lubrication.

We used three different hardness's of DLC that were coated on sliding bearings made of steel (SUJ2) as a substrate and a S55C steel disc as a counterpart. Boundary lubrication friction tests were conducted using a pin-on-disc tribometer. An additive-free mineral based oil was used as a lubricant to avoid the influence of any additives on both the friction and wear behaviors of DLC. After the friction tests, the worn area on the DLC coating was examined using Raman analysis, reflectance spectroscopy, and AFM scratch testing. Raman analysis was used during the friction tests to verify the graphitization process that generated the transformed layer at the topmost sliding interface. The thickness of the transformed layer was measured using reflectance spectroscopy. An AFM scratch test was used to determine the hardness of the transformed layer.

From the experimental results of the friction test in dry conditions, we attempted to relate the significant role of the transfer layer formation at the contact sliding interface to the friction behavior of the CNx coating under blowing dry Ar.

For the friction test in boundary oil lubrication conditions, the generation of a thin transformed layer at the topmost sliding interface of the DLC coating could be the main factor for low friction. We investigated the nano characteristics of transformed layer in term of its thickness and hardness. Then, we attempted to propose a friction model of low friction under boundary lubrication conditions in an additive-free mineral based oil.

In summary, the objectives of this study were as follows:

1. To clarify the effect of the CNx transfer layer area on the mating sapphire hemisphere on the friction properties under blowing dry Ar.
2. To clarify the effect of as-deposited hardness of DLC on friction and wear after friction test under boundary lubrication conditions in an additive-free mineral based oil.
3. To clarify the effect of the transformed layer's thickness on the tribological properties of the sliding bearing under boundary lubrication conditions in an additive-free mineral based oil.
4. To clarify the effect of the transformed layer's hardness on friction under boundary lubrication conditions in an additive-free mineral based oil.
5. To propose friction map and friction model for low friction of carbonaceous hard coatings.

1.5 Outline of dissertation

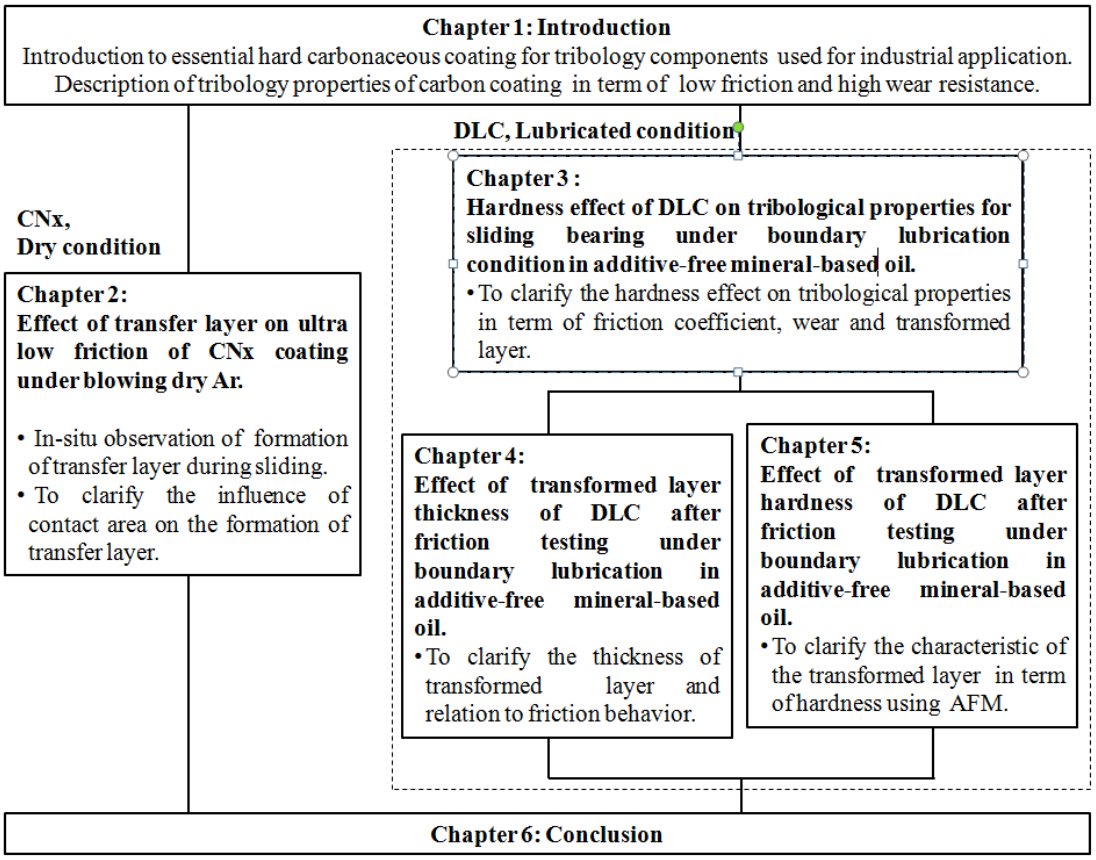

FIGURE 1.6: Outline of dissertation.

Chapter 2

Effect of transfer layer on ultra low friction of CNx coating under blowing dry Ar

2.1 Introduction

Carbonaceous hard coatings are used because those have good tribological properties, such as low friction, high hardness, and high wear resistance. Carbon Nitride (CNx) is expected as excellent materials with excellent tribological properties. CNx is a hybridized material that is composed of sp^3 and sp^2 Carbon-Nitrogen (C-N) bonding. CNx showed ultra low friction that is less than 0.01 of friction coefficient in dry Nitrogen gas [41]. The authors has tried to know the ultra low friction mechanism of CNx on the basis of surface analysis with Raman spectroscopy, XPS and AES because ultra low friction was observed after a number of repeated sliding in dry Nitrogen. As a result, we proposed the ultra low friction mechanism as the formation of thin graphite like layer that thickness is about 20 nm on the surface of CNx, the formation of transfer layer of graphite like wear particles and smoothing of friction surface [42]. However we have done the ex-observation after sliding test. Therefore we do not know the specific effect of the formation of transfer layer on the mating surface. In order to overcome this issue, we developed a friction tester with in-situ observation of transfer layer under sliding against a sapphire hemisphere in different species of gas such as Argon (Ar), Nitrogen (N_2) and ambient air.

In the case of ultra low friction under dry nitrogen and dry Argon, friction coefficient decreased with the increasing of the thickness of transfer layer. On the other hand, friction coefficient did not decrease with the increasing of the thickness of transfer layer in the case under ambient gas [43]. These results show the transfer layer from CNx to mating surface has the essential role in the ultra low friction mechanism of CNx.

In this chapter, we investigated the effect of the area of transfer layer on mating sapphire hemisphere on friction properties under blowing Ar gas. There is a possibility that the area of transfer layer can change contact pressure lead to the material properties of transfer layer. In-situ observation of transfer layer formation, and attachment at the sliding contact point, was observed using an optical microscope. Images were captured using a CCD camera. Meanwhile, an ex-situ observation was performed to analyze the transfer layer, wear track and wear debris, using Raman spectroscopy, SEM, AFM, and AES.

2.2 Experimental procedure

2.2.1 Test specimen

The Si(100) wafer disk was coated with a 100 μm thickness of CNx using Ion Beam Assisted Deposition (IBAD) method in this study. Further details of coating procedure can be seen in [26]. The nitrogen content in the CNx is about 10 %. A CNx surface roughness of 0.72 nmRa was measured using AFM. The hardness of the CNx coating was measured at approximately 25.2 GPa using nano indenter, with a maximum indentation load of 20 μN. A transparent sapphire hemisphere, with a radius of 4 mm, a hardness of about 35 GPa, and surface roughness of 30 nmRa, was chosen as a counter face.

2.2.2 Friction test

Figure 2.1 shows a ball-on-disk equipment with in-situ observation of contact point during sliding under blowing Ar gas. An electric motor was used to rotate the CNx coating, which was fixed on a rotatable disk holder, and the sapphire hemisphere was used as a stationary counter face at the upper side. The friction test was performed using the ball-on-disk tribometer, with a sliding speed of 83.8 mm/s, and a sliding track of 6 mm. The experiment was performed under ambient conditions, with room a temperature of 24 °C and a relative humidity of about 26 %. Dry Ar, with a 99.9999 % purity, was used in this experiment. Dry Ar came directly from the gas cylinder to the contact point between the CNx coating and the sapphire hemisphere, with a volume rate of 5 l/min throughout the sliding test. The O_2 content and humidity were measured at sliding interface using TORAY Oxygen Analyzer (LC-750) and Thermo Recorder (TR-72U) in order to clarify the impurities of blowing Ar. A normal load of 0.1 N was applied constantly to the sapphire hemisphere with a leaf spring. The initial mean Herztian's contact pressure was calculated at about 177 MPa, with a contact diameter of approximately 10 μm. The test's specimens were cleaned in an ultrasonic bath in acetone for 15 minutes before and after the friction test, in order to avoid any contamination on the specimen surface during testing and other analysis.

Transfer layer formation phenomena during contact sliding, which was generated by friction between the transparent sapphire hemisphere and the CNx coating,

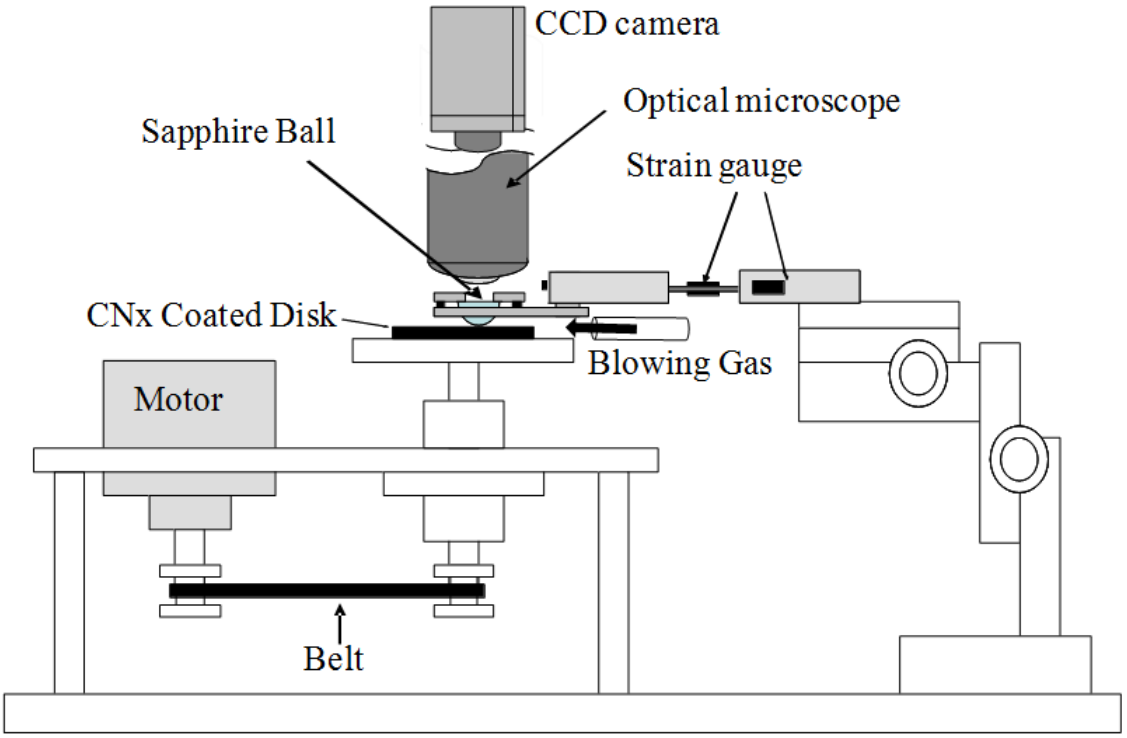

FIGURE 2.1: Test rig based on pin-on-disk method. Combination of optical microscope and CCD camera were used to observe the in-situ frictional behavior CNx coated disk against Sapphire hemisphere.

can be observed with optical microscope using CCD camera, through the sapphire hemisphere. Newton's ring can also be seen in the images and was used to estimate transfer layer thickness during the friction test. Pictures were taken every five cycles for 10,000 cycles.

2.2.3 Estimation of the thickness of transfer layer

The transfer layer thickness can be estimated by comparing the Newton's ring diameter images that were captured during the sliding test with an initial state image. The movement of Newton's ring can be observed during the sliding test. Inward movements of Newton's ring were caused by the elevation of the sapphire hemisphere, which corresponded to the increasing transfer layer thickness. The change of Newton's ring diameter during sliding test can be observed and measured from the images. The use of Newton's ring to quantify transfer layer thickness is given in [44, 45]. Pythagoras' theorem was used to estimate transfer layer thickness, as in Eqs. 2.1 and 2.2 and referring to the schematic illustration of transfer layer formation, as shown in Figure 2.2.

$$h = (X_2 + Z) - (X_1 + Z) \tag{2.1}$$

$$h = \sqrt{R^2 - {r_2}^2} - \sqrt{R^2 - {r_1}^2} \tag{2.2}$$

where h is transfer layer thickness; R is the radius of the sapphire hemisphere; Z is the height between the measured Newton's ring from the contact surface, $y_{1,2}$ are the height between the top of the sapphire hemisphere and the Newton's ring (*1*: before sliding, *2*: during sliding), $r_{1,2}$ are the estimated radius of Newton's ring (*1*: before sliding, *2*: during sliding).

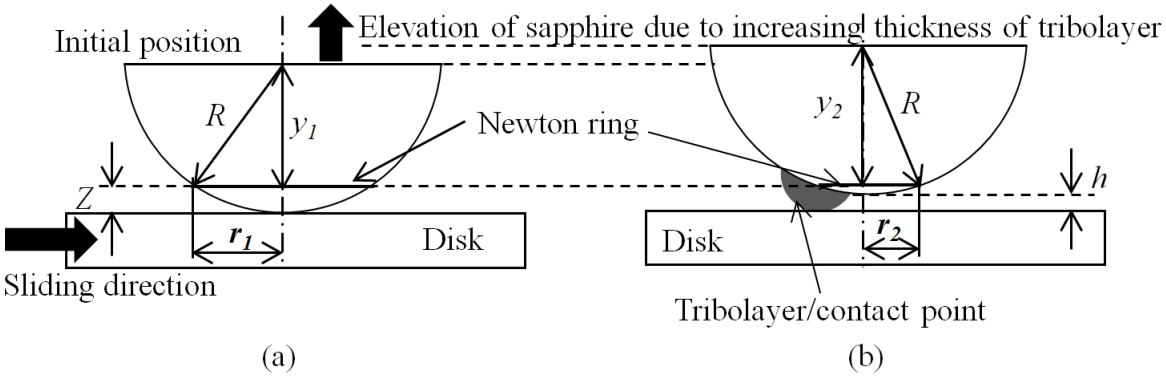

FIGURE 2.2: Schematic illustration ofrelationship between transfer layer and Newton's ring during sliding test for estimation of transfer layer thickness. (a) Initial state and (b) during sliding with the formation of transfer layer.

2.2.4 Raman and AES analyses

The Raman spectra was obtained using a Jasco Laser Raman spectrophotometer NRS-1000 equipped with a second harmonic Nd:YAG laser with a maximum laser power and wavelength of 10 mW and 532 nm, respectively. However, only 1% of the maximum power was applicable for the measurement without burning the surface and also to avoid the influence of the substrate underneath. The AES (ULVAC PHI-650) was used to obtain the depth profiles of chemical composition of test specimen with beam energy of 5 kV and a probe current of 100 nA. Before the measurement, the test specimen surface was cleaned by ion sputtering with a sputtering energy and a probe current of 3 kV and 25 mA, respectively.

2.3 Results and discussion

2.3.1 Effect of the thickness of transfer layer on friction coefficient

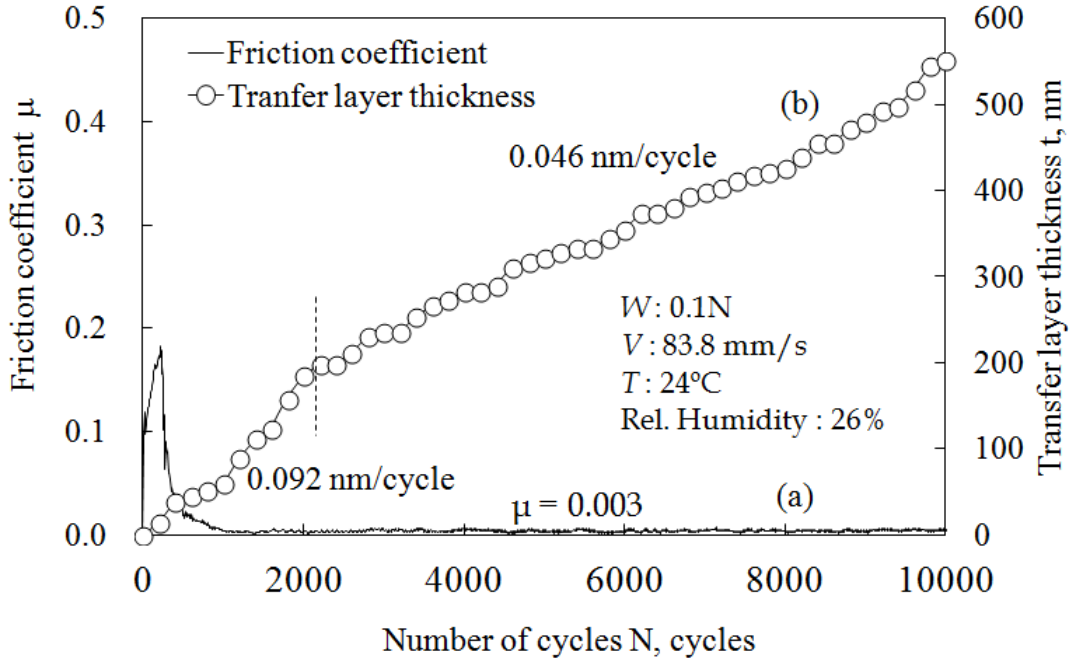

FIGURE 2.3: (a) The frictional behavior of CNx coating against Sapphire hemisphere as a function of sliding cycles and (b) Transfer layer thickness as a function of sliding cycles.

Figure 2.3 shows the coefficient of CNx coating against the sapphire hemisphere during the repeated sliding test under blowing dry Ar, as a function of the number of cycles. At approximately 300 cycles, the friction coefficient increased from 0.1 to 0.18. Then at 1000 cycles, the friction coefficient decreased drastically from 0.18 to 0.003. After a short running-in period, the friction coefficient was consistently ultra low until 10,000 cycles. Figure 2.4 shows images of transfer layer through a transparent sapphire hemisphere in each sliding cycles from 0 to 10,000 cycles.

The other experimental results show that the friction coefficient increased suddenly, due to a detachment of the transfer layer from the contact surface, as shown in Figure 2.5. Later, the transfer layer built-up again at the contact point, and the friction coefficient decreased slowly until it achieved a super low friction again. The images in Figure 2.4 show that the initial real contact point was at the centre (zero cycle), but later it deviated to the front of the sliding direction (400

cycles), where it remained for the rest of the sliding test, as illustrated in Figure 2.2.

Figure 2.4 shows the microscope images of Newton's rings that formed around the contact point of the two surfaces (i.e., the sapphire hemisphere and the CNx coating) with different diameters and light intensities. The Newton's rings were formed due to interference between the light waves reflected from the top and bottom surfaces.

The Newton's ring's diameters were measured and used to estimate transfer layer thickness using Eq. 2.2 from Pythagoras' theorem. The Newton's ring becomes smaller due to the elevation of the sapphire hemisphere corresponding to the formation of a transfer layer at the contact point, as illustrated in Figure 2.2. The results show that the friction coefficient decreased whilst the transfer layer thickness increased. See Figure 2.3(a). In addition, the higher rate of transfer layer generation (about 0.092 nm/cycle) was seen from the beginning of sliding test during the running-in period until approximately 2000 cycles. Then, the transfer layer generation rate became lower (at about 0.046 nm/cycle) from 2000 cycles onwards, and the friction coefficient reached a super low friction of 0.003, where it remained until 10,000 cycles. An ultra low friction of 0.003 was achieved when the transfer layer thickness was around 60 nm after 1000 sliding cycles. The transfer layer thickness increased consistently to 550 nm at 10,000 cycles, whilst the friction coefficient kept constant at super low. The higher rate of transfer layer generation during the running-in period showed that more graphitization occurred then, than the steady state period. This result indicates that more wear debris was produced from sliding at the beginning, due to the direct surface contact between the sapphire hemisphere and the coating disk. The wear debris accumulated at the sliding contact and became a thin transfer layer through compaction. As the transfer layer became thicker, the wear rate of the CNx coating decreased because the transfer layer could act as a protective layer to reduce wear.

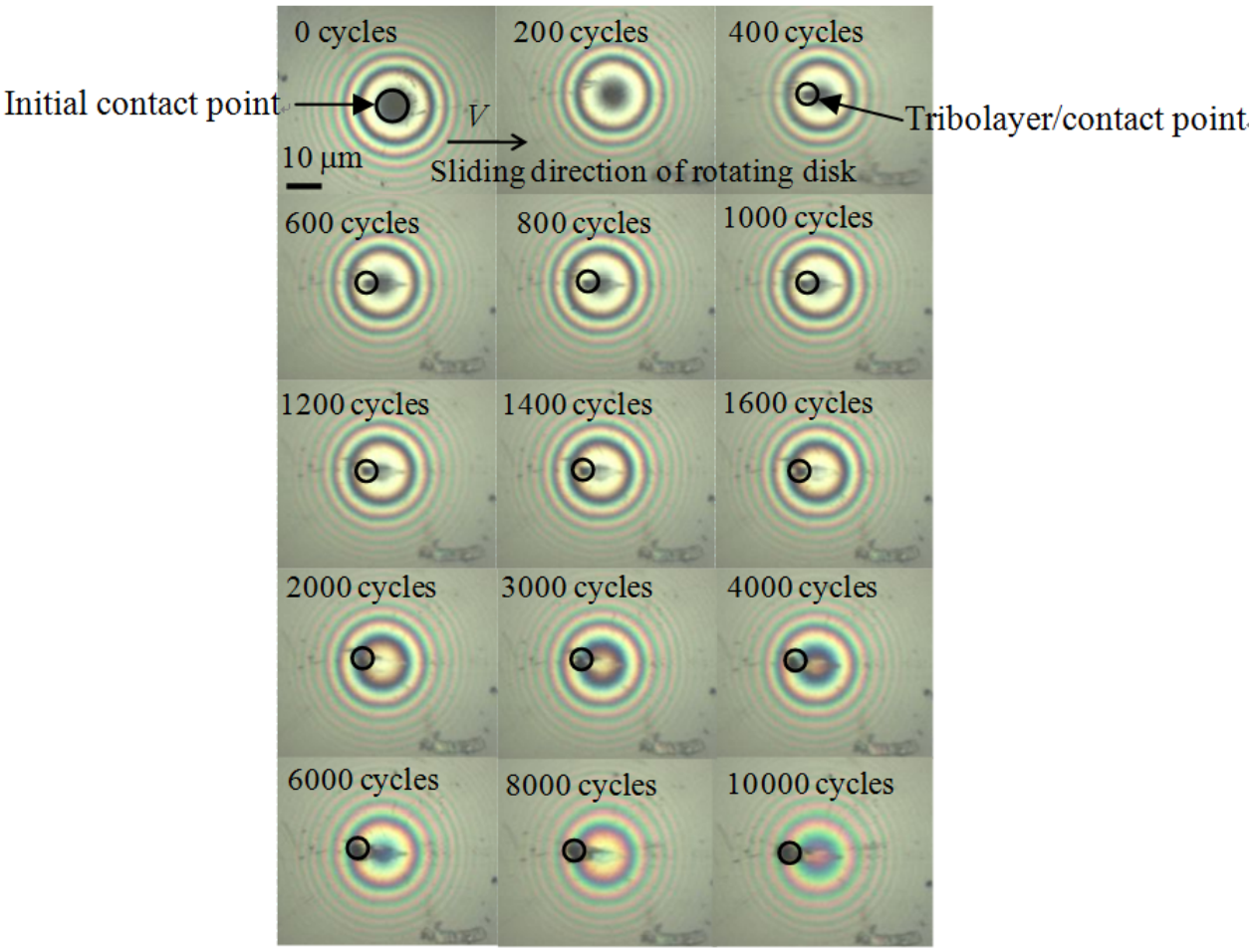

FIGURE 2.4: Microscopic images of Newton's ring and real contact area for estimation of transfer layer thickness and mean Hertzian's contact pressure respectively.

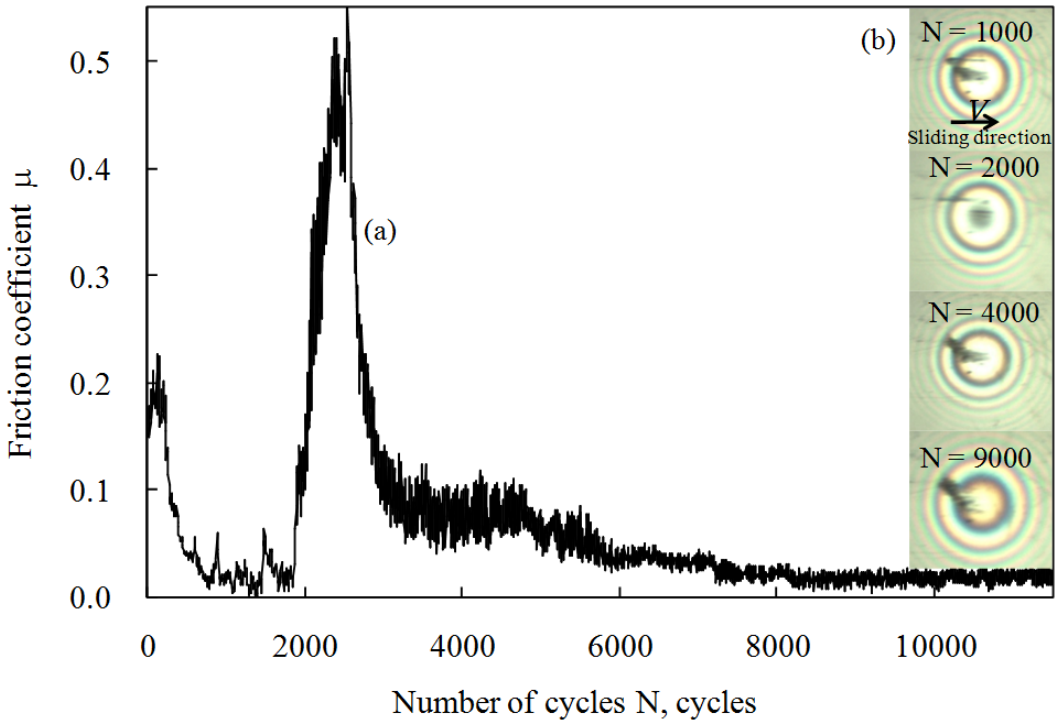

FIGURE 2.5: (a) Sudden increase of friction coefficient during sliding between CNx coatings against Sapphire hemisphere as a function of sliding cycles (b) Images of transfer layer and Newton's ring.

2.3.2 Effect of area of transfer layer and contact pressure on friction coefficient

As shown in Figure 2.4, the initial image of the dark circle at zero cycles shows the direct contact point between the sapphire hemisphere and the CNx coating. At the beginning of friction test, the contact between the sapphire hemisphere and the CNx coating forming the Hertzian's contact as shown in Figure 2.4 at 0 and 200 cycles. However, from 400 cycles of sliding rotation, transfer layer was generated, and the contact point moved from centre to the front side of the sliding direction. At this point, there was no more Hertzian's contact. The accumulation of wear debris at contact interface segregated the direct contact between sapphire hemisphere and CNx coating. The measured contact radius, decreased from 0 to 10000 cycles around 13 μm initially to 4 μm (10000 cycles). The changing contact radii were measured carefully from the captured images using CCD to be used later for the estimation of contact area, A. The measured radius of the Hertzian's contact point was 13 μm at initially state (i.e., zero cycles), which was confirmed by calculating the contact radius of 10 μm using Hertzian's contact mechanics; as per Eqs. 2.3 and 2.4 [46]. The different values, between measured and calculated Hertzian's contact point radii, are due to inaccurate measurements of the contact point using optical images. It is very difficult to obtain accurate value of Hertzian's contact radius by measurement because of the blurring of the contact edge as shown in Figure 2.4 (0 cycles). The difference between the measured contact point radius, r_c and the calculated Hertzian's contact radius, a was within a few micrometers, and are also reported elsewhere [45].

$$a = \left(\frac{3WR}{4E^*}\right)^{1/3} \tag{2.3}$$

where

$$\frac{1}{E^*} = \frac{1-{\upsilon_1}^2}{E_1} - \frac{1-{\upsilon_2}^2}{E_2} \tag{2.4}$$

Here, W is the applied load, R is the sapphire hemisphere's radius, E^* is the effective elastic modulus, υ_1 and υ_2 are the Poisson's ratio of the sapphire hemisphere and the CNx, respectively, and E_1 and E_2 are the Young's modulus of the sapphire hemisphere and the CNx, respectively. A measured contact point radius, r_c was used to calculate the mean pressure P_m using Eqs. 2.5 and 2.6.

$$P_m = \frac{W}{A} \tag{2.5}$$

where,F is the applied load, and A is the estimated contact area.

$$A = \pi {r_c}^2 \tag{2.6}$$

where, r_c is the measured contact radius.

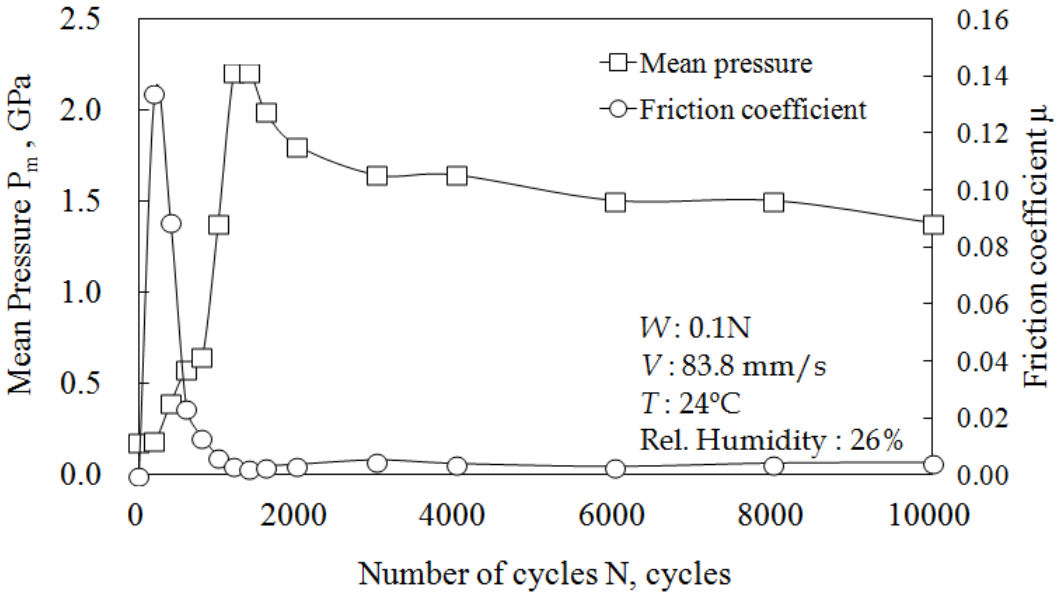

FIGURE 2.6: Relation between mean Hertzian's contact pressure and friction coefficient as a function of sliding cycles.

Figure 2.6 shows the relation between the estimated mean contact pressure and the friction coefficient, as a function of sliding cycles. The contact pressure increased drastically from 0.174 to 2.25 GPa, where the friction coefficient was shown to decrease to a super-low level of 0.003 until 10,000 cycles of rotation. Then, the

contact pressure decreased slowly from 2.25 to 1.5 GPa. The friction coefficient achieved a steady state condition at around 0.003, when the pressure was at a high value of around 1.5 GPa.

Another essential relation shown in this study is how the estimated mean Herztian's contact pressure affects the generation of the transfer layer as shown in Figure 2.7. It was observed that the thickness of transfer layer increase gradually, although the contact pressure slightly decrease after 2000 sliding cycle.

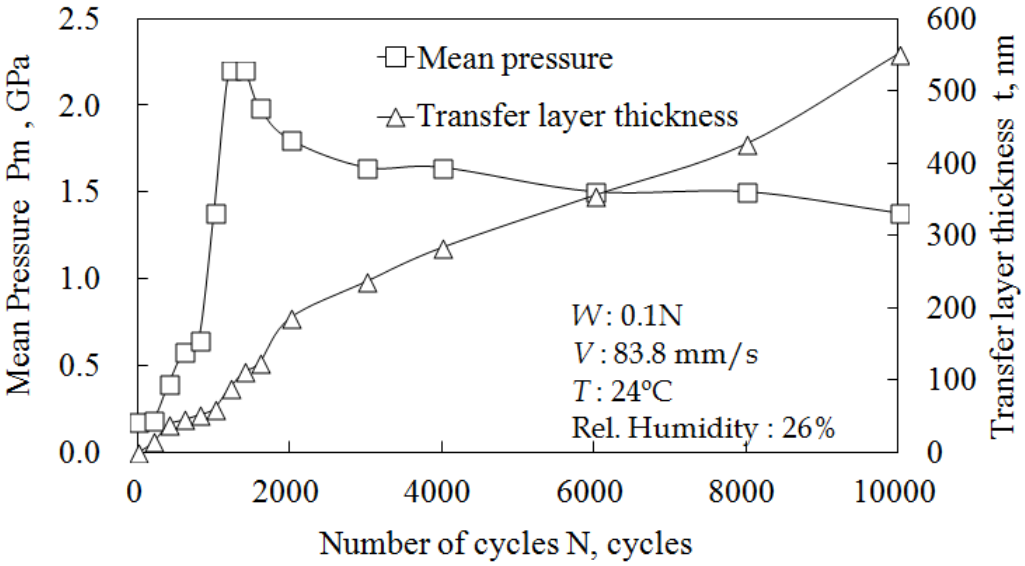

FIGURE 2.7: Relation between estimated mean Hertzian's constant pressure and transfer layer thickness as a function of sliding cycles.

2.3.3 Phase transition of CNx coating at sliding contact interfaces

CNx is a material with a combination of sp^3 and sp^2 carbon bonds, which the nitrogen substitutes into the sp^2-bonded ring to a saturation level of about one nitrogen to every three carbon atoms. This CNx structure provides good tribological properties, such as low friction, high hardness, and high wear resistance. CNx graphitization occurred when desorption of nitrogen atoms from the CNx matrix was caused by raising the annealing temperature. Generally, the transition temperature of CNx is about 200 °C, which corresponds to a sp^3-sp^2 transition temperature [47]. However, during sliding, the transition temperature can be decreased to a lower value, due to the high contact stress [48, 49]. The CNx transition

temperature can be calculated according to the Clapeyron law [50], with the functions of contact pressure and specific volume of low and high nitrogen contents of carbon nitride, as per Eq. 2.7.

$$T = T_c exp\left(\frac{-|\Delta v|}{L}\Delta p\right) \tag{2.7}$$

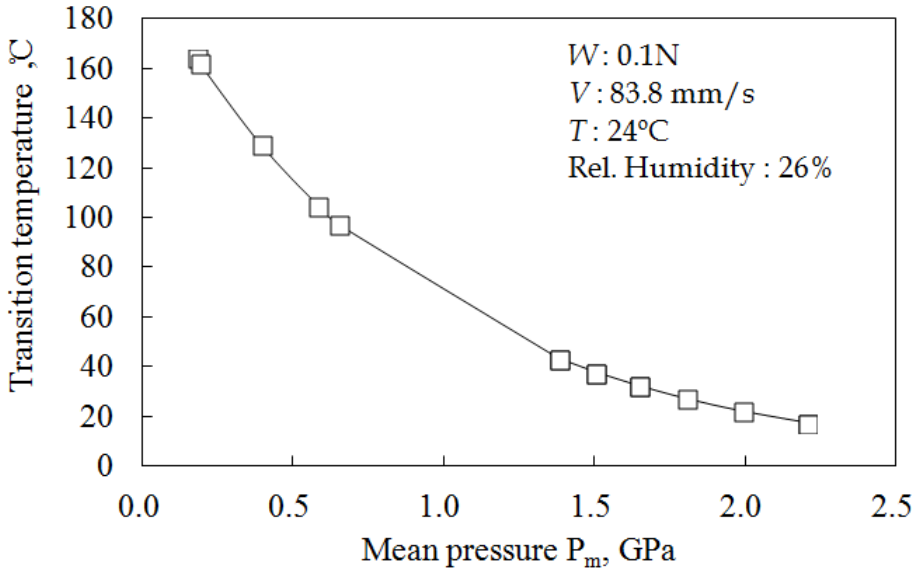

FIGURE 2.8: Calculated transition temperature of CNx coating as a function of Hertzian's contact pressure referring to Clapeyron law.

where T_c is the critical phase transition temperature of CNx (200 °C) [47], Δv is the difference between specific volume of low nitrogen content ($0.303{*}10^{-3}m^3kg^{-3}$) and high nitrogen content ($0.746 * 10^{-3}m^3kg^{-3}$) [21], Δp is the difference between Hertzian's contact pressure and atmospheric pressure. As explained previously, the contact area decreased throughout the sliding test, corresponding to increased contact pressure. Figure 2.8 shows that the phase transition temperature of CNx coatings decreased with an increase of Herztian's contact pressure at the sliding interface. Hence, a high contact pressure results in a lower transition temperature sp^3- sp^3 to as low as 20 °C. This explains that the graphitization process possibly occurred under high contact stress at room temperature, since the experiment was performed under room temperature (about 24 °C).

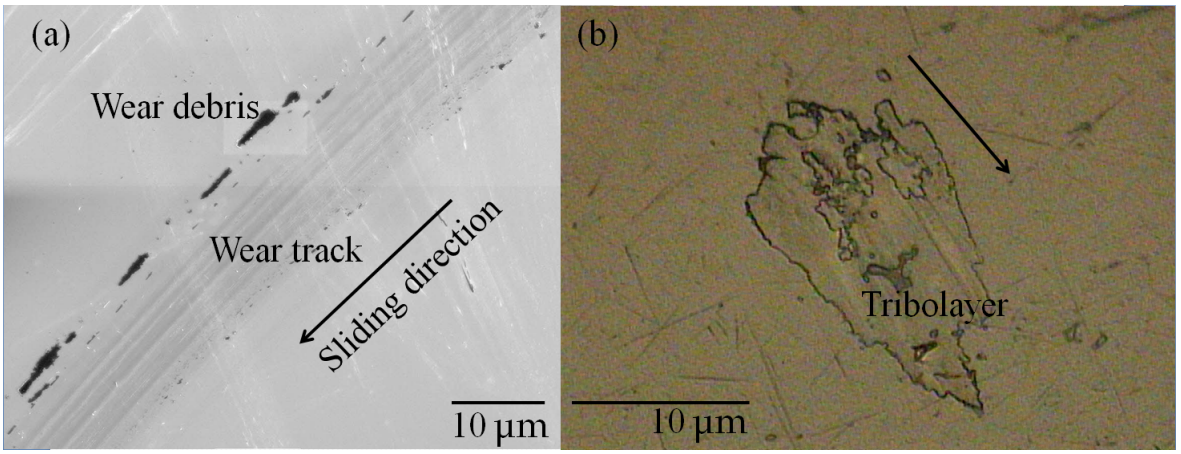

FIGURE 2.9: a) SEM observation of wear track and debris on CNx coating disk after sliding test.(b) Microscopic image of transfer layer on the sapphire hemisphere after sliding test.

2.3.4 Ex-observation of wear track with Optical microscope (OM), Raman spectroscopy and Auger Electron Spectroscopy (AES)

After the sliding test, the CNx coating and sapphire hemisphere was observed using SEM and an optical microscope. Figure 2.9(a) shows a picture of the compacted wear debris along the wear track on the CNx coating after the sliding test. No wear debris was found within the wear track because the wear debris was ejected outside of the wear track during the sliding. The generated transfer layer was transferred from the coating surface to the sapphire hemisphere's surface. The microscope image shows that the transfer layer is strongly adhered to the sapphire hemisphere, as shown in Figure 2.9(b).

Figure 2.10(a)-(d) show the Raman spectra of the as-deposited wear track, the transfer layer, and the wear debris, respectively. The Raman spectra shape, of the as-deposited of CNx, is comparable to other researcher's results [51]. The shape of Raman spectra on the wear track, after the sliding test, was the same as the as-deposited CNx; with the same Raman shift, G peak of 1576.5 1/cm. However, the Raman shifts of the G peak for both the wear debris and transfer layer show a different value of 1588.8 1/cm. This shifting G peak value, from a low to a higher frequency, means that transition of sp^3-sp^2 (also known graphitization) occurred during the sliding test [52].

The Raman shape of the wear debris and the transfer layer is comparable with pure graphite, as reported by other researchers [53]. This means that the graphitic material was removed from the CNx coating's wear track and accumulated as a transfer layer; which then adhered to the sapphire hemisphere and partially became wear debris.

Figure 2.11(a)-(c) show the results for Ar KLL, C KLL, N KLL, and O KLL peaks through AES analysis, between 150 and 550 eV on as-deposited CNx, wear track and wear debris, respectively. The kinetic energy of Ar KLL, C KLL, N KLL, and O KLL were approximately 220, 258, 374, and 510 eV, respectively. The intensity of the N KLL peaks on the wear debris is approximately zero. This means that there was almost no N content in the wear debris compared to the as-deposited CNx, and the wear track. This proves that desorption of N from the CNx coating during sliding was responsible for the graphitization process. Under high pressure stress, the C-N bonds tend to release their N content to become a more stable graphite-like structure [48, 50].

AES analysis does not detect the Ar content on the wear track or the debris after the sliding test. This means that the Ar gas, as an inert gas, was not involved in the tribochemical reaction with the dangling bonds [54]; which probably influenced the tribological performance. Oxygen molecules were not found on the coating surface, both before and after the sliding test. No oxidation process occurred on the coating surface before, during, or after the friction test, that influenced the results of the sliding test and the analysis.

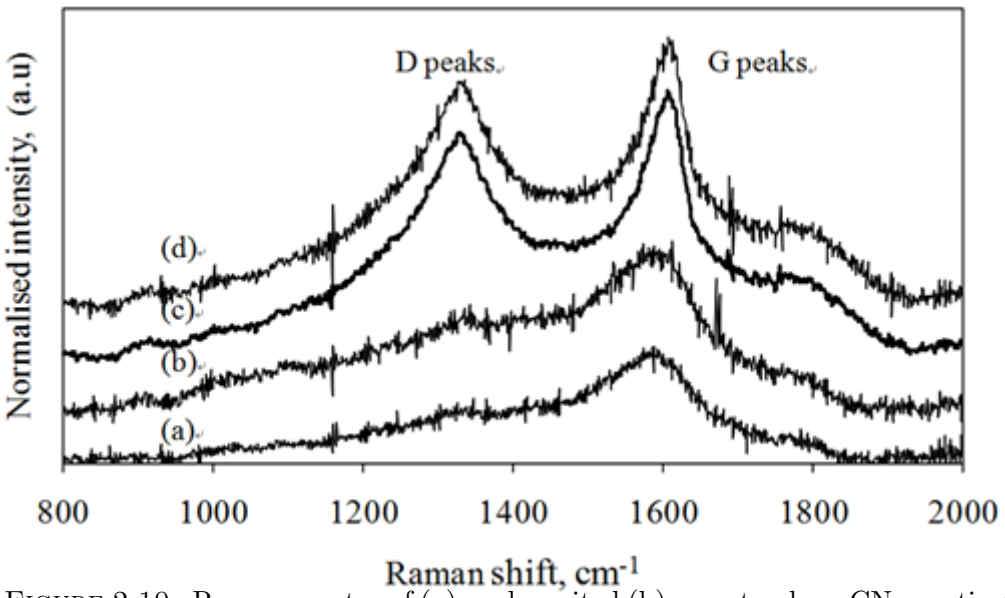

FIGURE 2.10: Raman spectra of (a) as-deposited (b) wear track on CNx coating (c) transfer layer on sapphire hemisphere and (d) wear debris on CNx coating.

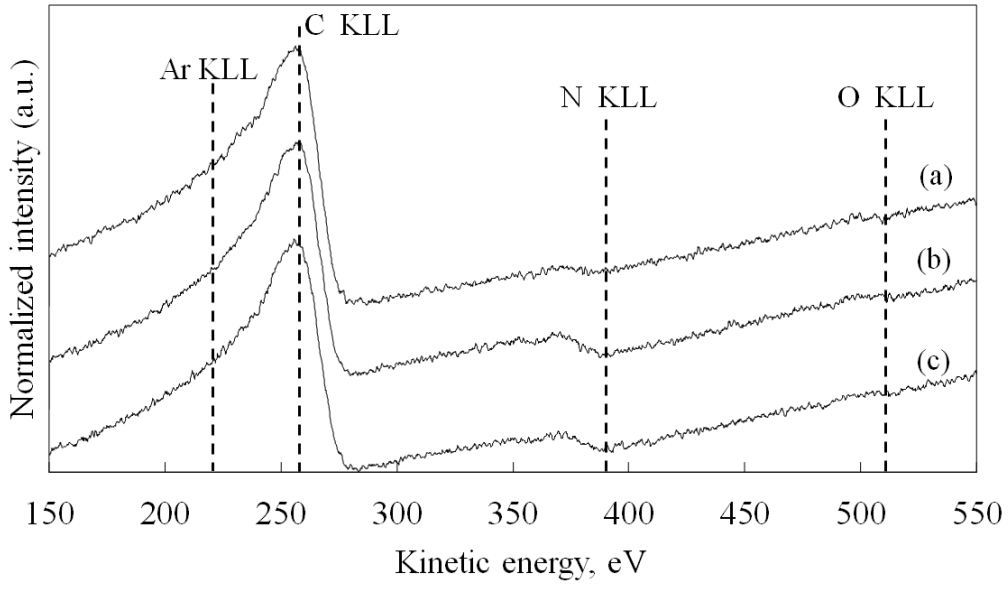

FIGURE 2.11: AES analysis for Ar, C, N and O content on CNx coating (a) as-deposited, (b) wear track and (c) wear debris.

2.3.5 Effect of transfer layer on ultra low friction of CNx coating

An ultra low friction level of 0.003 was observed during the sliding test, between the CNx coatings against the sapphire hemisphere, under blowing dry Ar gas directly onto the contact interface. In-situ observation confirmed that the generation of transfer layer at the contact point was responsible for reducing the friction coefficient to a super low level. It was also observed that the friction coefficient increased at the beginning of the friction test (up to 300 cycles), then the friction coefficient dropped to an ultra-low level of 0.18 to 0.003 at 1000 cycles. Sharp asperities that broke-off at the CNx coating's surface interface, which contributed to the nano particles, caused the increasing friction coefficient at the beginning of the sliding test.

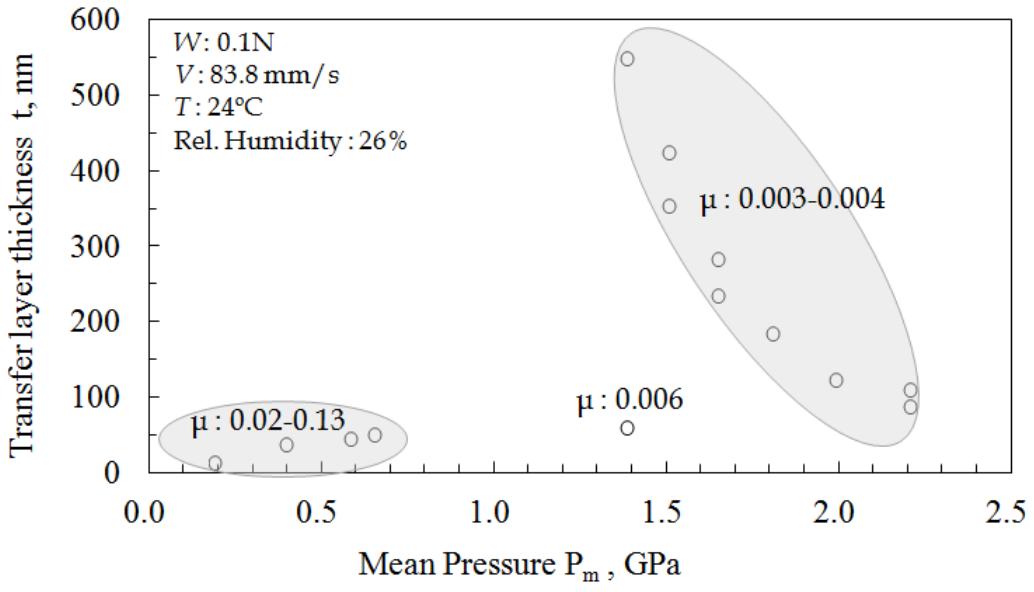

FIGURE 2.12: Relation between the thickness of transfer layer and contact pressure to friciton coefficient.

It is believed that the formation of the transfer layer began after 200 cycles (see Figure 2.4), by the compaction of nano wear particles between the CNx coating and the sapphire hemisphere. Accumulation of the transfer layer at the contact surface completely separated the contact between the CNx coating and the sapphire hemisphere. This provided a steady state value of super low friction between 1000 to 10,000 cycles. The transfer layer thickness was calculated and a significant relation between the friction coefficient and the transfer layer was found, which with a constantly increasing transfer layer, drops the friction coefficient to a lower

level. Super low friction can be achieved at a steady state through a sufficiently thick transfer layer at the contact interface, where it will remain throughout the sliding test. Figure 2.3 shows that a steady state of super low friction of 0.003 was achieved at 1000 cycles, with a sufficient transfer layer thickness of 60 nm. Further consistent increments of the transfer layer do not affect the friction coefficient anymore.

Figure 2.12 shows the relation between the thickness of transfer layer and contact pressure to friction coefficient. It was observed that the thickness of transfer layer below 50 nm, the value of friction coefficient is high in the range of 0.02-0.13. The super low friction achieved in the range 0.003-0.004 when the thickness of transformed layer above than 100 nm. A high contact pressure enhanced the generation of transfer layer at sliding contact interface. The accumulation of transfer layer at sliding interface increased the thickness of transfer layer.

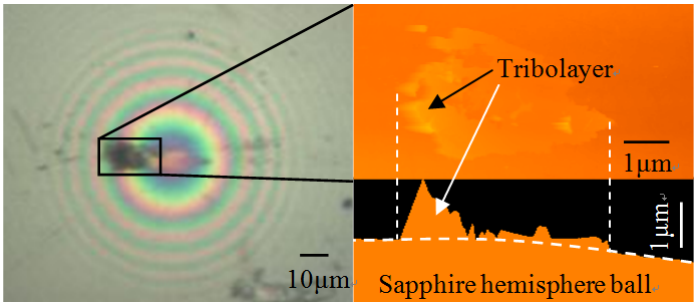

FIGURE 2.13: Microscopic and AFM images of transfer layer on sapphire hemisphere.

Figure 2.13 shows the ex-situ observation of the transfer layer on the sapphire hemisphere using AFM, after the sliding test. The thickness of the transfer layer was measured at approximately 550 nm. This value is comparable with that calculated at the end of the sliding test of 10,000 cycles, as discussed in Section 2.3.1. The transfer layer thickness is much higher than the RMS value of of 30 nm for the CNx coating and the sapphire hemisphere. It is believed that a steady state of super low friction was not influenced further by surface properties, such as the surface roughness of the CNx coatings and the sapphire hemisphere after 1000 cycles, but was fully controlled by the transfer layer; as long as the transfer layer was attached to the contact interface [55]. The Raman spectra of the transfer layer and the wear debris, as shown in Figure 2.10, proved that the transfer layer had graphite-like structures, which contributed to the super low friction during the friction test [56, 57]. AES analysis showed that no Ar molecule was found on the test specimen after the sliding test. As an inert gas, the function of Ar is to

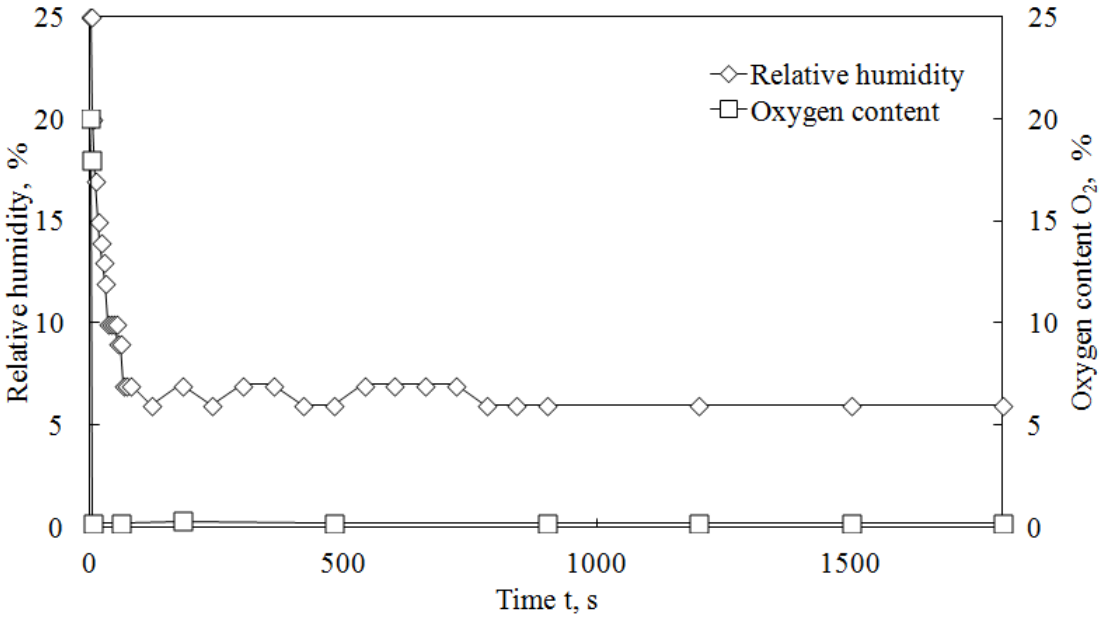

FIGURE 2.14: In-situ observation of relative humidity and oxygen content at sliding contact interface under blowing Ar.

protect accessibility of water and oxygen molecules from the environment to the sliding interface, which subsequently prevents chemical reaction that can cause an increment of friction coefficient [54]. Figure 2.14 shows the in-situ observation of relative humidity and O_2 content at the sliding interface during the sliding test. The relative humidity reduces significantly from 25 to 6 % after 1 minute. In addition, the O_2 content reduced drastically from 20 to 0.2 % after the Ar gas blew directly to the sliding contact interface. The very low value of relative humidity and O_2 was consistent throughout the sliding test. The influence of relative humidity and O_2 on friction coefficient is considered to be small in this experiment. High humidity and oxygen can cause high friction during friction test, as reported elsewhere [43, 54, 57]. As an inert gas, dry Ar gas flowed into the disorderly graphite structure without involving chemical interaction which attributed to the passivation of dangling covalent bonds [54]. This caused the atomic displacements from disorder into inter-lamellar layer of the lattice, which provided a highly slippery layer for super low friction, as reported elsewhere [57]. Since, no transfer layer was attached to the wear track of the CNx coating and the strongly adherent surface of the transfer layer on the sapphire hemisphere, it is suggested that a super low friction mechanism on the CNx coating against the sapphire hemisphere was provided by a low shear strength between the graphite-like transfer layer and the CNx coating.

2.4 Conclusions

In-situ observation successfully identified the transfer layer generation, which contributed to the friction behaviour of the CNx coating against the sapphire hemisphere. From this study, the following conclusions are as follows:

1. The transformation of CNx to graphite-like transfer layer is a consequence of high contact pressure 1.5 GPa at the contact interface.
2. The desorption of N content from the CNx coating during sliding was responsible for graphitization.
3. The shape of Raman spectra of the transfer layer is comparable with pure graphite.
4. Existing of a graphite-like transfer layer with the thickness of 60 nm between the CNx coating and the sapphire hemisphere, will significantly reduce the friction coefficient to an ultra low of 0.003.

The permanent attachment of a transfer layer at the contact interface is very important to maintain an ultra low friction during the friction test.

Chapter 3

Hardness effect of DLC on tribological properties for sliding bearing under boundary lubrication condition in additive-free mineral-based oil

3.1 Introduction

Many methods have been introduced in order to reduce friction and wear or as to increase the life span of mechanical components, and the efficiency of fuel consumption for engines. Surface topography, surface texturing, and the introduction of a lubricant at the contact of moving components have a significant influence on friction and the wear behaviour of engine components [58]. It has been reported that about 17% of energy is used to overcome friction in the engine and transmission system of passenger cars [5]. Thus, a new technology for engine systems is needed to increase fuel economy by introducing low friction materials, coatings, and lubricants [59–61].

Surface coating technology for engine components has been used in recent years under lubrication conditions in order to achieve ultra-low friction and low wear rates. One of the promising coating materials is diamond-like carbon (DLC) which

mainly provides high hardness, chemically inert, low friction and high wear resistance [62]. The tribological behaviour of DLCs depends on their structure, test environment and temperature [63]. High friction and wear occur mainly in a boundary lubrication regime. Although a DLC coating provides low friction and wear in these conditions, however what causes this good performance has not been fully clarified. It is important to understand the behaviour of DLC in terms of the structure changes that take the place in of DLC under these conditions in oil lubricants that have no additives.

In this chapter, we focus on the tribological behaviour of DLC with different hardness as a surface coating against steel as a mating surface under a boundary lubrication regime in an additive-free mineral-based oil lubrication.

3.2 Experimental details

DLC coatings with different hardness were deposited using plasma vapor deposition (PVD) and chemical vapor deposition (CVD) equipment on the same sliding roller of high carbon chrome steel (SUJ2) as the substrate. All the specimens were obtained from outside sources. Hydrogen-free DLC coating (DLC1) with a thickness of 1 μm was produced by an arc-PVD process. The detailed information of the arc-PVD process can be found elsewhere [64]. The Hydrogenated DLC coatings (DLC2 and DLC3) with the thickness of 4 and 10 μm respectively, were produced by a plasma enhanced CVD process . Different hardness was obtained by introducing different RF biases. S55C disks were used as counterpart for the friction test. Table 3.1 shows the mechanical properties of the as-deposited DLC coated sliding bearing and S55C disk.

Table 3.1: Properties of as-deposited DLC coated sliding bearing and disk.

Name	Roughness (R_a, nm)	Deposition method	Thickness (μm)
DLC1	50	PVD (FCVA)	1
DLC2	50	CVD (Plasma assisted CVD)	4
DLC3	50	CVD (Plasma assisted CVD)	10
S55C Disk	20	-	-

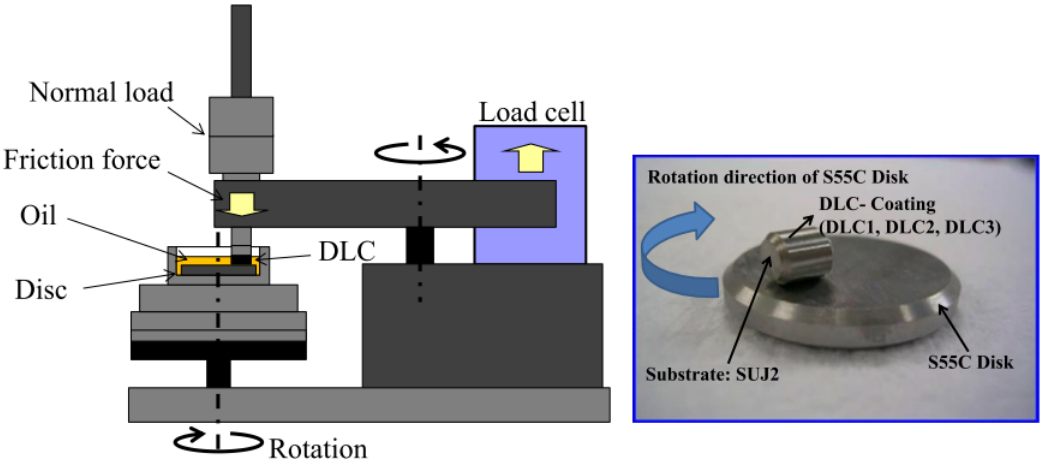

FIGURE 3.1: Schematic illustration of the pin-on-disk type tribometer.

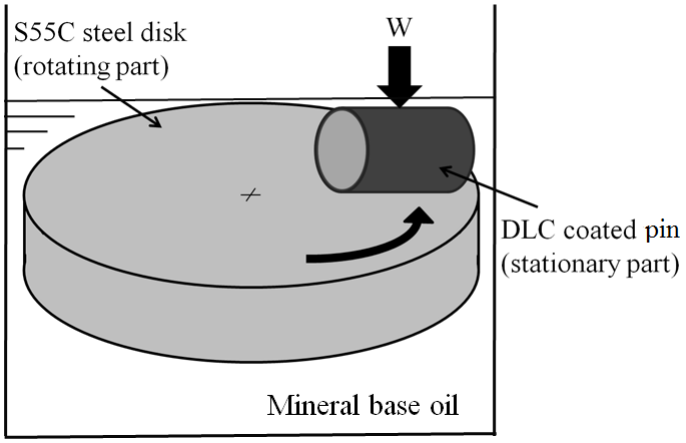

FIGURE 3.2: Schematic diagram of roller on disk friction test.

Pin on disk friction tests were carried out in order to investigate the effect of the hardness of DLC on the friction and wear behaviors under a constant load, W of 10 N (Hertzian's contact pressure of 208 MPa) at different oil temperatures of 25, 80, 120 and 160 °C. Figure 3.1 shows the schematic illustration of the pin-on-disk type tribometer of the friction test. The DLC-coated roller as the stationary part, is loaded in boundary lubrication conditions against a rotating disk of S55C immersed in an additive-free mineral-based oil as shown in Figure 3.2. The additive-free mineral-based oil had a kinetic viscosity of 95.2 mm^2/s (at 40 °C) and 10.8 mm^2/s (at 100 °C). The use of an additive-free mineral-based oil in this experiment enables the observation of the performance on the friction and wear of the DLC coating itself without any influence from the additive in lubricant. A contact load of 10 N was applied to the sliding bearing with a diameter of 4 mm and length of 5 mm during the sliding test with a sliding speed of 65 mm/s. The wear loss of the DLC films was investigated after 100 m sliding distance. The

worn surfaces of the films were observed by using an optical microscope and atomic force microscopy. Before sliding tests, the specimens were cleaned carefully in an ultrasonic bath with acetone solvent for 15 minutes. After the sliding tests, the tested specimens were cleaned in an ultrasonic bath with benzene for 15 minutes in order to remove all oil from the surface.

All the experiments were performed under a boundary lubrication regime where the calculated Λ value was less than unity. The Λ value, which was calculated using the EHL (elastohydrodynamic lubrication) theory, was controlled in the range of 0.07-0.1. The minimum film thickness of the oil and the dimensionless Λ value were calculated using Eqs. 3.1-3.6 [65].

$$h_{min} = 3.63RU^{0.68}G^{0.49}W^{-0.073}(1 - e^{-0.68k}) \tag{3.1}$$

where R is the radius of the roller,

U is the dimensionless speed parameter,

$$U = \frac{V\eta}{E^* R_x} \tag{3.2}$$

where

$$V = \left(\tilde{u}^2 + \tilde{v}^2\right)^{1/2} \tag{3.3}$$

G is the dimensionless materials parameter,

$$G = \xi E^* \tag{3.4}$$

W is the dimensionless load parameter,

$$W = \frac{w_z}{E^* R_x^2} \tag{3.5}$$

$$\Lambda = \frac{h_{min}}{\sqrt{R_{q,a}^2 + R_{q,b}^2}} \tag{3.6}$$

where η is the absolute viscosity at p=0 and constant temperature, E^* is the effective modulus of elasticity, R_x is the effective radius in x direction, $\tilde{u}$ is the mean surface velocity in x direction, $\tilde{v}$ is the mean surface velocity in y direction, ξ is the pressure-viscosity coefficient of the lubricant dependent on temperature and w_z is the normal load component.

The nanoidentation measurement system from Elionix (ENT-1100a) was used to measure the hardness of the as-deposited DLC. All measurements were carried out at a maximum indentation load of 1000 μN. The indentation depth was less than 10% of the thickness of the DLC coating in order to avoid the influence of the substrate material [66]. The structures of DLC coating surfaces were obtained before and after the friction test by using Raman spectroscopy in order to identify the structural changes in the topmost layer of DLC. The Raman spectra were obtained using a Jasco Laser Raman spectrophotometer NRS-1000 equipped with a second harmonic Nd:YAG laser with a maximum laser power and wavelength of 10 mW and 532 nm, respectively. However, only 1% of the maximum power was suitable for the measurement without burning the surface and also to avoid the influence of the steel substrate underneath. Three measurements were taken in order to reduce the uncertainty of the results from fitting the Raman peaks. Spectroscopy ellipsometry from Photal Otsuka Eletronics (FE-3000) was used to measure the thickness of transformed layer after the sliding test. Experimetal details about the measurement of the thickness of transformed layer is explained in the Chapter 4.

3.3 Results and discussion

3.3.1 Correlation between results with Raman spectroscopy and spectroscopic ellipsometry

The low friction coefficient obtained during the friction test is caused by structure changes in the surface of the DLC coating, which corresponds to graphitization. Graphitization during the rubbing was reported in many papers either under oil lubrication conditions [37, 67, 68] or dry conditions [52, 69]. Graphitization can be confirmed from the Raman spectra when the D and G peaks shifted to higher frequencies than the as-deposited DLC, and the intensity of the D peaks increased [37, 67]. The other indicator for graphitization from the Raman spectra is the ratio of I_D/I_G, in which the higher values of the I_D/I_G ratio of the DLC after rubbing compared to the as-deposited DLC mean the transformation of sp^3 to sp^2 [70].

Figure 3.3 shows the Raman shift of the D and G peaks, as well as the I_D/I_G ratios of all the DLCs at the various test temperatures before and afterthe sliding. Figure 3.4 and 3.5 show clearly, the shifting of the D and G peaks to higher frequencies as well as the increasing I_D/I_G values for all kinds of DLCs with increasing test temperatures, which correlate to graphitization. This means that the DLC structure at the topmost of the contact surface transforms from sp^3 to sp^2 and it is dependent on the oil temperature. Consequently, the topmost DLC coating becomes softer due to graphitization compared to the original surface, which results in more mechanical damage and wear [71, 72]. The wear results, indicate that the wear loss increases with increasing oil temperature. This means that the contact surface during rubbing becomes softer at higher temperatures under boundary lubrication conditions than at lower oil temperatures.

Spectroscopic ellipsometry was used to measure the transformed layer on the topmost DLC surfaces after the friction test. Figure 3.6 shows the thickness of transformed layer of all the DLCs at all the test temperatures. All the DLCs showed a significant increment in term of transformed layer thickness, where the thickness increases with increasing oil temperature. DLC1 shows the highest thickness 195 nm in the transformed layer at oil temperature of 120 °C. The thickness of transformed layer of DLC2 and DLC3 at oil temperature of 160 °C are 146 and 104 nm, respectively. The correlation between the D peaks from the Raman spectra and

transformed layer thickness from spectroscopic ellipsometry are shown in Figure 3.7. All the DLCs show the same trend, where the thickness of transformed layer increases with an increase in the intensity of the D peak.

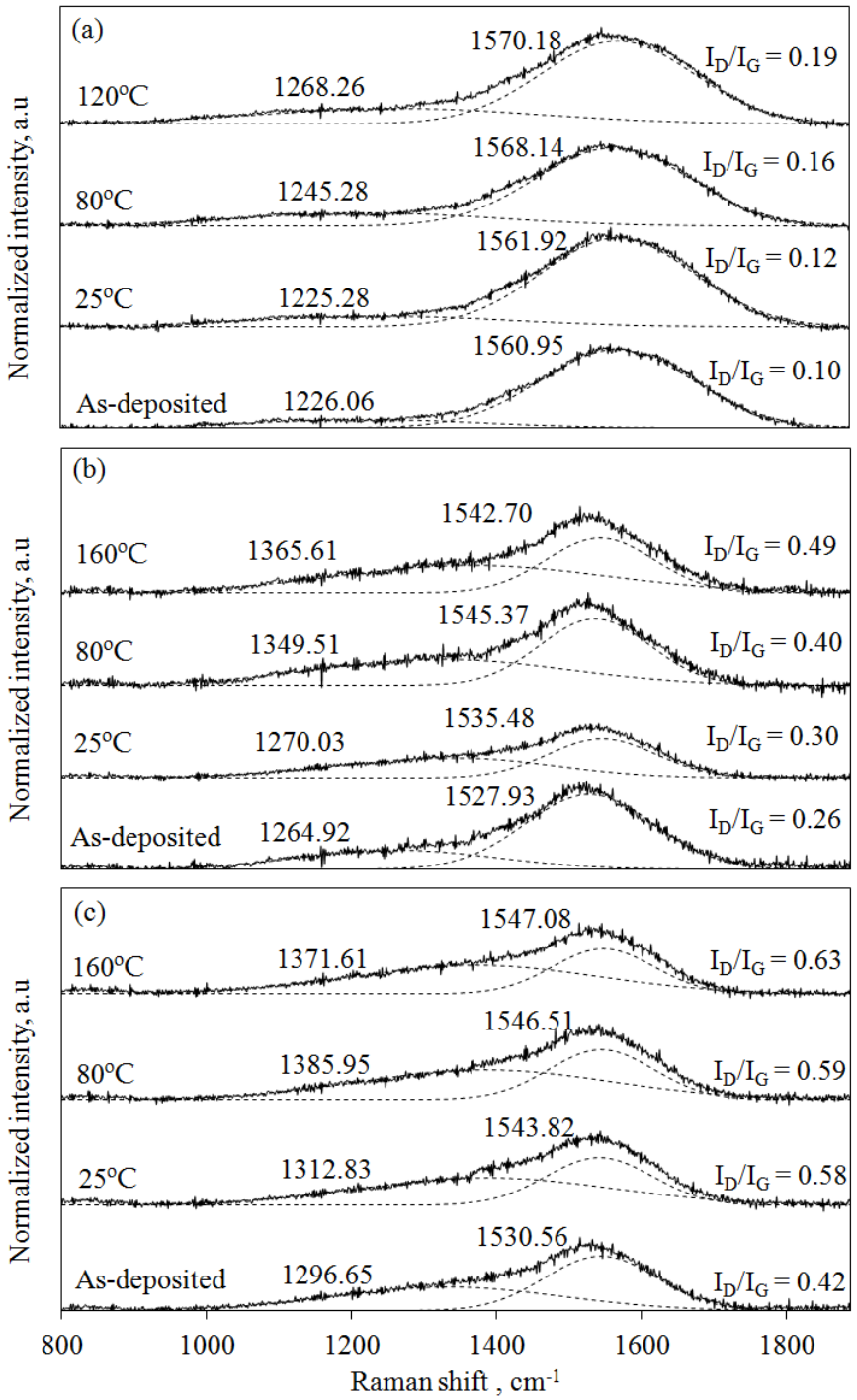

FIGURE 3.3: Raman spectroscopy of as-deposited DLC coatings before and after friction tests under different temperatures for (a) DLC1, (b) DLC2 and (c) DLC3.

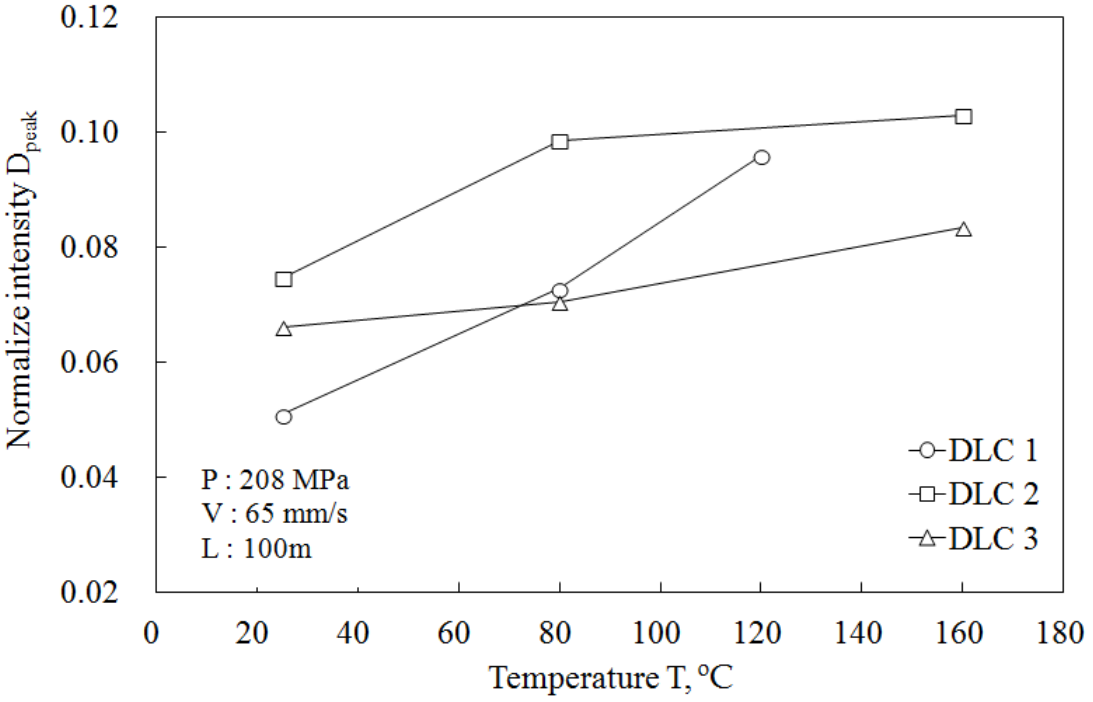

FIGURE 3.4: Intensity of D peak of DLC obtained by Raman spectroscopy as a function of oil temperature.

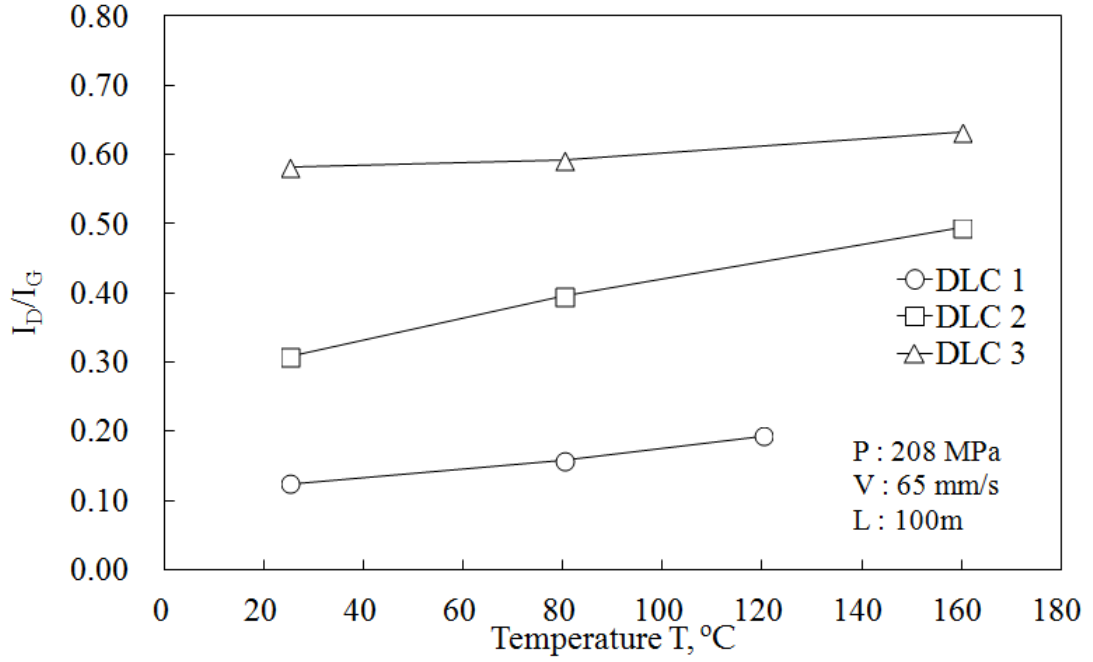

FIGURE 3.5: I_D/I_G ratio of DLC obtained by Raman spectroscopy as a function of oil temperature.

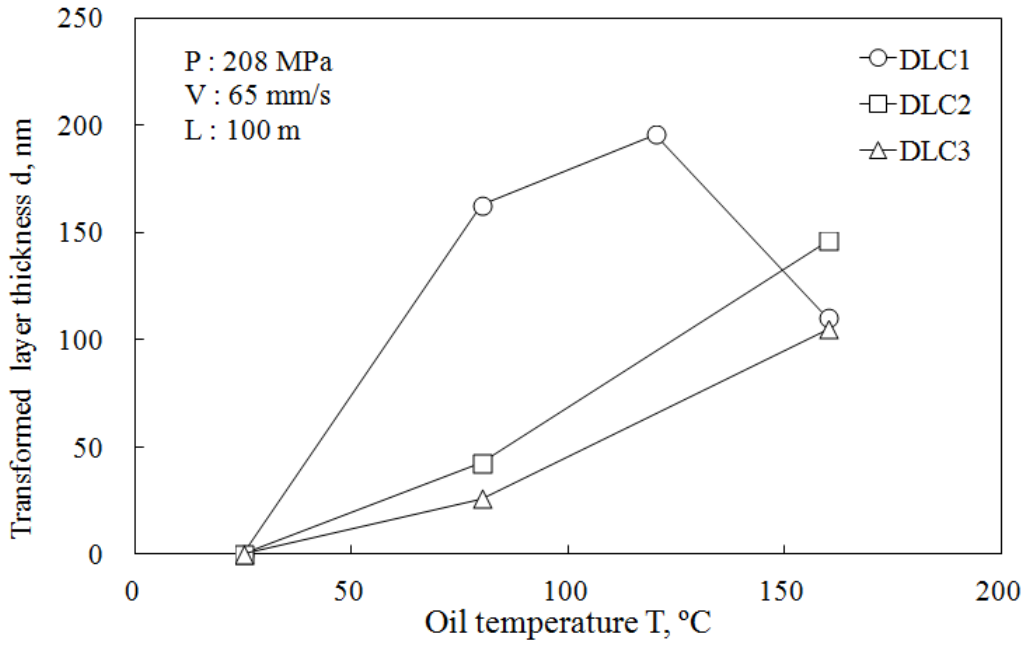

FIGURE 3.6: Thickness of the transformed layer after sliding in oil detected on wear track using spectroscopic ellipsometry as a function of oil temperature.

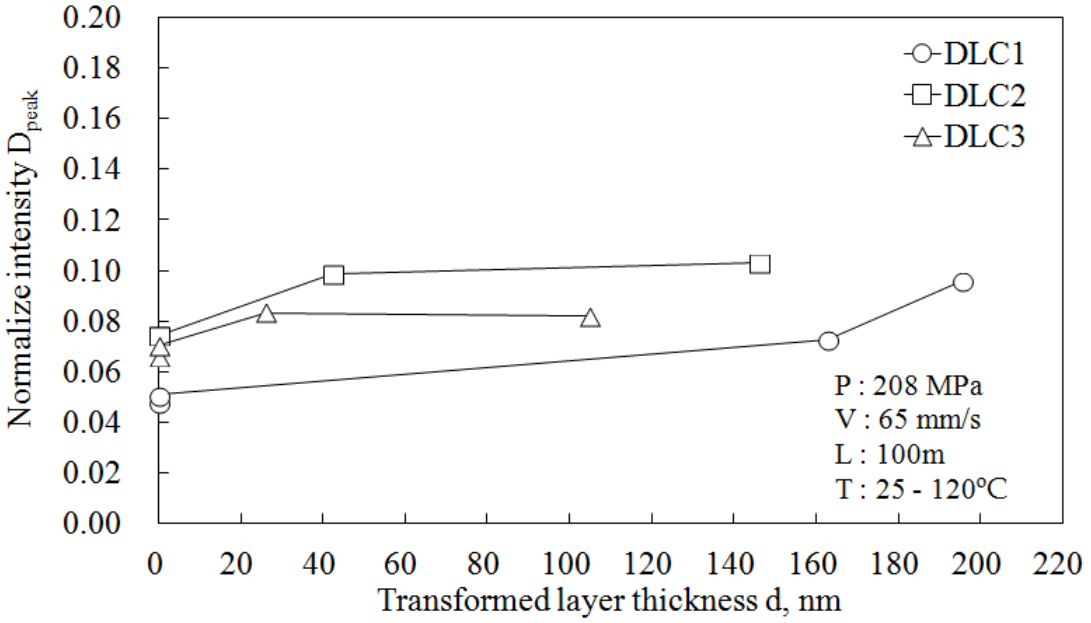

FIGURE 3.7: Correlation between intensity of D peaks and the thickness of transformed layer .

3.3.2 Hardness

The hardness was measured using a nanoindenter. An average of ten measurements was used to determine the hardness of the DLC coating in order to obtain a good statistical representation. The hardness of the DLC coatings DLC1, DLC2 and DLC3 were 47.1, 11.8 and 6.05 GPa, respectively as shown in Figure 3.8. Figure 3.9 shows the results of the indentation depths, where the depths of DLC1, DLC2 and DLC3 were 26.5, 70.04 and 90.2 nm at maximum indentation load of 1000 μN, respectively. This order is in agreement with the hardness of DLC coatings.

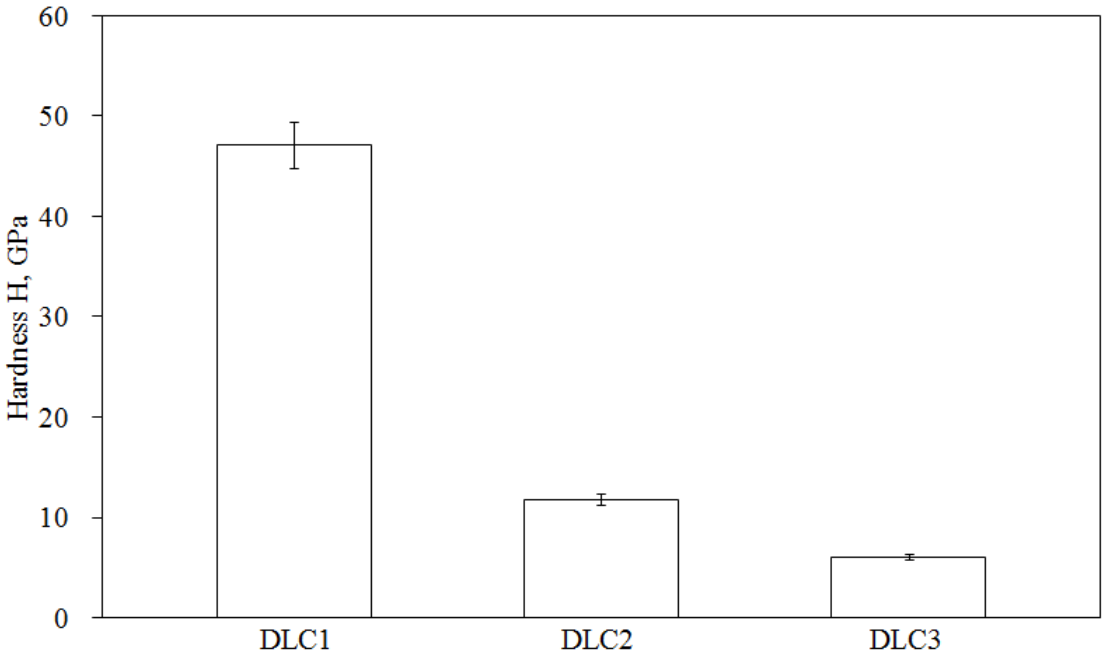

FIGURE 3.8: The hardness of DLC1, DLC2 and DLC3.

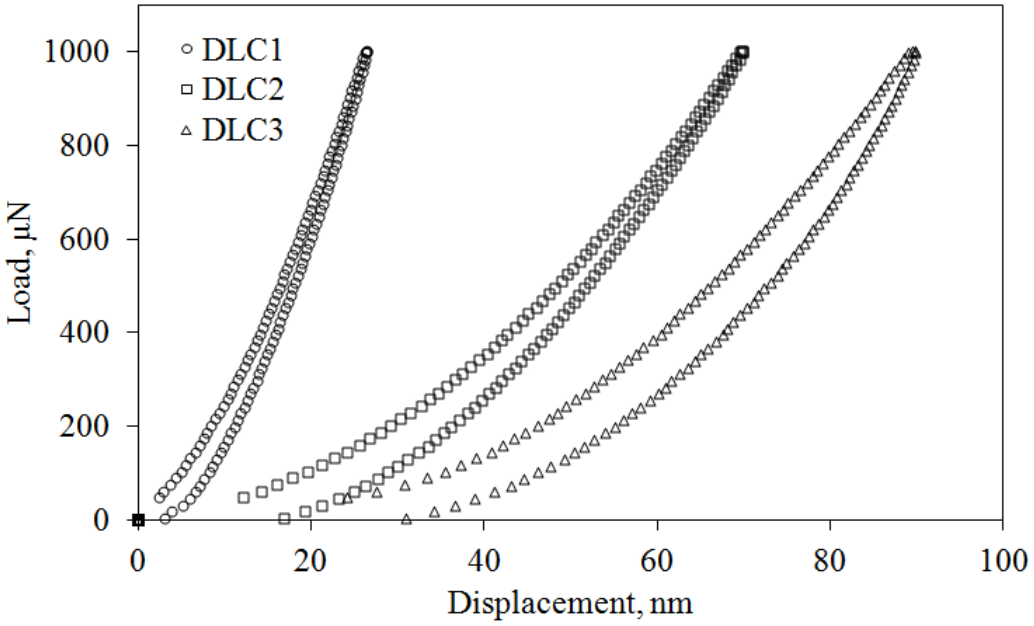

FIGURE 3.9: Load-displacement curves of different DLC by nanoindenter.

3.4 Friction and wear behaviors

Figure 3.10 shows the results of the friction coefficient of DLC1, DLC2 and DLC3 at different oil temperatures. All the DLCs showed the same friction behaviour where after the running-in, the friction coefficient reached a relatively steady and low value. It can be observed that DLC1 with the highest hardness showed a reduction of friction coefficient from 0.05 to 0.03 with increasing oil temperatures of 25, 80 and 120 °C. But DLC2 and DLC3 showed an increase in the friction coefficient at all oil temperatures. Figure 3.11 shows the relation between hardness and the average friction coefficient, where DLC1 with the highest hardness shows the lowest friction coefficient. Since, all the DLCs have the same initial surface roughness and have been coated on the same substrate, the friction behaviors depend strongly on the hardness of the DLC.

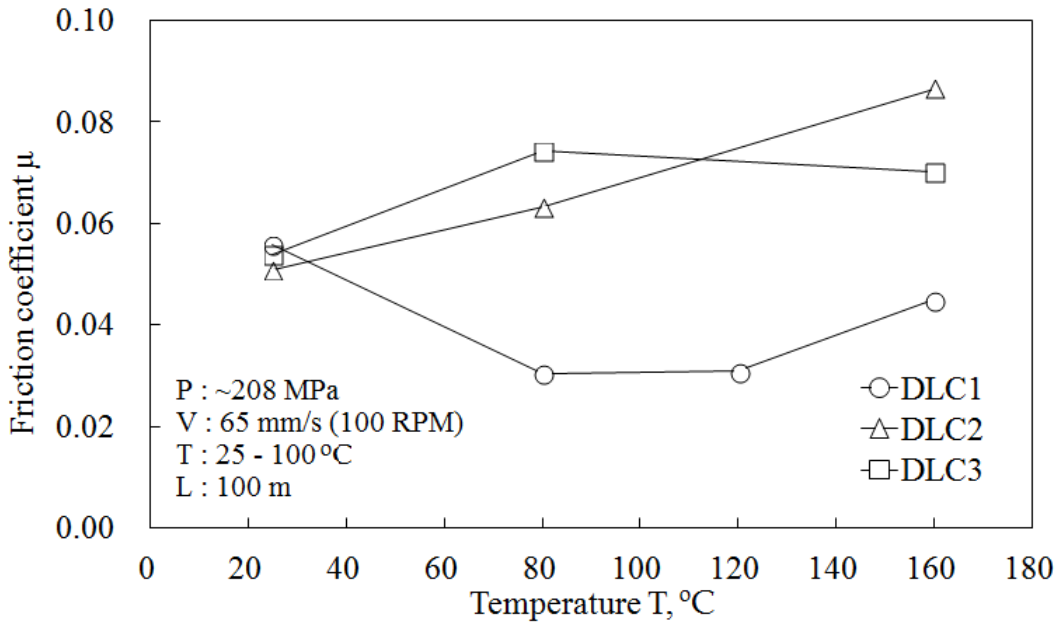

FIGURE 3.10: Friction coefficient of DLC as a function of oil temperature.

The wear loss of the DLC coatings can be obtained by observing the wear scar on the surface of the DLC coated roller. The wear volume, V (mm^3) of the DLC coating was measured by using the worn width and length of the DLC coated roller in an optical microscope and was calculated by using Eq. 3.7.

$$V = \left[R^2\left(\frac{\pi}{2} - Cos^{-1}\frac{b}{2R}\right) - \frac{b}{2}\sqrt{R^2 - \left(\frac{b}{2}\right)^2} \right] L \tag{3.7}$$

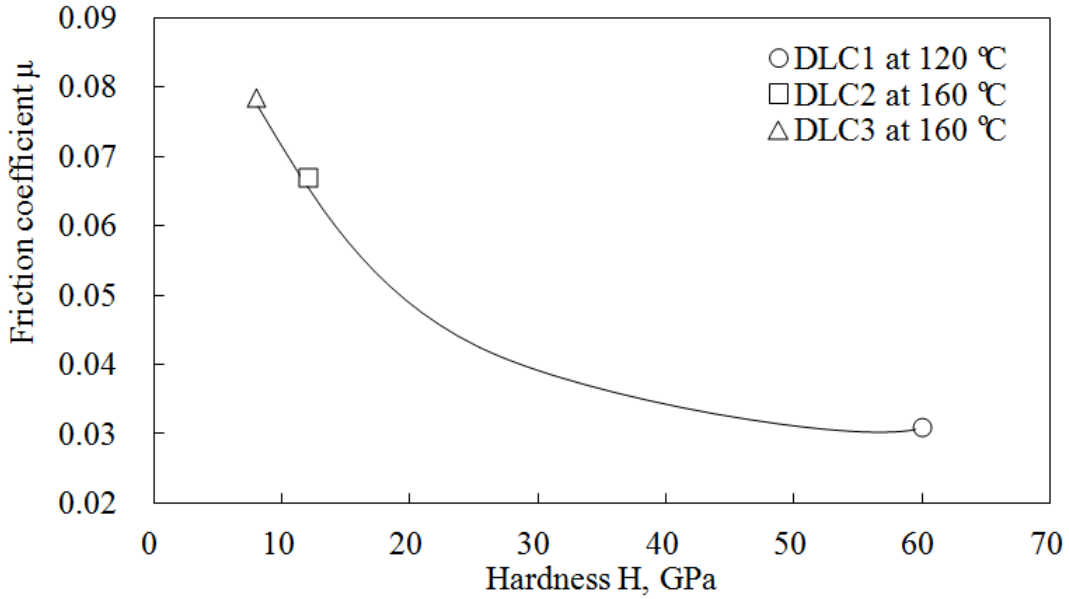

FIGURE 3.11: Correlation between friction coefficient and hardness of DLC.

where R is the radius of the roller (mm); b is the wear width (mm) and L is the wear length (mm).

The specific wear rate, W_s (mm^3/Nm) has been calculated using Archard wear equation as represented by Eq. 3.8.

$$W_s = \frac{V}{WL} \tag{3.8}$$

The effect of temperature on the wear behaviour of DLCs is shown in Figure 3.12. All the DLC showed the same trend with an increase in the specific wear rate as the oil temperature increased. The wear of the surface coatings increased with increasing oil temperature for all the DLCs mainly because of changes in the mechanical properties of the DLC coatings. The transformed layers at the contact interface were softer than the original DLC, and thus caused more wear [37]. The hardest DLC1 showed the lowest wear rate, followed by DLC2, and DLC3, which suffered the most wear. The specific wear rate of DLC1 was in the order of 10^{-11} mm^3/Nm, and DLC2 and DLC3 were at the order of 10^{-9} mm^3/Nm.

The relationship between the inverse hardness of DLC and the specific wear rate is shown in Figure 3.13. The specific wear rate decreases significantly with increases in the hardness of DLC.

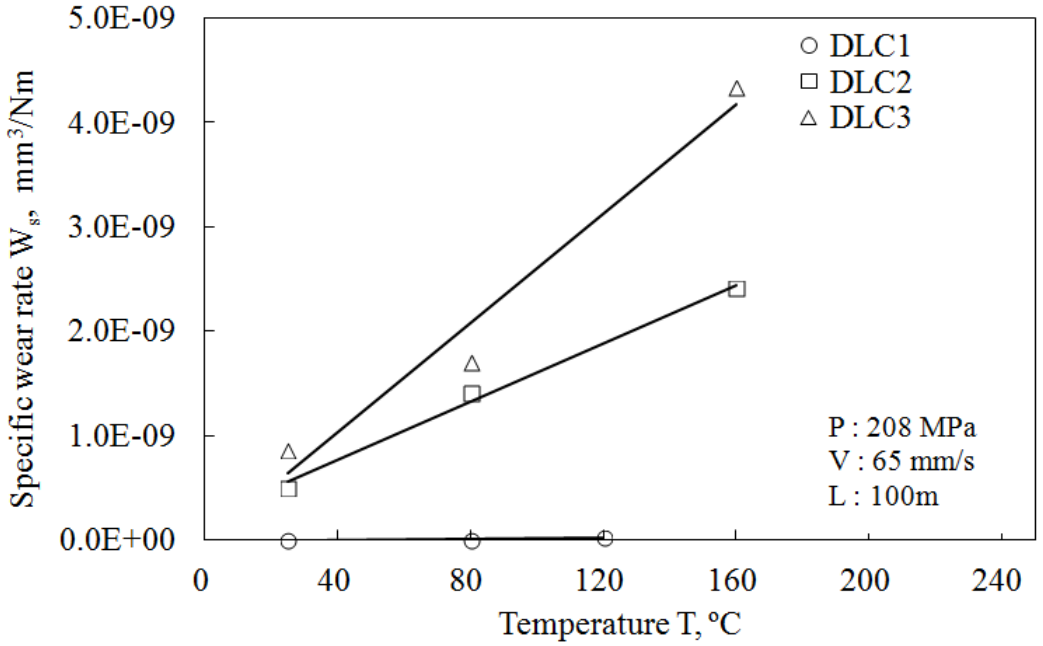

FIGURE 3.12: Specific wear rate of DLC as a function of oil temperature.

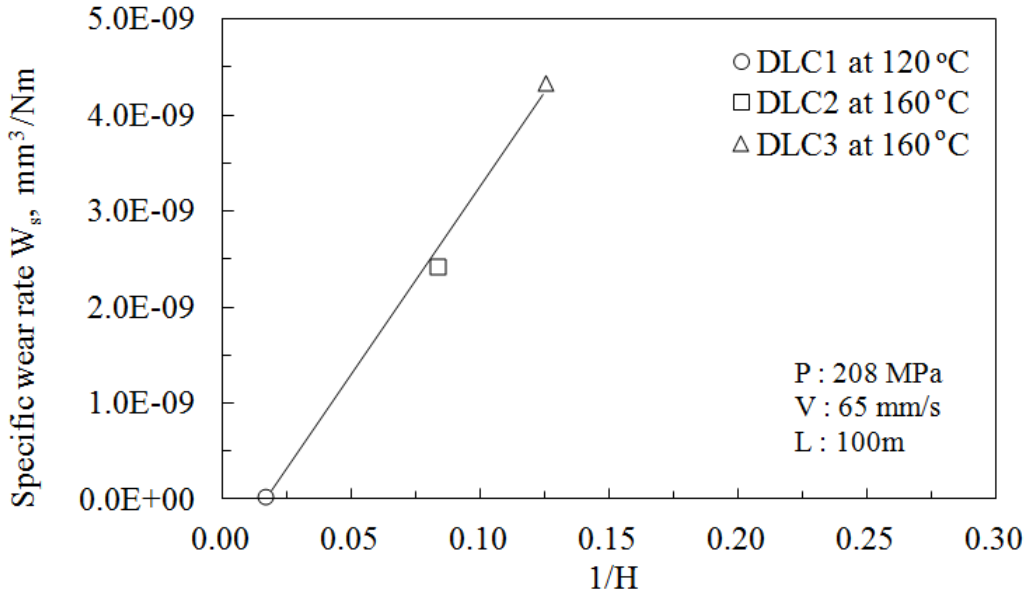

FIGURE 3.13: Relation between specific wear rate and inverse hardness of DLC.

It is suggested that the graphite-like transformed layer with low shear strength at contact interface could be responsible for the low friction coefficient. This is the most reasonable explanation for the low friction coefficient in this experiment for two reasons. Firstly, the influence of the lubricant is considered to be small because the oil film is very thin under the boundary lubrication conditions. The second reason is the absence of a low friction additive agent in the oil. On the other hand, we believed that the graphite-like transformed layer has some character such

as thickness and hardness that probably influence the friction behaviour. These nano characteristics is reported in the Chapter 4 and 5.

3.5 Conclusions

The tribological properties of different hardness of DLCs sliding against steel under boundary lubrication condition in additive-free mineral-based oil were investigated in order to determine the influence of the as-deposited DLC hardness on friction behaviour. The following conclusions were reached as follows:

1. The friction coefficient decreased with an increasing of the hardness of as-deposited DLC.
2. The specific wear rate decreases significantly with an increasing in the hardness of as-deposited DLC.
3. The formation of graphite-like transformed layer is due to graphitization process during friction test.

Further analysis on graphite-like transformed layer is needed in order to get the information about the nano character in term of its thickness and hardness.

Chapter 4

Effect of thickness of transformed layer on friction behaviour

4.1 Introduction

Diamond-like carbon (DLC) coatings are well known for their excellent low-friction and wear-resistance properties [11, 73]. Currently, these coatings are widely used in various mechanical systems. However, there are no clear systematic guidelines concerning for the use of DLC coatings in lubricated mechanical systems. This lack of guidelines in the use of DLC coatings is believed to be because the mechanism for the low friction of the DLC coating is unclear and because there are few models of DLC friction. Of course, there has been a report on the superlubricity mechanism for the ultra-low friction of glycerol-lubricated ta-coatings [74]. Furthermore, this report demonstrates that the adsorbed molecules from the oil additives play a critical role in obtaining ultra low friction. However, it is unclear what mechanism is valid for oil that does not contain any additives or mineral oil. Additionally, it has been reported that the transformed layer, which is a structure of a DLC surface enriched with sp^2 carbon, can reduce the friction of DLC under dry conditions [75].

However, it is only a qualitative factor, and this transformed layer cannot be easily observed under oil lubrication. Therefore, there is a need for quantitative methods to measure the thickness of the transformed layer of DLC under oil lubrication. A model for the friction of DLC under oil boundary lubrication is required to describe how the transformed layer of DLC functions. Several methods have been

developed for measuring the structure of DLC. For example, typical methods for this purpose include Raman spectroscopy, EELS, NEXAFS, NMR, PBS-ERDA and ESR. However, these methods are complex measurement techniques, and excessive amounts of time and costs are required to measure the DLC. Therefore, reflectance spectroscopy is considered to be a simple, rapid and low-cost method because once the optical models are defined, the thickness of the target film can be easily calculated. Spectroscopic reflectometry is a measurement technique that is based on an interferometric measurement. This method is a new method for the control of the thickness and the quality of the DLC. Reflectance spectrometry can measure the optical constant and film thickness of thin films from 1 to 5 nm in thickness based on the spectroscopic analysis of reflected light [76]. Furthermore, this system can measure the thickness with high resolution and accuracy. Therefore, spectroscopic reflectometry is expected to be an effective method for measuring the DLC film.

DLC films are thought to be predominantly amorphous, in which small clusters of microcrystalline structures with sp^3 and sp^2 bonding and an amorphous matrix coexist [77]. Therefore,the DLC can change its own structure from sp^3 to sp^2 with mechanochemical reaction under friction. Sanchez-Lopez et al. reported that friction-induced structural transformations of diamond-like carbon affect its friction coefficient under various atmospheres, such as in ambient air (RH 30-40 %),dry air (RH 1 %) and dry nitrogen (0-1 %) [74] . Mabuchi et al. observed that the DLC transformed its rich sp^2 carbon layer after sliding, which was obtained from friction under oil lubrication. They used transmission electron microscopy (TEM) and determined that the thickness of the transformed layer was a few nanometers [78] . This transformed layer had a π^* plasmon peak, which indicating that the transformed layer included a high content of sp^2 carbon. Therefore, it is believed that this transformed layer also had optical properties which were different than those of the original DLC. Consequently, the transformed layer could affect the friction coefficient of the DLC layer under oil boundary conditions. Therefore, the transformed layer of the DLC coating could be observed using reflective spectroscopy, and its thickness could also be quantitatively measured.

The transformed layer of the DLC on the original DLC surface can be considered to be a bi-layer [79] . However, there are no experimental examinations concerning this model because of the lack of quantitative measurement systems for the

transformed layer of DLC. Therefore, the purpose of this study is to develop are reflective spectroscopy method to quantitatively measure the transformed layer.

This chapter is composed of three parts. The first part details the optical model to explain the reflectance intensity spectrum of the DLC wear scar after sliding in oil. The second part reports on the influence of the oil temperature, contact pressure and sliding distance on the thickness of the transformed layer. In the third part, the relationship between the thickness of the transformed layer and the friction coefficient is clarified from the viewpoint of the friction model of DLC under oil boundary lubrication.

4.2 Experimental method and procedure

4.2.1 Test specimens and friction test

All materials and friction tests are same as in the Section 3.2.

Additional, the transformed layer thickness was measured using spectroscopic reflectometry measurement system (FE3000 made by Otsuka Electronics) as shown in Figure 4.1.

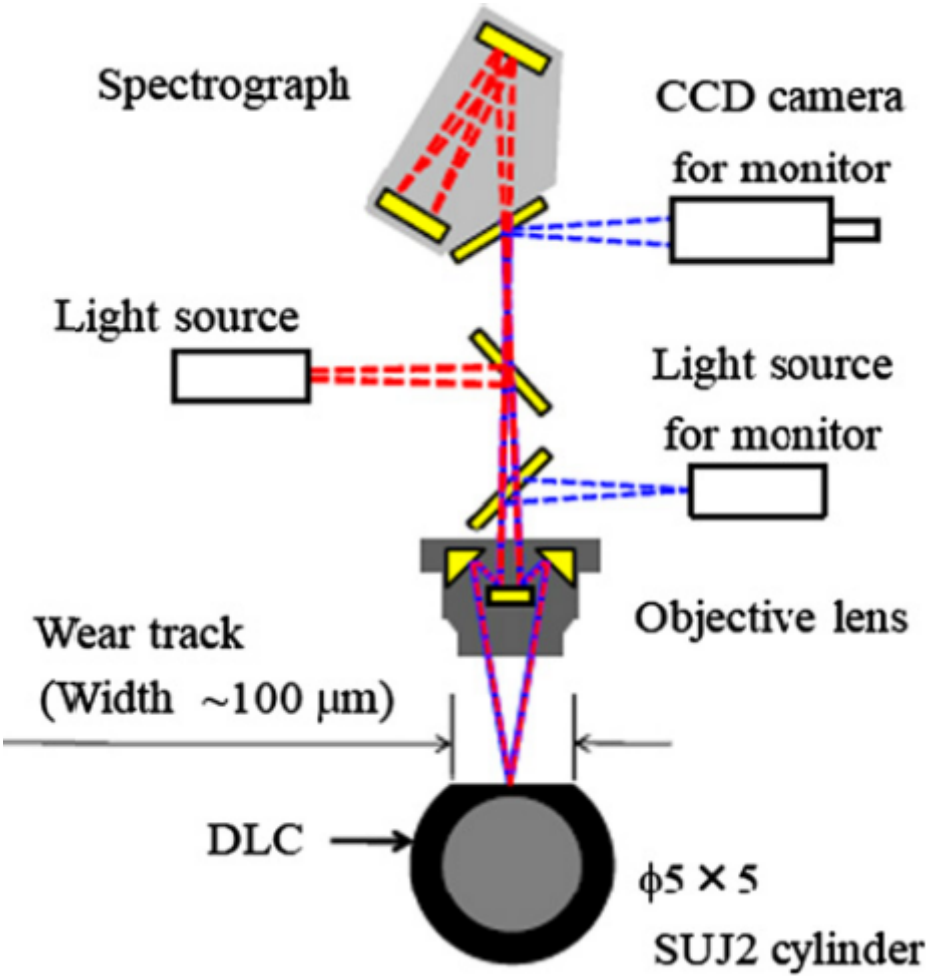

FIGURE 4.1: Schematic illustration of the reflectance spectrometry measurement for analysing the wear track on pin.

4.3 Spectroscopic reflectometry

A proper optical model for the material is needed in order to analyse the thickness and optical constant of the material using spectroscopic reflectometry. In this study, the materials, including DLC1, DLC2 and DLC3, were considered to have transformed layers on their topmost surfaces after the sliding test in additive-free mineral-based oil. Therefore, it was hypothesized that the specimens had two different layers on the SUJ2 substrate in the model. Figure 4.2 presents the cross-sectional image of the DLC1 coating cut using the FIB (Focused Ion Beam) and its elemental analysis by EDS (Energy Dispersive Spectroscopy). Figure 4.2 shows the DLC1 coating after sliding under an oil temperature of 80 °C within the region of the wear scar. The image was obtained by EDS/SEM with a tilting stage angle of 60 °. The SEM image showed different colour intensities with regard to different kinds of materials. The topmost surface showed that the transformed layer formatted during the friction test. The EDS analysis confirmed that the transformed layer consisted of the element carbon.

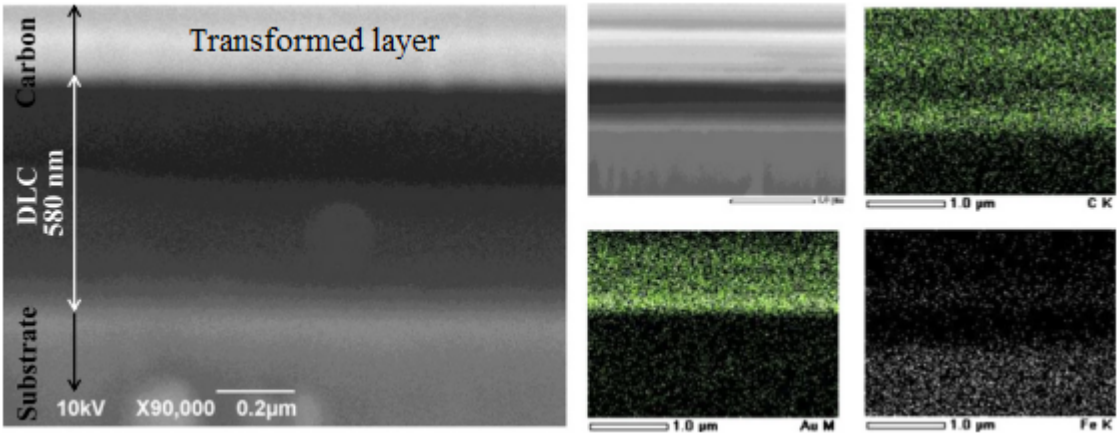

FIGURE 4.2: The cross-sectional image of the DLC1 coating cut by FIB and elemental analysis using EDS/SEM.

In this image, the bulk DLC, which is located between the transformed layer and the SUJ2 substrate., has a thickness of 580 nm. After recording an image, the real coating thickness (bulk DLC and transformed layer) was calculated to be 667 nm for DLC1. From this thickness, the optical properties of the original DLC1 film and the thickness and optical properties of the transformed layer could be estimated.

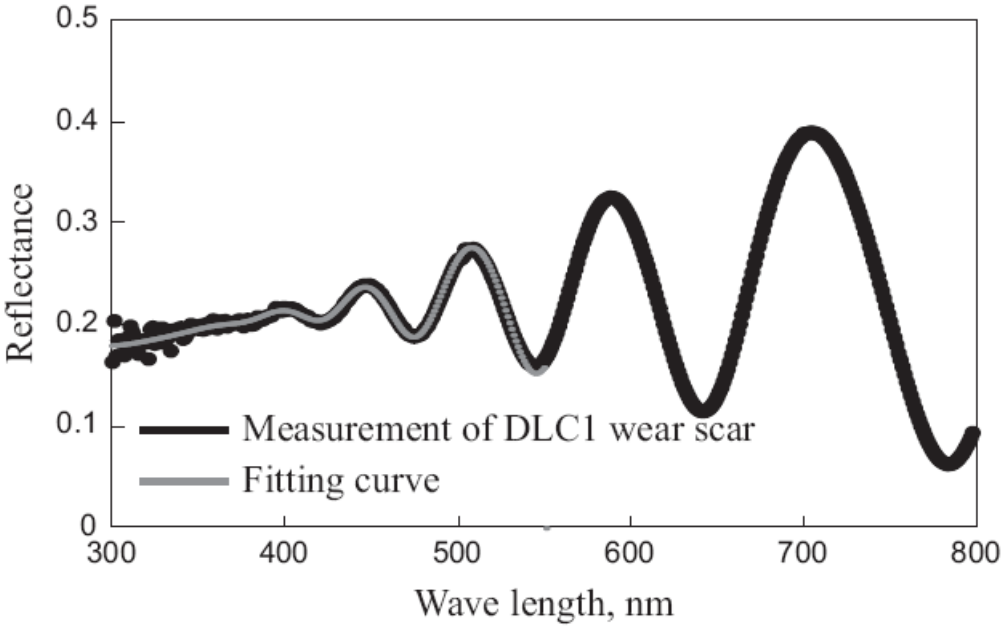

FIGURE 4.3: Reflectance intensity spectrum of the friction scar on the DLC1 coating after sliding.

Figure 4.3 presents the result of the reflectance intensity in the spectrum of a friction scar of DLC1 after sliding in oil. Figure 4.3 exhibits a fringe pattern along with the wavelength, which clearly indicates that the specimen contained a bi-layer. By fitting the spectrum with a theoretical curve, it was possible to estimate the thickness of the transformed layer on DLC1 after sliding in oil. The spectrum was fitted with the theoretical curve within the wavelength range of 300-550 nm. This wavelength range was selected because the penetration depth of 550-800 nm light was too deep to measure the optical properties of the transformed layer. Therefore, the penetration depth was calculated from the extinction index of the original DLC1 layer. Subsequently, the wavelength range was selected, for which the penetration depth of light was less than tens of nanometres, as shown in Figure 4.4.

Therefore, the optical model for DLC1 could be obtained as a bi-layer with a 10 nm transformed layer on the DLC1 films over the SUJ2 substrates. The optical models for DLC2 and DLC3. were also considered. It was determined that these two coatings had quite different models from that of the DLC1 coating, as a single-layer model. The reason for this difference was that the extinction index was too high to transmit the those films to the substrates.

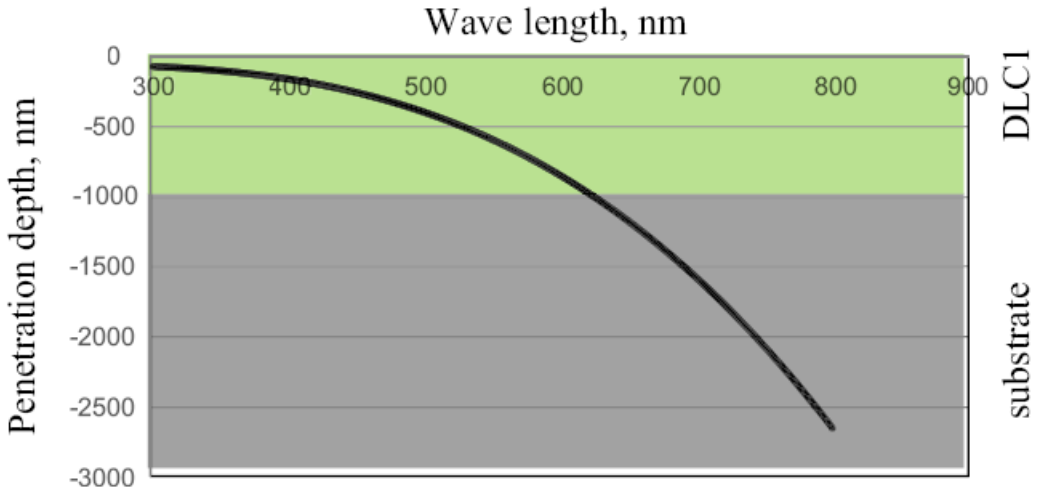

FIGURE 4.4: Penetration depth for each wavelength of light and the corresponding thickness of the DLC coating.

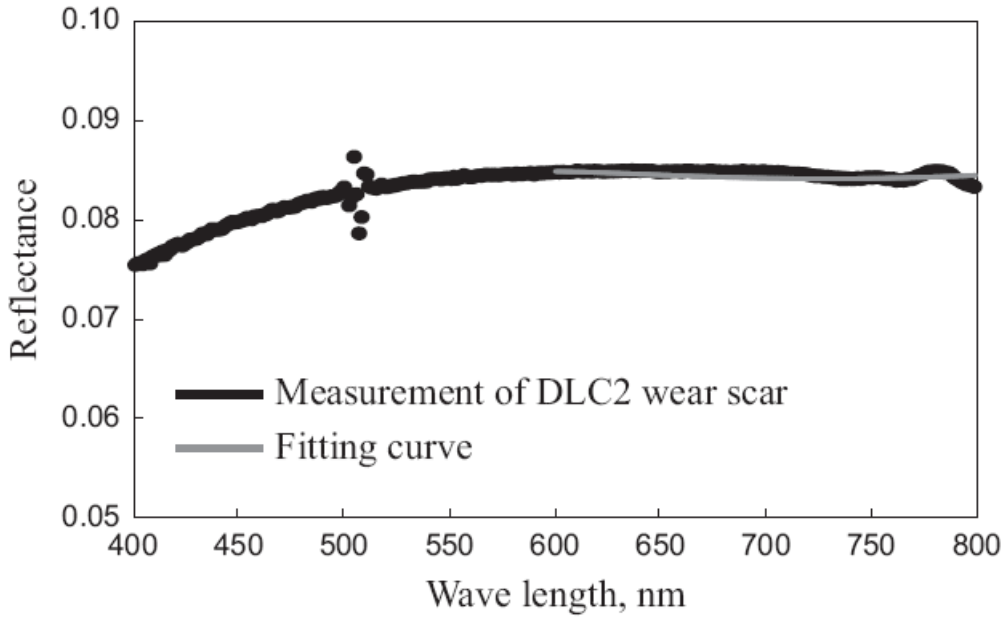

FIGURE 4.5: Reflectance intensity spectrum of the friction scar on the DLC2 coating after sliding.

Figure 4.5 shows the typical result of the reflectance intensity of a friction scar in the DLC coating (DLC2 and DLC3) after sliding in oil under different wavelengths. Figure 4.4 shows that no long wavelengths could penetrate those films, which is why there are no obvious fringe images in Figure 4.5. Figure 4.6 shows the penetration depth of each wavelength of light through the coating.

However, the penetration depths of light at 600-800 nm were sufficient to transmit the transformed layers of those DLCs. There, the optical model for the DLC2 and DLC3 coatings were obtained after sliding as a single model of transformed layers on the DLC2 and DLC3 substrates.

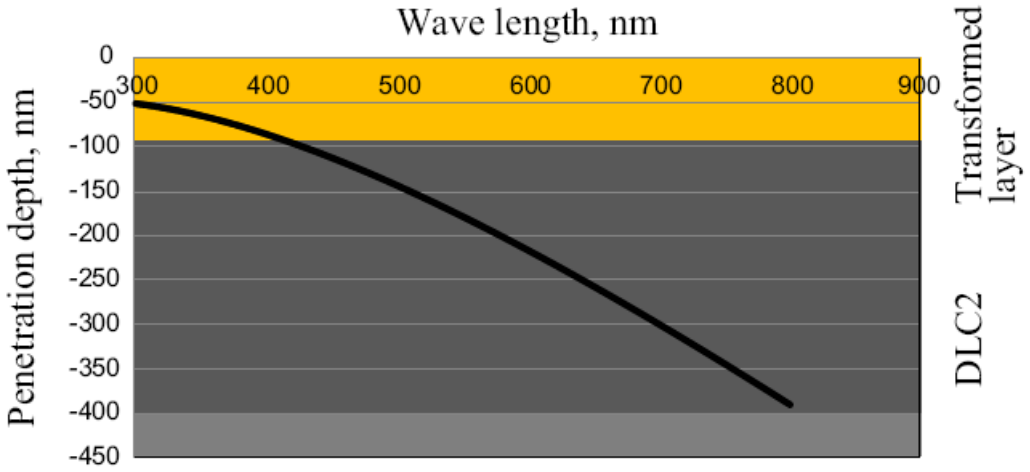

FIGURE 4.6: Penetration depth of each wavelength of light through the coating.

4.4 Results

4.4.1 The effect of oil temperature on the reflectance intensity

Figures 4.7-4.9 show the influence of the oil temperature on the intensity of the reflectance spectra of the wear scar in the DLC1, DLC2 and DLC3 films after sliding.

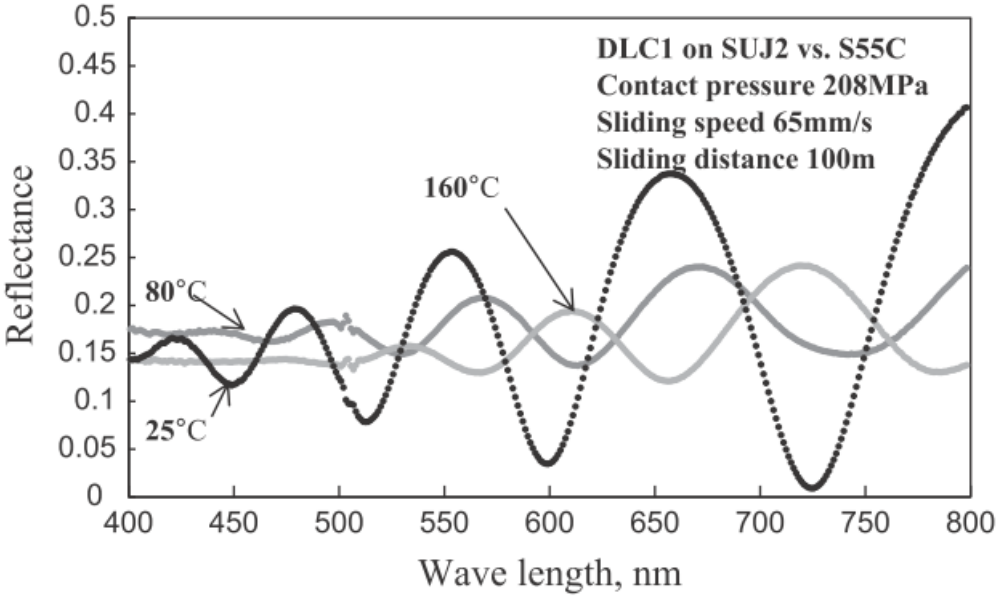

FIGURE 4.7: Reflectance intensity spectrum of the friction scar in the DLC1 coating after sliding under various contact pressures.

Figure 4.7 reveals that the reflectance intensity of DLC1 decreased with increasing oil temperature and phase (fringe pattern starting point) shifts to larger wavelengths with increasing oil temperature. In contrast, Figures 4.8 and 4.9 show a fringe image at wavelengths greater than 750-800 nm for DLC2 and DLC3. The fringe image in the wavelength range of 750-800 nm disappeared with increasing oil temperature.

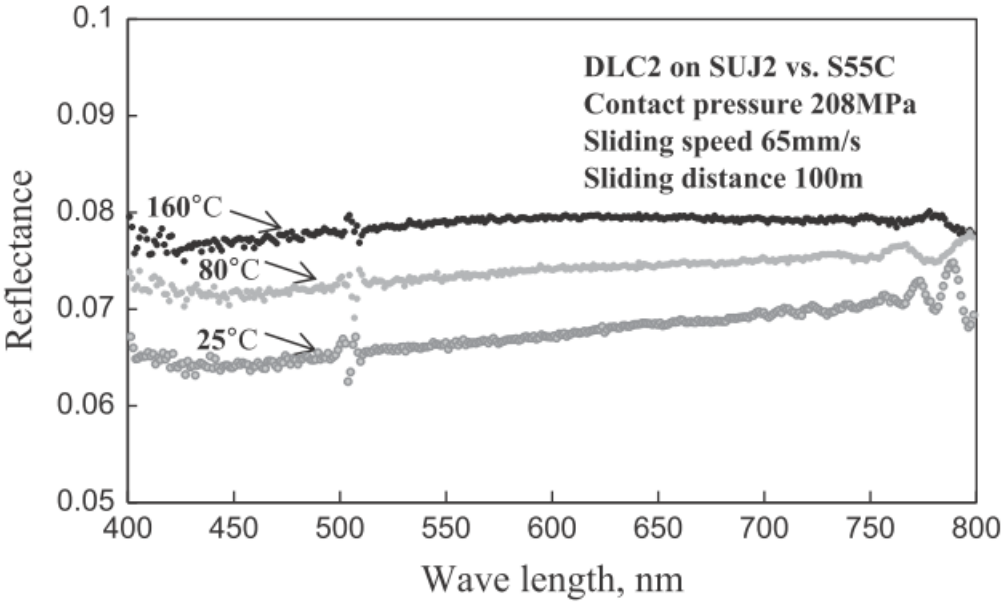

FIGURE 4.8: Reflectance intensity spectrum of the friction scar in the DLC2 coating after sliding under various contact pressures.

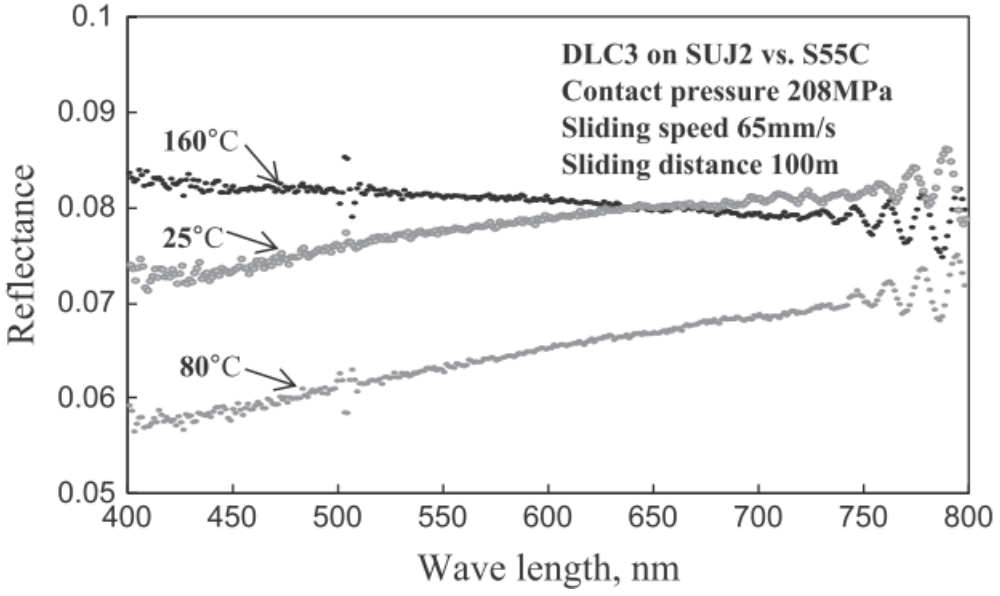

FIGURE 4.9: Reflectance intensity spectrum of the friction scar in the DLC3 coating after sliding under various contact pressures.

4.4.2 The effects of contact pressure and sliding distance on the reflectance intensity

After several friction tests with different contact pressures, Figure 4.10 shows the influence of contact pressure on the reflectance intensity of the friction scar in the DLC1 coating. The reflectance intensity decreased with increasing contact pressure and phase shifting was observed.

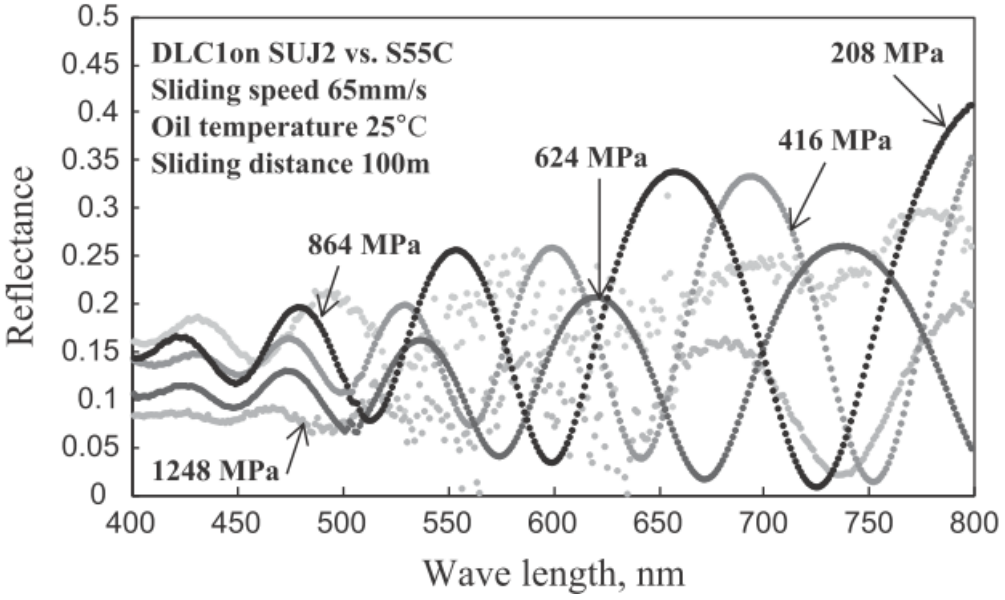

FIGURE 4.10: Reflectance intensity spectrum of the friction scar in the DLC1 coating after sliding under various contact pressures.

Figure 4.11 shows the influence of the sliding distance on the reflectance intensity of the friction scar in the DLC1 coating. The reflectance intensity decreased with increasing sliding distance, and phase shifting was observed.

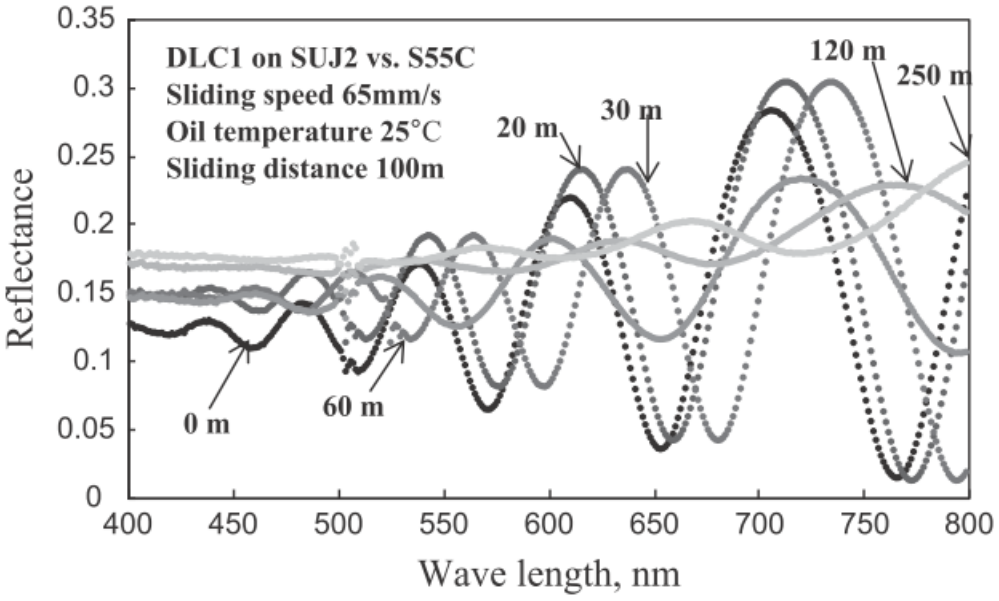

FIGURE 4.11: Reflectance intensity spectrum of the friction scar in the DLC1 coating after sliding under various sliding distances.

4.4.3 The effects of friction conditions on the thickness of the transformed DLC layer using spectroscopic reflectometry

After several friction tests, the relationships between the thickness of the transformed layer and the friction coefficient under various oil temperatures, contact pressures and sliding distances, were summarized. Figures 4.12-4.14 show the effects of the friction conditions on the thickness of the transformed layers, which were obtained from the results of Figures 4.7-4.11 with the theoretical curve fittings.

4.4.3.1 The effect of oil temperature on the thickness of the transformed DLC layer using spectroscopic reflectometry

Figure 4.12 shows the relationship between the thickness of the transformed layer and oil temperature. It can be seen that the thickness of the transformed layer increased with increasing oil temperature for all the DLC coatings. The hydrogen-free DLC coating (DLC1) exhibited a thick transformed layer at each oil temperature. When the friction coefficient of DLC1 decreased, the thickness of the transformed layer of DLC1 simultaneously increased. However, the friction coefficients of the DLC2 and DLC3 coatings increased with increasing thickness of the transformed layers on these films.

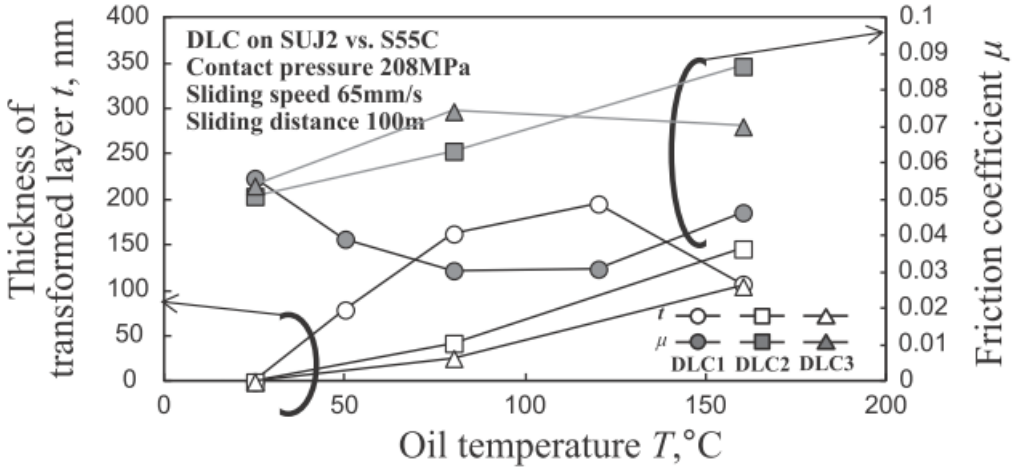

FIGURE 4.12: Effect of oil temperature on the thickness of the transformed layer and friction coefficient of various DLC coatings after sliding in the based oil.

4.4.3.2 The effects of contact pressure on the thickness of the transformed DLC layer using spectroscopic reflectometry

Figure 4.13 shows the effect of contact pressure on the thickness of the transformed layer and the friction coefficient of DLC1 after sliding in based oil at room temperature. The effects of the contact pressures on the thicknesses of the transformed layers were substantially less than the influence of the oil temperature. Subsequently, there was no obvious correlation between the friction coefficient and the thickness of the transformed layer.

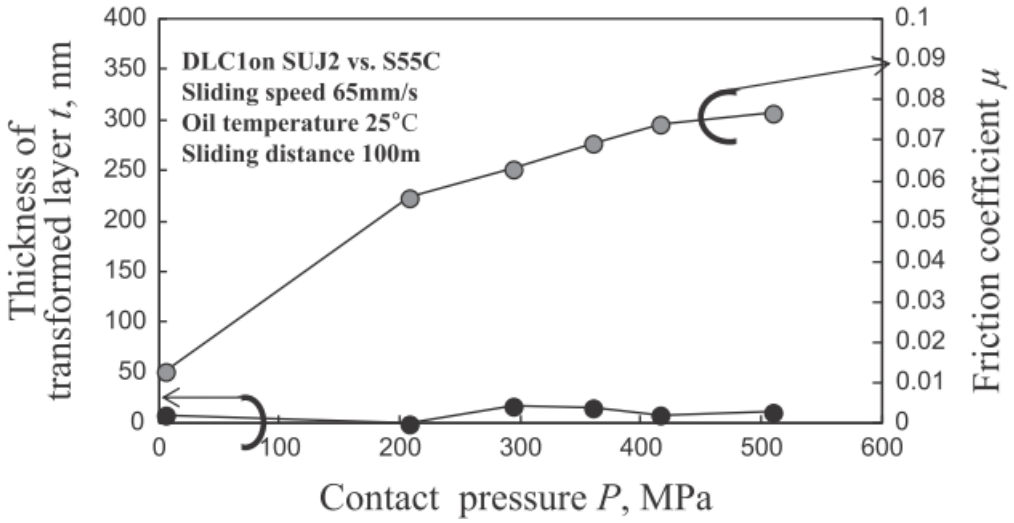

FIGURE 4.13: Effect of contact pressure on the thickness of the transformed layer, t, and friction coefficient, μ, of the DLC1 coating after sliding in the based oil at a temperature of 25 $°C$.

4.4.3.3 The effects of sliding distance on the transformed layer thickness of DLC with spectroscopic reflectometry

Figure 4.14 shows the effects of the sliding distance on the thickness of the transformed layer and the friction coefficient of DLC1 after sliding in the based oil with a temperature of 80 °C and approximately under 104 MPa of contact pressure. The thickness of the transformed layer increased with increasing sliding distance. In contrast, the friction coefficient decreased with increasing sliding distance. At the beginning of the friction test, there was no generation of the transformed layer. After several meters of sliding distance, the transformed layer was generated and increased with an increase in the sliding distance. The thickness of the transformed layer on the DLC coating outside the scar surface was measured at oil temperatures of 80 and 160 °C. The result showed that no transformed layer was generated under annealing temperatures at 80 and 160 °C. Since, the experimental oil temperature is below the transition temperature of 300 °C for DLC, the sliding distance is also one of the factors for the graphitization process which leads to pressure-induced graphitization [48, 49].

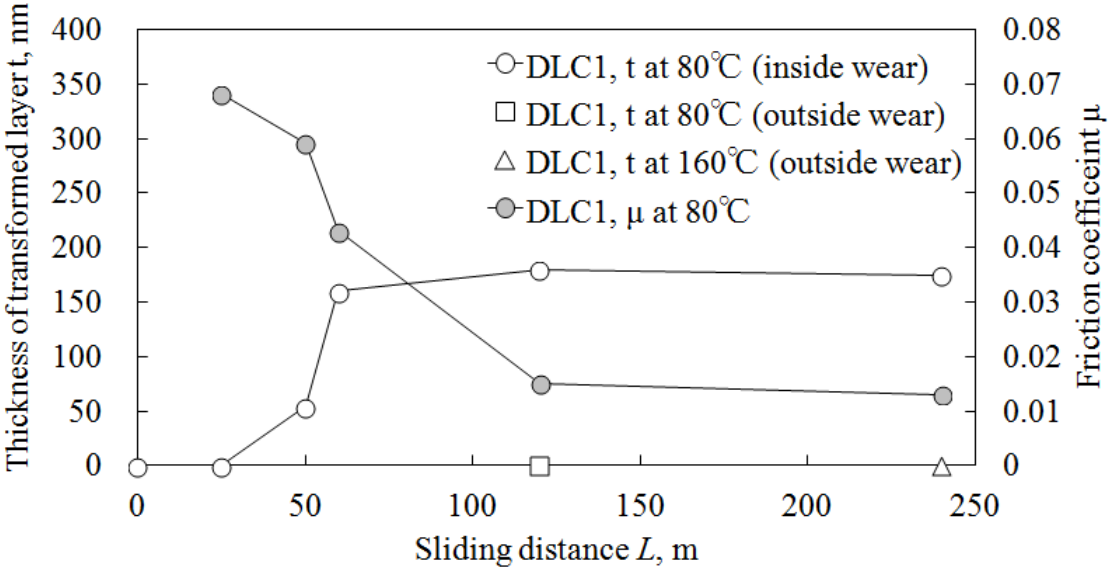

FIGURE 4.14: Effect of sliding distance on the thickness of the transformed layer, t, and the friction coefficient, μ, of the DLC1 coating after sliding in the mineral-based oil at a temperature of 80 °C.

4.4.4 The effects of the friction condition on the surface roughness of the DLC coatings using spectroscopic reflectometry

From the viewpoint of the friction coefficient, the surface roughness was assumed to have a significant effect. Dayson reported on the possibility of breaking of the solid lubricant film from this compound surface model [80]. Therefore, the deviation of roughness height, σ^* was measured on the wear track of DLC1, DLC2 and DLC3 using AFM, and these results are shown in Figures 4.15-4.17.

4.4.4.1 The effects of oil temperature on the surface roughness of the DLC coatings using spectroscopic reflectometry

Figure 4.15 shows the relationship between σ^* and the oil temperature. The DLC1 exhibited a remarkable change in σ^* with increasing oil temperature. However, it was difficult to correlate the σ^* of all the DLCs with oil temperature.

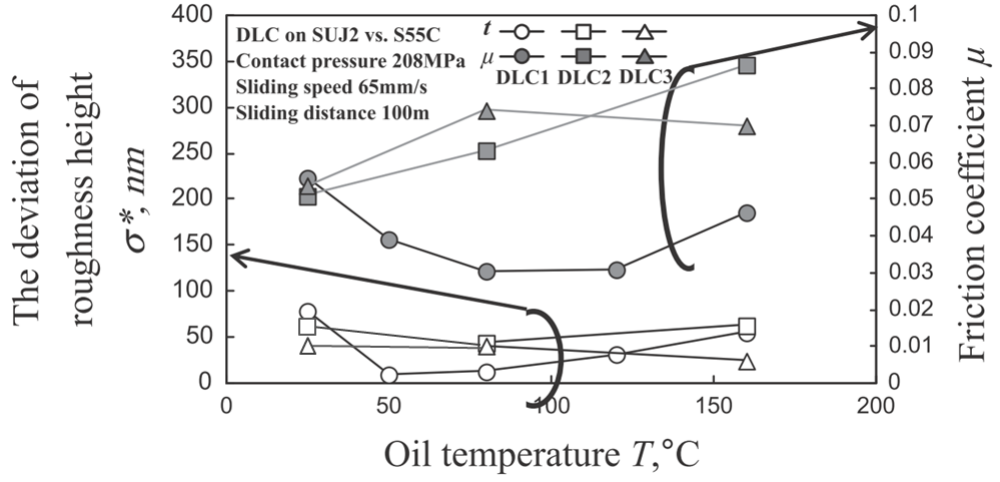

FIGURE 4.15: Effect of oil temperature on the deviation of the roughness height, σ^* and friction coefficient, μ, of various DLC coatings after sliding in the mineral-based oil.

4.4.4.2 The effects of the contact pressure on the surface roughness of the DLC coatings using spectroscopic reflectometry

Figure 4.16 shows the effects of the contact pressures on the $\sigma^*$and the friction coefficient of DLC1 after sliding in additive-free mineral-based oil. at room temperature. The σ^* decreased as the contact pressure increased from 200 to 300 MPa, and remained constant with further increases of contact pressure. It was clear that the contact pressure did not have a significant effect on either σ^*.

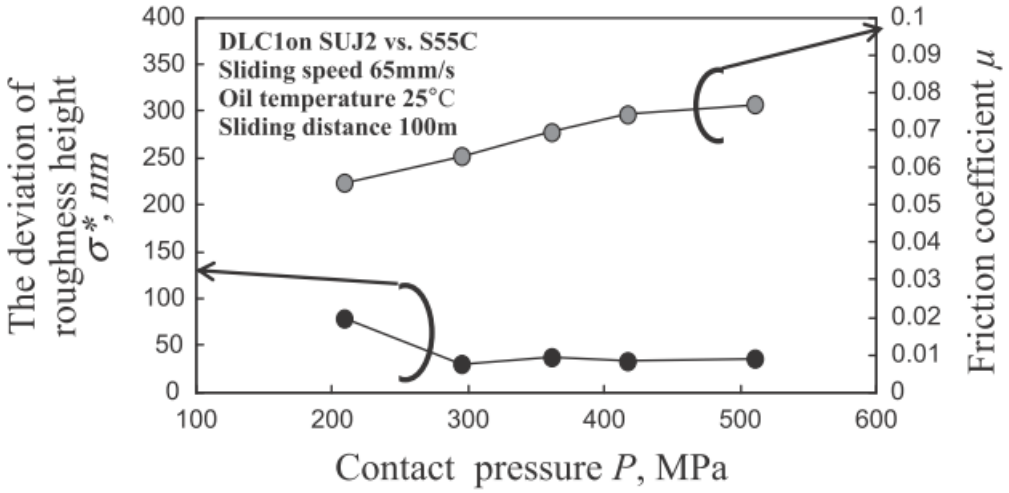

FIGURE 4.16: Effect of contact pressure on the deviation of the roughness height,σ^* and the friction coefficient, μ, of the DLC1 coating after sliding in the mineral-based oil with a temperature of 25 $°C$.

4.4.4.3 The effects of sliding distance on the surface roughness of the DLC coatings using spectroscopic reflectometry

Figure 4.17 shows the effect of the sliding distance on the σ^* and the friction coefficient of DLC1 after sliding in mineral-based oil with a temperature of 80 $°C$ and approximately under 104 MPa of contact pressure. The σ^* first increased to 50 nm with increasing sliding distance and then σ^* decreased to 10 nm after 50 m of sliding distance. In contrast, the friction coefficient decreased with increasing sliding distance. Therefore, there was no clear correlation between the sliding distance and σ^*.

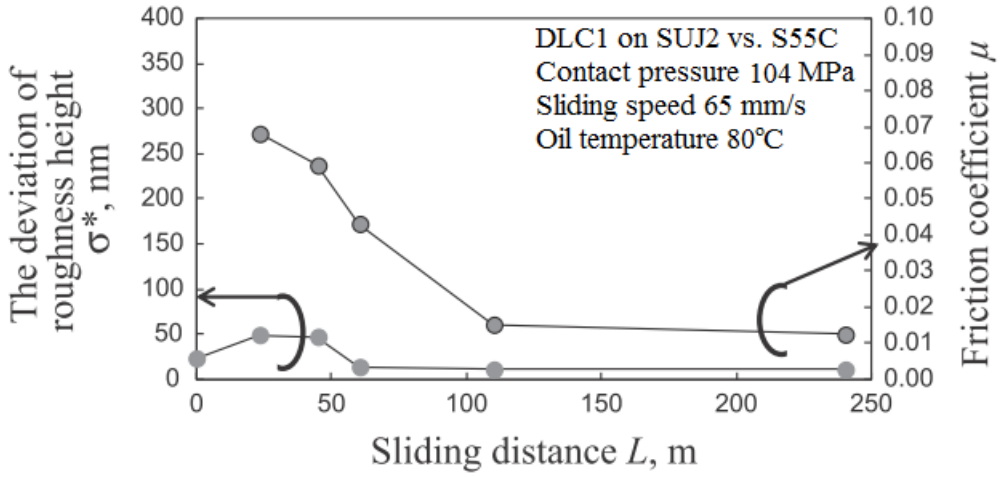

FIGURE 4.17: Effect of sliding distance on the deviation of the roughness height, σ^* and friction coefficient, μ,of the DLC1 coatings after sliding in the mineral-based oil with a temperature of 80 $°C$.

4.5 Discussion

Figure 4.18 shows the friction coefficient, μ as a function of the transformed layer thickness, t. In case of increasing of oil temperature, the friction coefficient of DLC1 decreases with an increasing of the thickness of transformed layer. The effect of sliding distance of DLC1 shows that the friction coefficient decreases with an increasing of the thickness of transformed layer. However, the effect of pressure, the thickness of transformed layer was not increased with an increasing of contact pressure. DLC2 and DLC3 shows the friction coefficient increase with an increasing of the thickness of transformed layer. From this result, it is difficult to find concrete relation between the friction coefficient and the thickness of transformed layer.

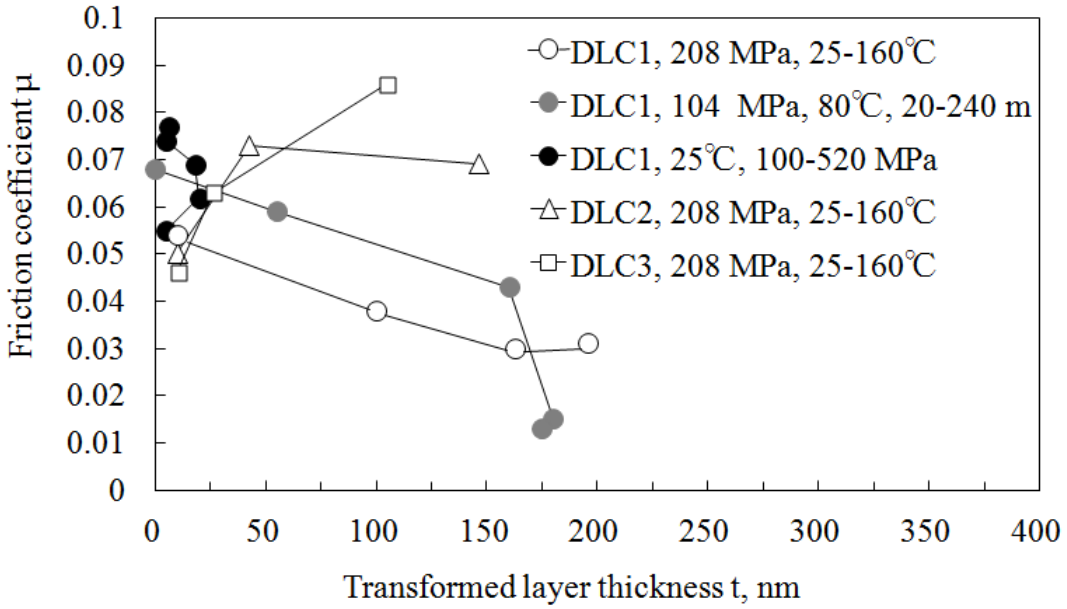

FIGURE 4.18: Relation between transformed layer thickness, t and friction coefficient, μ.

Figure 4.19 shows the friction coefficient, μ as a function of the deviation of the roughness height, σ^*. The friction coefficient increases drastically with an increasing of the deviation of roughness height in the range of 10-20 nm. Then, the σ^* don't have significant influence on friction coefficient when the σ^* value higher than 20 nm.

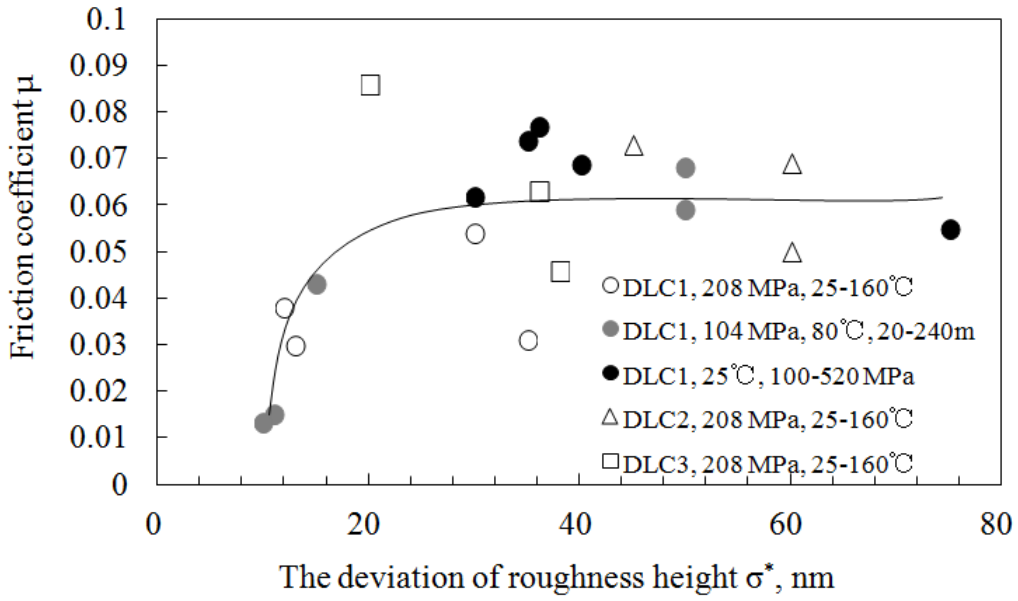

FIGURE 4.19: Relation between the deviation of the roughness height, σ^* and friction coefficient, μ.

Figure 4.20 shows the effect of t/σ^* on the friction coefficient of various DLC coatings after sliding in the mineral-based oil. The friction coefficient did not change when the value of t/σ^* below than 1. The friction coefficient decreases significantly with an increasing of t/σ^* value above 1. This figure showed that the low friction coefficient can achieve if the thickness of transformed layer much higher than the the σ^* value.

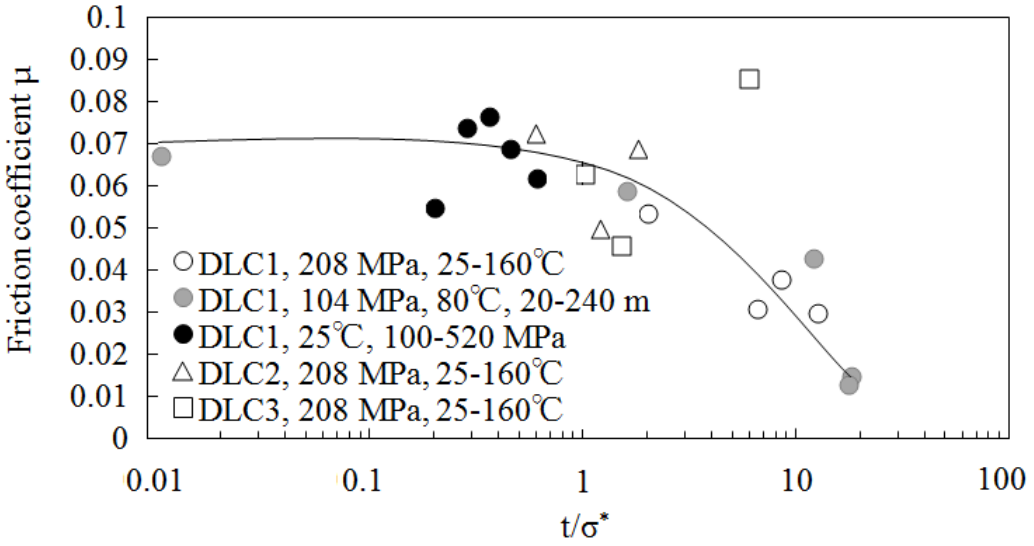

FIGURE 4.20: The effect of t/σ^* on the friction coefficient of various DLC coatings after sliding in the mineral-based oil.

4.6 Conclusions

The thickness of transformed layer of DLC sliding against steel under boundary lubrication condition in additive-free mineral-based oil were successfully measured by using reflectance spectroscopy. From the experimental results, following conclusions are as follows:

1. The thickness of the transformed layer has an effect to reduce friction coefficient in the case of DLC1.
2. It was observed that the temperature and the sliding distance has a significant effect on DLC1 for generating transformed layer during sliding test.
3. The significant decrement of friction coefficient when the t/σ^* value is higher than 1, where t is the thickness of transformed layer of DLC and σ^* is the effective root mean square roughness.

Chapter 5

Characteristics of transformed layer of DLC after friction test under boundary lubrication in additive-free mineral-based oil

5.1 Introduction

Diamond-like carbon (DLC) provide very excellence performance in term of friction coefficient and wear resistance under boundary lubrication in mineral based oil with or without additives [81–84]. DLC became more interesting as a coating material in tribological applications especially in the automotive industry in order to reduce the fuel consumption [5], because of their significant tribological properties such as low friction, high hardness, and high wear resistance. Improvements in coating technology have made the DLC coating suitable for various machine components that operate under severe conditions i.e under boundary lubrication. The low friction mechanism in the DLC coating under friction tests in either dry or boundary-lubricated conditions is due to the formation of a graphite-like layer in the non- lubricated [37, 52, 69, 85] or transformed layer [37, 86] which provides low shear strength at the contact interface. The transition phase of the as-deposited DLC to graphite-like structure at the topmost sliding interface is due to graphitization by conversion of sp^3 to sp^2. This transition phase has been reported in

other studies as a friction-induced transformation of the topmost sliding interface of the DLC coating [87, 88].

However, the nano characteristic of the transformed layer has not been studied in-terms of its hardness which is believed to have a significant effect in the tribological performance, such as a low friction coefficient under boundary lubrication conditions. The most important finding in this study is the scratch hardness of the transformed layer at the topmost of the sliding interface of the DLC from the AFM scratch test under different oil temperatures.

5.2 Experimental details

5.2.1 Friction test and Raman analysis

The detailed explanation about materials, friction test and Raman analysis are same as in the Section 3.2.

5.2.2 Scratch test

A scratch hardness test was performed to find the hardness of the transformed layer that is believed to have been formed at the topmost worn surface during the friction test. The scratch test was carried out using a commercial AFM (SII, SPA-400) in ambient temperature and humidity of 25 °C and 40 %, respectively. The poly-crystal diamond (PCD) tip cantilever from the Nano World AG, which has a tip radius of 150 nm and a spring constant of 42 Nm^{-1}, was used to perform the scratch test. Figure 5.1 shows the scanning and the scratch area when the scanning process was done before and after the scratch hardness test in order to obtain different surface profiles of the worn area. The load was applied to the cantilever for the scanning and hardness scratch of 50 and 1000 nN, respectively. The AFM stage speed of 1 μms^{-1} was set for both the scanning and scratch hardness test. The scratch movement of the PDC tip was programmed to be the same in all the tests. As shown in Figure 5.1, the initial position of the scratch hardness was at the bottom-left corner of the scratch area and then moved in a straight line by 500 nm along the y axis with a constant normal load and scratch speed. Then the PCD tip detached from the surface, and moved to the bottom position and was translated by 4 nm of x axis. These movements were repeated for 125 times for 1 cycle in order to create a scratch area of 500×500 nm^2.

The advantage of the scratch method compared to the nano-indentation in terms of the determination of the thin layer hardness is that the influence of the substrate hardness can be minimized [89]. The hardness of the transformed layer can be directly calculated using the depth of the scratch area (h') that is measured after 1 cycle of the scratch test as shown in Figure 5.2. The scratch hardness is commonly defined as a normal load per one half of the projected contact area by a single line scratch [90, 91]. In this experiment, the scratch test was done in area, a. So, the effective contact was defined as only one quarter of the vertically projected area.

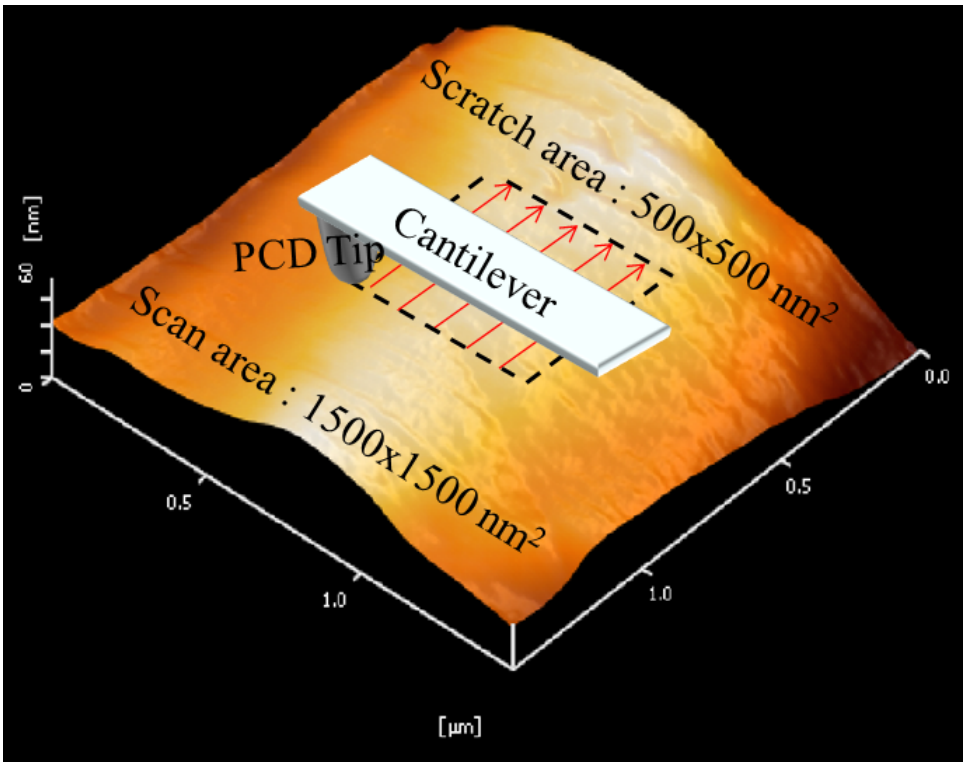

FIGURE 5.1: Schematic diagram of scan and nanoscratch test area at worn surface of DLC coating after friction test.

Figure 5.2 shows the schematic diagram of the nano-scratch test. The appropriate scratch hardness H formula that was used to calculate the hardness of the transformed layer is as follows [92].

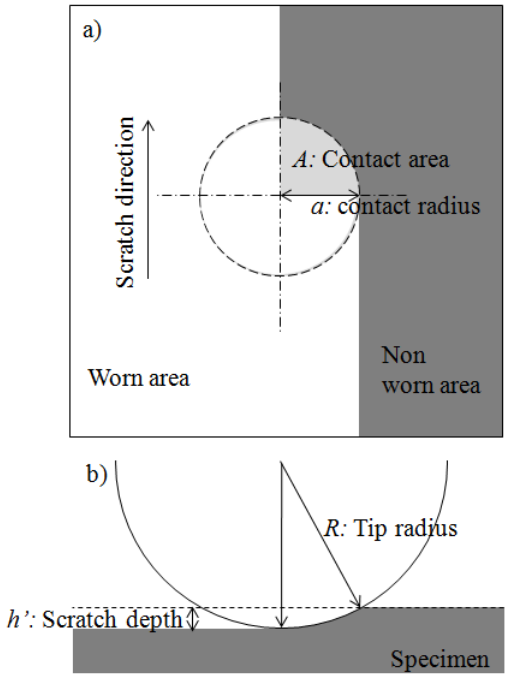

FIGURE 5.2: Schematic diagram of nano-scratch area a) top-view b) side-view.

$$H = \frac{4W}{\pi a^2} = \frac{4W}{\pi(2kRh' - k^2h'^2)} \tag{5.1}$$

$$k = \frac{R - \sqrt{R^2 - \frac{(4W)}{\pi H}}}{h'} \tag{5.2}$$

where W is the scratch test applied load, a is the radius of the projected area of contact, R is the tip radius, k is the correction factor, h' is the scratch depth and H is the hardness of the known material.

The AFM scratch hardness is depend on the stiffness of the PCD tip cantilever that used for scratch test. The correction factor, k can be determine by scratching the known material. This k value is used for calculating the hardness of transformed layer.

5.3 Results and discussion

5.3.1 Raman spectroscopy results

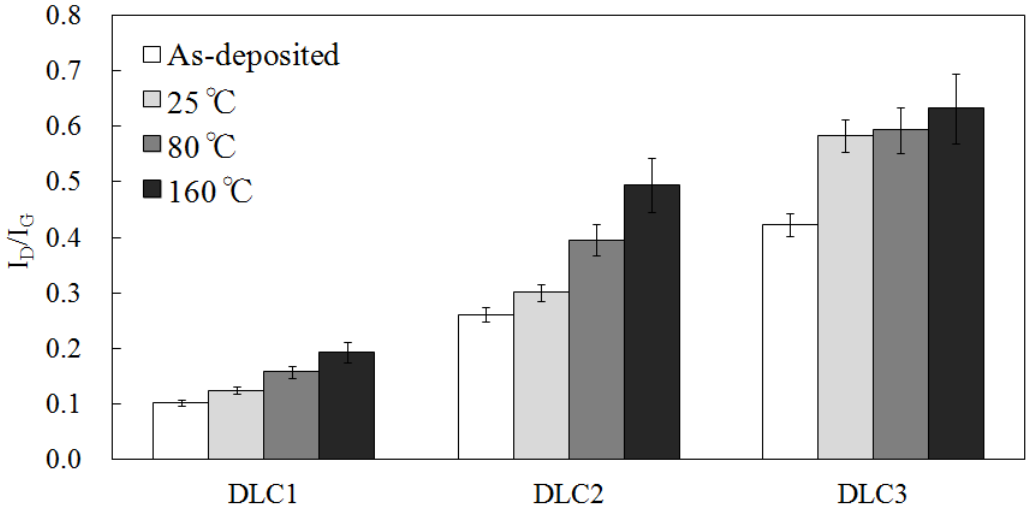

FIGURE 5.3: I_D/I_G ratios by Raman spectroscopy on wear track for each DLC as a function of oil temperature.

Raman analysis is used commonly used to investigate the changes in the DLC structure. The DLC structure can be indicated using Raman spectra by the height of disordered (D) peak near a wavelength of 1380 cm^{-1} and the graphite (G) peak near a wavelength of 1580 cm^{-1} [15]. Figure 5.3 shows the I_D/I_G values of each coating as a function of the oil temperature. Soft DLCs showed higher intensities of I_D/I_G ratios compared to harder DLCs. These results are similar to the data reported by other researchers [15]. In addition, all DLCs showed the same trend where the I_D/I_G value tended to increase after the friction test by elevated temperatures. These shows that the phase transition of sp^3 - sp^2 occurred at the topmost sliding interface during the friction test. The higher value of I_D/I_G indicated that more sp^3 transformed into sp^2 through graphitization. Generally, the transition temperatures for DLC coatings are in the range of 300-500 °C. However, according to the Clayperon law, the phase transition temperature of DLC coatings decreases with an increase in the Hertzian's contact stress. The phase transition of DLC could be reduced to a lower value of 100 °C during the sliding test [50]. This shows that the DLC coating surface can be transformed from sp^3 into sp^2 at lower than phase transition temperatures due to increased contact stress during sliding. It suggests that the friction-induced graphitization was responsible for the structural

changes. These surface modifications created a graphite-like transformed layer at the sliding interface.

5.3.2 Dependence of scratch depth on oil test temperature

A scratch test was carried out to investigate the hardness properties of transformed layer of all DLCs after the friction test in different oil test temperatures from 25 to 160 °C. Figure 5.4(a) shows the surface topography after the scratch hardness test on DLC1, DLC2 and DLC3 with different oil temperatures of the friction test. These AFM images showed that an apparent worn area was created after the scratch test. Figure 5.4(b) shows the cross-sectional profile of the worn area. All types of DLCs showed the same behaviour in that the scratch depth increased with increases in oil temperature. The deepest scratch depth for all the DLCs showed at a high oil test temperature with the value of 5.5, 12.7 and 29.2 nm for DLC1, DLC2 and DLC3, respectively. This scratch depth was used later for the determination of the hardness of the transformed layer.

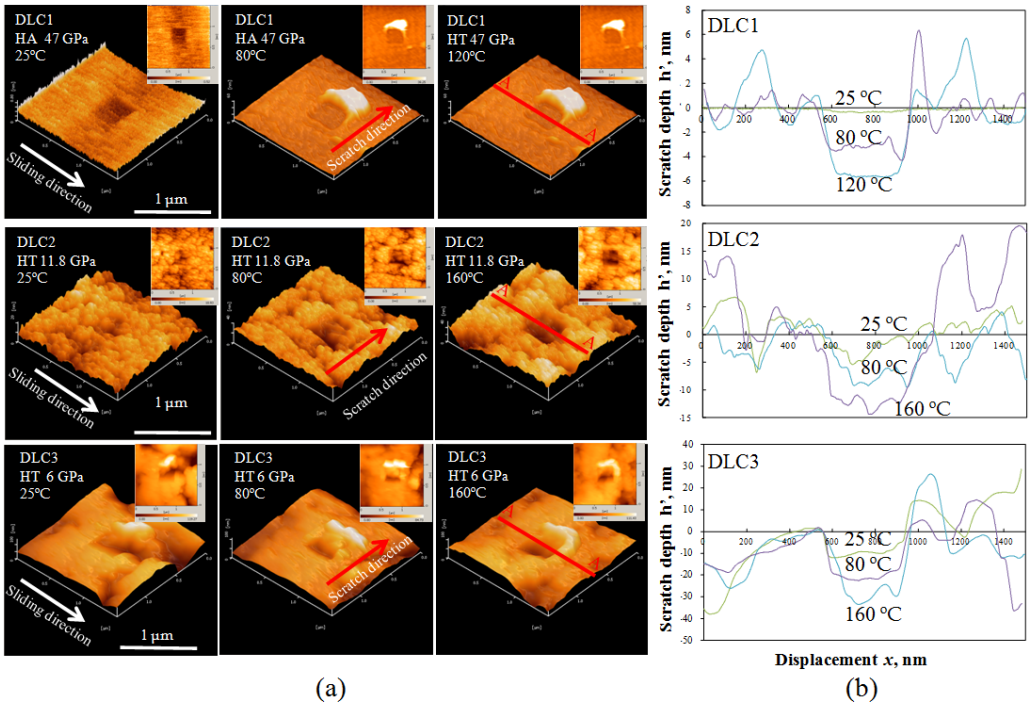

FIGURE 5.4: a) Surface topography after scratch hardness test b) cross-section profile of A-A and wear depth at different oil test temperatures.

In Figure 5.5, the scratch depth values of all the DLCs have been plotted as a function of the oil temperature. The increase in the scratch depth by increasing the oil temperature showed that the DLC coating became softer during the

friction test and was influenced by the oil temperature [37]. As explained in the previous subsection, the structure of the coating at the sliding contact interfaces has transformed the DLC into a graphite-like layer due to the friction-induced graphitization process [50]. The graphite-like transformed layer has a more sp^2 structure compared to the as- deposited DLC. The friction-induced graphitization process softened the contact interface during sliding.

5.3.3 Scratch hardness of transformed layer

The scratch hardness was calculated by Eqs. 5.1 and 5.2 using the applied normal load and the scratch depth. The scratch depth was measured from the cross-sectional profile of the scratch area from AFM as shown in Figure 5.4(b). The scratch hardness results were plotted as a function of oil temperature as shown in Figure 5.6.

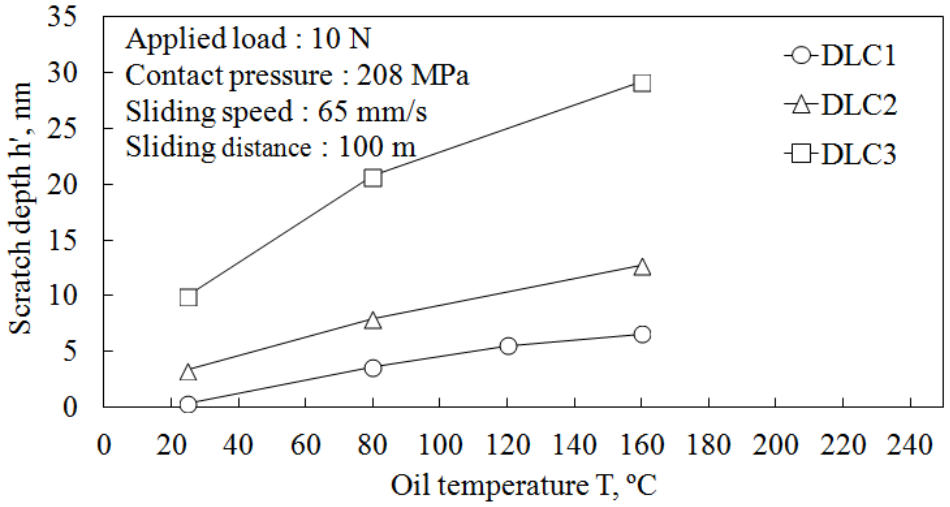

FIGURE 5.5: Scratch depth as a function of oil temperature for DLC1, DLC2 and DLC3.

The result showed a significant decrease in the scratch hardness of the transformed layer compared to the as-deposited DLC by the elevated oil temperature for all types of DLCs. The hardness of the transformed layers was lower than the hardness of the S55C mating material. In addition, the scratch hardness of the transformed layer decreased by increasing the oil temperature. The hardness of the transformed layer of DLC1 showed drastic reduction from the as-deposited coating hardness of 47 GPa to 4.3 GPa at 80 °C. The low hardness of the transformed layer with the sp^2-rich structure provided a low shear strength at the contact interface that influenced the friction behaviour. The lowest scratch hardness of 0.5 GPa was shown by the softest coating (DLC3) at an oil temperature of 160 °C, and the hardest coating (DLC1) showed the lowest scratch hardness of 2.5 GPa at an oil temperature of 160 °C.

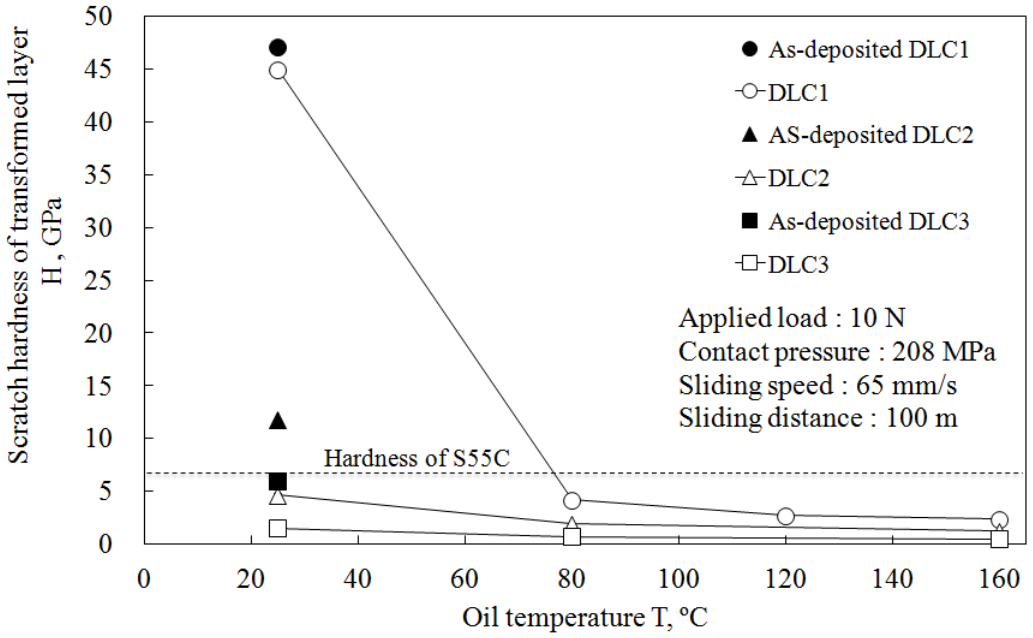

FIGURE 5.6: Scratch hardness as a function of oil temperature for DCL1, DLC2 and DLC3.

5.3.4 Dependence of friction coefficient on the scratch hardness of the transformed layer

The relation between friction coefficient and oil temperatures is discussed in section 3.4. The friction coefficient of DLC1 decreased from 0.05 to 0.03 with an increase in oil temperature. However, the friction coefficient of DLC1 increased from 0.03 to 0.04 when the oil temperature increased from 120 to 160 °C. DLC2 and DLC3 showed the opposite behaviour, where the friction coefficient increased with elevated oil temperatures, and the value was higher than DLC1. From these results, it is difficult to explain why the different hardness of as-deposited DLC showed different friction behaviour.

In order to understand the situation, the friction coefficient was plotted as a function of the hardness of the transformed layer. Figure 5.7 shows the relation between the friction coefficient and the hardness of the transformed layer. This figure can be divided into 3 regions. The first region is the soft transformed layer, where the friction coefficient is high and the value is around 0.08. Then the friction coefficient decreased as the hardness of the transformed layer increased. The lowest friction coefficient of 0.03 was achieved at a moderate hardness of the transformed layer

within the range of 2.8-4.3 GPa. However, any further increment of the hardness of the transformed layer results an increasing in the friction coefficient.

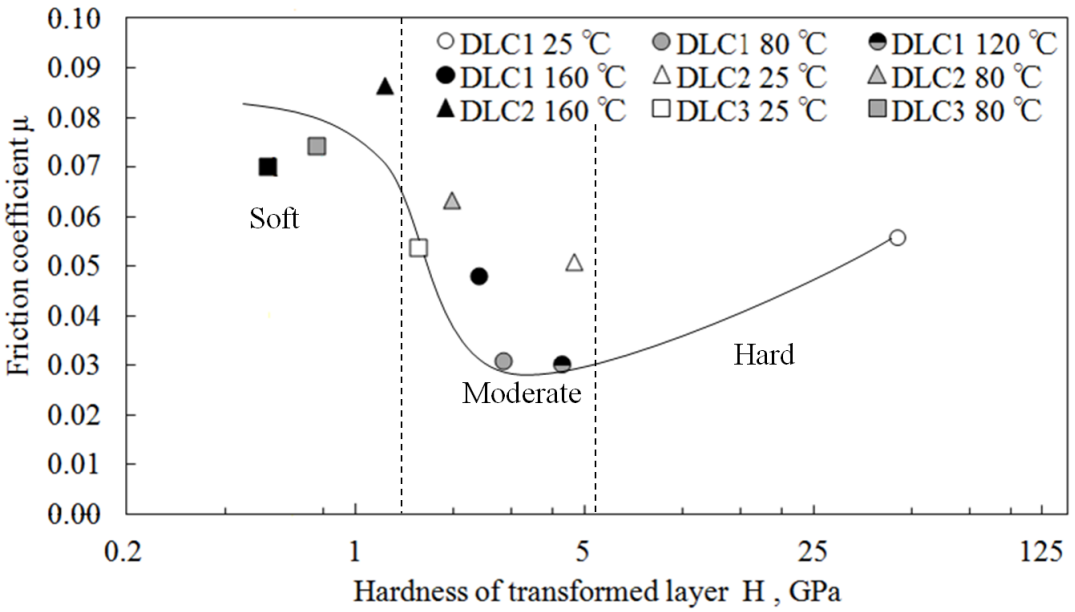

FIGURE 5.7: Friction coefficient as a function of hardness of transformed layer for DLC1, DLC2 and DLC3.

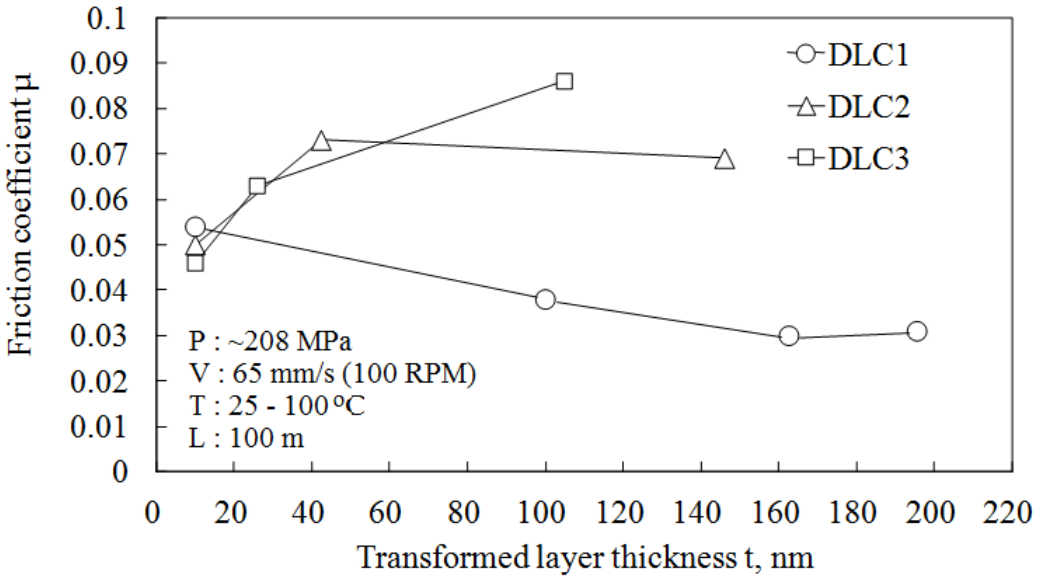

FIGURE 5.8: Friction coefficient as a function of transformed layer thickness.

Figure 5.8 shows the friciton coefficient as a function of transformed layer thickness as reported in Chapter 4. The friction coefficient of DLC1 decreased with an increasing oil temperature. In contrast, DLC2 and DLC3 showed an increasing in the friction coefficient as the oil temperature increased.

Further investigation is needed in order to understand the influence of the thickness and hardness of the transformed layer on the friction behaviour. Therefore, the friction coefficient map as a function of the thickness and hardness of the transformed layer is developed as shown in Figure 5.9. A high friction coefficient in the range of 0.07 - 0.08 is given by the combination LH-TnTL and LH-TkTL. The thickness of the transformed layer did not play a significant role in these combinations because the transformed layer was too soft. It was thought that the high friction coefficient in the soft region was because the asperities of the mating surface could penetrate easily into the transformed layer, and subsequently the mating surface had full contact with hard bulk DLC as shown in 5.10(a). The graphite-like transformed layer did not function as a slippery surface because the direct contact between the mating surface and the bulk DLC controlled the behaviour.

The combination of LH, MH, HH, and Tn gives the friction coefficient in the range of 0.05 - 0.07. In this case, the hardness of the transformed layer did not influence the friction coefficient. Because of the thickness of the transformed layer, the asperities of the mating surface could touch the hard bulk DLC as shown in Figure 5.10(c). The friction between the hard bulk DLC surfaces with the mating surface still provided a high friction coefficient.

The lowest friction coefficient of 0.03 was given by the MH-TkTL combination. Because of its moderate hardness, the transformed layer, could avoid direct contact between the asperities of the mating surface and the hard bulk DLC. Subsequently, the mating surface could smoothly slide on the transformed layer because the graphite-like transformed layer provided a slippery surface.

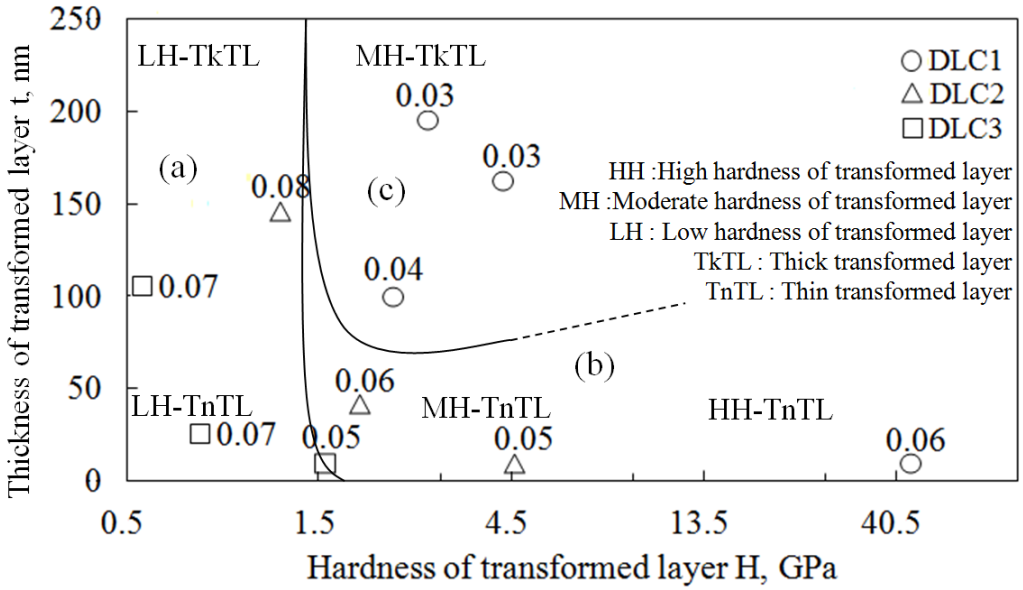

FIGURE 5.9: Friction coefficient map as a function of the thickness and hardness of the transformed layer.

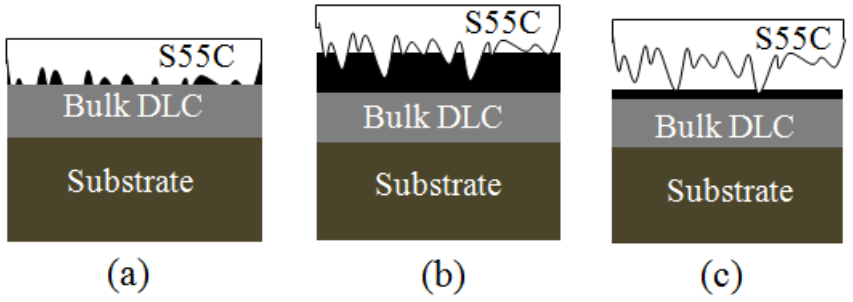

FIGURE 5.10: Friction model regarding the combination of thickness and hardness of the transformed layer. (a) LH-TkTL and LH-TnTL. (b) MH-TnTL and MH-TnTL. (c) MH-TkTL.

5.4 Conclusion

DLC is well known as a coating material that has essential properties for tribological applications due to its low friction coefficient, high hardness and wear resistance. The low friction coefficient that achieved during the friction test was due to the phase transformation of the hard DLC coating into a soft graphite-like transformed layer. This study presented the scratch hardness of the transformed layer was obtained from the AFM scratch test that governs the friction behaviour of DLC. A friction map was also developed as a function of the thickness and hardness of the transformed layer. The following conclusions were reached as follows:

1. The hardness of the transformed layer depends on the oil temperature, where the sliding interface of DLC softened during the friction test due to graphitization.

2. It is suggested that the combination of moderate hardness and thick transformed layer leads to a low friction.

Chapter 6

Conclusion

Carbonaceous hard coatings attract more attention for coating technology especially for tribological components, because of their high hardness, low friction and high wear resistance. Carbonaceous hard coatings can also provide low friction either under dry conditions or boundary lubrication in oil. After the friction test, an ex-situ observation in dry conditions showed that the transfer layer could easily be found on the surface. of the counterpart. This transfer layer is believed to be responsible for the low friction, with the transfer layer acting as a third body and providing a slippery interlayer between the carbonaceous and mating surface. The transfer layer separated the direct contact between the two surfaces and controlled the friction behaviour. Therefore, an in-situ observation was needed to observe the formation of a transfer layer that influenced the friction behaviour under dry conditions. However, no reports exist about in-situ observations of the formation of a transfer layer during friction testing under dry conditions.

However, the transfer layer could not be found on the surface of the counterpart using ex-situ observation after friction, in the case of oil lubrication. The oil would not allow the adhesive bonding of the transfer layer to the counterpart. However, after the ex-situ surface analysis of the carbonaceous coating worn area, the results of a Raman analysis after the friction test, showed that the carbonaceous hard coating structure had changed and was then known as the transformed layer.

This change was due to graphitization, where the structure of sp^3 was converted to sp^2 . The sp^2 rich topmost surface could provide a low shear strength that resulted the low friction. It is believed that due to a lack of oil in the boundary lubrication friction test, the properties of the carbonaceous hard coating topmost

surface (transformed layer) could control the friction behaviour. It is therefore very important to investigate the mechanical properties of the topmost contact interface.

The findings in this work can be summarized as follows:

1. In-situ observation successfully identified the transfer layer generation, which contributed to the friction behaviour of the CNx coating against the sapphire hemisphere. From this study, the following conclusions are as follows:

   (a) The transformation of CNx to graphite-like transfer layer is a consequence of high contact pressure 1.5 GPa at the contact interface.

   (b) The desorption of N content from the CNx coating during sliding was responsible for graphitization.

   (c) The shape of Raman spectra of the transfer layer is comparable with pure graphite.

   (d) Existing of a graphite-like transfer layer with the thickness of 60 nm between the CNx coating and the sapphire hemisphere, will significantly reduce the friction coefficient to an ultra low of 0.003.

   The permanent attachment of a transfer layer at the contact interface is very important to maintain an ultra low friction during the friction test.

2. The tribological properties of different hardness of DLCs sliding against steel under boundary lubrication condition in additive-free mineral-based oil were investigated in order to determine the influence of the as-deposited DLC hardness on friction behaviour. The following conclusions were reached as follows:

   (a) The friction coefficient decreased with an increasing of the hardness of as-deposited DLC.

   (b) The specific wear rate decreases significantly with an increasing in the hardness of as-deposited DLC.

   (c) The formation of graphite-like transformed layer is due to graphitization process during friction test.

3. The thickness of transformed layer of DLC sliding against steel under boundary lubrication condition in additive-free mineral-based oil were successfully measured by using reflectance spectroscopy. From the experimental results, following conclusions are as follows:

   (a) The thickness of the transformed layer has an effect to reduce friction coefficient in the case of DLC1.

   (b) It was observed that the temperature and the sliding distance has a significant effect on DLC1 for generating transformed layer during sliding test.

   (c) The significant decrement of friction coefficient when the t/σ^* value is higher than 1, where t is the thickness of transformed layer of DLC and σ^* is the effective root mean square roughness.

4. DLC is well known as a coating material that has essential properties for tribological applications due to its low friction coefficient, high hardness and wear resistance. The low friction coefficient that achieved during the friction test was due to the phase transformation of the hard DLC coating into a soft graphite-like transformed layer. This study presented the scratch hardness of the transformed layer was obtained from the AFM scratch test that governs the friction behaviour of DLC. A friction map was also developed as a function of the thickness and hardness of the transformed layer. The following conclusions were reached as follows:

   (a) The hardness of the transformed layer depends on the oil temperature, where the sliding interface of DLC softened during the friction test due to graphitization.

   (b) It is suggested that the combination of moderate hardness and thick transformed layer leads to a low friction.

References

[1] Dowson, D., 2nd edition, Professional engineering published limited, London, UK, Tribology Transactions, (1998).

[2] Jost, P., Lubricant tribology, Education and Research Report, London, Department Education and Science, Her Majestry's Stationary Office, (1998).

[3] Taylor, R.I., Improved fuel efficiency by lubricant design: A review, Proceedings of the Institution of Mechanical Engineers, 214J (2000) 1-15.

[4] Fessler, R.R., Fenske, G.R.I., Multiyear program plan: Reducing friction and wear in heavy vehicles, U.S. Department of Energy, Office of Heavy Vehicle Technologies, Workshop Report, Argonne National Laboratory, Argonne, (1999).

[5] Holmberg, K., Andersson, P., Erdemir, A., Global energy consumption due to friction in passenger cars, Tribology International, 47 (2012) 221-234.

[6] Hogmark, S., Progress report on WG3: Tribochemistry, Triboscience and Tribotechnology, Workgroup meeting, Prague, (2005).

[7] Podgornik, B., Vizintin, J., Jacobson, S., Hogmark, S., Tribological behaviour of WC/C coatings operating under different lubricant regimes, Surface and Coatings Technology, 177-178 (2004) 558-565.

[8] Bhusan, B., Introduction to Tribology, John Wiley & Sons, Inc., New York, (2002).

[9] Hainsworth, S.V., Uhure, N., Diamond-like carbon coatings for tribology applications, Int. Mater. Rev., 52 (2007) 153-158.

[10] Stachowiak, G.W., Wear: Materials, Mechanisms and Practice, John Wiley & Sons, Inc., New York, (2006).

[11] Robertson, J., Diamond-like amorphous carbon, Materials Science and Engineering, R: Reports, 37 (2002) 129-281.

[12] Kelly, B.T., Physics of graphite, Applied Science Publishers, London, (1981).

[13] Kelly, B.T., Essentials of materials science, McGraw-Hill, Inc., New York, US, (1976).

[14] Bushan, B., Principles and applications of tribology, John Wiley & Sons, Inc., New York, USA, (1999).

[15] Ferrari, A.C., Robertson J., Interpretation of Raman spectra of disordered and amorphous carbon, Physic Rev. B., 61 (2000) 14095-14106.

[16] Moon, M.W., Jensen, H.M., Hutchinson, J.W., Oh, O.H., Evans, J., Mech. Phys. Solids, 50 (2002) 2355-2365.

[17] Mattox, D.M., Handbook of physical vapor deposition (PVD) processing film formation, adhesion, surface preparation and contamination control, Noyes Publication, (1998).

[18] Erdemir, A., Donnet, C., Modern tribology handbook, Boca Raton, FL., CRC Press, (2000) 871-908.

[19] Bruno, P., Cicala, G., Losacco, A.M., Decuzzi, P., Mechanical properties of PECVD hydrogenated amorphous carbon coatings via nanoindentation and nanoscratching techniques, Surface and Coatings Technology, 180 (2004) 259-264.

[20] Ferrari, A.C., Robertson, J., Pastorelli, R., Beghi, M.G., Bottanii, C.E., Elastic constants of tetrahedral amorphous carbon films by surface Brillouin scattering, Applied Physics Letters, 75 (1999) 1893-1895.

[21] Hu, J., Lieber, C., Yang P., Nitrogen-driven sp^3 to sp^2 transformation in carbon nitride materials, Physical Review B, 57 (1998) 3185-3188.

[22] Liu, A.I., Cohen, M.L., Prediction of new low compressibility solid, Science, 245 (1989) 841-842.

[23] Cohen, M.L., Predicting useful materials, Science, 261 (1993) 307-308.

[24] Wang, D.F., Kato, K., Friction studies of ion beam, assisted carbon nitride coating sliding against diamond tip in water vapour, Wear, 217 (1998) 307-311.

[25] McCann, R., Roy, S.S., Papakonstantinou, P., Abbas, G., McLaughlin, G.A., The effect of thickness and arc current on the structural properties of FCVA synthesised ta-C and ta-C:N films, Diamond Related Materials, 14 (2004) 983-988.

[26] Tokoroyama, T., Goto, M., Umehara, N., Nakamura, T., Honda, F., Effect of nitrogen atoms desorption on the friction of the CNx against Si_3N_4 ball in nitrogen gas, Tribology letters, 22 (2006) 215-220.

[27] Svahn, F., Kassman-Rudolphi, A., Wallen, E., The influence of surface roughness on friction and wear of machine element coatings, Wear, 254 (2003) 1092-1098.

[28] Zhang, W., Tanaka, A., Wazumi, K., Koga Y., Effect of environment on friction and wear properties of diamond-like carbon film, Thin Solid Films, 413 (2002) 104-109.

[29] Erdemir, A., Fenske, G.R., Terry, J., Wilbur, P., Effect of source gas and deposition method on friction and wear performance of diamond-like carbon films, Surface and Coatings Technology, 94-95 (1997) 525-530.

[30] Yoon, E.S., Kong, H., Lee, K.R. Tribological behavior of sliding diamond-like carbon films under various environments, Wear, 217 (1998) 262-271.

[31] Fontaine, J., Donnet, C., Grill, A., LeMogne, T., Tribochemistry between hydrogen and diamond-like carbon films, Surface and Coatings Technology, 146-147 (2001) 286-291.

[32] Fontaine, J., Belin, M., Le Mogne, T., Grill A., How to restore superlow friction of DLC: The healing effect of hydrogen gas, Tribology International, 37 (2004) 869-877.

[33] Donnet, C., Le Mogne, T., Ponsonnet, L., Belin, M., Grill A., Patel V., Jahnes, C., The respective role of oxygen and water vapor on the tribology of hydrogenated diamond-like carbon coatings, Tribology Letters, 4 (1998) 259-265.

[34] Liu, Y., Erdemir, A., Meletis, E.I., Influence of environmental parameters on the frictional behavior of DLC coatings, Surface and Coatings Technology, 93-95 (1997) 363-168.

[35] Liu, Y., Meletis, E. I., Evidence of graphitization of diamond-like carbon films during sliding wear, Journal of Materials Science, 32 (1997) 3491-3495.

[36] Vengudusamy, B., Mufti, R.A., Lamb, G.D., Green J.H., Spikes, H.A., Friction properties of DLC/DLC contacts in base oil, Tribology International, 44 (2011) 922-932.

[37] Kalin, M., Roman, E., Vizintin, J., The effect of temperature on the tribological mechanisms and reactivity of hydrogenated, amorphous diamond-like carbon coatings under oil-lubricated conditions, Thin Solid Films, 515 (2007) 3644-3652.

[38] Khurshudov, A.G., Kato, K., Tribological properties of carbon nitride overcoat for thin-film magnetic rigid disks, Surface and Coatings Technology, 86-87 (1996) 664-671.

[39] Fernandez, A., Fernandez-Ramos, C., Sanchez-Lopez, J.C., Preparation, microstructural characterisation and tribological behaviour of CNx coatings, Surface and Coatings Technology, 163-164 (2003) 527-534.

[40] Qi, J., Chan, C.Y., Bello, I., Lee, C.S., Lee, S.T., Luo, J. B., Wen, S.Z., Film thickness effects on mechanical and tribological properties of nitrogenated diamond-like carbon films, Surface and Coatings Technology, 145 (2001) 38-43.

[41] Kato, K., Umehara, N., Adachi, K., Friction, wear and N_2-lubrication of carbon nitride coatings: A review, Wear, 254 (2003) 1062-1069.

[42] Umehara, N., Tatsuno, M., Kato, K., Nitrogen lubricated sliding between CNx coatings and ceramic balls, Proceedings of the International Tribology Conference, Nagasaki, (2000) 1007-1012.

[43] Miyahira, Y., Tokoroyama, T., Umehara N., Effect of atmosphere gas on ultra low friction properties of CNx coating, The Japan Society of Mechanical Engineers, (2010) 1116-1120 (In Japanese).

[44] Chromik, R.R., Baker, C.C., Voevodin, A.A., Wahl, K.J., In situ tribometry of solid lubricant nanocomposite coatings, Wear, (2007) 1239-1252.

[45] Wahl, K.J., Chromik, R.R., Lee, G.Y., Quantitative in situ measurement of transfer film thickness by a Newton's rings method, Wear, 264 (2008) 731-736.

[46] Johnson, K.L., Contact mechanics, Cambridge University Press, (1985).

[47] McCulloch, D.G., Merchant, A.R., The effect of annealing on the structure of cathodic arc deposited amorphous carbon nitride films, Thin Solid Film, (1996) 99-102.

[48] Zhou, Z.F., Li, K.Y., Bello, I., Lee, C.S., Lee, S.T., Study of tribological performance of ECR-CVD diamond-like carbon coatings on steel substrates: Part 2. The analysis of wear mechanism, Wear, 258 (2005) 1589-1599.

[49] Haque, T., Morina, A., Neville, A., Kapadia, R., Arrowsmith, A., Effect of oil additives on the durability of hydrogenated DLC coating under boundary lubrication conditions, Wear, 266 (2009) 147-157.

[50] Huu, T.L., Zaidi, H., Paulmier, D., Voumard, P., Transformation of sp^3 to sp^2 sites of diamond like carbon coatings during friction in vacuum and under water vapour environment, Thin Solid Films, (1996) 126-130.

[51] Tokoroyama, T., Umehara, N., Effect of nitrogen atom included in CNx coatings on friction sliding against Si_3N_4 ball in nitrogen gas, International Symposium on Micro-Nano Mechatronics and Human Science, (2007) 568-591.

[52] Liu, Y., Erdemir, A., Meletis, E.I., An investigation of the relationship between graphitization and frictional behavior of DLC coatings, Surface and Coatings Technology, 86-87 (1996) 564-568.

[53] Reich, S., Thomsen, C., Raman spectroscopy of graphite, Philosophical Transactions of the Royal Society of London A., 362 (2004) 2271-228.

[54] Sanchez-Lopez, J.C., Belin, M., Quiro, C., Elizalde, E., Friction mechanisms of amorphous carbon nitride films under variable environments: A triboscopic study, Surface and Coatings Technology, 160 (2002) 138-144.

[55] Scharf, T.W., Singer, I.L., Tribology of diamond-like carbon films: Fundamental and applications, Springer, (2008) 210-237.

[56] Zaidi, H., Robert, F., Paulmier, D., Influence of absorbed gases on the surface energy of graphite: consequences on the friction behavior, Thin solid films, 264 (1995) 46-51.

[57] Kumar, N., Dash, S., Tyagi, A.K., Raj, B., Super low to high friction of turbo static graphite under various atmospheric test conditions, Tribology International, 44 (2011) 1969-1978.

[58] Kovalchenko, A., Ajayi, O., Erdemir, A., Fensk, G., Etsion, I., The effect of laser texturing of steel surfaces and speed-load parameters on the transition of lubrication regime from boundary to hydrodynamic, Tribology Transactions, 47 (2010) 299-307.

[59] Beardsley, M.B., Happoldt, P.G., Kelley, K.C., Rejda, E.F., Socie, D.F., Thermal barrier coatings for low emission, high efficiency diesel engine applications, SAE, 01 (1999) 2255-2265.

[60] Johnson, D.R., Diamond, S., Heavy vehicle propulsion materials: Recent progress and future plans, SAE, 01 (2001) 2061-2070.

[61] Singh, G., Graves, R.L., Storey, J.M., Partridge, W.P., Thomas, J.F., Penetrante, B.M., Brusasco, R.M., Merritt, B.T., Vogtlin, G.E, Aardahl, C.L., Habeger, C.F., Balmer, M. L., Emission control research to enable fuel efficiency, SAE, 01 (2000) 2198-2215.

[62] Kalin, M., Velkavrhand, I., Vizintinand, J., Ozbolt L., Review of boundary lubrication mechanisms of DLC coatings used in mechanical applications, Meccanica, 43 (2008) 623-637.

[63] Semenov, A.P., Khrushchov, M.M., Influence of environment and temperature on tribological behavior of diamond and diamond-like coatings, Journal of Friction and Wear, 31 (2010) 142-158.

[64] Hosfall, R.H., Commercial applications using non-hydrogenated carbon films for industrial uses such as cutting tools and wear components, Proceedings of the 41st Annual Technical Conference, Society of Vacuum Coaters, (1998) 60-65.

[65] Hamrock, B.J., Schmid, S.R., Jacobson, B. O., Fundamentals of fluid film lubrication, CRC Press, (2004).

[66] Fischer-Cripps, A.C., Critical review of analysis and interpretation of nanoindentation test data, Surface and Coatings Technology, 200 (2006) 4153-4165.

[67] Tamor, M. A., Vassell, W.C., Raman "fingerprint" of amorphous carbons films, Journal Applied Physics, 76 (1999) 3823-3830.

[68] Prawer, S., Nugent, K.W., Lifshiz, Y., Lempert, G.D., Grossman, E., Kulik, J., Avigal, I., Kalish, R., Systematic variation of the Raman spectra of DLC films as a function of sp^2:sp^3 composition, Diamond and Related Materials, 5 (1996) 433-438.

[69] Sanchez-Lopez, J.C., Erdemir, A., Donnet, C., Rojasa, T.C., Friction-induced structural transformations of diamond-like carbon coatings under various atmospheres, Surface and Coatings Technology, 163 (2003) 444-450.

[70] Scheibe, H.J., Drescher, D., Alers, P., Raman characterization of amorphous carbon films, Fresenius' Journal of Analytical Chemistry, 353 (1995) 695-697.

[71] Waara, P., Hannu, J., Norrby, T., Byheden, A., Additive influence on wear and friction performance of environmentally adapted lubricants, Tribology International, 34 (2001) 547-556.

[72] Spikes, H., The history and mechanisms of ZDDP, Tribology Letters, (2004) 17-3.

[73] Kalin, M., Dohda, K., Jahanmir, S., Erdemir, A., Vizintin. J., Diamond-like carbon films, Tribology of mechanical systems, NewYork: ASME Press, (2004) 139-156.

[74] De Barros Bouches, M.I., Matta, C., Kano, M., Superlubricity mechanism of diamond-like carbon with glycerol, Coupling of experimental and simulation studies, Journal of Physics: Conference Series, (2007) 89-90.

[75] Sanchez-Lopez, J.C., Erdemir, A., Donnet, C., Rojas, T.C., Friction-induced structural transformations of diamond like carbon coatings under various atmospheres, Surface and Coatings Technology, (2003) 163-164.

[76] Johnston, G.J., Wayte, R., Spikes, H.A., The measurement and study of very thin lubricant films in concentrated contacts, Tribology Transactions, 34 (1991) 187-194.

[77] Spencer, E.G., Schmidt, P.H., Joy, D.C., Sansalone, F.J., Ion beam deposited polycrystalline diamond-like films, Applied Physics Letters, 29 (1976) 118-120.

[78] Higuchi, T., Mabuchi, Y., Structure transformation of hydrogen free DLC surface with friction, Proceedings of the JAST tribology conference, Tokyo, (2011) 135-140.

[79] Momozono, S., Nakahara, T., Effects of mechanical properties of solid-like film and substrate, film thickness and roughness parameters on static boundary friction, Proceedings of the 3rd Asia international conference of tribology, Kanazawa, (2006) 85-86.

[80] Dayson, C., The friction of very thin solid film lubricants on surface of finite roughness, STLE Transactions, 14 (1971) 105-115.

[81] De Barros Bouchet, M.I., Martin, J.M., Le-Mogne, T., Vacher, B., Boundary lubrication mechanisms of carbon coatings by MoDTC and ZDDP additives, Tribology International, 38 (2005) 257-264.

[82] Stallard, J., Mercs, D., Jarratt, M., Teer, D.G., Shipway, P.H., A study of the tribological behaviour of three carbon-based coatings, tested in air, water and oil environments at high loads, Surface and Coatings Technology, 177 (2004) 545-551.

[83] Ouyung, J.H., Sasaki, S., Friction and wear characteristics of a Ti-containing diamond-like carbon coating with an SRV tester at high contact load and elevated temperature, Surface and Coatings Technology, 195 (2005) 234-244.

[84] Miyake, S., Tadashi, F., Yasuda, Y., Okamoto, Y., Kano, M., Improvement of boundary lubrication properties of diamond-like carbon (DLC) films due to metal addition, Tribology International, 37 (2004) 751-761.

[85] Liu, Y., Erdemir, A., Meletis, E.I., An investigation of the relationship between graphitization and frictional behavior of DLC coatings, Surface and Coatings Technology, 86 (1996) 564-568.

[86] Ohara, K., Masripan, N.A., Umehara, N., Kousaka, H., Tokoroyama, T., Inami, S., Zushi, K., Fujita, M., Evaluation of transformed layer of DLC after sliding in oil with spectroscopic reflectometry, Tribology International, (2013) in press.

[87] Erdemir, A., Bindal, C., Pagan, J., Wilbur, P., Characterization of transfer layers on steel surfaces sliding against diamond-like hydrocarbon films in dry nitrogen, Surface and Coatings Technology, 76 (1995) 559-563.

[88] Voevodin, A.A., Phelps, A.W., Zabinski, J.S., Donley, M.S., Friction induced phase transformation of pulsed laser deposited diamond-like carbon, Diamond and Related Materials, 5 (1996) 1264-1269.

[89] Beegan, D., Chowdhury, C., Laugier, M.T., Comparison between nanoindentation and scratch test hardness (scratch hardness) values of cooper thin films on oxidised silicon, Surface and Coatings Technology, 201 (2007) 5804-5808.

[90] Ahn, J., Mittal, K.L., MacQueen, R.H., Adhesion measurement of thin films, thick films and bulk coatings, ASTM, 640 (1978) 74.

[91] Thomas, A., Walters, R.P., Wear and scratch hardness of 304 stainless steel investigated with a single scratch test, Wear, 74 (1993) 713-720.

[92] Kimura, H., Tsukiyama, Y., Tokoroyama, T., Umehara, N., Evaluation of mechanical properties of the superficial layer of CNx with ultra low friction in N_2 gas, Transactions of the Japan Society of Mechanical Engineer Series C, 772 (2010) 3794-3799.

Publication lists

[1] **Nor Azmmi Bin Masripan**, Yuki Miyahira, Hidenori Nishimura, Takayuki Tokoroyama, Noritsugu Umehara, Yoshio Fuwa. Effect of transfer layer on ultra low friction of CNx coating under blowing dry Ar. Triboligy Online,
8,3 (2013) 219-226.

[2] **Nor Azmmi Bin Masripan**, Kenji Ohara, Noritsugu Umehara, Hiroyuki Kousaka, Takayuki Tokoroyama,Shigeru Inami, Koji Zushi, Masahito Fujita Hardness effect of DLC on tribological properties for sliding bearing under boundary lubrication condition in additive-free mineral base oil.
Tribology International, (2013) in press.

[3] Kenji Ohara, **Nor Azmmi Bin Masripan**, Noritsugu Umehara, Hiroyuki Kousaka, Takayuki Tokoroyama, Shigeru Inami, Koji Zushi, Masahito Fujita. Evaluation of the transformed layer of DLC coatings after sliding in oil using spectroscopic reflectometry. Tribology International, (2013) in press.

International Conference

[1] **Nor Azmmi Bin Masripan**, Yuki Miyahira, Hidenori Nishimura, Takayuki Tokoroyama, Noritsugu Umehara, Yoshio Fuwa. Effect of transfer layer on ultra low friction of CNx coating under blowing dry Ar. International Tribology conference Hiroshima 2011, 30 Oct. – 3 Nov. 2011.

[2] **Nor Azmmi Bin Masripan**, Kenji Ohara, Noritsugu Umehara, Hiroyuki Kousaka, Takayuki Tokoroyama,Shigeru Inami, Koji Zushi, Masahito Fujita Hardness effect of DLC on tribological properties for sliding bearing under boundary lubrication condition in additive-free mineral base oil.
39th Leeds-Lyon Symposium on Tribology, 4-7 Sept. 2012, Leeds Trinity University College, Leeds.

[3] Kenji Ohara, **Nor Azmmi Bin Masripan**, Noritsugu Umehara, Hiroyuki Kousaka, Takayuki Tokoroyama, Shigeru Inami, Koji Zushi, Masahito Fujita Evaluation of the transformed layer of DLC coatings after sliding in oil using spectroscopic reflectometry. 39th Leeds-Lyon Symposium on Tribology, 4-7 Sept. 2012, Leeds Trinity University College, Leeds.